12-2009

Title Geometry and Electronic Structure of Doped Clusters via the Coalescence Kick Method

Boris Averkiev
Utah State University

Utah State University
MERRILL-CAZIER LIBRARY

5-1-2009

Geometry and Electronic Structure of Doped Clusters via the Coalescence Kick Method

Boris Averkiev
Utah State University

Recommended Citation

GEOMETRY AND ELECTRONIC STRUCTURE OF DOPED

CLUSTERS VIA THE COALESCENCE

KICK METHOD

by

Boris Averkiev

A dissertation submitted in partial fulfillment
of requirements for the degree

of

DOCTOR OF PHILISOPHY

in

Chemistry
(Physical Chemistry)

Approved:

_____   _____
Alexander Boldyrev   Steve Scheiner
Major Professor   Committee Member

_____   _____
David Farrelly   Stephen Bialkowski
Committee Member   Committee Member

_____   _____
T.C. Shen   Byron Burnham
Committee Member   Dean of Graduate Studies

UTAH STATE UNIVERSITY
Logan, Utah

2009

ABSTRACT

Geometry and Electronic Structure of Doped Clusters via the

Coalescence Kick Method

by

Boris Averkiev, Doctor of Philosophy

Utah State University, 2009

Major Professor: Dr. Alexander I. Boldyrev
Department: Chemistry and Biochemistry

Developing chemical bonding models in clusters is one of the most challenging tasks of modern theoretical chemistry. There are two reasons for this. The first one is that clusters are relatively new objects in chemistry and have been extensively studied since the middle of the 20th century. The second reason is that clusters require high-level quantum-chemical calculations; while for many classical molecules their geometry and properties can be reasonably predicted by simpler methods.

The aim of this dissertation was to study doped clusters and explain their chemical bonding. The research was focused on three classes of compounds: aluminum clusters doped with one nitrogen atom, planar compounds with hypercoordinate central atom, partially mixed carbon-boron clusters, and transition metal clusters. The geometry of the two latter classes of compounds was explained using the concept of aromaticity, previously developed in our group.

Also the Coalescence Kick Method for finding global minima structure and low-lying isomers was implemented, tested, and applied to the considered cluster systems. Tests showed that the Kick Method works faster than other methods and provides reliable results. It finds global minima even for such large clusters as B_{17}^- and B_{19}^- in reasonable time.

(404 pages)

ACKNOWLEDGMENTS

I would like to express my sincere gratitude to my advisor, Professor Alexander I Boldyrev. His advice and explanations were invaluable in both my research and my life here in Logan. He helped me greatly to develop my skills in quantum chemistry, to broaden my scientific vision. I am very thankful that such a person as Dr. Boldyrev has been my advisor and mentor.

I would like to thank all the members of my supervisory committee: Dr. Steve Scheiner, Dr. David Farrelly, Dr. Stephen Bialkowski, Dr. T.C. Shen, and also Dr. Robert Brown, who was a committee member on my Final Defense. I appreciate their support and openness for questions and discussions, which had much influence on my progress and professional growth.

Biological and Environmental Research and located at Pacific Northwest National Laboratory, which is operated for DOE by Battelle.

<div align="right">Boris B. Averkiev</div>

CONTENTS

LIST OF TABLES

LIST OF FIGURES

CHAPTER 1

INTRODUCTION

Developing chemical bonding models in clusters is one of the most challenging tasks of modern theoretical chemistry. There are two reasons for this, the first one is that clusters are relatively new objects in chemistry and have been extensively studied since the middle of the 20th century. The second reason is that clusters require high-level quantum-chemical calculations. For many organic molecules, simplified methods were suggested: the Huckel method and a number of semi-empirical methods. Due to the limited number of bond types in a majority of organic compounds, it is possible to find reasonable parameters for theses methods and calculate feasible geometry and properties. The geometry of many organic molecules can be predicted even via molecular mechanics. The diversity of clusters and different types of bonding elements in clusters make it impossible to study them by semi-empirical methods. Therefore, the study of clusters has to be performed at high-level *ab initio* quantum-chemical methods. Such methods have been incorporated in available software packages and, thus, become possible for use in routine calculations only in the last 20 years.

We still do not have a chemical bonding model capable of predicting the structure, stability, and chemical reactivity of clusters. In the study of some particular type of clusters, we start with investigating small clusters and then apply the gained knowledge to more complex systems composed of hundreds of atoms, including various elements, such as transition metals or even lanthanides and actinides. This approach leads

to the establishment of further understanding of structure and bonding in novel nanoparticles and nanomaterials in general.

In this dissertation, I calculated the structures of isomers for some small (less than 12 atoms) clusters and analyzed the nature of chemical bonding in them. There are three groups of studied clusters: aluminum clusters doped with one nitrogen atom, mixed carbon-boron clusters, and clusters of transition elements.

Chapter 2 is a literature review of methods that have been previously implemented for global minimum search, as well as models of chemical bonding in clusters. Chapter 3 is dedicated to Coalescence Kick method, which was suggested, implemented, and tested in our group. This method is the simplest one from all methods described in literature, but our tests showed that it works faster and provides reliable results. It finds global minima even for such big clusters as B_{19}^- in reasonable time.

In Chapters 4-7, the aluminum clusters doped with nitrogen atom: Al_xN and Al_xN^- for x=3-8 are discussed. In this project, we showed how impurities affect the structure and properties of aluminum clusters. Chapter 4 is devoted to the Al_xN and Al_xN^- (x=3-5) clusters. It was shown that for x=5 there is a transition occurring from planar to 3-dimensional structures for Al_xN and Al_xN^- clusters. In Chapter 5, structures for Al_6N and Al_6N^- are discussed. Chapters 6 and 7 describe structures for Al_7N and Al_7N^-, and Al_8N and Al_8N^- clusters, respectively.

Chapters 8-11 describe probability of designing planar molecules with hyper-coordinate central atom. In chapters 8 and 9 we developed a new chemical bonding model capable of explaining why carbon atom avoids the central position in the wheel

structure of carbon-boron clusters CB_6^-, CB_6^{2-}, $C_2B_5^-$, and CB_7^-. Some authors suggested using such molecules as building blocks in other compounds. However, we showed that this is impossible because hexa- and hepta-coordinate carbon clusters, though being local minima, are not viable chemical species (high-lying isomers) and, thus, of no interest for experimentalists. Using our model of chemical bonding in clusters, one can see why clusters with hypercoordinate carbon atom are not stable. This model also allows one to predict what planar structures with hypercoordinate central atom will be low-lying isomers. In Chapter 10, we showed that planar AlB_9 structure with central hypercoordinate Al atom is the global minima or a low-lying isomer for AlB_9 cluster. This is an example of predictive power of aromaticity conception in cluster chemistry. In Chapter 11, we summarized ideas from Chapters 8-10 about aromaticity in planar structures with hypercoordinate planar atom. Also, we reported structure and analysis of electron density in CB_8^- cluster.

In Chapters 12-15, aromaticity and antiaromaticity in transition-metal systems are described. The conception of aromaticity is applied to transition metal compounds. $Ta_3O_3^-$ in a $^1A_1'$ D_{3h} state was shown to be the first example of δ-aromatic compound. This is the topic of Chapter 12. Theoretical calculation of first example of triply (σ, π, δ)-aromatic system Hf_3 is described in Chapter 13. The aromaticity in transition metal systems previously reported in literature is reviewed in Chapter 14. In Chapter 15, theoretical models for aromatic orbitals in transition metals are discussed. The diagrams for different aromatic orbitals in 3- and 4-member metallic cycles are presented.

CHAPTER 2

LITERATURE REVIEW

2-1. Introduction

One of the most important targets of modern science is the design of new materials with desired properties. It can be done by experimental synthesis of compounds, followed by testing of their properties, or by *ab initio* calculations of yet unsynthesized molecules with calculation of their properties. Using quantum chemical calculations, one can predict myriads of unique compounds with unusual properties. However, it is not enough just to predict unique structure with desired properties. Only global minima or low-lying isomer will be feasible for synthesis, and so, can be used to design new materials. High-energy isomers, which are about 5 kcal/mol higher in energy than the global minimum structure, will be unstable. Hence, the global minima search is a very important step in designing new materials with desirable properties. Mathematically, the process of global minima search is represented by exploring the Potential Energy Surface (PES) – the 3n+1-dimensional surface, where energy variable depends on 3n coordinates of n-atomic system. The result of such a search should be a set of isomers corresponding to local minima structures and the global minimum structure. The main obstacle is that the number of minima increases exponentially with the number of atoms in the system, especially when there are several types of atoms in system.[1,2] While for simple systems containing 2-5 atoms possible minima structures are usually obvious, and thus, can be manually constructed, for more complicated systems such a manual search is

impossible. Even for relatively small systems containing just 6-12 atoms, the manual search of global minima and low-lying isomers becomes tedious. Hence, we need unbiased computational methods for global minima search.

2-2. Algorithms for Global Minima Search

There were several algorithms proposed for solving this problem, with the most popular being Simulated Annealing,[2-4] Genetic Algorithm,[5-9] Particle Swarm Optimization,[10-13] Kick Method,[14,15] Basin Hopping,[16,17] and Minima Hopping.[18,19] All of them utilize random structure generation of initial populations.

The easiest and most straightforward algorithm is a Kick Method,[14,15] where the large population of randomly generated structures is optimized to the nearest local minima. Generating big enough population, one can obtain all minima on PES, including the global one. The process is finished when the method does not generate new structures anymore.

Other algorithms generate smaller initial population of random structures, which is then used to generate other structures. In Simulated Annealing, Particle Swarm Optimization, Basin Hopping, and Minima Hopping approaches, each structure from initial population is slightly transformed in each step of process, so that the PES is gradually explored by "walking" of each of the initially generated structure. Because we are interested in minima of PES, we are looking for transformed structures with energies lower than energies of their untransformed "parents." However, we also need to accept some structures with higher energies, otherwise we will stay in the same basin – area of

PES, where optimization of all structures will lead to the same local minima. Hence, when the energy of transformed structure is higher, it will be accepted with some probability. The algorithms mentioned above are differentiated by method of exploring of PES, i.e. how program generates new structures from initial population and which of them will be further accepted.

The Simulated Annealing was the first method suggested for global minima search. The classic simulated annealing paper by Kirkpatrick[2] has been cited over 8,600 times since 1983. The Simulated Annealing, as one can see from its name, is based on a procedure simulating the process of self-organizing of clusters when we heat them to a high temperature and then gradually cool them down. We believe that, in this case, atoms will be assembled into the most stable structure, which has the lowest energy, i.e. global minima. Technically, it means that we allow the initial structure to be changed randomly in any direction of PES. The probability of acceptance depends on the energy difference between the initial and transformed structures and also on temperature. The higher the temperature, the more the probability that the transformation will be accepted, even if the transformation has increased the energy of the structure. The process starts at high temperature, so at the beginning of Simulated Annealing, most the steps are accepted. That allows one to overcome the barriers of PES and not to stay in one local minima basin. At the end of the process, the temperature decreases, along with the number of accepted transformations. The process is finished when the number of accepted transformations is less than some small value, e.g. 10%.

Basin Hopping algorithm, proposed by Wales,[16,17] can be considered as a modification of Simulated Annealing. In Basin Hopping algorithm "basin energies" of initial and transformed structures are used to calculate the probability of acceptance of the transformed structure. "Basin energy" is the energy of the local minimum of basin to which structure belongs. Mathematically, it means that, in this case, we deal with modified PES, where energies of all points are replaced by energies of corresponding local minima (see Figure 1-1). This modification helps structures to overcome barriers between basins, so it speeds up the exploring of PES. Strictly speaking, Basin Hopping is not an algorithm, but rather, a procedure, which can be incorporated in other methods, for example, in Particle Swarm Optimization method, which is briefly described next.

Particle Swarm Optimization[10-13] simulates behaviors of swarms of insects or flocks of birds. Unlike previously described methods, where structures on each step are transformed randomly, in this method the transformation of each structure depends on transformations of other structures from initial population. The lower the energy of some obtained structure in whole population the higher the probability that all other structures will be transformed in the same direction in PES.

Minima Hopping Algorithm,[18,19] recently proposed by Goedecker, is another modification of Simulated Annealing. In this approach, authors used molecular dynamics simulations to explore PES. The probability that structure crosses a barrier in PES depends on kinetic energy of the atoms, which is an adjustable variable. Hence, the system "hops" from one minimum to another when a barrier between two basins is smaller than the kinetic energy. In this method, a program keeps history of all obtained

local minima, so that when the procedure do not obtain any new basins, the kinetic energy parameter is increased and that allows the system to explore other parts of PES. Goedecker emphasizes that this method works in cases where even Basin Hopping method does not work – in case when two basins are separated by other basins with higher energies and the difference between barrier and local minima is not big (Figure 2-1).

Genetic Algorithm[5-9] is different from above-mentioned algorithms, because the new structures in this method are obtained via mating of two "parent" structures. It is based on Darwin's theory of Evolution, where mating of two parents produces a child that takes best properties from his parents. In terms of global minima search, it means that when we use two structures with low energies there is a high probability that their combination will result in a child structure with low energy too. In Gradient Embedded Genetic Algorithm (GEGA),[8,9] designed by Alexandrova, all structures are first optimized to local minima, and afterwars breed new generation of structures. Besides breeding Genetic Algorithm implements mutations – random changes of parent structures. This prevents the search to be entrapped in some local minima.

In our group Simulated Annealing, Particle Swarm Optimization and Gradient Embedded Genetic Algorithm were implemented by Seth Call and Anastasia Alexandrova. While all these methods were effective for the calculation of relatively small molecules, they were not very efficient when we tried to deal with larger molecules containing more than 12 atoms. Hence, one more algorithm was implemented which is described in the next chapter.

2-3. Structures and Chemical Bonding of Inorganic Clusters

The investigation of the structure of matter is one of the most intriguing and important tasks of science. Usually, all compounds are divided into two main classes: organic and inorganic compounds. The first step in the theory of structure of organic compounds was made by Butlerov at the end of the 19th century, where he explained isomerism of organic compounds using concept of valency. The principles of chemical bonding in organic and simple inorganic molecules were developed on the basis of Lewis model[20] in the first part of the 20th century. In this model, the structure of molecule is described as a group of atoms, connected by 2-center 2-electron bonds (2c-2e bonds). Atoms also can have lone pairs (1c-2e electrons). Inorganic compounds usually exist as crystals, and chemical bonding in them can be described as ionic (like in NaCl), metallic (like in Cu), or covalent (like in diamond).

Starting from the 1950's the first clusters were studied.[21] There is still no precise definition of a cluster. A cluster can be defined as an aggregate of atoms, which is stable in vacuum (gas phase), but usually is not stable as a bulk material. Unlike molecules, clusters can be charged. Clusters can contain from several to hundreds of atoms. Examples of classic small clusters are $B_{12}H_{12}^{2-}$, $Co_4(CO)_{12}$, $Fe_2(CO)_9$, $Re_2Cl_8^{2-}$. The challenging feature of clusters is that their chemical bonding pattern cannot be described in terms of classical 2c-2e bonds. Hence, we need to develop a new definition of chemical bonding, a definition, which will describe the geometry and properties of clusters.

Usually, clusters are produced by laser vaporization technique.[22] Atoms from the source bulk material (for example, metal) are evaporated to gas phase and are assembled into clusters with different composition. Clusters containing N, O atoms can be produced by vaporization of metal in an atmosphere of N_2 or O_2, respectively. Using mass-spectroscopy, these clusters can be separated, and some of their properties (like photoelectronic spectra) can be studied.

Mass spectra show that some clusters with a certain composition are more abundant than others. This reflects the increased stability of clusters with such specific composition. For example, mass-spectra of C_x clusters show that, at x=60, clusters should be especially stable.[23,24] This is the famous fullerene cluster C_{60}. Analogously, for Al_x^- clusters, a very pronounced peak of mass-spectra corresponds to x=13,[25] for Al_xC^-, x=7,[26] for Al_xSi, x=12.[27] These specific numbers are so-called "magic numbers." One of the purposes of the chemical bonding theory in clusters is to explain the nature of these magic numbers.

Before 80's, the structure of the clusters, obtained from bulk material had not ever been discussed, since it was implicitly supposed that their structure is just some piece of original bulk material. The most famous example is carbon clusters, which were first produced by Rohlfing et al. in 1984.[23] The authors noticed that cluster C_{60} is very stable, but they didn't consider its structure, suggesting that it should be just a piece of graphite lattice. Only in 1985, in the famous paper of Kroto et al. in Nature, it was suggested that this cluster has an unusual, football (mathematically strictly speaking

truncated icosahedron) structure, and it was called buckminsterfullerene (in short, fullerene), named after the American architect R. Buckminster Fuller.[24]

Hence, it occurred that cluster structure is not the same as that of the corresponding crystal. Moreover, the structure of clusters dramatically depends on the number of atoms. Addition of just one atom can dramatically change the cluster's geometry and electronic structure. Also, structure depends on the charge of cluster. For example, bulk aluminum has face-centered cubic crystal structure. Al_{13}^{-}, cluster, however, is a perfect icosahedron.[27] This situation is common for many metal clusters. Search for global minima of gold clusters[19] revealed that, depending on the number of atoms, the structure a of gold cluster can be described as amorphous (without any symmetry), fivefold symmetry cluster, cluster based on face centered cubic lattice, and cluster based on twinned face centered cubic lattice.

The simplest theory, describing the stability of clusters, is the Jellium Model.[28] It was shown that it works well for sodium clusters.[29] Mass spectra of Na clusters showed large peaks with N=8, 20, 40, 58, and 92. The main idea of this model is that a metallic cluster with approximately spherical shape can be considered as a superatom, where nucleus and core electrons make the core of this superatom, with valence electrons occupying atomic orbitals of this superatom. Because of spherical symmetry, these orbitals can be characterized by quantum numbers l and m. However, since the spherical potential, created by many nuclei, is not the same as that created by a single nucleus, for this superatom angular quantum number l is not restricted by a principle quantum number n - there are 1s, 1p, 1d orbitals. According to calculations, the order of the occupation of

orbitals is $1s^2$, $1p^6$, $1d^{10}$, $2s^2$, $1f^{14}$, $2p^6$ … Hence, superatoms with 2, 8, 18, 20, 34, 40,

… electrons should have enhanced stability, analogously to atoms with completed sub-

shells that have more stable electronic configurations.

However, the Jellium Model works only for metal clusters, and it does not

explain the structure of clusters. Some authors tried to apply it to explain the stability of

doped metal cluster Al_7C^-.[26] This cluster contains 26 valence electrons, which doesn't fit

the Jellium Model. Authors suggested that this cluster could be considered as

combinations of two superatoms, Al_6 and AlC^-, with 18 and 8 valence electrons,

respectively. However, as it was noticed later on,[30] this model did not work, because the

structure of Al_7C^- with carbon atom, located in the center of the cluster, is not in

consistence with this explanation.

The second model, proposed to explain structure and bonding in clusters, is

conception of aromaticity. The application of aromaticity to chemical bonding in clusters

was first introduced by Kuznetsov et al.[31] The authors suggested expanding the concept

of aromaticity from organic chemistry to clusters. Like in case of organic molecules,

aromatic clusters possess high symmetry and increased stability. The first examples of

aromatic clusters were clusters containing Al_4^{2-} fragment[31] $NaAl_4^-$ and $CuAl_4^-$, as well as

XAl_3^- (X=Si, Ge, Sn, Pb).[32] The details of these works are given in Kuznetsov's PhD

dissertation.[33]

Because of the diversity of clusters, the conception of aromaticity occurred to be

even more fruitful than in organic chemistry. The striking feature of chemical bonding in

clusters is the possibility of the multi-fold nature of aromaticity, antiaromaticity and

conflicting aromaticity. Like in aromatic organic structures, molecular orbitals in planar clusters can be classified as σ- and π-orbitals. Huckel rules should be applied for each of these subsystems separately. Consequently, there are four possibilities for planar clusters composed out of main group elements:

1) both aromatic σ and π systems – double aromatic clusters.

2) both antiaromatic σ and π systems – double antiaromatic clusters.

3) σ aromatic, π antiaromatic – clusters with conflicting aromaticity

4) σ antiaromatic, π aromatic – clusters with conflicting aromaticity

Alexandrova et al. analyzed structures of pure boron clusters on the basis of conception of multiple aromaticity and antiaromaticity.[34] In particular, they showed that B_9^- cluster is doubly aromatic, which results in stable high-symmetry planar structure of this cluster. The details of analysis of boron clusters are given in Alexandrova's PhD dissertation.[35]

From quantum-chemical calculations, one can obtain molecular orbitals – wave functions, describing space distribution of electrons with certain energy. Natural Bond Orbitals (NBO) Analysis, developed by Weinhold,[36,37] let us transform molecular orbitals to localized objects, which can be interpreted as atom-atom 2c-2e bonds and lone pairs (1c-2e bond) in classical molecules without delocalized bonding. Therefore, NBO Analysis fails for structures with delocalized bonding, like aromatic compounds. Hence, we cannot apply this analysis to many clusters, which could be explained on the basis of aromaticity conceptions. In 2008, Zubarev developed the Adaptive Natural Density Partitioning (AdNDP) method,[38] which is an extension of NBO analysis. This method

localizes all 2c-2e bonds and lone pairs, but in addition to that, it also reveals bonds, localized over more than 2 atoms: 3c-2e, 4c-2e, and so on (such bonds are called delocalized). Hence, this method is a very powerful tool for analyzing electron distribution in clusters and molecules, and it allows describing bonding pattern in terms of 2c-2e bonds and aromaticity. This method was already applied to gold cluster[39] and classical aromatic molecules.[40] The details of this method are given in Zubarev's PhD dissertation.[41]

References

(1) Wales, D. J. *Science*, **1999**, *285*, 1368.

(2) Kirkpatrick, S.; Gelatt, C. D., Jr.; Vecchi, M. P. *Science*, **1983**, *220*, 671

(3) Hamad, S.; Catlow, C. R. A.; Spanó, E.; Matxain, J. M.; Ugalde J. M. *J. Phys. Chem. B* **2005**, *109*, 2703.

(4) Corcelli, S. A.; Kelley, J. A.; Tully, J. C.; Johnson, M. A. *J. Phys. Chem. A* **2002**, *106*, 4872.

(5) Deaven, D. M.; Ho, K. M. *Phys. Rev. Lett.* **1995**, *75*, 288.

(6) White R. P.; Niesse J. A.; Mayne H. R. *J. Chem. Phys.* **1998**, *108*, 2208.

(7) Kabrede, H.; Hentschke, R. *J. Phys. Chem. B* **2002**, *106*, 10089.

(8) Alexandrova, A. N.; Boldyrev, A. I.; Fu, Y.-J.; Yang, X.; Wang, X.-B.; Wang L. S. *J. Chem. Phys.* **2004**, *121*, 5709.

(9) Alexandrova, A. N.; Boldyrev. A. I. *J. Chem. Theory and Comput.* **2005**, *1*, 566.

(10) Kennedy, J.; Eberhart, R. In Proceedings IEEE International Conference on Neural Networks, Vol. IV; 1995; p. 1942.

(11) Eberhart, R.; Kennedy, J. In Proceedings of the 6th International Symposium on Micro Machine and Human Science; 1995 p. 39.

(12) Eberhart, R. C.; Shi, Y. In Proceedings of the IEEE Congress on Evolutionary Computation, Seoul, Korea, 2001, p. 81

(13) Call, S. T.; Zubarev, D. Yu.; Boldyrev, A. I. *J. Comput. Chem.* **2007**, *28*, 1177.

(14) Bera, P. P.; Sattelmeyer, K. W.; Saunders, M.; Schaefer, H. F.; Schleyer, P. v. R. *J. Phys. Chem. A,* **2006**, *110*, 4287.

(15) Addicoat, M. A.; Metha, G. F. *J. Comput. Chem.* **2009**, *30*, 57.

(16) Wales, D. J.; Doyle, J. P. K. *J. Phys. Chem. A* **1997**, *101*, 5111.

(17) Wales, D. J. *Energy Landscapes: Applications to Clusters, Biomolecules and Glasses*; Cambridge University Press, 2003.

(18) Goedecker, S. *J. Chem. Phys.* **2004**, *120*, 9911.

(19) Bao, K.; Goedecker, S.; Koga, K.; Lançon, F.; Neelov, A. *Phys. Rev. B* **2009**, *79*, 041405-1.

(20) Lewis, G. N. *J. Am. Chem. Soc.* **1916**, *38*, 762.

(21) Moskovits, M. *Metal Clusters*; John Wiley & Sons Inc, 1986.

(22) Dietz, T. G. ; Duncan, M. A.; Powers, D. E.; Smalley, R. E. *J. Chem. Phys.* **1981**, *74*, 6511.

(23) Eric A. Rohlfing, D. M. Cox, and A. Kaldor *J. Chem. Phys.* **1984**, *81*, 3322.

(24) Kroto, H. W.; Heath, J. R.; O'Brien, S. C.; Curl, R. F.; Smalley, R. E. *Nature* **1985**, *318*, 162.

(25) Li, X.; Wang L.-S. *Eur. Phys. J. D.* **2005**, *34* 9.

(26) Leskiw B. D.; Castleman A. W., Jr. *Chem. Phys. Lett.* **2000**, *316*, 31.

(27) Akutsu, M.; Koyasu, K.; Atobe, J.; Hosoya, N.; Miyajima, K.; Mitsui, M.; Nakajima, A. *J. Phys. Chem. A* **2006**, *110,* 12073.

(28) Lang, N. D.; Kohn, W. *Phys. Rev. B* **1970**, *1*, 4555

(29) Knight, W. D.; Clemenger, K.; De Heer, W. A.; Saunders, W. A.; Chou, M. Y.; Cohen M. L. *Phys. Rev. Lett.* **1984**, *52*, 2141.

(30) Reveles, J. U.; Khanna, S. N.; Roach, P. J.; Castleman, A. W., Jr. *PNAS* **2006**, *103*, 18405.

(31) Li, X.; Kuznetsov, A. E.; Zhang, H.-F.; Boldyrev, A. I.; Wang, L. S. *Science* **2001**, *291*, 859.

(32) Li, X.; Zhang, H.-F.; Kuznetsov, A. E.; Cannon, N. A.; Wang, L. S.; Boldyrev, A. I. *Angew. Chem. Int. Ed.* **2001**, *40*, 1867.

(33) Kuznetsov, A. E. *Aromaticity and Antiaromaticity in All-metal Systems*; PhD Dissertation, USU 2003.

(34) Alexandrova, A. N.; Boldyrev, A. I.; Zhai, H.-J.; Wang, L. S. *Coord. Chem. Rev* **2006**, *250*, 2811.

(35) Alexandrova, A. N. *Multiply Aromatic Clusters via Ab Initio Genetic Algorithm*; PhD Dissertation, USU 2005.

(36) Foster, J. P.; Weinhold, F. *J Am. Chem. Soc.* **1980**, *102*, 7211

(37) Reed, A. E.; Curtiss, L. A.; Weinhold, F. *Chem. Rev.* **1988**, *88*, 899.

(38) Zubarev, D. Yu.; Boldyrev, A. I. *Phys. Chem. Chem. Phys.* **2008**, *10*, 5207.

(39) Zubarev, D. Yu.; Boldyrev, A. I. *J. Phys. Chem.* **2009**, *113*, 866.

(40) Zubarev, D. Yu. Boldyrev, A. I. *J. Org. Chem.* **2008**, *73*, 9251.

(41) Zubarev, D. Yu. *Analysis of Chemical Bonding in Clusters by Means of the Adaptive Natural Density Partitioning*; PhD Dissertation, USU 2008.
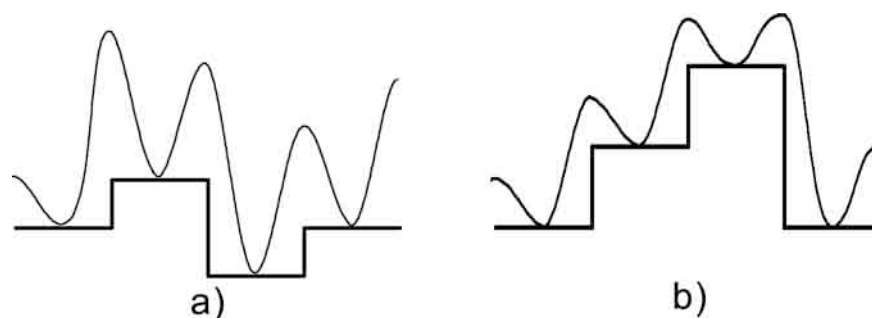
Figure 2-1. Examples of transformation of PES in Basin Hopping method.

a) Basin Hopping method works, b) Basin Hopping method does not work

CHAPTER 3

COALESCENCE KICK METHOD

3-1. Introduction

Different methods of global minimum search were discussed in the previous chapter. Three from the above-mentioned methods – GEGA, Simulated Annealing, and Particle Swarm Optimization were already implemented in our group by A. Alexandrova[1,2] and S. Call.[3,4]

While all these methods were effective for calculation of relatively small molecules, they occurred not to be very efficient when we tried to deal with larger molecules containing more than 12 atoms. There were several problems, resulting from the fact that the main purpose of these methods is search for the global minimum, but not exploring PES for other minima. The first problem is repeated visits of certain configurations in PES. The closer programs get to the global minimum, the more often it generates structures from the global minimum basin or from neighboring basins. Hence, programs spend a lot of computational time to optimize different initial geometries leading to the same structure. The second problem is that programs can miss some low-lying isomers. A low-lying isomer, which is not the global minimum structure at low-level calculation, can become global minimum at high-level calculations. High-level calculations can change the order of isomers, and even result in a different global minimum structure.

It should be emphasized that a searching program usually performs more than a thousand calculations (depending on the number of atoms in structure), so nowadays for such a vast number of calculations one can afford only low-level quantum-chemical methods. Hence, a program should search not only for global minimum, but also for isomers lying within some reasonable energy gap from the energy of the global minimum at the current level of calculations. Usually this energy gap is about 20-30 kcal/mol. For chemical species, which are described in this dissertation, we report structures lying within 10-20 kcal/mol energy gaps from global minimum structures.

Hence, increasing complexity of structures investigated in our group stimulated us to implement one more program featuring fast and simple Kick Method. In original version of this method program generates random structures without checking connectivity or short atom-atom distances. Generated structures are submitted to another program, which optimizes them to local minima. It was estimated that only 10-50% out of all generated structures are optimized completely and represent possible isomers for the cluster. All other initial structures have too bad, unreasonable, geometry if treated by quantum-chemical programs. There are two types of structures with bad geometry:

1) Initially generated structure containing too short atom-atom distances. In this case it is impossible to calculate initial wave function because self-consistent field (SCF) convergence cannot be achieved, hence the quantum-chemical program abandons the structure from the beginning.

2) Fragmented initially generated structure. This is the worst and the most common case. The fragmentation of structure results in very slow conversion of SCF. At

best SCF will result in convergence failure with quantum-chemical program abandoning the structure like in the case of structures of too short atom-atom distances. If SCF is converged then a process of optimization starts next. However, this process is much slower than for non-fragmented structures, so it slows down calculations dramatically, and does not lead to new isomers. Only in rare cases initial fragmented structure is optimized into a non-fragmented one.

While all these problems did not play crucial role for small molecules, they became the main obstacle when we tried to calculate medium size clusters with more than 12 atoms: $Al_{12}N^-$ and B_{17}^-, B_{18}^-, B_{19}^-. The program just could not create the initial wavefunction for any of randomly generated structures.

To avoid above-mentioned drawbacks of the original version of Kick Method, we designed the modified "Coalescence" Kick Method. In this method initially generated random structure is first checked for connectivity, and then if the structure is fragmented, the coalescence procedure is applied to it. Two atoms are considered to be connected if the interatomic distance satisfies the sum of their covalent (or van der Waals) radii.

There are several algorithms that can be implemented to transform fragmented structure to non-fragmented one. They can be classified into two groups:

1) Program connects different fragments of initial structure step by step, starting from the fragments that are closest to each other. This approach was used by S. Call in his program of Simulated Annealing[4] and Particle Swarm Optimization.[3]

2) Program pushes all fragments of structure to the center of mass simultaneously. This approach is used in Coalescence Kick Method.

In spite of seeming simplicity of the former approach, the latter is easier to implement and it better preserves the mutual arrangement of atoms of initially generated random structure.

3-2. Coalescence Kick Method Algorithm

The current version of "Coalescence" Kick Method program is designed for search of global minimum as for single molecules of desired composition, as well as for complexes of molecules like solvated anions (e.g. $SO_4^{2-}*4H_2O$), where the initial geometry of each molecule is specified in the input file. The program can also search for clusters with a desired core, for example, when we are looking only for the $Al_{10}N^-$ clusters that contain Al_6N octahedral fragment.

The process of global minimum search is divided in four steps.

1) The generation of a random structure.

Because the structure can contain both atoms and fragments, there are two procedures of generation. Atomic position is assigned using three random coordinates x, y, z. The position of a fragment is defined by its center of mass being assigned three random coordinates x, y, z. The orientation of a fragment is defined by three random Euler angles ϕ, θ, ψ. The range of possible values of coordinates x, y, z depends on "box size," which defines maximum values of coordinates. The box size is chosen to be very large to avoid initial structures with very short interatomic distances. The program uses 4*(sum of atomic covalent radii) for all three linear dimensions of box.

2) Analysis of system connectivity.

By connectivity we mean not only when atoms are directly connected to each other, but also in case atoms belong to the same fragment of the structure, that is they are connected indirectly, via other directly connected atoms.

The information of connectivity between atoms in structure is represented by the matrix of connectivity. The calculation of the matrix is an iterative process. The initial matrix shows only directly connected pair of atoms. If two atoms i-th and j-th are directly connected to each other, then elements [i,j] and [j,i] are equal to 1. Otherwise, [i,j] and [j,i] are equal to 0. After that program checks the connections of the 2-nd order - two atoms are considered to belong to the same fragment when they are directly connected to the same atom. Then connectivities of the 3-rd order are checked (when i-th atom is connected to j-th atom via k-th atom, where connection i-k is the 2-nd order connection). This procedure starts from the first atom in the list of atoms. When all atoms that belong to the part of the first atom are obtained, the same procedure is applied to atoms that do not belong to this fragment. The number of atoms in the fragment of i-th atom is kept in element [i,i] of the matrix. This information will be used in coalescence procedure, which is the next step of our method. The [j,j] element for the j-th atom which already belongs to i-th fragment (i < j) is set to 0, so program skips the j-th element. The following three matrices demonstrate the calculation of the matrix of connectivity for a system of water molecule and hydrogen peroxide molecule ($H_2O+H_2O_2$). The first matrix represents the initially generated matrix, in the second one the program revealed that first three atoms belong to the same fragment (water), the third matrix represents the final matrix of connectivity, where both water and hydrogen peroxide fragments are revealed.

$$\begin{pmatrix} 1 & 1 & 1 & 0 & 0 & 0 & 0 \\ 1 & 1 & 0 & 0 & 0 & 0 & 0 \\ 1 & 0 & 1 & 0 & 0 & 0 & 0 \\ 0 & 0 & 0 & 1 & 1 & 1 & 0 \\ 0 & 0 & 0 & 1 & 1 & 0 & 0 \\ 0 & 0 & 0 & 1 & 0 & 1 & 1 \\ 0 & 0 & 0 & 0 & 0 & 1 & 1 \end{pmatrix} \Rightarrow \begin{pmatrix} 3 & 1 & 1 & 0 & 0 & 0 & 0 \\ 1 & 0 & 0 & 0 & 0 & 0 & 0 \\ 1 & 0 & 0 & 0 & 0 & 0 & 0 \\ 0 & 0 & 0 & 1 & 1 & 1 & 0 \\ 0 & 0 & 0 & 1 & 1 & 0 & 0 \\ 0 & 0 & 0 & 1 & 0 & 1 & 1 \\ 0 & 0 & 0 & 0 & 0 & 1 & 1 \end{pmatrix} \Rightarrow \begin{pmatrix} 3 & 1 & 1 & 0 & 0 & 0 & 0 \\ 1 & 0 & 0 & 0 & 0 & 0 & 0 \\ 1 & 0 & 0 & 0 & 0 & 0 & 0 \\ 0 & 0 & 0 & 4 & 1 & 1 & 1 \\ 0 & 0 & 0 & 1 & 0 & 0 & 0 \\ 0 & 0 & 0 & 1 & 0 & 0 & 1 \\ 0 & 0 & 0 & 0 & 0 & 1 & 0 \end{pmatrix}$$

3) The coalescence procedure.

The structure obtained from the first step is fragmented. This step is intended to push all atoms and fragments toward the center of mass of the system. If several atoms belong to the same fragment, they are pushed to the center of mass of the system not independently, but as a whole fragment, so that their interatomic distances do not change. When two or more atoms approach each other and are considered to be connected by connectivity analysis, they are treated as one fragment. The process is repeated unless the system is non-fragmented.

The magnitude of shift should be small enough so that atoms do not approach each other too close, but it should be large enough so that procedure converges in reasonable time. In the current version of program we use 0.2 A shift.

The example of changing the geometry of system during the coalescence procedure is given in Figure 3-1 for system B_7.

4) Submitting generated structure to an optimizing program.

The optimization procedure uses Schlegel's analytical gradient method.[5] This program is a subroutine of Gaussian 03 program.[6] The attainment of the energy minimum is achieved if four following criteria are satisfied:

a) The maximum force on atoms is less than 0.00045 hartree/bohr.

b) The root mean-squared (rms) force on atoms is less than 0.00030 hartree/bohr.

c) The maximum displacement of atoms during optimization step is less than 0.0018 A.

d) The rms displacement of atoms during optimization step is less than 0.0012 A.

Currently we are using Gaussian 03 program, however, in principle it can be any other quantum-chemical or molecular-mechanical program, which optimizes geometry of a molecule to minimize its energy.

The examples of generated non-fragmented structures are given in Figure 3-2. Using this method we predicted global minimum structures for $B_3H_7^-$, Al_8N^-, B_{17}^-, and B_{19}^- clusters (Figure 3-3). Our tests showed that Kick Method generates mostly different structures, so computational time is not wasted for calculation of the same structure for several times. For $B_3H_7^-$ and Al_8N^- clusters the global minimum structures were predicted within 200 trials of randomly generated structures, while for B_{17}^-, and B_{19}^- the number of random structures was about 1000. Certainly, to be sure that program did not miss global minima structure, the number of generated structures should be 2-3 times more than above-mentioned. The process of optimization of initially generated non-fragmented structure to the final isomer is presented in Figure 3-4 for the second low-lying isomer of B_{19}^-.

References

(1) Alexandrova, A. N.; Boldyrev, A. I.; Fu, Y.-J.; Yang, X.; Wang, X.-B.; Wang L. S. *J. Chem. Phys.* **2004**, *121*, 5709.

(2) Alexandrova, A. N.; Boldyrev. A. I. *J. Chem. Theory and Comput.* **2005**, *1*, 566.

(3) Call, S. T.; Zubarev, D. Yu.; Boldyrev, A. I. *J. Comput. Chem.* **2007**, *28*, 1177.

(4) Averkiev, B. B.; Call, S.; Boldyrev, A. I.; Wang, L. M.; Huang, W.; Wang, L. S. *J. Phys. Chem. A*, **2008**, *112*, 1873.

(5) Schlegel. H. B. *J. Comput. Chem.* **1982**, *3*, 214.

(6) Frisch, M. J.; Trucks, G. W.; Schlegel, H. B.; Scuseria, G. E.; Robb, M. A.; Cheeseman, J. R.; Montgomery, Jr., J. A.; Vreven, T.; Kudin, K. N.; Burant, J. C.; Millam, J. M.; Iyengar, S. S.; Tomasi, J.; Barone, V.; Mennucci, B.; Cossi, M.; Scalmani, G.; Rega, N.; Petersson, G. A.; Nakatsuji, H.; Hada, M.; Ehara, M.; Toyota, K.; Fukuda, R.; Hasegawa, J.; Ishida, M.; Nakajima, T.; Honda, Y.; Kitao, O.; Nakai, H.; Klene, M.; Li, X.; Knox, J. E.; Hratchian, H. P.; Cross, J. B.; Bakken, V.; Adamo, C.; Jaramillo, J.; Gomperts, R.; Stratmann, R. E.; Yazyev, O.; Austin, A. J.; Cammi, R.; Pomelli, C.; Ochterski, J. W.; Ayala, P. Y.; Morokuma, K.; Voth, G. A.; Salvador, P.; Dannenberg, J. J.; Zakrzewski, V. G.; Dapprich, S.; Daniels, A. D.; Strain, M. C.; Farkas, O.; Malick, D. K.; Rabuck, A. D.; Raghavachari, K.; Foresman, J. B.; Ortiz, J. V.; Cui, Q.; Baboul, A. G.; Clifford, S.; Cioslowski, J.; Stefanov, B. B.; Liu, G.; Liashenko, A.; Piskorz, P.; Komaromi, I.; Martin, R. L.; Fox, D. J.; Keith, T.; Al-Laham, M. A.; Peng, C. Y.; Nanayakkara, A.; Challacombe, M.; Gill, P. M. W.; Johnson, B.; Chen, W.; Wong, M. W.; Gonzalez, C.; and Pople, J. A. Gaussian 03, Revision C.02; Gaussian, Inc.: Wallingford, CT, 2004.

Figure 3-1. Coalescence procedure for B_7 cluster.
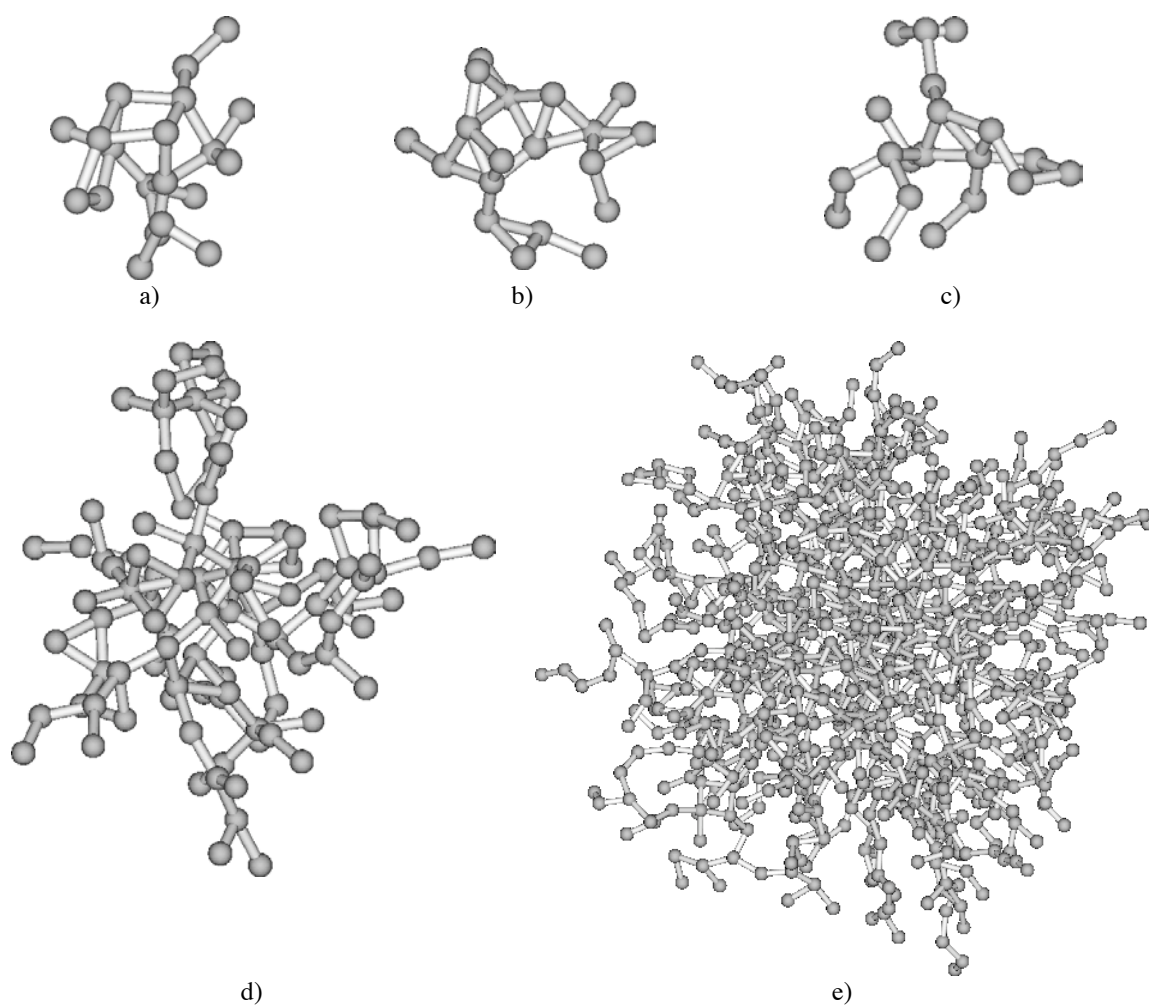
Figure 3-2. Initial non-fragmented structures generated by "Coalescence" Kick Method. a)-c) 20 atomic structures, d) 100 atomic structure, e) 1000 atomic structure
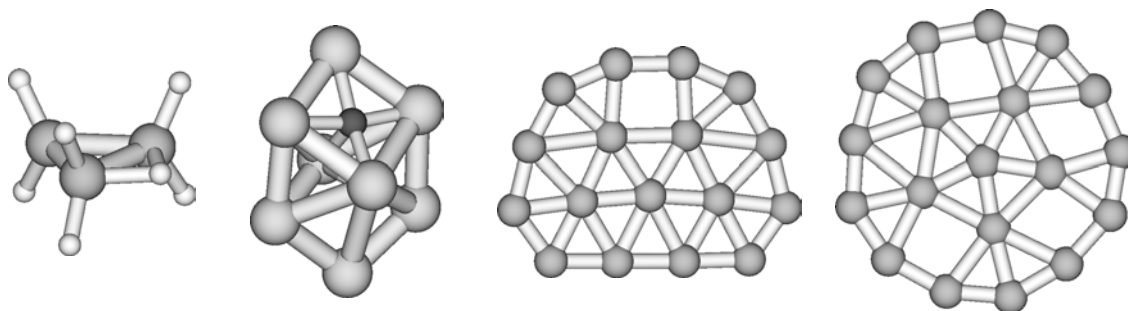
Figure 3-3. Global minimum structures for $B_3H_7^-$, Al_8N^-, B_{17}^-, and B_{19}^- clusters.
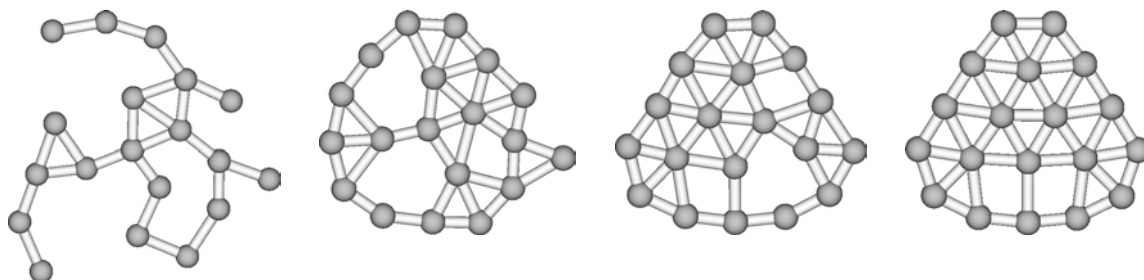
Figure 3-4. Initially generated random structure, intermediate structures, and the optimized structure for the second low-lying isomer of B_{19}^- cluster.

CHAPTER 4

PLANAR NITROGEN-DOPED ALUMINUM

CLUSTERS Al_xN^- (x = 3-5)[1]

Abstract

The electronic and geometrical structures of three nitrogen-doped aluminum clusters, Al_xN^- (x = 3-5), are investigated using photoelectron spectroscopy and ab initio calculations. Well-resolved photoelectron spectra have been obtained for the nitrogen doped aluminum clusters at four photon energies (532, 355, 266, and 193 nm). Global minimum structure searches for Al_xN^- (x = 3-5) and their corresponding neutrals are performed using several theoretical methods. Vertical electron detachment energies are calculated using three different methods for the lowest energy structures and low-lying isomers are compared with the experimental observations. Planar structures have been established for all the three Al_xN^- (x = 3-5) anions from the joint experimental and theoretical studies. For Al_5N^-, a low-lying non-planar isomer is also found to contribute to the experimental spectra, signifying the onset of 2D-to-3D transition in nitrogen-doped aluminum clusters. The chemical bonding in all the planar clusters have been elucidated on the basis of molecular orbital and natural bond analyses.

4-1. Introduction

By doping pure metal clusters with one or more "impurity" atoms one can generate novel chemical species and manipulate their physical and chemical properties. Understanding how impurities affect the chemical bonding in doped clusters can provide valuable information in understanding nanomaterials, nanostructure interfaces, and may be an important step in developing a robust chemical bonding model which could be used in the rational design of the smallest electronic devices based on nanoclusters. Aluminum is widely used as conductor in electronic devices and aluminum nitride (AlN) is an important semiconductor material. Several prior experimental and theoretical studies have been reported on small aluminum nitride Al_nN_m clusters.[1-11] In particular, Nayak *et al*. have reported a combined experimental and density functional study on Al_3N^- and Al_4N^-.[4] Recently, Li and Wang reported an extensive set of photoelectron spectra of Al_xN^- clusters from x = 2-22 at 193 nm and compared them to those of pure Al_x^- clusters.[10]

The present contribution focuses on a detailed investigation of the electronic structure and chemical bonding in three small aluminum clusters doped with one impurity N atom, Al_xN^- and Al_xN^- (x = 3-5). An extensive set of photoelectron spectra has been obtained for each anion at four detachment photon energies (532, 355, 266, and 193 nm). Well resolved spectral features were interpreted using ab initio theoretical calculations at several levels of theory, which allow us to unequivocally elucidate the electronic and geometrical structures, stability, and low-lying isomers of these three anions and their

corresponding neutrals. The ground states of all three species are found to be planar. Molecular orbital and natural bond analyses have been carried out to understand the chemical bonding in the planar clusters. We also find a non-planar isomer of Al_5N^-, which is very close in energy to the planar ground state isomer and is present in the molecular beam, suggesting the onset of 2D to 3D structural transitions.

4-2. Experimental Method

The experiment was performed using a magnetic-bottle photoelectron spectroscopy apparatus with a laser vaporization cluster source. Details of this apparatus have been published elsewhere.[12] Briefly, the Al_xN^- clusters were produced by laser vaporization of either a pure Al or an AlN alloy disk target with a 5% N_2/He carrier gas. The anion clusters of interest were size-selected and photoelectron spectra were taken at several different photon energies. The electron energy resolution was better than 30 meV for 1 eV electrons. We have measured photodetachment spectra of Al_xN^- for $x = 2-45$ at 193 nm and reported those data up to $x = 22$ recently.[10] In current study, we obtained the photoelectron spectra of Al_xN^- with $x = 3$-5 at four photon energies, 532 nm (2.331 eV), 355 (3.496 eV), 266 (4.661eV), and 193 6.424 eV) nm, as shown in Figures 4-1 – 4-3, respectively.

4-3. Theoretical Methods

The initial search for most stable structures was performed using our gradient embedded genetic algorithm (GEGA) program written by Alexandrova.[13,14] We used a hybrid method known in the literature as B3LYP[15-17] with the small split-valence basis

sets (3-21G).[18] for energy, gradient and force calculations. The lowest few structures in every system were recalculated using the B3LYP, a second order Moller-Plesset perturbation theory (MP2)[19], and coupled-cluster method with single, double, and noniterative triple excitations (CCSD(T))[20-22] based on the UHF formalism for open-shell systems and all with the polarized split-valence basis sets (6-311+G*).[23-25] Total energies of these structures were also calculated using the extended 6-311+G(2df) basis sets. In order to test the validity of the one-electron approximation, single point calculations were performed using the multi-configuration self-consistent field method (CASSCF(X,Y)[26,27] with X active electrons and Y active molecular orbitals.

The vertical electron detachment energies were calculated using R(U)CCSD(T)/6-311+G(2df), the outer valence Green Function method (R(U)OVGF/6-311+G(2df))[28-32] and CCSD(T)/6-311+G(2df) at the CCSD(T)/6-311+G* geometries, as well as at the time-dependent DFT method[33,34] (TD B3LYP/6-311+G(2df)) at the B3LYP/6-311+G* geometries. Core electrons were frozen in treating the electron correlation at the R(U)CCSD(T) and R(U)OVGF levels of theory.

The B3LYP, MP2, R(U)CCSD(T), R(U)OVGF ab initio calculations were performed using the Gaussian 98 and 03 programs.[35,36] Molecular orbital visualization has been done using the MOLDEN3.4 program.[37]

4-4. Experimental Results

The 193 nm spectrum of Al_3N^- (Figure 4-1) reveals six spectral bands below 5.8 eV, labeled as X, A, B, C, D, and E, respectively. The features X (around 0.96 eV) and E

(around 5.2 eV) are very broad. The onset of the first two transitions at 0.96 and 2.72 eV represent a large energy gap, suggesting that the neutral Al_3N cluster is likely to be closed-shell with a large HOMO-LUMO gap. The broad nature of the X band indicates that there is a significant geometry change between the ground states of the anion and neutral. The spectral features are better resolved in the lower photon energy spectra and the obtained vertical detachment energies (VDEs) are given in Table 4-1.

The spectra of Al_4N^- (Figure 4-2) are surprisingly simple with only intense bands observed in the 193 nm spectrum. The X band at 2.32 eV in the 355 and 266 nm spectra is very sharp with no indication of any vibrational structure, whereas the 3.41 eV feature (A) is broad with a partially resolved vibrational progression, which yields a vibrational frequency of 810 ± 50 cm^{-1}. A shoulder on the higher binding energy side of the A band is identified as another electronic transition, labeled as B. A weak band (C) is observed in the 193 nm at very high binding energies. There are also other weak features present in the spectra of Al_4N^-. The features, occurring at around 1.76 and 1.93 eV, are resolved more clearly at lower photon energies, especially at 532 nm. There are also weak signals around 2.7 eV. The intensities of these features depend on the source conditions slightly, but could not be eliminated. All these weak features are most likely due to excited states or different isomers of Al_4N^-.

The spectra of Al_5N^- are quite complicated with numerous well-defined features (X, A, B, C, D, E, and F) at both 266 nm (Figure 4-3); and more features are also revealed at higher binding energies in 193 nm. A strong feature around 2.01 eV (x) at both 532 and 355 nm is resolved, which appears to be merged with the X band. The

complicated spectra of Al_5N^- suggest the possible population of closely lying isomers, as born out from our theoretical calculations.

The VDEs of the main spectral features for Al_xN^- ($x = 3, 4,$ and 5) are all given in Table 4-1 and are compared with ab initio results in Tables 5, 6, and 7, respectively (*vide infra*).

4-5. Theoretical Results

We performed extensive searchs for the global minimum structures of Al_xN^- ($x =$ 3-5) and their neutrals using our GEGA program at B3LYP/3-21G level of theory.

A. Al_3N and Al_3N^-.

The planar D_{3h} ($^1A_1$', $1a_1'^2 1e'^4 2a_2''^2 2a_1'^2 2e'^4 3e'^0$) structure I (Figure 4-1) was found to be the global minimum structure for Al_3N from prior ab initio calculations[3-6] and from infrared matrix investigations.[6] Andrews and co-workers assigned two sharp bands at 777.9 cm^{-1} and 770.3 cm^{-1} to e' antisymmetric stretching mode of Al_3N split by interaction in nitrogen matrix. The major peak at 773.1 cm^{-1} in argon matrix was assigned to the same mode. Our calculations of the planar D_{3h} ($^1A_1$') geometric structure for the Al_3N (Table 2) at our highest level of theory (CCSD(T)/6-311+G*) reveal $w_3(e') = 776$ cm^{-1}, in excellent agreement with the matrix experiment.

For the Al_3N^- anion we performed GEGA search at the B3LYP/3-21G level of theory. The two lowest (below 20 kcal/mol) doublet structures are presented in Figure 4. The planar T-shaped C_{2v} ($^2B_2$, $1a_1^2 1b_2^2 2a_1^2 1b_1^2 3a_1^2 2b_2^2 4a_1^2 3b_2^1$) structure II is predicted by GEGA to be the global minimum structure, similar to that reported previously by Nayak

et al.[4] using DFT calculations. The second C_{2v} ($^2A_1$) configuration originated from the $1a_1'^2 1e'^4 2a_2''^2 2a_1'^2 2e'^4 3e'^1$ occupation is a first order saddle point on the intramolecular rearrangement of the anion from one global minimum structure into another. We performed single point calculations at the CASSCF(7,8)/6-311+G*, CASSCF(7,10)/6-311+G* and CASSCF(13,12)/6-311+G* and found that the Hartree-Fock wave function was dominant ($C_{HF} = 0.949$, $C_{HF} = 0.943$, and $C_{HF} = 0.945$, respectively) in the CASSCF expansion, thus confirming applicability of MP2 and CCSD(T) theoretical methods. However, at our highest level of theory (CCSD(T)/6-311+G*) the planar T-shaped C_{2v} ($^2B_2$) structure is a saddle point with the $w_3(b_1) = 37i$ cm^{-1} imaginary frequency (Table 4-2). Geometry optimization following the imaginary frequency leads to a very slightly non-planar structure C_s ($^2A''$) with the nitrogen atom being out of plane by 0.04 Å. The energy difference between the planar and non-planar structure is only 5.6×10^{-4} kcal/mol and that value is significantly lower than the difference in zero point energy (ZPE) corrections (0.065 kcal/mol) for the two structures. Thus, the vibrationally averaged Al_3N^- structure is actually planar and for all practical purpose we will consider Al_3N^- as being planar in the following discussion. The lowest alternative structure III (C_{2v}, $^2B_1$, $1a_1^2 2a_1^2 1b_2^2 1b_1^2 3a_1^2 2b_2^2 4a_1^2 2b_1^1$) corresponds to a local minimum, which is substantially higher in energy and will not be further discussed.

The T shape for the isoelectronic Al_3O cluster was predicted before by Boldyrev and Schleyer[38] and Sun et al.[39] with quite similar molecular parameters. The $CAlSi_2$ cluster, another 15 valence electron tetra-atomic molecule, was, however, found to have a Y-type structure by Boldyrev, Li, and Wang.[40] When an additional electron is added to

Al_3N^-, the resulting 16 valence electronic Al_3N^{2-} cluster was found to have the T-shape again, which has been found to be the ground state for all other studied isoelectronic species such as BSi_3^-, $CAlSi_2^-$, CSi_3, NSi_3^+, NAl_2Si^-, Al_3O^-, and Al_3F.[40]

B. Al_4N and Al_4N^-.

For Al_4N the GEGA search led to a global minimum planar D_{4h} ($^2B_{2g}$, $1a_{1g}^2 1e_u^4 1a_{2u}^2 2a_{1g}^2 1b_{1g}^2 2e_u^4 1b_{2g}^1$) structure IV (Figure 4-5), in agreement with several previously reported theoretical studies.[3-5,7,9] At our highest level of theory CCSD(T)/6-311+G* the D_{4h} ($^2B_{2g}$) structure is a saddle point. Distortion along the b_{2u} mode of imaginary frequency leads to a slightly non-planar butterfly distorted structure D_{2d} ($^2B_1$). However, the energy difference between D_{2d} ($^2B_1$) and D_{4h} ($^2B_{2g}$) is only 0.192 kcal/mol, which is smaller than the difference in ZPE (0.206 kcal/mol). Therefore, the vibrationally averaged structure is actually planar and in the following discussion we will consider the Al_4N cluster to be planar. The similar small deviation from planarity was previously reported for the valence isoelectronic Al_4C^- anion.[41] The planar structure was also found to be a global minimum structure for other 18 valence electron penta-atomic species: Al_4O,[1,38,39] Al_2Si_2C,[1,42] Al_2Ge_2C,[1,42] Al_3SiC^-,[43] Al_3GeC^-,[43] as well as for other 17 valence electron penta-atomic species: Al_4C^-,[41] Al_3SiC,[43] and Al_3GeC.[43] Hence, the 18 and 17 electron rule[1,38,42-45] for planarity of penta-atomic clusters is a general rule for these species.

For the neutral Al_4N cluster, in addition to the global minimum D_{4h} ($^2B_{2g}$) structure IV, we also found two low-lying isomers C_{2v} ($^2A_1$) (structure V in Figure 4-5)

and C_{2v} ($^2B_1$) (structure VI in Figure 4-5), which are 5.4 kcal/mol and 10.9 kcal/mol above the global minimum at the CCSD(T)/6-311+G(2df)//B3LYP/6-311+G* level of theory.

The planar D_{4h} ($^1A_{1g}$) structure for Al_4N^- was first computationally predicted by Schleyer and Boldyrev[1] on the basis of molecular orbital analysis for the five-atomic 18 valence electron systems and was confirmed in follow up calculations.[2,4,5,7] In order to confirm these results for the Al_4N^- anion we run GEGA calculations for both singlet and triplet states of the Al_4N^- anion. The lowest (less than about 20 kcal/mol) singlet and triplet structures found by GEGA are presented in Figure 4-5. The GEGA search found the planar D_{4h} ($^1A_{1g}$, $1a_{1g}^2 1e_u^4 1a_{2u}^2 2a_{1g}^2 1b_{1g}^2 2e_u^4 1b_{2g}^2$) structure VII to be the global minimum, in agreement with previously reported theoretical results.[1,2,4,5,7] We performed single point calculations at the CASSCF(8,8)/6-311+G*, CASSCF(12,12)/6-311+G* and CASSCF(8,14)/6-311+G* and found that the Hartree-Fock wave function was dominant ($C_{HF} = 0.980$, $C_{HF} = 0.969$, and $C_{HF} = 0.958$, respectively) in the CASSCF expansion. We found that the next lowest isomer is a triplet C_{2v} ($^3B_1$ $1a_1^2 2a_1^2 1b_2^2 3a_1^2 1b_1^2 4a_1^2 2b_2^2 5a_1^2 6a_1^1 2b_1^1$) structure VIII (20.6 kcal/mol higher at CCSD(T)/6-311+G(2df)//B3LYP/6-311+G*), which is similar to previously reported triplet structure by Nayak et al.[4] using DFT calculations, though they did not specify the spectroscopic state of their triplet isomer. We also found one singlet structure IX (C_s, $^1A'$ $1a'^2 2a'^2 3a'^2 4a'^2 1a''^2 5a'^2 6a'^2 7a'^2 8a'^2$), which is more than 20 kcal/mol higher.

C. Al$_5$N and Al$_5$N$^-$.

For Al$_5$N the GEGA (B3LYP/3-21G) search found many structures (Figure 4-6, X-XXI) with the planar C$_{2v}$ (^{1}A$_1$, 1a$_1^2$2a$_1^2$1b$_2^2$3a$_1^2$1b$_1^2$4a$_1^2$2b$_2^2$3b$_2^2$5a$_1^2$6a$_1^2$) structure being the global minimum. The refinement at B3LYP/6-311+G* and at CCSD(T)/6-311+G(2df)//B3LYP/6-311+G* confirmed our GEGA results. However, at MP2/6-311+G* and CCSD(T)/6-311+G* it has one imaginary frequency (Table 4-4). The most stable structure C$_s$ (^{1}A') at the last two levels of theory is only slightly distorted from the C$_{2v}$ symmetry and after ZPE corrections it is effectively C$_{2v}$ symmetry. The C$_{2v}$ (^{1}A$_1$) structure X was also reported to be the global minimum structure by Guo and Wu[9] who used two B3LYP/6-311+G* and SVWN/6-311+G* theoretical methods. According to Ling, Song and Cao[8] the global minimum of Al$_5$N corresponds to the structure XVIII at the full-potential linear-muffin-tin-orbital molecular dynamics (FP-LMTO-MD) method. We found that this structure is a second order saddle point, which is 17.3 kcal/mol higher in energy at B3LYP/6-311+G* (13.5 kcal/mol at CCSD(T)/6-311+G(2df)//B3LYP/6-311+G*). Geometry optimization of the structure XVIII following the imaginary frequency led initially to the structure XII; and geometry optimization following the imaginary in the structure XII led eventually to the global minimum structure X. Thus, the structure XVIII can be safely excluded from being a global minimum structure of Al$_5$N. Nayak, Khanna, and Jena[3] reported that the structure XI is the global minimum structure for the Al$_5$N cluster using the BPW91/6-311G** level of theory. The same global minimum structure was also reported by Leskiw et al.[7] According to our calculations, the structure XI is a first order saddle point at B3LYP/6-311+G*. Geometry

optimization of the structure XI following the imaginary frequency led to a slightly distorted structure C_2 (^1A) in which the top Al atom still located on the C_2 axis with the beneath tetrahedral type Al_4 cluster being slightly distorted. The energy difference between the C_{2v} ($^1A_1$) structure XI and slightly distorted local minimum structure is only 0.021 kcal/mol, which is significantly lower than the difference in ZPE corrections (0.063 kcal/mol) for the two structures. At the MP2/6-311+G* and CCSD(T)/6-311+G* levels of theory the C_{2v} ($^1A_1$) structure was found to be a minimum. Thus, for all practical purpose we will consider the structure XI of Al_5N as being C_{2v} symmetry. The structure XI is 6.8 kcal/mol higher in energy than the structure X at B3LYP/6-311+G*, but this difference is only 1.3 kcal/mol at CCSD(T)/6-311+G(2df)//B3LYP/6-311+G* and 1.3 at CCSD(T)/6-311+G(2df)//CCSD(T)/6-311+G*. Thus, these two structures are almost degenerate at our highest level of theory. Two structures (XIV and XVI) were found to have 2 and 1 imaginary frequencies at B3LYP/6-311+G* level of theory, however, they have effective C_{2v} symmetry after ZPE corrections. The other structures identified in our calculations, within 20 kcal/mol above the ground state, are summarized in Figure 4-6.

The structure of the Al_5N^- anion has been previously studied by Leskiw et al.,[7] who reported that the global minimum structure XXIII is similar to the structure XI for Al_5N neutral. Our GEGA search at B3LYP/3-21G for Al_5N^- found the planar C_{2v} ($^2B_1$ $1a_1^2 2a_1^2 1b_2^2 3a_1^2 1b_1^2 4a_1^2 2b_2^2 3b_2^2 5a_1^2 6a_1^2 2b_1^1$) structure XXII to be the global minimum, which is similar to the global minimum of the neutral (structure X). We also performed single point calculations at CASSCF(13,11)/6-311+G*, CASSCF(11,11)/6-311+G* and CASSCF(11,12)/6-311+G* and found that the Hartree-Fock wave function was dominant

($C_{HF}= 0.932$, $C_{HF}= 0.925$, and $C_{HF}= 0.912$, respectively) in the CASSCF expansion. At MP2/6-311+G* and CCSD(T)/6-311+G* it has one and two imaginary frequencies, respectively (Table 4-4). However, the vibrationally averaged global minimum structure can be considered to have the C_{2v} symmetry. The second lowest energy structure C_s ($^2A'$) in our calculations at B3LYP/3-21G, B3LYP/6-311+G* and MP2/6-311+G* is similar to the global minimum structure XXIII proposed by Leskiw et al.[7], though in our case it has lower symmetry C_s instead of C_{2v}. It relative energy is 5.3 kcal/mol at B3LYP/6-311+G* and 2.9 kcal/mol at CCSD(T)/6-311+G(2df)//B3LYP/6-311+G*. Geometry optimization at the CCSD(T)/6-311+G* level of theory revealed that C_s ($^2A'$) structure collapsed into the C_{2v} ($^2A_1$) structure XXIII. The structure XXIII is 2.6 kcal/mol (CCSD(T)/6-311+G(2df)//CCSD(T)/6-311+G*) higher in energy than the global minimum. The third lowest energy structure XXIV C_s ($^2A'$) lies 6.2 kcal/mol at B3LYP/6-311+G*, 4.2 kcal/mol at CCSD(T)/6-311+G(2df)//B3LYP/6-311+G* and 4.0 at CCSD(T)/6-311+G(2df)//CCSD(T)/6-311+G* higher in energy than the global minimum. In addition, two more structures XXV and XXVI were found to be about 6-8 kcal/mol (CCSD(T)/6-311+G(2df)//CCSD(T)/6-311+G*) above the global minimum. The other structures identified in our calculations, within 20 kcal/mol above the global minimum, are also shown in Figure 4-6.

4-6. Comparison of Calculated VDEs with Experiment

A. Al_3N^-.

The ab initio VDEs calculated at the TD-B3LYP/6-311+G(2df), ROVGF/6-311+G(2df) and CCSD(T)/6-311+G(2df) levels for Al_3N^- are compared with the experimental data in Table 4-5 and good agreement is obtained among the different levels of theory and between the theory and experiment.

The global minimum of Al_3N^- was found to be the planar structure II (C_{2v}, $^2B_2$) with the valence electronic configuration: $1a_1^2 1b_2^2 2a_1^2 1b_1^2 3a_1^2 2b_2^2 4a_1^2 3b_2^1$. As given in Table 4-5, our calculated VDE for removal of an electron from the HOMO of the global minimum is 1.06 eV at the UCCSD(T)/6-311+G(2df) level of theory, 1.16 eV at the UOVGF/6-311+G(2df) level of theory, and 1.15 eV at the TD-B3LYP/6-311+G(2df) level of theory. The pole strength (UOVGF) was found to be 0.90, indicating that the detachment channel can be primarily described by a one-electron detachment process. These calculated first VDE for the structure-II (C_{2v}, $^2B_2$) is in excellent agreement with the measured VDE of 1.19 ± 0.04 eV for this feature (Table 4-5). The $3b_2$-HOMO of Al_3N^- is a bonding orbital within the triangular wing Al-Al-Al in the global minimum structure (Figure 4-7). Detachment of the electron from this orbital results in a significant geometry relaxation from C_{2v} in the anion to D_{3h} in the neutral. The large geometry change is consistent with the broad PES band width observed for this transition (Figure 4-1). The calculated adiabatic electron detachment energy (ADE) is 0.73 eV (CCSD(T)/6-311+G(2df)//CCSD(T)/6-311+G*+ZPE//CCSD(T)/6-311+G*), in good

agreement with the experimental threshold (~0.7 eV) for the X band. Because of the large geometry changes and the lack of vibrational resolution, the ADE cannot be accurately determined from the experimental PES spectra.

Electron detachment from the doubly occupied MOs could result in either triplet or singlet final states at the C_{2v} global minimum structure. The two triplet $^3B_2$ $(1a_1^21b_2^22a_1^21b_1^23a_1^22b_2^24a_1^13b_2^1)$ and $^3A_1$ $(1a_1^21b_2^22a_1^2\ 1b_1^23a_1^22b_2^24a_1^13b_2^1)$ states are assigned to the sharp features A and B, respectively (Table 4-5) and the corresponding singlet $^1B_2$ $(1a_1^21b_2^22a_1^21b_1^23a_1^22b_2^24a_1^13b_2^1)$ and $^1A_1$ $(1a_1^21b_2^22a_1^21b_1^2\ 3a_1^22b_2^14a_1^23b_2^1)$ states are assigned to the relatively weak features C and D (Table 4-5). The $4a_1$ and $2b_2$ MOs are essentially non-bonding (Figure 4-7), consistent with the relatively sharp spectral features observed for bands A, B, C, and D. Finally, the broad feature E most probably corresponds to several transitions involving the two triplet $^3B_2$ $(1a_1^21b_2^22a_1^21b_1^23a_1^1\ 2b_2^24a_1^23b_2^1)$ and $^3A_2$ $(1a_1^21b_2^22a_1^21b_1^13a_1^22b_2^24a_1^23b_2^1)$ states (Table 4-5). The $3a_1$ and $1b_1$ orbitals are strongly bonding MOs (Figure 4-7), consistent with the broad E band.

B. Al_4N^-.

The calculated VDE's for the global minimum structure VII, as well as for the low-lying isomer VIII of Al_4N^- are compared with the experimental data in Table 4-6. The calculated VDE from the $1b_{2g}$-HOMO of the planar square D_{4h} structure VII at three levels of theory is 2.16 eV (TD-B3LYP/6-311+G(2df)), 2.26 eV (ROVGF/6-311+G(2df)), and 2.29 eV (CCSD(T)/6-311+G(2df)), agreeing very well with the

experimental value 2.32 ± 0.02 eV (Table 4-6). The calculated adiabatic electron detachment energy (ADE) is 2.28 eV (CCSD(T)/6-311+G(2df)//CCSD(T)/6-311+G*+ZPE//CCSD(T)/6-311+G*), in good agreement with the experimental value 2.29 eV.[4]

The broad band (A&B) in the experimental spectra (Figure 4-2) are due to detachment from HOMO-1 ($2e_u$) and HOMO-2 ($1b_{1g}$) (Table 4-6), which are very close to each other, resulting in the overlap of the two detachment bands. Because of the order of the ^2E_u and $^2B_{1g}$ states is different at TD-B3LYP and OVGF, we cannot be sure with certainty which spectroscopic state is actually lower in energy. The next rather weak feature C could be assigned to detachment from HOMO-3 ($2a_{1g}$). According to our calculations there should be one detachment channel from HOMO-4 ($1a_{2u}$)) around 6 eV (Table 4-6), which may be underestimated because no major detachment band was observed in the higher binding energy side. Overall, the calculated VDE's from the planar D_{4h} global minimum are in good agreement with the experiment, in particular for the first three detachment channels.

The weak features, observed in the low energy part (<2.3 eV) of the spectrum and in between the intense peaks X and A (Figure 4-2), cannot be explained by the global minimum D_{4h} structure and they should belong to either alternative isomers or to impurities. Nayak et al.[4] explained these small features by contributions from a triplet isomer. According to our calculations there are two lowest isomers: a triplet C_{2v} ($^3B_1$) structure VIII (19.8 kcal/mol higher at CCSD(T)/6-311+G(2df)//B3LYP/6-311+G*) and singlet a C_s structure IX (21.8 kcal/mol higher at CCSD(T)/6-311+G(2df)//B3LYP/6-

311+G*) (Figure 4-5). Indeed the triplet C_{2v} ($^3B_1$) structure VIII gives calculated VDEs, which fall in the right energy ranges for the weak features in the PES spectra of Al_4N^- (Table 4-6). Our result agrees with the previous assignment by Nayak et al.,[4] whose DFT calculations suggests that the triplet isomer is 0.97 eV (22.3 kcal/mol) above the D_{4h} ground state. It is very surprising that such a high energy isomer can be populated at all in the experiment. The explanation suggested by Nayak et al. that such a high energy isomer is "spin-protected" seems reasonable, i.e., the triplet isomer once formed is prevented from being relaxed to the D_{4h} ground state because it is spin-forbidden. Although this is unusual, we have increasingly observed in several cluster systems population of high energy triplet isomers, for example in B_7^- and B_{13}^-.[46,47]

C. Al_5N^-.

We computed the VDEs from the three low-lying isomers for Al_5N^- and compared them with the experimental data in Tables 4-7 – 4-9. Clearly, at least two isomers are needed to interpret the observed spectra of Al_5N^-. The OVGF and TD-DFT methods give similar first VDE for all three isomers and cannot be used to distinguish them. However, our most accurate $\Delta CCSD(T)$ method gives a first VDE of 2.01 eV for structure XXII, which is in good agreement with that of feature x (2.01 eV); whereas the first VDE for structure XXIII from $\Delta CCSD(T)$ is 1.83 eV in very good agreement with that of feature X (1.89 eV), suggesting the observed first two detachment bands come from two different isomers of Al_5N^-. The fact that the two features have similar intensities suggest

that the two isomers are most likely degenerate, consistent with the close energies of the two isomers (Figure 4-6).

The calculated second VDE from ΔCCSD(T) for the planar C_{2v} structure XXII of Al_5N^- is 2.63 eV, in good agreement with that of band B (2.66 eV). The second ΔCCSD(T) VDE for the C_{2v} structure XXIII is 2.23 eV, in excellent agreement with that of band A (2.29 eV). The next ΔCCSD(T) detachment channel for both isomers is at much higher energies, thus preventing us from making more definitive assignments for the higher binding energies features. However, our TD-DFT data suggest that each of the higher binding energy feature may contain contributions from both isomers. We also computed the VDEs for isomer XXIV (Table 4-9), which seem to be all similar to those of the planar isomer XXII. Since this isomer is higher in energy, we suspect that it may not be significantly populated. Its minor contribution to the observed spectra is likely to be obscured.

Al_5N^- is a rare case, where two or more isomers are nearly degenerate and seem to be equally populated experimentally. The two isomers of Al_5N^- are very different, one planar (2D) (structure XXII) and the other 3D (structure XXIII). Al_3N^-, Al_3N, Al_4N^-, and Al_4N are all overwhelmingly stable as 2D structures. However, the 2D and 3D structures for Al_5N^- are nearly degenerate, signifying the onset of 2D to 3D transitions.

4-7. Chemical Bonding Analyses

A. Al$_3$N$^-$ and Al$_3$N.

The peculiar T-shape for Al$_3$N$^-$ can be understood on the basis of MO analysis, as shown in Figure 4-7. The four lowest valence MOs (HOMO-7, HOMO-6, HOMO-5 and HOMO-4) are primarily formed from 2s (HOMO-7), 2p$_x$ (HOMO-4), 2p$_y$ (HOMO-6), and 2p$_z$ (HOMO-5) AOs of N. The next three MOs (HOMO-1, HOMO-2 and HOMO-3) corresponding to three lone pairs are formed primarily by 3S-AOs of Al. When only these MOs are occupied as that is in Al$_3$N, then the resulting structure is a perfect triangule with N being at the center and formal charge distribution is close to ionic [(Al$^+$)$_3$(N^{3-})], i.e., Al is acting as a valence +1 atom. Indeed, our calculated NBO effective charges q(N) = -2.46 |e| and q(Al) = +0.82 |e| (B3LYP/6-311+G*) support this simple ionic picture. The central N atom has already a full octet of valence electrons and it should not form any additional bonds. Thus one would expect that the Al$_3$N$^-$ anion may not be an electronically stable species. That is indeed the case for NH$_3$, which does not bind an access electron.[48] However, the Al$_3$N$^-$ anion is quite electronically stable with a VDE of 1.19 ± 0.04 eV. The stability of the Al$_3$N$^-$ anion comes from the extra electron occupying 3b$_2$-HOMO, which is a pure ligand (Al-Al) bonding orbital (Figure 4-7). Calculated NBO effective charges q(N) = -2.32 |e|, q(Al$_a$) = +0.20 |e| and q(Al$_e$) = +0.56 |e| (B3LYP/6-311+G*) support this description. The bonding character of the 3b$_2$-HOMO is responsible for the electronic stability of this anion and for its T-shape. The lower symmetry of Al$_3$N$^-$ can be also understood as a Jahn-Teller distortion of the initial

D_{3h} structure of Al_3N when an additional electron occupies its double degenerate LUMO (3e').

B. Al_4N^- and Al_4N.

The planar square structure of Al_4N^- can also be understood on the basis of the MO analysis, as shown in Figure 8. The four lowest valence MOs (HOMO-6, HOMO-5, HOMO-5' and HOMO-4) are again primarily formed from 2s (HOMO-6), $2p_x$ (HOMO-5'), $2p_y$ (HOMO-5), $2p_z$ (HOMO-4) AOs of N. The next four MOs (HOMO-1, HOMO-2, HOMO-2' and HOMO-3) corresponding to four lone pairs are formed primarily by 3S-AOs of aluminum. When only these MOs are occupied as in Al_4N^+, the resulting structure is a tetrahedron with N being at the center and a formal charge distribution close to ionic, similar to the isoelectronic Al_4C molecule.[41,44] The tetrahedral Al_4C molecule has the following electron configuration $1a^2 1t_2^6 2a_1^2 2t_2^6 1e^0$. When one or two electrons occupy one of the doubly degenerate 1e-LUMO, the resulting anions Al_4C^- and Al_4C^{2-} undergo Jahn-Teller distortion toward the planar D_{4h} structure.[41,45] Similarly, occupation of 1e-LUMO in the tetrahedral Al_4N^+ should result in the geometric distortion towards D_{4h} structure in Al_4N and Al_4N^-. In Al_4N^+ the central atom N has a full octet and formally the hyper-stoichiometric molecules Al_4N and Al_4N^- should not be stable. However, the ligand-ligand bonding HOMO in Al_4N and Al_4N^- is responsible for the electron and geometric stability of these species. Al_4N and Al_4N^- are analogs of the first experimentally discovered pentaatomic tetracoordinate planar carbon molecules, Al_4C^- and Al_4C^{2-}.[41-45]

C. Al$_5$N$^-$ and Al$_5$N.

The geometries of the structures X of Al$_5$N and XXII of Al$_5$N$^-$ (Figure 4-6) hint that they could be formally considered as Al$^+$ or Al coordinated to the edge of the planar Al$_4$N$^-$ anionic structure IV (Figure 4-5), respectively. Calculated NBO charges (B3LYP/6-311+G*) on the central nitrogen atom (-2.31 and -2.33 |e|) are almost the same in Al$_4$N$^-$ (IV), Al$_5$N (X), and Al$_5$N$^-$ (XXII). The NBO charge on the apex Al atom in Al$_5$N is +0.30 |e|, which is lower than ionic limit +1.0 |e|, but that is qualitatively consistent with the formal [Al$_4$N]$^-$Al$^+$ formulation, indicating the structural stability of the planar tetracoordinate [Al$_4$N]$^-$. In the anionic Al$_5$N$^-$ cluster, a significant portion of the additional electron goes to the apex Al atom, which now has a NBO charge of -0.25 |e|. The molecular orbital pictures for Al$_5$N and Al$_5$N$^-$ (Figure 9) are also consistent with the chemical bonding described above. One can see that molecular orbitals: HOMO-1, HOMO-2, HOMO-3, HOMO-4, HOMO-5, HOMO-6, HOMO-8, HOMO-9, and HOMO-10 in Al$_5$N$^-$ can be approximately correlated to the molecular orbitals: HOMO, HOMO-1, HOMO-2, HOMO-2', HOMO-3, HOMO-4, HOMO-5, HOMO-5', and HOMO-6 in Al$_4$N$^-$, respectively. The HOMO and HOMO-7 are responsible for the p- and s-covalent bonding between the apex Al atom and the Al$_4$N$^-$ cluster.

The second lowest isomer of Al$_5$N (XI) could be formally considered as AlN^{2-} coordinated to the edge of the tetrahedral Al$_4^{2+}$ dication. It was previously shown,[38] that the Al$_4^{2+}$ dication has a tetrahedral structure. Calculated NBO charge (B3LYP/6-311+G*) on the AlN group is -1.42 |e| and that is qualitatively consistent with the formal

$[Al_4]^{2+}(NAl)^{2-}$ formulation. According to our NBO analysis of Al_5N^- (XXIII), an additional electron in Al_5N^- goes to the Al_4 unit.

4-8. Conclusions

Well-resolved photoelectron spectra were obtained for three nitrogen doped aluminum clusters Al_3N^-, Al_4N^- and Al_5N^- at four photon energies (532, 355, 266, and 193 nm) and compared with theoretical calculations to elucidate their electronic structure and chemcial bonding. Global minimum structures of Al_3N^-, Al_4N^- and Al_5N^- were identified first by using Gradient Embedded Genetic Algorithm (B3LYP/3-21G) followed by B3LYP/6-311+G*, MP2/6-311+G* and CCSD(T)/6-311+G* geometry and frequency calculations. By comparing the theoretical VDEs with the experimental data we established that NAl_3 is D_{3h} and Al_3N^- has a T-shape structure (II) C_{2v} ($^2B_2$). The ground state of Al_4N and Al_4N^- are both square-planar in agreement with previously reported results. For the Al_5N^- anion we found two quasi degenerate structures XXII (C_{2v}, $^2B_1$) and XXIII (C_{2v}, $^2A_1$), which are almost equally populated experimentally. We also computationally identified three other low energy structures: XXIV (C_s, $^2A'$), XXV (C_{2v}, $^2A_1$), XXVI (C_s, $^2A''$), which lie with 6-8 kcal/mol above the ground state. The low-lying isomers of the neutral Al_5N cluster are found to be similar to those its anion.

Chemical bonding analysis revealed that Al_3N can be described as an ionic cluster $(Al^+)_3(N^{3-})$. In the planar C_{2v} structure of Al_3N^-, an additional electron occupies the peripheral ligand-ligand bonding HOMO, resulting in the structural distortion to the T-shape. Both Al_4N and Al_4N^- have planar structure with a central nitrogen atom. The

planarity of this structure is due to the singly or doubly occupied $1b_{2g}$-HOMO, which is a peripheral four-center ligand-ligand bonding orbital, similar to the tetracoordinate planar carbon molecules, CAl_4^- and CAl_4^{2-}. Finally, the Al_5N and Al_5N^- species two nearly degenerate structures competing for ground state, a planar one and a 3D one. The planar structure can be viewed as an Al coordinated to the planar Al_4N: $[Al_4N]^-Al^+$ or $[Al_4N]^-Al$, whereas the 3D structure can be viewed as an AlN unit interacting with a tetrahedral Al_4 motif: $[Al_4]^{2+}(NAl)^{2-}$ or $([Al_4]^+(NAl)^{2-})$.

References

[1] P. v. R. Schleyer and A. I. Boldyrev, J. Chem. Soc. Chem. Commun. 1536 (1991).

[2] V. G. Zakrzewski, W. v. Niessen, A. I. Boldyrev, and P. v. R. Schleyer, Chem. Phys. **174**, 167 (1993).

[3] S. K. Nayak, S. N. Khana, and P. Jena, Phys. Rev. B, **57**, 3787 (1998).

[4] S. K. Nayak, B. K. Rao, P. Jena, X. Li, and L. S. Wang, Chem. Lett. **301**, 379 (1999).

[5] B. H. Boo and Z. Liu, J. Phys. Chem. A, **103**, 1250 (1999).

[6] L. Andrews, M. Zhou, G. V. Chertihin, W. D. Bare, Y. Hannachi, J. Phys. A, **104**, 1656 (2000).

[7] B. R. Leskiw, A. W. Castleman, Jr., C. Ashman, S. N. Khanna, J. Chem. Phys. **114**, 1165 (2001).

[8] L. Ling, B. Song, and P.-L. Cao, J. Mol. Struct. Theochem, **728**, 215 (2005).

[9] L. Gou and H.-S. Wu, Int. J. Quant. Chem. 106, 1250 (2006).

[10] X. Li and L. S. Wang, Eur. Phys. J. D, **34**, 9 (2005).

[11] G. Meloni, S. M. Sheehan, B. F. Parsons, and D. M. Neumark, J. Phys. Chem. A, **110**, 3527 (2006).

[12] L. S. Wang, H. S. Cheng, and J. Fan, J. Chem. Phys. **102**, 9480 (1995).

[13] A. N. Alexandrova, A. I. Boldyrev, Y-J. Fu, X.-B. Wang, and L. S. Wang, J. Chem. Phys. **121**, 5709 (2004).

[14] A. N. Alexandrova and A. I. Boldyrev, J. Chem. Theory and Comput. **1**, 566 (2005).

[15] A. D. Becke, J. Chem. Phys. **98**, 5648, (1993).

[16] S. H. Vosko, L. Wilk, and M. Nusair, Can. J. Phys. **58**, 1200 (1980).

[17] C. Lee, W. Yang, R. G. Parr, Phys. Rev. B, **37**, 785 (1988).

[18] (a) J. S. Binkley, J. A. Pople, and W. J. Hehre, J. Am. Chem. Soc. **102**, 939 (1980); (b) M. S. Gordon, J. S. Binkley, J. A. Pople, W. J. Pietro, and W. J. Hehre, J. Am. Chem. Soc. **104**, 2797 (1982); (c) W. J. Pietro, M. M. Francl, W. J. Hehre, D. J. Defrees, J. A. Pople, and J. S. Binkley, J. Am. Chem. Soc. **104**, 5039 (1982).

[19] M. Head-Gordon, J. A. Pople, and M. J. Frisch, Chem. Phys. Lett. **153**, 503 (1988).

[20] J. Cizek, Adv. Chem. Phys. **14**, 35 (1969).

[21] P. J. Knowles, C. Hampel, and H.-J.Werner, J. Chem. Phys. **99**, 5219 (1993).

[22] K. Raghavachari, G. W. Trucks, J. A. Pople, M. Head-Gordon, Chem. Phys. Lett. **157**, 479 (1989).

[23] A. D. McLean and G. S. Chandler J. Chem. Phys. **72**, 5639 (1980).

[24] T. Clark, J. Chandrasekhar, G. W. Spitznagel, and P. v. R. Schleyer, J. Comput. Chem. **4**, 294 (1983).

[25] M. J. Frisch, J. A. Pople, and J. S. Binkley, J. Chem. Phys. **80**, 3265 (1984).

[26] F. Bernardi, A. Bottini, J. J. W. McDougall, M. A. Robb, and H. B. Schlegel, Faraday Symp. Chem. Soc. 19, 137 (1979).

[27] M. J. Frisch, I. N. Ragazos, M. A. Robb, and H. B. Schlegel, Chem. Phys. Lett. **189**, 524 (1992).

[28] L. Cederbaum, J. Phys B, **8**, 290 (1975).

[29] W. von Niessen, J. Shirmer, and L. S. Cederbaum, Comput. Phys. Rep. **1**, 57 (1984).

[30] V. G. Zakrzewski and W. von Niessen W. J. Comput. Chem. **14**, 13 (1993).

[31] (a) J. V. Ortiz, Int. *J. Quant. Chem., Quant. Chem. Symp.* **1989,** 23, 321; (b) J. S. Lin and J. V. Ortiz, Chem. Phys. Lett. 171, 197 (1990).

[32] V. G. Zakrzewski, J. V. Ortiz, J. A. Nichols, D. Heryadi, D. L. Yeager, and J. T. Golab, Int. J. Quant. Chem., Quant. 60, 29 (1996).

[33] R. Bauernshmitt and R. Alrichs, R. Chem. Phys. Lett. 256, 454 (1996).

[34] M. E. Casida, C. Jamorski, K. C. Casida, and D. R. Salahub, J. Chem. Phys. 108, 4439 (1998).

[35] Gaussian 98 (revision A.7). M. J. Frisch, G. M. Trucks, H. B. Schlegel, G. E. Scuseria, M. A. Robb, J. R. Cheeseman, V. G. Zakrzewski, J. A. Montgomery, Jr., R. E. Stratmann, J. C. Burant, S. Dapprich, J. M. Millam, A. D. Daniels, K. N. Kudin, M. C.

Strain, O. Farkas, J. Tomasi, V. Barone, M. Cossi, R. Cammi, B. Mennucci, C. Pomelli, C. Adamo, S. Clifford, J. Ocheterski, G. A. Petersson, P. Y. Ayala, Q. Cui, K. Morokuma, D. K. Malick, A. D. Rabuck, K. Raghavachari, J. B. Foresman, J. Cioslowski, J. V. Ortiz, A. G. Baboul, B. B. Stefanov, G. Liu, A. Liashenko, P. Piskorz, I. Komaromi, R. Gomperts, R. L. Martin, D. J. Fox, T. Keith, M. A. Al-Laham, C. Y. Peng, A. Nanayakkara, C. Gonzales, M. Challacombe, P. M. W. Gill, B. G. Johnson, W. Chen, M. W. Wong, J. L. Andres, M. Head-Gordon, E. S. Replogle and J. A. Pople, (Gaussian, Inc., Pittsburgh PA, 1998).

[36] Gaussian 03 (revision A.1). M. J. Frisch, G. M. Trucks, H. B. Schlegel, G. E. Scuseria, M. A. Robb, J. R. Cheeseman, J. A. Montgomery, T. Vreven, K. N. Kudin, J. C. Burant, J. M. Millam, S. S. Iyengar, J. Tomasi, V. Barone, B. Mennucci, M. Cossi, G. Scalmani, N. Rega, G. A. Petersson, H. Nakatsuji, O. Kitao, H. Nakai, M. Klene, X. Li, J. E. Knox, H. P. Hratchian, J. B. Cross, C. Adamo, J. Jaramillo, R. Gomperts, R. E. Stratmann, O. Yazyev, A. J.Austin, R. Cammi, C. Pomelli, J. W. Ochterski, P. Y. Ayala, K. Morokuma, G. A. Voth, P. Salvador, J. J. Dannenberg, V. G. Zakrzewski, S. Dapprich, A. D. Daniels, M. C. Strain, O. Farkas, D. K. Malick, A. D. Rabuck, K. Raghavachari, J. B. Foresman, J. V. Ortiz, Q. Cui, A. G. Baboul, S. Clifford, J. Cioslowski, B. B. Stefanov, A.Liu, A. Liashenko, P. Piskorz, I. Komaromi, R. L. Martin, D. J. Fox, T. Keith, M. A. Al-Laham, C. Y. Peng, A. Nanayakkara, M. Challacombe, P. M. W. Gill, B. G. Johnson, W. Chen, M. W. Wang, C. Gonzales, and J. A. Pople (Gaussian, Inc., Pittsburgh PA, 2003).

[37] MOLDEN3.4. Schaftenaar, G. MOLDEN3.4, CAOS/CAMM Center, The Netherlands (1998).

[38] A. I. Boldyrev and P. v. R. Schleyer, J. Am. Chem. Soc. **113**, 9045 (1991).

[39] J. Sun, W. C. Lu, H. Wang, Z.-S. Li, and C.-C. Sun, J. Phys. Chem. A, **110**, 2729 (2006).

[40] A. I. Boldyrev, X. Li, and L. S. Wang, J. Phys. Chem. **104**, 5358 (2000).

[41] X. Li, L. W. Chen, L. S. Wang, A. I. Boldyrev, and J. Simons, J. Am. Chem. Soc. **121**, 6033 (1999).

[42] A. I. Boldyrev and J. Simons, J. Am. Chem. Soc. **120**, 7967 (1998).

[43] L. S. Wang, A. I. Boldyrev, X. Li, and J. Simons, J. Am. Chem. Soc. **122**, 7681 (2000).

[44] D. Yu. Zubarev and A. I. Boldyrev, **122**, 144322 (2005).

[45] X. Li, H.-F. Zhang, L. S. Wang, G. D. Geske, and A. I. Boldyrev, Angew. Chem. Int. Ed. **39**, 3630 (2000).

[46] A. N. Alexandrova, A. I. Boldyrev, H. J. Zhai, and L. S. Wang, J. Phys. Chem. A **108**, 3509 (2004).

[47] H. J. Zhai, B. Kiran, J. Li, and L. S. Wang, Nature Materials **2**, 827 (2003).

[48] H. W. Sarkas, S. T. Arnold, J. G. Eaton, G. H. Lee, and K. H. Bowen, J. Chem. Phys. **116**, 5731 (2002).

Table 4-1. Experimental vertical detachment energies in eV for the Al_3N^-, Al_4N^-, and Al_5N^- anions from the photoelectron spectra. The number in parentheses represents the uncertainty of the last digit.

	X	A	B	C	D	E	F
Al_3N^-	1.19 (4)	2.78 (3)	3.06 (3)	3.39 (4)	3.69 (4)	5.20 (5)	
Al_4N^-	2.32 (3)	3.41 (2)	3.74 (3)	5.40 (5)			
Al_5N^-	1.89 (4)	2.29 (3)	2.66 (3)	2.90 (3)	3.27(3)	3.51(3)	3.87 (3)

Table 4-2. The molecular properties of the global minimum Al_3N^- and Al_3N structures.

	Al_3N^- (C_{2v}, $^2B_2$')			Al_3N^- (C_s, ^2A")
Molecular Parameter	B3LYP/ 6-311+G*	MP2/ 6-311+G*	CCSD(T)/ 6-311+G*	CCSD(T)/ 6-311+G*,b
E, a.u.	-782.2040	-780.6194	-780.6674376	-780.6674385[c]
R(N-Al_1), Å	1.916	1.923	1.916	1.916
R(N-$Al_{2,3}$), Å	1.822	1.827	1.821	1.821
<$Al_1NAl_{2,3}$, ^{0}	102.9	101.8	102.4	102.4
w_1 (a_1), cm^{-1}	560 (80.2)[a]	569 (101.5)[a]	577	577
w_2 (a_1), cm^{-1}	444 (0.6)[a]	445 (1.0)[a]	452	452
w_3 (a_1), cm^{-1}	152 (8.3)[a]	156 (12.2)[a]	153	153
w_3 (b_1), cm^{-1}	164 (4.1)[a]	57 (2.9)[a]	37i	46
w_4 (b_2), cm^{-1}	801 (4.7)[a]	822 (1.2)[a]	822	821
w_4 (b_2), cm^{-1}	140 (22.8)[a]	175 (27.9)[a]	136	137

Al_3N (D_{3h}, $^1A_1$')			
Molecular Parameter	B3LYP/ 6-311+G*	MP2/ 6-311+G*	CCSD(T)/ 6-311+G*d
E, a.u.	-782.1750	-780.6034	-780.6512
R(N-Al), Å	1.850	1.851	1.847
w_1 (a_1'), cm^{-1}	426 (0.0)[a]	428 (0.0)[a]	438
w_2 (a_2"), cm^{-1}	218 (0.1)[a]	133 (0.0)[a]	137
w_3 (e'), cm^{-1}	749 (328.1)[a]	765 (334.7)[a]	776
w_4 (e'), cm^{-1}	154 (2.8)[a]	150 (3.2)[a]	151

[a] Values in parentheses represent relative absorbance intensities in the IR spectrum.

[b] Nitrogen atom comes out of the Al_3-plane by 0.039 Å.

[c] E_{tot}=-780.735852 a.u.,

[d] E_{tot}=-780.709937 a.u. (all at CCSD(T)/6-311+G(2df)//CCSD(T)/6-311+G*).

Table 4-3. The molecular properties of the Al_4N^- and Al_4N species.

	Al_4N^- $(D_{4h}, {}^1A_1)$			Al_4N $(D_{4h}, {}^2B_{2g})$			Al_4N $(D_{2d}, {}^2B_1)$
Molecular Parameter	B3LYP/ 6-311+G*	MP2/ 6-311+G*	CCSD(T)/ 6-311+G*,b	B3LYP/ 6-311+G*	MP2/ 6-311+G*	CCSD(T)/ 6-311+G*,c	CCSD(T)/ 6-311+G*,c
E, a.u.	-1024.6857	-1022.6343	-1022.6869	-1024.6060	-1022.5538	-1022.6130	-1022.6133
R(N-Al), Å	1.936	1.938	1.936	1.964	1.968	1.962	1.961
$w_1(a_{1g})$, cm^{-1}	400 (0.0)	403 (0.0)	407	379 (0.0)	381 (0.0)	387	386
$w_2(a_{2u})$, cm^{-1}	214 (14.1)	118 (15.5)	117	223 (5.6)	159 (8.5)	151	220
$w_3(b_{1g})$, cm^{-1}	265 (0.0)	280 (0.0)	277	216 (0.0)	231 (0.0)	232	236
$w_4(b_{2g})$, cm^{-1}	268 (0.0)	278 (0.0)	275	223 (0.0)	244 (0.0)	245	265
$w_5(b_{2u})$, cm^{-1}	90 (0.0)	71 (0.0)	55	46 (0.0)	52 (0.0)	46i	47
$w_6(e_u)$, cm^{-1}	666 (238.8)	709 (345.2)	680	521 (123.5)	711 (505.5)	554	555
$w_7(e_u)$, cm^{-1}	217 (14.9)	251 (17.4)	226	97 (0.2)	316 (0.2)	159	160

[a] Values in parentheses represent relative absorbance intensities in the IR spectrum (km/mol).

[b] E_{tot}=-1022.770084 a.u.,

[c] E_{tot}=-1022.686211 a.u. (all at CCSD(T)/6-311+G(2df)//CCSD(T)/6-311+G*).

Table 4-4. The molecular properties of the Al_5N^- and Al_5N species.

Molecular Parameter	Al₅N⁻ (C₂ᵥ, ²B₁)			Al₅N (C₂ᵥ, ¹A₁)		
	B3LYP/ 6-311+G*	MP2/ 6-311+G*	CCSD(T)/ 6-311+G*,b	B3LYP/ 6-311+G*	MP2/ 6-311+G*	CCSD(T)/ 6-311+G*,c
E, a.u.	-1267.1276	-1264.5970	-1264.6622	-1267.0636	-1264.5370	-1264.6025
R(N-Al₁), Å	3.859	3.796	3.847	3.885	3.858	3.878
R(N-Al₂,₃), Å	1.934	1.929	1.940	1.890	1.888	1.896
R(N-Al₄,₅), Å	1.921	1.932	1.915	1.975	1.977	1.971
<Al₁NAl₂,₃, °	42.7	42.8	42.2	46.9	46.9	46.2
<Al₁NAl₄,₅, °	134.3	135.7	133.5	136.3	136.4	135.8
w₁ (a₁), cm⁻¹	666 (311)ᵃ	806 (1237)	707	697 (271)ᵃ	738 (356)	707
w₂ (a₁), cm⁻¹	411 (6)ᵃ	493 (28)	418	402 (32)ᵃ	407 (29)	408
w₃ (a₁), cm⁻¹	304 (1)ᵃ	353 (0)	327	284 (14)ᵃ	297 (18)	297
w₄ (a₁), cm⁻¹	243 (19)ᵃ	295 (6)	251	238 (3)ᵃ	256 (4)	242
w₅ (a₁), cm⁻¹	211 (4)ᵃ	246 (18)	224	196 (37)ᵃ	206 (51)	204
w₆ (a₂), cm⁻¹	67 (0)ᵃ	7 (0)	43i	82 (0)ᵃ	65 (0)	38
w₇ (b₁), cm⁻¹	213 (5)ᵃ	46 (0)	28	200 (2)ᵃ	10 (0)	72
w₈ (b₁), cm⁻¹	29 (2)ᵃ	78i (9)	62i	34 (3)ᵃ	31i (5)	32i
w₉ (b₂), cm⁻¹	628 (67)ᵃ	660 (64)	642	655 (110)ᵃ	717 (160)	663
w₁₀ (b₂), cm⁻¹	262 (3)ᵃ	284 (5)	268	246 (6)ᵃ	281 (7)	261
w₁₁ (b₂), cm⁻¹	209 (8)ᵃ	239 (7)	220	226 (1)ᵃ	256 (1)	234
w₁₂ (b₂), cm⁻¹	115 (0)ᵃ	166 (3)	117	106 (3)ᵃ	122 (3)	109

ᵃ Values in parentheses represent relative absorbance intensities in the IR spectrum (km/mol).

ᵇ E_tot=- a.u., ᶜ E_tot=- a.u. (all at CCSD(T)/6-311+G(2df)//CCSD(T)/6-311+G*).

ᶜ E_tot=- a.u., ᶜ E_tot=- a.u. (all at CCSD(T)/6-311+G(2df)//CCSD(T)/6-311+G*).

Table 4-5. Comparison of the experimental VDE's to calculated VDE's for structure

II of the Al_3N^- anion.

Feature	VDE (exp.) eV	Final State and Electronic Configuration	VDE (theo.), eV		
			TD-B3LYP[b]	OVGF[b]	ΔCCSD(T)[b]
X	1.19 (4)	$^1A_1$, $1b_1^2 3a_1^2 2b_2^2 4a_1^2 3b_2^0$	1.15	1.16 (0.90)[a]	1.06
A	2.78 (3)	$^3B_2$, $1b_1^2 3a_1^2 2b_2^2 4a_1^1 3b_2^1$	2.78	2.92 (0.85)	2.71
B	3.06 (3)	$^3A_1$, $1b_1^2 3a_1^2 2b_2^1 4a_1^2 3b_2^1$	2.99	3.37 (0.85)[a]	3.15
C	3.39 (4)	$^1B_2$, $1b_1^2 3a_1^2 2b_2^2 4a_1^1 3b_2^1$	3.33		
D	3.69 (4)	$^1A_1$, $1b_1^2 3a_1^2 2b_2^1 4a_1^2 3b_2^1$	3.33		
E	5.20 (5)	$^3B_2$, $1b_1^2 3a_1^1 2b_2^2 4a_1^2 3b_2^1$	4.39	4.71 (0.79)[a]	
		$^3A_2$, $1b_1^1 3a_1^2 2b_2^2 4a_1^2 3b_2^1$	4.88	5.45 (0.90)[a]	

[a] Values in parentheses represent the pole strength of the OVGF calculation.

[b] 6-311+G(2df) basis set.

Table 4-6. Comparison of the experimental VDE's to calculated VDE's for Al_4N^-.

Feature	VDE (exp.) eV	Final State and Electronic Configuration	VDE (theo.), eV		
			TD-B3LYP[c]	OVGF[c]	ΔCCSD(T)[c]
Structure VII					
X	2.32 (3)	$^2B_{2g}$, $1a_{2u}^2 2a_{1g}^2 1b_{1g}^2 2e_u^4 1b_{2g}^1$	2.16	2.26 (0.87)	2.29
A	3.41 (2)	^2E_u, $1a_{2u}^2 2a_{1g}^2 1b_{1g}^2 2e_u^3 1b_{2g}^2$	3.38	3.63 (0.84)	3.52
B	3.74 (5)	$^2B_{1g}$, $1a_{2u}^2 2a_{1g}^2 1b_{1g}^1 2e_u^4 1b_{2g}^2$	3.47	3.56 (0.85)	3.53
C	5.40 (5)	$^2A_{1g}$, $1a_{2u}^2 2a_{1g}^1 1b_{1g}^2 2e_u^4 1b_{2g}^2$	5.21	5.79 (0.75)[b]	
D		$^2A_{2u}$, $1a_{2u}^1 2a_{1g}^2 1b_{1g}^2 2e_u^4 1b_{2g}^2$	5.83		5.97
Structure VIII					
	1.7-1.8	$^2A_1$, $1b_1^2 4a_1^2 2b_2^2 5a_1^2 6a_1^1$	1.63	1.84	1.72
	1.9	$^2B_1$, $1b_1^2 4a_1^2 2b_2^2 5a_1^2 2b_1^1$	1.90	2.01	2.03
	2.8	$^4B_1$, $1b_1^2 4a_1^2 2b_2^2 5a_1^1 6a_1^1 2b_1^1$	2.79	2.82	2.82

[a] Values in parentheses represent the pole strength of the OVGF calculation.

[b] The pole strength is too low. This value is not reliable.

[c] 6-311+G(2df) basis set.

Table 4-7. Comparison of the experimental VDE's to calculated VDE's for the structure XXII of Al_5N^-.

Feature	VDE (exp.) eV	Final State and Electronic Configuration	VDE (theo.), eV		
			TD-B3LYP[d]	UOVGF[d]	ΔCCSD(T)[d]
X	1.89 (4)				
x	2.01 (4)	$^1A_1$, $1b_1^2 4a_1^2 2b_2^2 3b_2^2 5a_1^2 6a_1^2 2b_1^0$	1.92	2.06 (0.88)	2.01
A	2.29 (3)				
B	2.66 (3)	$^3B_1$, $1b_1^2 4a_1^2 2b_2^2 3b_2^2 5a_1^2 6a_1^1 2b_1^1$	2.52	2.61 (0.86)	2.63
C	2.90 (3)	$^1B_1$, $1b_1^2 4a_1^2 2b_2^2 3b_2^2 5a_1^2 6a_1^1 2b_1^1$	2.77	b	b
D	3.27 (3)	$^3B_1$, $1b_1^2 4a_1^2 2b_2^2 3b_2^2 5a_1^1 6a_1^2 2b_1^1$	3.22	3.29 (0.84)	b
E	3.51 (3)	$^1B_1$, $1b_1^2 4a_1^2 2b_2^2 3b_2^2 5a_1^1 6a_1^2 2b_1^1$	3.47	b	b
F	3.87 (3)	$^1A_2$, $1b_1^2 4a_1^2 2b_2^2 3b_2^1 5a_1^2 6a_1^2 2b_1^1$	3.72	b	b
		$^3A_2$, $1b_1^2 4a_1^2 2b_2^2 3b_2^1 5a_1^2 6a_1^2 2b_1^1$	3.75	4.17 (0.84)	3.92
		$^3A_2$, $1b_1^2 4a_1^1 2b_2^1 3b_2^1 5a_1^2 6a_1^2 2b_1^1$	4.07	4.08 (0.83)	b
		$^1A_2$, $1b_1^2 4a_1^2 2b_2^1 3b_2^1 5a_1^2 6a_1^2 2b_1^1$	4.52	b	b
		$^3B_1$, $1b_1^2 4a_1^1 2b_2^2 3b_2^2 5a_1^2 6a_1^2 2b_1^1$	4.79	5.40 (0.78)[c]	b

[a] Values in parentheses represent the pole strength of the UOVGF calculation.

[b] This value cannot be calculated at the this level of theory.

[c] The pole strength is too low. This value is not reliable.

[d] 6-311+G(2df) basis set.

Table 4-8. Comparison of the experimental VDE's to calculated VDE's for the structure XXIII of Al_5N^-.

Feature	VDE (exp.) eV	Final State and Electronic Configuration	VDE (theo.), eV		
			TD-B3LYP[d]	OVGF[d]	ΔCCSD(T)[d]
X	1.89 (4)	$^1A_1$, $2b_1^2 4a_1^2 2b_2^2 5a_1^2 6a_1^2 7a_1^0$	1.82	2.04 (0.86)	1.80
x	2.01 (4)				
A	2.29 (3)	$^3A_1$, $2b_1^2 4a_1^2 2b_2^2 5a_1^2 6a_1^1 7a_1^1$	2.04	2.17 (0.87)	2.23
B	2.66 (3)	$^1A_1$, $2b_1^2 4a_1^2 2b_2^2 5a_1^2 6a_1^1 7a_1^1$	2.64	b	b
C	2.90 (3)				
D	3.27 (3)	$^3A_1$, $2b_1^2 4a_1^2 2b_2^2 5a_1^1 6a_1^2 7a_1^1$	3.33	3.61 (0.85)	b
E	3.51 (3)	$^1A_1$, $2b_1^2 4a_1^2 2b_2^2 5a_1^1 6a_1^2 7a_1^1$	3.56	b	b
F	3.87 (3)				
		$^3B_2$, $2b_1^2 4a_1^2 2b_2^1 5a_1^2 6a_1^2 7a_1^1$	4.37	4.24 (0.79)c	4.16
		$^1B_2$, $2b_1^2 4a_1^2 2b_2^1 5a_1^2 6a_1^2 7a_1^1$	4.48	b	b
		$^3A_1$, $2b_1^2 4a_1^1 2b_2^2 5a_1^2 6a_1^2 7a_1^1$	4.40	5.17 (0.85)	b
		$^3B_1$, $2b_1^1 4a_1^2 2b_2^2 5a_1^2 6a_1^2 7a_1^1$	4.48	4.53 (0.82)	4.37
		$^1A_1$, $2b_1^2 4a_1^1 2b_2^2 5a_1^2 6a_1^2 7a_1^1$	4.84	b	b
		$^1B_1$, $2b_1^1 4a_1^2 2b_2^2 5a_1^2 6a_1^2 7a_1^1$	5.09	b	b

[a] Values in parentheses represent the pole strength of the OVGF calculation.

[b] This value cannot be calculated at the this level of theory.

[c] The pole strength is too low. This value is not reliable.

[d] 6-311+G(2df) basis set.

Table 4-9. Comparison of the experimental VDE's to calculated VDE's for the structure XXIV of $Al_5N^{..}$.

Feature	VDE (exp.) eV	Final State and Electronic Configuration	VDE (theo.), eV		
			TD-B3LYP[c]	OVGF[c]	ΔCCSD(T)[c]
X	1.89 (4)				
x	2.01 (4)	$^1A'$, $4a'^25a'^26a'^22a''^27a'^23a''^28a'^0$	1.98	2.12(0.88)	2.01
A	2.29 (3)				
B	2.66 (3)	$^3A''$, $4a'^25a'^26a'^22a''^27a'^23a''^18a'^1$	2.44	2.50(0.87)	2.60
		$^1A''$, $4a'^25a'^26a'^22a''^27a'^23a''^18a'^1$	2.65		
C	2.90 (3)			[b]	[b]
D	3.27 (3)	$^3A'$, $4a'^25a'^26a'^22a''^27a'^13a''^28a'^1$	3.34	3.44(0.86)	3.44
E	3.51 (3)	$^1A'$, $4a'^25a'^26a'^22a''^27a'^13a''^28a'^1$	3.56	[b]	[b]
F	3.87 (3)	$^3A'$, $4a'^25a'^26a'^12a''^27a'^23a''^28a'^1$	3.68	3.94(0.85)	[b]
		$^3A''$, $4a'^25a'^26a'^22a''^17a'^23a''^28a'^1$	3.81	3.72(0.86)	[b]
		$^1A''$, $4a'^25a'^26a'^22a''^17a'^23a''^28a'^1$	3.99	[b]	[b]
		$^3A'$, $4a'^25a'^16a'^22a''^27a'^23a''^28a'^1$	4.27	4.42(0.84)	[b]
		$^1A'$, $4a'^25a'^16a'^22a''^27a'^23a''^28a'^1$	4.37	[b]	[b]
		$^1A'$, $4a'^15a'^26a'^22a''^27a'^23a''^28a'^1$	4.81	[b]	[b]

[a] Values in parentheses represent the pole strength of the OVGF calculation.
[b] This value cannot be calculated at the this level of theory.
[c] 6-311+G(2df) basis set.
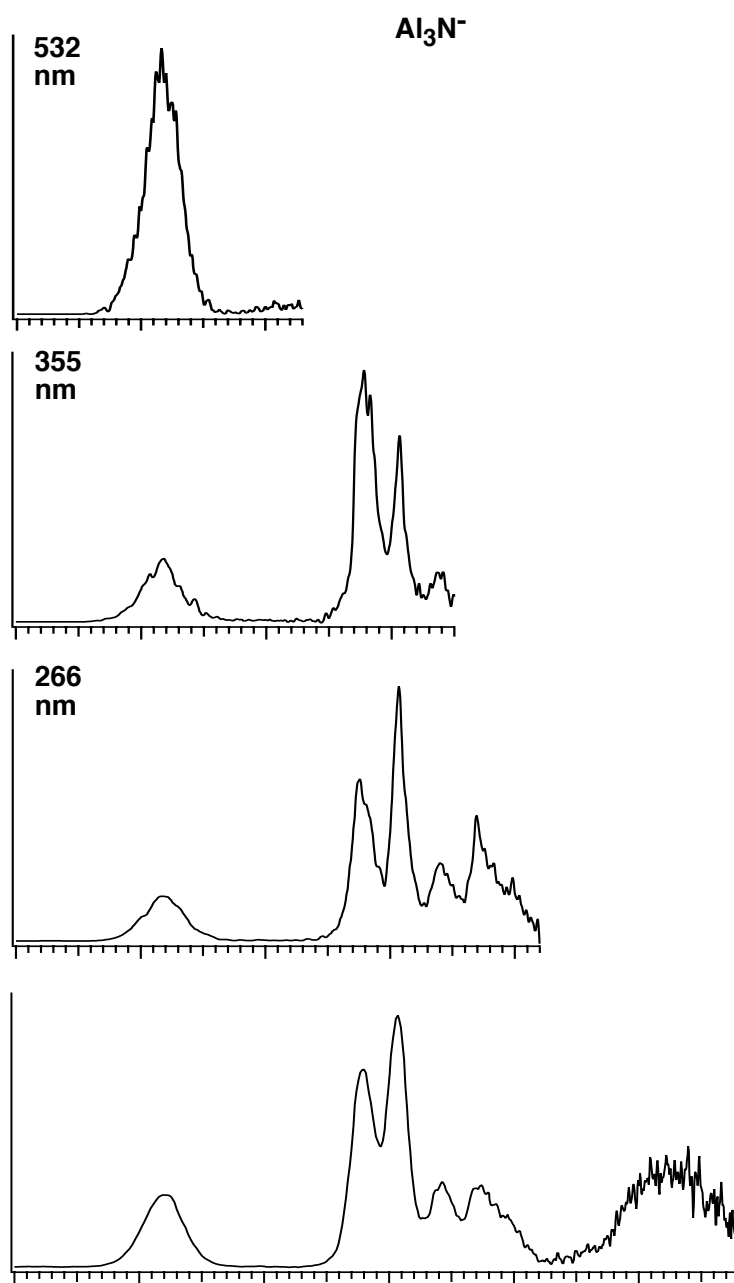
Figure 4-1. Photoelectron spectra of Al_3N^- at four photon energies: 532 (2.331 eV), 355 (3.496 eV), 266 (4.661 eV), and 193 nm (6.424 eV).
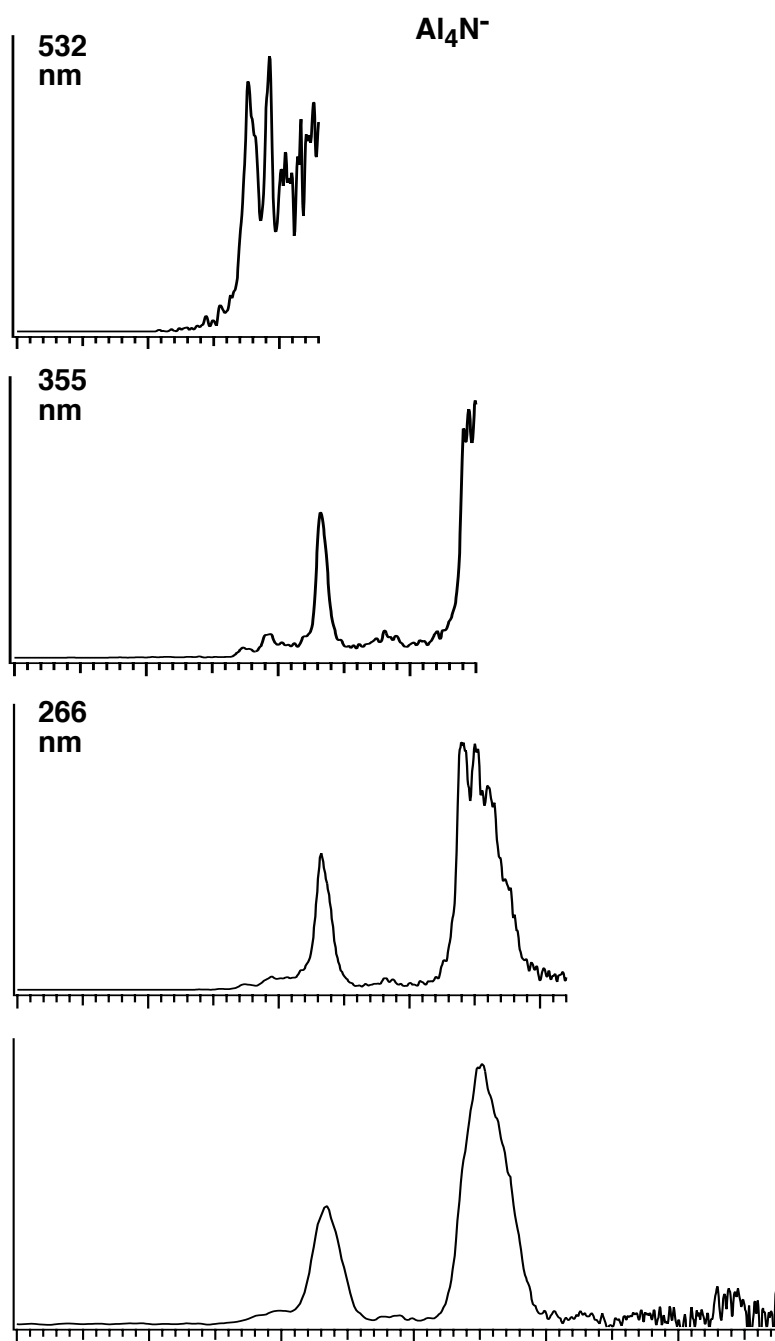
Figure 4-2. Photoelectron spectra of Al$_4$N$^-$ at four photon energies: 532 (2.331 eV), 355 (3.496 eV), 266 (4.661 eV), and 193 nm (6.424 eV).
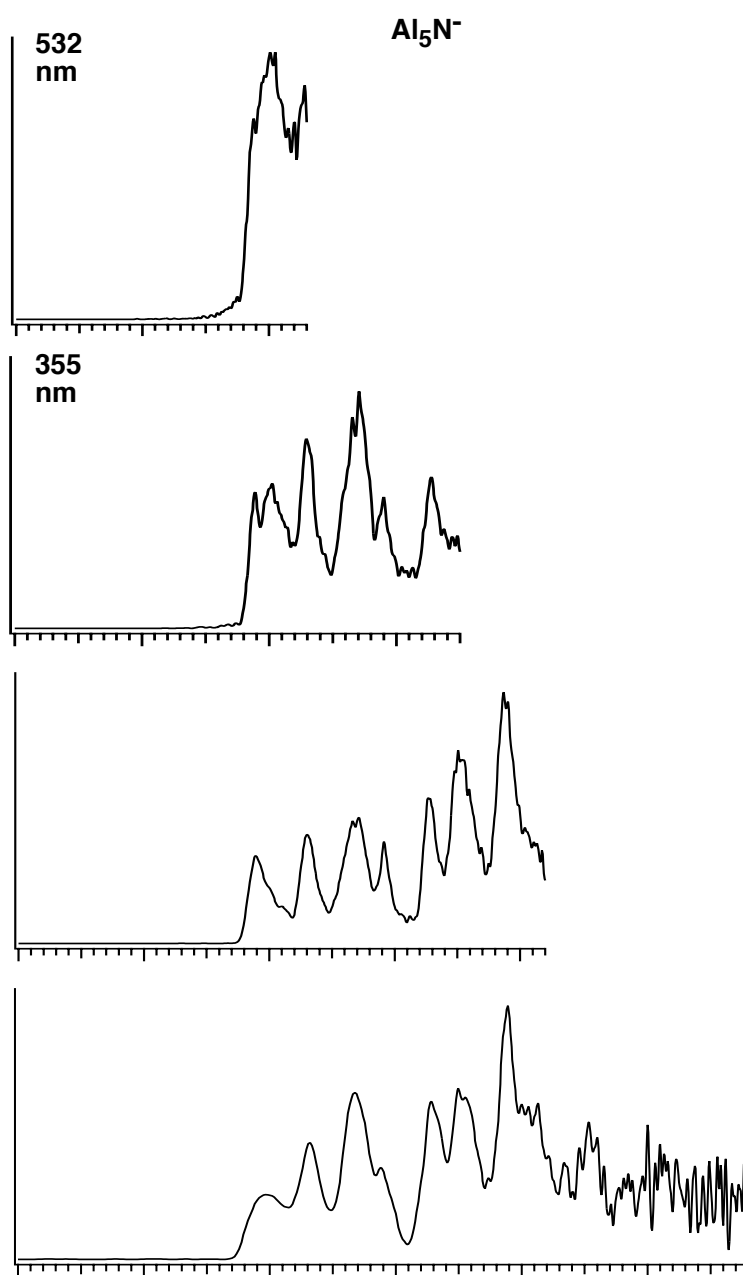
Figure 4-3. Photoelectron spectra of Al$_5$N$^-$ at four photon energies: 532 (2.331 eV), 355 (3.496 eV), 266 (4.661 eV), and 193 nm (6.424 eV).
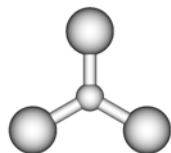
Al$_3$N

I. D$_{3h}$ (^{1}A$_1$)
ΔE = 0.0 kcal/mol
[ΔE = 0.0 kcal/mol]
NImag=0
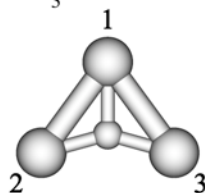
Al$_3$N$^-$
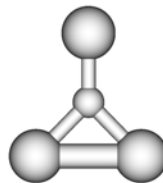
II. C$_{2v}$ (^{2}B$_2$)   III. C$_{2v}$ (^{2}B$_1$)
ΔE = 0.0 kcal/mol   ΔE = 19.7 kcal/mol
[ΔE = 0.0 kcal/mol]   [ΔE = 17.2 kcal/mol]
NImag=0   NImag=0

Figure 4-4. The lowest isomers for Al$_3$N and Al$_3$N$^-$. Relative energies are presented at CCSD(T)/6-311+G(2df)//B3LYP/6-311+G* and at B3LYP/6-311+G* in brackets. Nimag is the number of imaginary frequencies calculated at B3LYP/6-311+G*.

Al$_4$N

IV. D$_{4h}$ (^{2}B$_{2g}$)
ΔE = 0.0 kcal/mol
[ΔE = 0.0 kcal/mol]
NImag=0

V. C$_{2v}$ (^{2}A$_1$)
ΔE = 5.4 kcal/mol
[ΔE = 3.3 kcal/mol]
NImag=0

VI. C$_{2v}$ (^{2}B$_1$)
ΔE = 10.9 kcal/mol
[ΔE = 10.7 kcal/mol]
NImag=0

Al$_4$N$^-$

VII. D$_{4h}$ (^{1}A$_{1g}$)
ΔE = 0.0 kcal/mol
[ΔE = 0.0 kcal/mol]
NImag=0

VIII. C$_{2v}$ (^{3}B$_1$)
ΔE = 20.6 kcal/mol
[ΔE = 18.7 kcal/mol]
NImag=0

IX. C$_s$ (^{1}A')
ΔE = 21.5 kcal/mol
[ΔE = 20.0 kcal/mol]
NImag=0
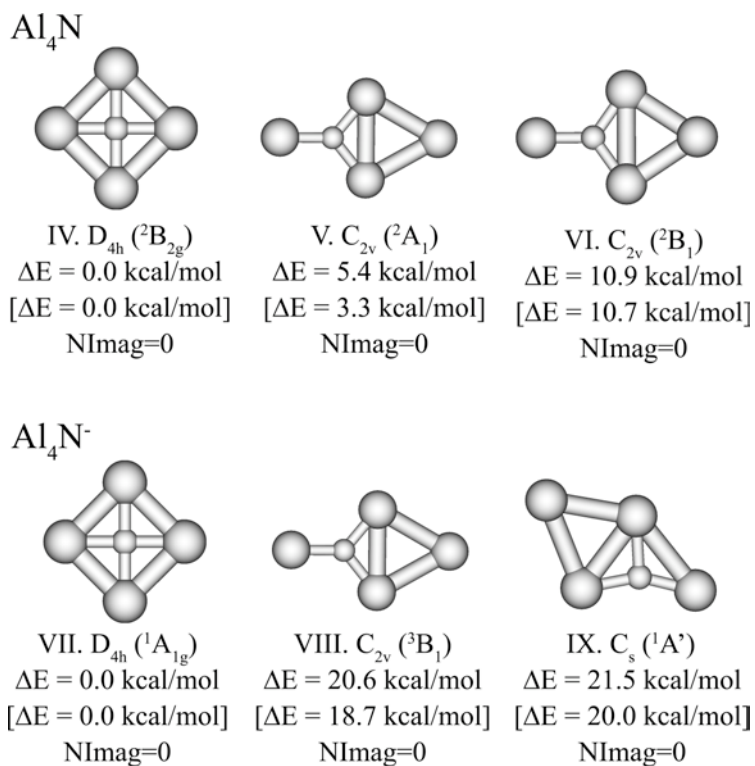
Figure 4-5. The lowest isomers for Al$_4$N and Al$_4$N$^-$. Relative energies are presented at CCSD(T)/6-311+G(2df)//B3LYP/6-311+G* and at B3LYP/6-311+G* in brackets. Nimag is the number of imaginary frequencies calculated at B3LYP/6-311+G*.

Al_5N

X. C_{2v} ($^1A_1$)
ΔE = 0.0 kcal/mol
[ΔE = 0.0 kcal/mol]
NImag = 0

XI. C_{2v} ($^1A_1$)
ΔE = 1.3 kcal/mol
[ΔE = 6.8 kcal/mol]
NImag = 1

XII. C_s ($^1A'$)
ΔE = 5.9 kcal/mol
[ΔE = 9.4 kcal/mol]
NImag = 1

XIII. C_{2v} ($^1A_1$)
ΔE = 7.5 kcal/mol
[ΔE = 9.9 kcal/mol]
NImag = 0

XIV. C_{2v} ($^3A_1$)
ΔE = 10.5 kcal/mol
[ΔE = 10.9 kcal/mol]
NImag = 2

XV. C_{2v} ($^3B_1$)
ΔE = 12.1 kcal/mol
[ΔE = 13.6 kcal/mol]
NImag = 0

XVI. C_{2v} ($^3B_2$)
ΔE = 12.2 kcal/mol
[ΔE = 11.3 kcal/mol]
NImag = 1

XVII. C_{3v} ($^3A_1$)
ΔE = 13.4 kcal/mol
[ΔE = 13.5 kcal/mol]
NImag = 0

XVIII. C_{4v} ($^1A_1$)
ΔE = 13.5 kcal/mol
[ΔE = 23.0 kcal/mol]
NImag = 2

XIX. C_{4v} ($^1A_1$)
ΔE = 13.6 kcal/mol
[ΔE = 15.7 kcal/mol]
NImag = 2

XX. C_s ($^3A''$)
ΔE = 15.6 kcal/mol
[ΔE = 16.0 kcal/mol]
NImag = 0

XXI. C_{2v} ($^1A_1$)
ΔE = 16.5 kcal/mol
[ΔE = 14.5 kcal/mol]
NImag = 0

Al_5N^-

XXII. C_{2v} ($^2B_1$)
ΔE = 0.0 kcal/mol
[ΔE = 0.0 kcal/mol]
NImag = 0

XXIII. C_{2v} ($^2A_1$)
ΔE = 3.0 kcal/mol
[ΔE = 5.4 kcal/mol]
NImag = 1

XXIV. C_s ($^2A'$)
ΔE = 4.2 kcal/mol
[ΔE = 6.2 kcal/mol]
NImag = 0

XXV. C_s ($^2A''$)
ΔE = 6.3 kcal/mol
[ΔE = 6.3 kcal/mol]
NImag = 0

XXVI. C_{2v} ($^2A_1$)
ΔE = 8.7 kcal/mol
[ΔE = 7.1 kcal/mol]
NImag = 0

XXVII. C_s ($^4A''$)
ΔE = 15.9 kcal/mol
[ΔE = 14.6 kcal/mol]
NImag = 0

XXVIII. C_{2v} ($^4A_1$)
ΔE = 18.4 kcal/mol
[ΔE = 19.9 kcal/mol]
NImag = 0

XXIX. C_{2v} ($^2B_1$)
ΔE = 20.0 kcal/mol
[ΔE = 14.5 kcal/mol]
NImag = 1

Figure 4-6. The lowest isomers for Al_5N and Al_5N^-. Relative energies are presented at CCSD(T)/6-311+G(2df)//B3LYP/6-311+G* and at B3LYP/6-311+G* in brackets. Nimag is the number of imaginary frequencies calculated at B3LYP/6-311+G*.

HOMO, 3b$_2$ HOMO-1, 4a$_1$ HOMO-2, 2b$_2$ HOMO-3, 3a$_1$

HOMO-4, 1b$_1$ HOMO-5, 2a$_1$ HOMO-6, 1b$_2$ HOMO-7, 1a$_1$
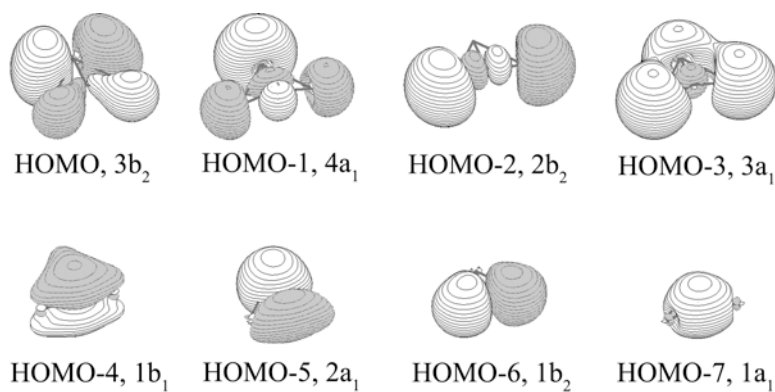
Figure 4-7. Valence molecular orbitals for the structure II of Al$_3$N$^-$ (UHF/6-311+G*).

HOMO, 1b$_{2g}$ HOMO-1, 1b$_{1g}$ HOMO-2, 2e$_u$

HOMO-2', 2e$_u$ HOMO-3, 2a$_{1g}$ HOMO-4, 1a$_{2u}$

HOMO-5, 1e$_u$ HOMO-5', 1e$_u$ HOMO-6, 1a$_{1g}$
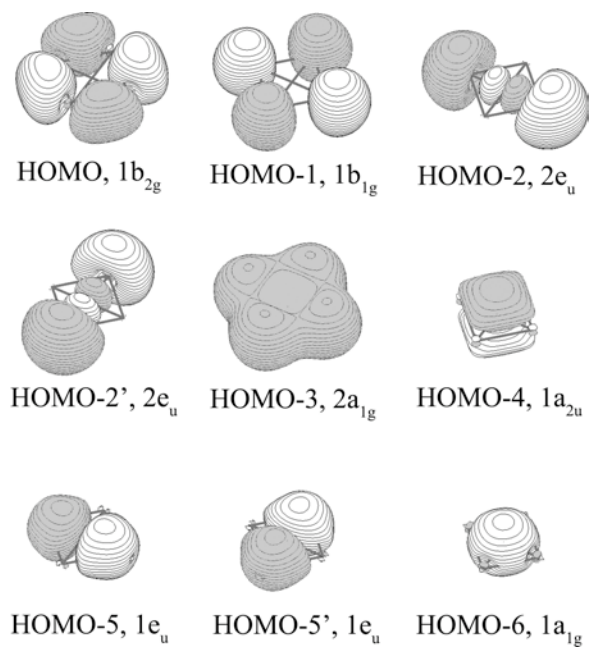
Figure 4-8. Valence molecule orbitals for the structure VII of Al$_4$N$^-$ (RHF/6-311+G*).

71

HOMO, 1b₁   HOMO-1, 7a₁   HOMO-2, 6a₁   HOMO-3, 3b₂

HOMO-4, 2b₂   HOMO-5, 5a₁   HOMO-6, 4a₁   HOMO-7, 3a₁

HOMO-8, 1b₂   HOMO-9, 2a₁   HOMO-10, 1a₁
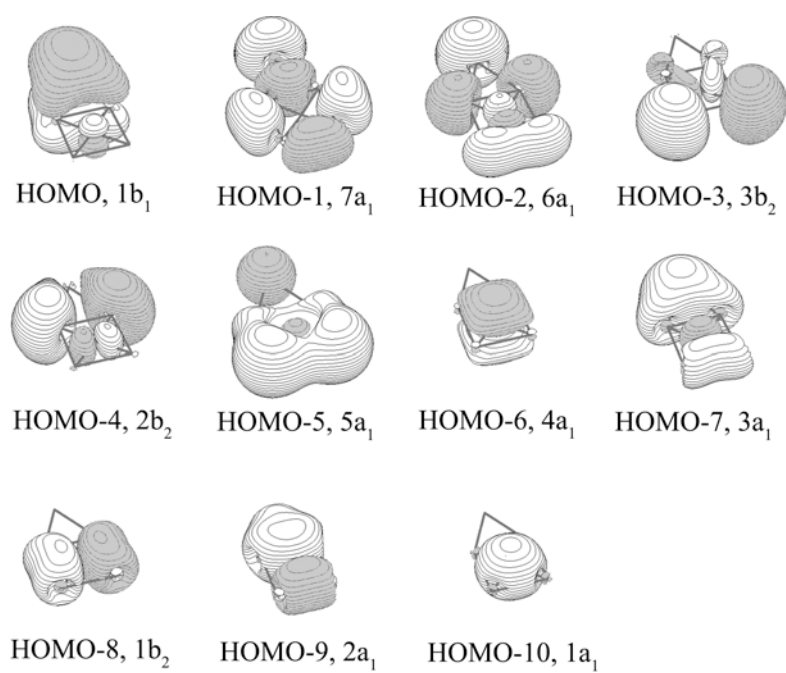
Figure 4-9. Valence molecule orbitals for the structure XXII of Al_5N^- (UHF/6-311+G*).

CHAPTER 5

PROBING THE STRUCTURE AND BONDING IN Al_6N^- AND Al_6N BY

PHOTOELECTRON SPECTROSCOPY AND AB INITIO CALCULATIONS[1]

Abstract

The electronic and geometrical structure of a nitrogen-doped Al_6^- cluster (Al_6N^-) is investigated using photoelectron spectroscopy and ab initio calculations. Photoelectron spectra of Al_6N^- have been obtained at three photon energies with seven resolved spectral features. The electron affinity of Al_6N has been determined to be 2.58 ± 0.04 eV. Global minimum structure searches for A_6N^- and its corresponding neutral are performed using several theoretical methods. Vertical electron detachment energies, calculated using three different methods for the lowest energy structure and a low-lying isomer, are compared with the experimental data. The ground state structure of Al_6N^- is established from the joint experimental and theoretical study to consist of an Al_2 dimer bonded to the top of a quasi-planar tetracoordinated N unit, Al_4N^- or it can be viewed as a distorted trigonal prism structure with the N atom bonded in one of the prism faces. For neutral Al_6N, three low-lying isomers are found to compete for the global minimum, two of which are built from the tetracoordinated Al_4N unit. The chemical bonding in Al_6N^- is discussed on the basis of molecular orbital and natural bond analyses.

5-1. Introduction

Aluminum nitride is an important semiconductor material, but there have been relatively few experimental and theoretical studies on small aluminum nitride clusters.[1-11] Recently, Li and Wang reported an extensive set of photoelectron spectra of Al_xN^- clusters from $x = 2\text{-}22$ at 193 nm and compared them to those of pure Al_x^- clusters.[10] They found spectral similarity between Al_xN^- and Al_{x-1}^- and suggested that there is a strong charge transfer to form formally N^{3-} in the nitrogen-doped aluminum clusters. In a very recent study,[12] we combined photoelectron spectroscopy (PES) with global minimum structural search, using a gradient embedded genetic algorithm followed by high level ab initio calculations, to elucidate the structures and bonding for a series of nitrogen doped small aluminum clusters, Al_xN^- ($x = 3\text{-}5$). Vertical electron detachment energies calculated for the lowest energy structures were found to be in excellent agreement with the experimental observations. Planar structures were established for all the three Al_xN^- ($x = 3\text{-}5$) anions. In particular, we found that Al_4N^- is a highly stable cluster, isoelectronic to the penaatomic tetracoordianted planar carbon molecule, CAl_4^{2-}.[13,14] The global minimum structure of Al_5N^- simply consists of a planar Al_4N^- with the extra Al atom bonded to its side in the same plane,[12] suggesting the stability and robustness of the planar tetracoordinated N structural unit. In the current article, we report a joint PES and ab inito study on Al_6N^- and Al_6N to examine if the planar Al_4N structural unit plays any role in larger N-doped aluminum clusters.

For the Al_6N cluster, a number of different structures have been suggested from prior theoretical studies,[3,7-9] but there is no consensus about its global minimum. Nayak,

Khanna and Jena[3] reported a global minimum structure with the N atom capping the triangular face of a distorted Al_6 octahedron. Leskiw *et al.*[7] and Guo and Wu[9] reported a global minimum structure with the N atom located inside a distorted Al_6 octahedron. Ling, Song, and Cao[8] reported a very low-symmetry structure, which can be approximately viewed as a N atom inside a highly distorted Al_6 prism structure.

In the current work, well-resolved photoelectron spectra of Al_6N^- at three photon energies are compared to theoretical calculations. We found that Al_6N^- possesses a C_{2v} global minimum structure, which consists of an Al_2 dimer bonded on the top of a planar Al_4N^- unit. It can also be viewed as an N atom located in one of the faces of a distorted Al_6 trigonal prism. For neutral Al_6N, we found three low-lying isomers with very close energies competing for the global minimum. Two of the three low-lying structures are related to the planar Al_4N, confirming the stability and robustness of the planar tetracoordinated N structural unit.

5-2. Experimental Method

The experiment was performed using a magnetic-bottle PES apparatus with a laser vaporization cluster source, details of which have been published elsewhere.[15] Briefly, the Al_6N^- clusters were produced by laser vaporization of a pure Al disk target with a 5% N_2/He carrier gas. Under this condition, only clusters doped with one nitrogen atom were formed.[10] The Al_6N^- anion clusters of interest were size-selected and decelerated before crossing with a detachment laser beam. We have reported PES spectra of Al_xN^- for x = 2– 22 at 193 nm (6.424 eV) recently along with the Al_xN^- mass

distribution.[10] In the current study, we have obtained additional photoelectron spectra for Al_6N^- at two lower photon energies, 355 (3.496 eV) and 266 (4.661eV). The lower photon energy spectra yielded better resolved spectra, which were necessary to compare with theoretical calculations. The electron energy resolution of our PES apparatus was DE/E ~ 3%, i.e. about 30 meV for 1 eV electrons.

5-3. Theoretical Methods

We performed initial search for the global minimum of Al_6N^- and Al_6N using our gradient embedded genetic algorithm (GEGA) program.[16,17] We used a hybrid method known in the literature as B3LYP[18-20] with the small split-valence basis sets (3-21G)[21] for energy, gradient and force calculations. We reoptimized geometries and calculated frequencies for all isomers found for Al_6N^- and Al_6N at the B3LYP/6-311+G* level of theory. We also recalculated the two lowest energy structures of Al_6N^- using a coupled-cluster method with single, double, and noniterative triple excitations (CCSD(T))[22-24] based on the RHF formalism with the polarized split-valence basis sets (6-311+G*).[25-27] Total energies of the local minimum structures were also recalculated at the CCSD(T)/6-311+G(2df)//B3LYP/6-311+G* level of theory. We performed additional single point calculations at the multi-configuration self-consistent field method (CASSCF(X,Y)[28,29] with X active electrons and Y active molecular orbitals in order to test the validity of the one-electron approximation.

The Al_6N^- vertical electron detachment energies (VDEs) were calculated using the R(U)CCSD(T)/6-311+G(2df), the outer valence Green Function method (ROVGF/6-

311+G(2df))[30-34] at the RCCSD(T)/6-311+G* geometries, and the time-dependent DFT method[35,36] (TD B3LYP/6-311+G(2df)) at the B3LYP/6-311+G* geometries. Core electrons were frozen in treating the electron correlation at the RCCSD(T) and ROVGF levels of theory.

The B3LYP, R(U)CCSD(T), R(U)OVGF ab initio calculations were performed using the Gaussian 98 and 03 programs.[37,38] Molecular orbital visualization has been done using the MOLDEN3.4 program.[39]

5-4. Experimental Results

The PES spectra of Al_6N^- at three photon energies are shown in Figure 5-1. Two bands were observed in the 355 nm spectrum (Figure 5-1a), a relatively sharp band (X) at a VDE of 2.66 eV and a broad band, which seemed to consist of two overlapping features (A and B). A long tail was observed at the lower binding energy side, which depended on the detachment photon flux at 355 nm and was due to thermionic emission processes.[40] The thermionic emission was less severe at higher photon energies because of the relatively lower photon fluxes used. The X band was relatively sharp, suggesting a small geometrical change from the ground state of Al_6N^- to that of neutral Al_6N. From the onset of the X band, we obtained an adiabatic detachment energy (ADE) of 2.58 ± 0.04 eV, which defines the electron affinity of neutral Al_6N. At 266 nm (Figure 5-1b), the bands A and B were resolved more clearly and a number of new features were also revealed. Two relatively sharp peaks were observed at 4.00 eV (C) and 4.06 eV (D), which could be due to the 0-0 and 0-1 transitions of a vibrational progression. However,

since there were no other regular peaks with a similar spacing at higher binding energies beyond peak D, we tentatively assigned the C and D as the origins of two electronic transitions. As will be shown below, these assignments were born out in our theoretical calculations. At 193 nm (Figure 5-1c), two more closely spaced bands were observed at VDEs of 4.51 eV (E) and 4.70 eV (F). In addition, the relative intensities of the A and B bands, as well as the C and D bands, appeared to increase with the photon energies.

The VDEs of all the observed bands are given in Tables 5-1 and 5-2, where they are compared with theoretical calculations for the two lowest-lying isomers of Al_6N^-.

5-5. Theoretical Results

Al_6N^-. We initially performed the GEGA search for the global minimum structure at B3LYP/3-21G level of theory separately for both singlet and triplet states. Figure 5-2 displays the low-lying structures found by the GEGA search and recalculated at the B3LYP/6-311+G* geometry with relative total energies at CCSD(T)/6-311+G(2df)//B3LYP/6-311+G*.

The structure II (Figure 5-2) was found by GEGA at the B3LYP/3-21G level to be the global minimum, which is the same as reported by Leskiw et al.[7] and Guo and Wu[9]. However, at the B3LYP/6-311+G*, CCSD(T)/6-311+G*, and CCSD(T)/6-311+G(2df)//B3LYP/6-311+G* levels of theory, the global minimum is the structure I, which is more stable than the structure II at the above levels of theory by 0.8, 2.4, and 1.5 kcal/mol, respectively. The Hatree-Fock function was found to be dominant (C_{HF}=0.951

out of 31,8787 configurations) in CASSCF(10,10)/6-311+G* calculations for the structure I. The global minimum structure I seems to have been missed in previous studies of Al_6N^-. At CCSD(T)/6-311+G* the structure II has one imaginary frequency (Table 5-3). However, the vibrationally averaged structure II can be considered to have the C_{2v} symmetry. Among other low-lying isomers, we mention the structure III, which consists of an NAl moiety bonded to a capped-tetrahedral Al_5 cluster, is higher in energy than the global minimum structure by 7.7 kcal/mol (B3LYP/6-311+G*) and 10.1 (CCSD(T)/6-311+G(2df)//B3LYP/6-311+G*). The lowest triplet structure IV, which is related to the singlet structure II, is higher in energy than the global minimum structure by 10.5 kcal/mol (B3LYP/6-311+G*) and 12.4 (CCSD(T)/6-311+G(2df)//B3LYP/6-311+G*). We also identified a number of local minimum structures (Figure 5-2) with energies between 14 and 32 kcal/mol above the global minimum.

Al_6N. We initially performed the GEGA search for the global minimum structure of neutral Al_6N at B3LYP/3-21G level of theory separately for doublet and quartet states. Figure 5-3 shows the low-lying structures found by the GEGA search and recalculated at the B3LYP/6-311+G* geometry with relative total energies at CCSD(T)/6-311+G(2df)//B3LYP/6-311+G*.

The global minimum structure XVIII (Figure 5-3) at the B3LYP/3-21G level found by GEGA is the same as reported by Leskiw et al.[7] and Guo and Wu[9]. Ling, Song, and Cao[8] found a global minimum structure similar to the structure XVIII, but without any symmetry. Note the structure XVIII in Figure 5-3 possesses C_{2v} symmetry. Nayak, Khanna and Jena[3] reported a global minimum structure for Al_6N, in which a nitrogen

atom is coordinated outside the face of a distorted Al_6 octahedron. However, at the B3LYP/6-311+G* level of theory the global minimum is the structure XIX, which has never been reported in the literature. At our highest CCSD(T)/6-311+G(2df)//B3LYP/6-311+G* level of theory the structure XVIII again becomes the most stable one, but it is only more stable than structure XIX by 0.7 kcal/mol. We also found that the structure XX, which corresponds to the global minimum of the anion (structure I), is also a very stable structure for the neutral, only 3.3 kcal/mol (B3LYP/6-311+G*) and 0.8 kcal/mol (CCSD(T)/6-311+G(2df)//B3LYP/6-311+G*) higher than the structure XVIII. In order to avoid the problem with a different spin-contamination at the UCCSD(T)/6-311+G(2df) level of theory for structures XVIII-XX, we evaluated energies of the structures XVIII-XX as a difference between total energy of the anion at the geometry of the neutral species (at RCCSD(T)/6-311+G(2df)//B3LYP/6-311+G*) and the first vertical electron detachment energy for the anion (at ROVGF/6-311+G(2df)//B3LYP/6-311+G*) at the geometry of the neutral species. In that approach the $<S^2>$ values are exactly 0.750. The structure XVIII was found again to be the global minimum with relative energies equal to 3.7 kcal/mol for the structure XIX and 1.8 kcal/mol for the structure XX. The energy differences for the three low-lying structures of Al_6N (XVIII, XIX, XX) are too small to allow us to conclude with certainty which one is the true global minimum. Notably, all other isomers, XXI-XXXI in Figure 5-3, are significantly higher in energy and will not be discussed further.

The molecular properties for the two low-lying structures of Al_6N^- (I and II) and the three low-lying structures of Al_6N (XVIII, XIX, and XX) are summarized in Tables 5-3 and 5-4, respectively.

5-6. Interpretations of the PES Spectra and

Comparison with the Calculated VDEs

We calculated the VDEs for structures I and II of Al_6N^- at the TD-B3LYP/6-311+G(2df), ROVGF/6-311+G(2df) and CCSD(T)/6-311+G(2df) levels of theory. The theoretical results are compared with the experimental data in Tables 5-1 and 5-2 for the two isomers, respectively.

The global minimum structure I has the $1a_1^2 1b_2^2 1b_1^2 2a_1^2 3a_1^2 2b_2^2 4a_1^2 2b_1^2 1a_2^2 3b_2^2 5a_1^2 3b_1^2$ ($^1A_1$) electronic configuration according to the ROVGF/6-311+G(2df) calculations. The calculated VDE from the $3b_1$-HOMO at three levels of theory is 2.41 eV (TD-B3LYP/6-311+G(2df)), 2.53 eV (ROVGF/6-311+G(2df)), and 2.63 eV (CCSD(T)/6-311+G(2df)), agreeing well with the experimental value for the ground state transition (X) with the measured VDE of 2.66 eV (Table 5-1). The next two detachment channels from $5a_1$-HOMO-1 and $3b_2$-HOMO-2 give very close VDEs in all three methods. Again the TD-DFT method gives slightly lower VDEs for these two detachment channels (3.14 and 3.22 eV). But the OVGF values (3.36 and 3.44 eV) are almost identical to the CCSD(T) values (3.36 and 3.44 eV), which are in excellent agreement the experimental measurements (3.25 and 3.40 eV). The calculated VDEs from the $1a_2$-HOMO-3 and $2b_1$-HOMO-4 from TD-DFT again

differ from the OVGE values, which are more reliable from the above discussion. The

OVGF values (4.20 and 4.21 eV) for these two detachment channels are somewhat larger

than the experiment (4.00 and 4.06 eV). We also note that the OVGF values for the two

relatively high-energy detachment channels, $4a_1$-HOMO-5 and $2b_2$–HOMO-6, are in

excellent agreement with the PES data (Table 5-1). The pole strength (UOVGF) in the

OVGF calculations was found to be between 0.81 and 0.86 for all the seven detachment

channels (Table 5-1), indicating that electron detachments from Al_6N^- can be primarily

described by one-electron processes. The overall agreement between the calculated

VDEs for the structure I and the experimental VDEs is excellent.

Since the structure II was found to be very close to the global minimum structure,

we also computed the VDEs for this isomer and compared them with the experimental

data in Table 5-2. The electronic configuration for the structure II was found to be

$1a_1^2 1b_2^2 2a_1^2 1b_1^2 3a_1^2 2b_2^2 4a_1^2 2b_1^2\ 3b_2^2 5a_1^2 1a_2^2 6a_1^2$ ($^1A_1$) at the ROVGF/6-311+G(2df) level

of theory. The calculated VDE from the $6a_1$-HOMO at three levels of theory is 2.56 eV

(TD-B3LYP/6-311+G(2df)), 2.67 eV (ROVGF/6-311+G(2df)), and XXX eV

(CCSD(T)/6-311+G(2df)), which also agrees well with the experimental VDE for the

ground state transition at 2.66 eV (Table 5-4). However, the calculated VDEs for the

higher binding energy channels completely disagree with the experiment. For example,

the experiment showed that the bands A and B have very close VDEs, whereas the

calculated VDEs for $1a_2$-HOMO-1 and $5a_1$-HOMO-2 show a very large separation in all

three methods (Table 5-2). The spectral pattern for the higher binding energy channels

also display large discrepancy with the PES data. Thus, we can rule out structure II as the carrier of the PES spectra for Al_6N^-.

Our results demonstrate again the sensitivity of the calculated PES spectra to cluster structures. Even though both structures I and II are very close in total energies and give similar first VDEs, their overall spectral patterns are totally different. The excellent agreement between the calculated VDEs for structure I and the experiment unequivocally confirms it as the global minimum for the Al_6N^- cluster.

5-7. Chemical Bonding in Al_6N^-

The global minimum structure I and the low-lying isomer II are both related to the planar tetracoordinate nitrogen molecule Al_4N^-. Our recent work[12] showed that Al_4N^- is isoelectronic to the first penta-atomic planar tetracoordiante carbon, Al_4C^{2-},[13,14] and is a very stable structural unit. We also found in that work that Al_5N^- is build upon the planar Al_4N^- unit with the extra Al bonded to one side of Al_4N^- in the same plane.[12] The ground state of Al_6N^- can be viewed as an Al_4N^- unit with the two extra Al atoms bonded to its top, whereas the low-lying isomer II can be viewed as an Al_4N^- unit with the two Al atoms bonded to each side of it on one edge. In neutral Al_6N, among the three lowest-lying isomers structures XIX and XX are built from the planar Al_4N unit. These observations suggest the robustness and stability of the planar Al_4N^- and Al_4N structural units, which may also play major roles in larger Al_xN^- clusters.

The ground state structure I and the low-lying isomer II for Al_6N^- can also be understood as a Jahn-Teller distortion from the corresponding high symmetry D_{3h} and O_h

structures, respectively. In order to proof these structural relationships, we added an extra pair of electrons to the lowest unoccupied MO in both structures (Figures 5-4 and 5-5). Geometry optimizations for Al_6N^{3-} started from the geometries of structures I and II led to high symmetry D_{3h} ($^1A_1'$, $1a_{1g}^2 1t_{1u}^6 2a_{1g}^2 2t_{1u}^6 1e_g^4 1t_{2g}^6$) and O_h ($^1A_{1g}$, $1a_1'^2 1a_2'' 1e'^4 2a_1'^2$ $2a_2''^2 2e'^4 1e''^4 3a_1'^2 3e'^4$) structures (see MOs in Figures 5-6 and 5-7). While isolated Al_6N^{3-} is not electronically stable, it has a repulsive Coulomb barrier on the electron ejection pathway and therefore it has a certain lifetime at the optimized O_h geometry. We discuss this metastable trianion only for showing that the low-symmetry global minimum structure of Al_6N^- can be explained on the basis of the Jahn-Teller effect. At the B3LYP/6-311+G* level of theory, the O_h ($^1A_{1g}$) structure is a local minimum and the D_{3h} ($^1A_1'$) structure was found to be a first order saddle point being 8.9 kcal/mol (B3LYP/6-311+G*) and 15.2 kcal/mol (CCSD(T)/6-311+G(2df)//B3LYP/6-311+G*) higher in energy than the O_h structure. Geometry optimization of the D_{3h} ($^1A_1'$) structure along the imaginary frequency mode led to the O_h structure. Thus, when a pair of electrons are removed from the $1t_{2g}$-HOMO (O_h) or from the $3e'$-HOMO (D_{3h}), the ensuring Jahn-Teller distortion lead to the structures II and I, respectively.

Calculated NBO charges at B3LYP/6-311+G* for the two lowest structures of Al_6N^- and Al_6N are summarized in Figure 5-8. In all four structures the effective charge on the central N atom is almost the same (-2.30 – -2.40 |e|), which is close to the ionic limit -3.00 |e|. Upon electron detachment from Al_6N^- the electron density is reduced primarily on aluminum atoms. That can be easily understood from the MO pictures of Al_6N^- (structures I and II) presented in Figures 5-5 and 5-6 because the the $3b_1$-HOMO in the

structure I and the $6a_1$-HOMO in the structure II are composed purely of aluminum

AO's only. Thus, the N atom in Al_6N^- and Al_6N can be viewed as N^{3-}, consistent with the

previous observation by Li and Wang that the electronic structures of Al_xN^- are similar to

pure aluminum clusters with one less aluminum, Al_{x-1}^-.[10]

The O_h structure of Al_6N^{3-} can be related to the recently reported O_h structure of

the isolated Al_6^{2-} cluster.[41] In Al_6^{2-}, the six lowest valence occupied MOs could be

approximately assigned to six lone pairs formed by primarily 3s-AOs of Al with one lone

pair at every Al atom. That takes 12 valence electrons out of 20. The remaining 8

valence electrons fill a completely delocalized $2a_{1g}$ MO, which is formed by the radial 3p-

AOs of six aluminum atoms, and a delocalized triply degenerate $1t_{2g}$-HOMO, which is

formed by the tangential 3p-AOs of the six aluminum atoms. This results in double

spherical aromaticity, where the $2a_{1g}$-MO is a spherical analog of a p-aromatic MO and

the $1t_{2g}$-MO is a spherical analog of s-aromatic MOs in planar aromatic systems (see

recent review ref. 42 for details). MOs for the O_h structure of Al_6N^{3-} are presented in

Figure 5-8. The lowest valence $1a_{1g}$-MO is primarily 2s-AO of the central nitrogen atom.

The next triply degenerate $1t_{1u}$-MO can be assigned to three $2p_x$-, $2p_y$-, and $2p_z$-AOs of

the nitrogen. The next six valence MOs ($2a_{1g}$, $2t_{1u}$, and $1e_g$) are primarily formed by the

3s-AOs of the aluminum atoms. Finally, the triply degenerate $1t_{2g}$-HOMO is formed by

the tangential 3p-AOs of the Al atoms, similar to the $1t_{2g}$-HOMO in Al_6^{2-}. Thus, in the O_h

structure of Al_6N^{3-} the chemical bonding can be approximately described as the central

atom carrying a effective charge -3 (N^{3-}), which is ionically bound to the octahedral Al_6

cluster. The Al_6 cluster keeps its octahedral structure in Al_6N^{3-}, because N^{3-} can perfectly

fit in the cavity of the octahedron and N^{3-} with its 8 valence electrons substitute a pair of electrons on the completely bonding $2a_{1g}$-MO in Al_6^{2-}. The tangential peripheral Al-Al bonding is the same in both clusters and thus Al_6N^{3-} is also tangential aromatic.

5-8. Conclusions

We combined photoelectron spectroscopy and theoretical calculations to elucidate the electronic structure and chemical bonding of Al_6N^-. Seven detachment channels were observed and compared with the calculated VDEs. Global minimum structures of Al_6N^- and Al_6N were identified first by using Gradient Embedded Genetic Algorithm (B3LYP/3-21G) followed by B3LYP/6-311+G* geometry and frequency calculations. The energies of the optimized structures were than refined at the CCSD(T)/6-311+G(2df)//B3LYP/6-311+G* level of theory. By comparing the theoretical VDEs with the experimental data we established that Al_6N^- has a distorted trigonal prism structure I (C_{2v}, $^1A_1$), which is build from a planar Al_4N^- unit with the two extra Al atoms bonded to its top on one side. Three low-lying isomers with close total energies were identified for the neutral Al_6N cluster, competing for the global minimum structure. The current work provides another example of the robustness and stability of the planar Al_4N unit, which may play a major structural role in larger N-doped aluminum clusters.

References

(1) Schleyer, P. v. R.; Boldyrev, A. I. *J. Chem. Soc., Chem. Comm.* **1991**, 1536.

(2) Zakrzewski, V. G.; Niessen, W. v.; Boldyrev, A. I.; Schleyer, P. v. R. *Chem. Phys.* **1993**, *174*, 167.

(3) Nayak, S. K.; Khana, S. N.; Jena, P. *Phys. Rev*. B, **1998**, *57*, 3787.

(4) Nayak, S. K.; Rao, B. K.; Jena, P.; Li, X.; Wang, L. S. *Chem. Phys. Lett*. **1999**, *301*, 379.

(5) Boo, B. H.; Liu, Z.; *J. Phys. Chem*. A, **1999**, *103*, 1250.

(6) Andrews, L.; Zhou, M.; Chertihin, G. V.; Bare, W. D.; Hannachi, Y.; *J. Phys. A*, **2000**, *104*, 1656.

(7) Leskiw, B. R.; Castleman, A. W. Jr., Ashman, C.; Khanna, S. N. *J. Chem. Phys*. **2001**, *114*, 1165.

(8) Ling, L.; Song, B.; Cao, P.-L. *J. Mol. Struct. Theochem*, **2005**, *728*, 215.

(9) Gou, L.; Wu, H.-S. *Int. J. Quant. Chem*. **2006**, *106,* 1250.

(10) Li, X.; Wang, L. S. *Eur. Phys. J. D*, **2005,** *34*, 9.

(11) Meloni, G.; Sheehan, S. M.; Parsons, B. F.; Neumark, D. M. *J. Phys. Chem. A*, **2006**, *110*, 3527.

(12) Averkiev, B. B.; Boldyrev, A. I.; Li, X.; Wang, L. S. *J. Chem. Phys*. in press.

(13) Li, X.; Wang, L. S.; Boldyrev, A. I.; Simons, J.   *J. Am. Chem. Soc*. **1999**, *121*, 6033.

(14) Li, X.; Zhang, H. F.; Wang, L. S.; Geske, G. D.; Boldyrev, A. I. *Angew. Chem. Int. Ed*. **2000**, *39*, 3630.

(15) Wang, L. S.; Cheng, H. S.; Fan, J. *J. Chem. Phys*. **1995**, *102*, 9480.

(16) Alexandrova, A. N.; Boldyrev, A. I.; Fu, Y-J.; Wang, X.-B.; Wang, L. S. *J. Chem. Phys*. **2004**, *121*, 5709.

(17) Alexandrova, A. N.; Boldyrev, A. I. *J. Chem. Theory and Comput*. **2005**, *1*, 566.

(18) Becke, A. D. *J. Chem. Phys.* **1993**, *98*, 5648.

(19) Vosko, S. H.; Wilk, L.; Nusair, M. *Can. J. Phys.* **1980**, *58*, 1200.

(20) Lee, C.; Yang, W.; Parr, R. G.; *Phys. Rev. B*, **1988**, *37*, 785.

(21) (a) Binkley, J. S.; Pople, J. A.; Hehre, W. J. *J. Am. Chem. Soc.* **1980**, *102*, 939; (b) Gordon, M. S.; Binkley, J. S.; Pople, J. A.; Pietro, W. J.; Hehre, W. J. *J. Am. Chem. Soc.* **1982**, *104*, 2797; (c) Pietro, W. J.; Francl, M. M.; Hehre, W. J.; Defrees, D. J.; Pople, J. A.; Binkley, J. S. *J. Am. Chem. Soc.* **1982**, *104*, 5039.

(22) Cizek, J. *Adv. Chem. Phys.* **1969**, *14*, 35.

(23) Knowles, P. J.; Hampel, C.; Werner, H.-J. *J. Chem. Phys.* **1993**, *99*, 5219.

(24) Raghavachari, K.; Trucks, G. W.; Pople, J. A.; Head-Gordon, M. *Chem. Phys. Lett.* **1989**, *157*, 479.

(25) McLean, A. D.; Chandler, G. S. *J. Chem. Phys.* **1980**, *72*, 5639.

(26) Clark, T.; Chandrasekhar, J.; Spitznagel, G. W.; Schleyer, P. v. R. *J. Comput. Chem.* **1983**, *4*, 294.

(27) Frisch, M. J.; Pople, J. A.; Binkley, J. S. *J. Chem. Phys.* **1984**, *80*, 3265.

(28) Bernardi, F.; Bottini, A.; McDougall, J. J. W.; Robb, M. A.; Schlegel, H. B. *Faraday Symp. Chem. Soc.* **1979**, *19*, 137.

(29) Frisch, M. J.; Ragazos, I. N.; Robb, M. A.; Schlegel, H. B. *Chem. Phys. Lett.* **1992**, *189*, 524.

(30) Cederbaum, L. S. *J. Phys B*, **1975**, *8*, 290.

(31) Niessen, W. v.; Shirmer, J.; Cederbaum, L. S. *Comput. Phys. Rep.* **1984,** *1*, 57.

(32) Zakrzewski, V. G.; Niessen, W. v. *J. Comput. Chem.* **1993**, *14*, 13.

(33) (a) Ortiz, J. V. *Int. J. Quant. Chem., Quant. Chem. Symp.* **1989,** 23, 321; (b) Lin, J. S.; Ortiz, J. V. *Chem. Phys. Lett.* **1990**, *171*, 197.

(34) Zakrzewski, V. G.; Ortiz, J. V.; Nichols, J. A.; Heryadi, D.; Yeager, D. L.; Golab, J. T. *Int. J. Quant. Chem.* **1996**, *60*, 29.

(35) Bauernshmitt, R.; Alrichs, R. *Chem. Phys. Lett.* **1996**, *256*, 454.

(36) Casida, M. E.; Jamorski, C.; Casida, K. C.; Salahub, D. R. *J. Chem. Phys.* **1998,** *108*, 4439.

(37) Frisch, M. J.; Trucks, G. M.; Schlegel, H. B.; Scuseria, G. E.; Robb, M. A.; Cheeseman, J. R.; Zakrzewski, V. G.; Montgomery, J. A.; Stratmann, R. E.; Burant, J. C.; Dapprich, S.; Millam, J. M.; Daniels, A. D.; Kudin, K. N.; Strain, M. C.; Farkas, O.; Tomasi, J.; Barone, V.; Cossi, M.; Cammi, R.; Mennucci, B.; Pomelli, C.; Adamo, C.; Clifford, S.; Ochterski, J. W.; Petersson, G. A.; Ayala, P. Y.; Cui, Q.; Morokuma, K.; Malick, D. K.; Rabuck, A. D.; Raghavachari, K.; Foresman, J. B.; Cioslowski, J.; Ortiz, J. V.; Stefanov, B. B.; Liu, G.; Liashenko, A.; Piskorz, P.; Komaromi, I.; Gomperts, R.; Martin, R. L.; Fox, D. J.; Keith, T.; Al-Laham, M. A.; Peng, C. Y.; Nanayakkara, A.; Gonzales, C. ; Challacombe, M.; Gill, P. M. W.; Johnson, B. G.; Chen, W.; Wong, M. W.; Andres, J. L.; Head-Gordon, M.; Replogle, E. S.; Pople, J. A. Gaussian 98 (revision A.1); Gaussian, Inc.: Pittsburgh, PA, 1998.

(38) Frisch, M. J.; Trucks, G. W.; Schlegel, H. B.; Scuseria, G. E.; Robb, M. A.; Cheeseman, J. R.; Montgomery, Jr., J. A.; Vreven, T.; Kudin, K. N.; Burant, J. C.; Millam, J. M.; Iyengar, S. S.; Tomasi, J.; Barone, V.; Mennucci, B.; Cossi, M.; Scalmani, G.; Rega, N.; Petersson, G. A.; Nakatsuji, H.; Hada, M.; Ehara, M.; Toyota, K.; Fukuda,

R.; Hasegawa, J.; Ishida, M.; Nakajima, T.; Honda, Y.; Kitao, O.; Nakai, H.; Klene, M.; Li, X.; Knox, J. E.; Hratchian, H. P.; Cross, J. B.; Bakken, V.; Adamo, C.; Jaramillo, J.; Gomperts, R.; Stratmann, R. E.; Yazyev, O.; Austin, A. J.; Cammi, R.; Pomelli, C.; Ochterski, J. W.; Ayala, P. Y.; Morokuma, K.; Voth, G. A.; Salvador, P.; Dannenberg, J. J.; Zakrzewski, V. G.; Dapprich, S.; Daniels, A. D.; Strain, M. C.; Farkas, O.; Malick, D. K.; Rabuck, A. D.; Raghavachari, K.; Foresman, J. B.; Ortiz, J. V.; Cui, Q.; Baboul, A. G.; Clifford, S.; Cioslowski, J.; Stefanov, B. B.; Liu, G.; Liashenko, A.; Piskorz, P.; Komaromi, I.; Martin, R. L.; Fox, D. J.; Keith, T.; Al-Laham, M. A.; Peng, C. Y.; Nanayakkara, A.; Challacombe, M.; Gill, P. M. W.; Johnson, B.; Chen, W.; Wong, M. W.; Gonzalez, C.; and Pople, J. A. Gaussian 03, Revision C.02; Gaussian, Inc.: Wallingford, CT, 2004

(39) MOLDEN3.4. Schaftenaar, G. MOLDEN3.4, CAOS/CAMM Center, The Netherlands (1998).

(40) Wang, L. S.; Conceicao, J.; Jin, C.; Smalley, R. E. *Chem*. *Phys*. *Lett*. **1991**, *182*, 5.

(41) Kuznetsov, A. E.; Boldyrev, A. I.; Zhai, H-J.; Li, X.; Wang, L. S. *J*. *Amer*. *Chem*. *Soc*. **2002**, *124*, 11801.

(42) Boldyrev, A. I.; Wang, L. S. *Chem*. *Rev*. **2005**, *105*, 3716.

Table 5-1. Comparison of the experimental VDEs to the calculated VDEs for the structure I of Al_6N^-. All energies are in eV.

Feature	VDE (exp.) [a]	Final State and Electronic Configuration	VDE (theo.)		
			TD-B3LYP	OVGF [b]	ΔCCSD(T)
X	2.66 (3)	$^2B_1,\ 2b_2^2 4a_1^2 2b_1^2 1a_2^2 3b_2^2 5a_1^2 3b_1^1$	2.41	2.53 (0.86)	2.63
A	3.25 (5)	$^2A_1,\ 2b_2^2 4a_1^2 2b_1^2 1a_2^2 3b_2^2 5a_1^1 3b_1^2$	3.14	3.30 (0.86)	3.36
B	3.40 (4)	$^2B_2,\ 2b_2^2 4a_1^2 2b_1^2 1a_2^2 3b_2^1 5a_1^2 3b_1^2$	3.22	3.44 (0.86)	3.44
C	4.00 (3)	$^2A_2,\ 2b_2^2 4a_1^2 2b_1^2 1a_2^1 3b_2^2 5a_1^2 3b_1^2$	4.21	4.20 (0.83)	4.23
D	4.06 (3)	$^2B_1,\ 2b_2^2 4a_1^2 2b_1^1 1a_2^2 3b_2^2 5a_1^2 3b_1^2$	4.00	4.21 (0.82)	c
E	4.50 (5)	$^2A_1,\ 2b_2^2 4a_1^1 2b_1^2 1a_2^2 3b_2^2 5a_1^2 3b_1^2$	4.40	4.51 (0.81)	c
F	4.70 (5)	$^2B_2,\ 2b_2^1 4a_1^2 2b_1^2 1a_2^2 3b_2^2 5a_1^2 3b_1^2$	4.62	4.70 (0.81)	c

[a] Numbers in parentheses represent the uncertainty in the last digit.

[b] Values in parentheses represent the pole strength of the OVGF calculation.

[c] This value cannot be calculated at the this level of theory.

Table 5-2. Comparison of the experimental VDE's to calculated VDE's for the structure II of Al_6N^-. All energies are in eV.

Feature	VDE (exp.) [a]	Final State and Electronic Configuration	VDE (theo.)		
			TD-B3LYP	OVGF [b]	ΔCCSD(T)
X	2.66 (3)	$^2A_1$, $2b_2^2 2b_1^2 4a_1^2 3b_2^2 5a_1^2 1a_2^2 6a_1^1$	2.56	2.67 (0.86)	2.79
A	3.25 (5)	$^2A_2$, $2b_2^2 2b_1^2 4a_1^2 3b_2^2 5a_1^2 1a_2^1 6a_1^2$	2.78	2.95 (0.86)	2.99
B	3.40 (4)	$^2A_1$, $2b_2^2 2b_1^2 4a_1^2 3b_2^2 5a_1^1 1a_2^2 6a_1^2$	3.64	3.73 (0.86)	c
C	4.00 (3)	$^2B_2$, $2b_2^2 2b_1^2 4a_1^2 3b_2^1 5a_1^2 1a_2^2 6a_1^2$	3.87	4.10 (0.84)	3.98
D	4.06 (3)	$^2A_1$, $2b_2^2 2b_1^2 4a_1^1 3b_2^1 5a_1^2 1a_2^2 6a_1^2$	4.11	4.31 (0.82)	c
E	4.50 (5)	$^2B_1$, $2b_2^2 2b_1^1 4a_1^2 3b_2^2 5a_1^2 1a_2^2 6a_1^2$	4.06	4.29 (0.80)	4.23
F	4.70 (5)	$^2B_2$, $2b_2^1 2b_1^2 4a_1^2 3b_2^2 5a_1^2 1a_2^2 6a_1^2$	4.81	4.89 (0.79)	c

[a] Numbers in parentheses represent the uncertainty in the last digit.

[b] Values in parentheses represent the pole strength of the OVGF calculation.

[c] This value cannot be calculated at the this level of theory.

Table 5-3. The molecular properties of the Al_6N^- species.

Molecular Parameter	I (C_{2v}, $^1A_1$)		II (C_{2v}, $^1A_1$)		II (C_s, $^1A'$)
	B3LYP/ 6-311+G*	CCSD(T)/ 6-311+G*	B3LYP/ 6-311+G*	CCSD(T)/ 6-311+G*	CCSD(T)/ 6-311+G*
E, a.u.	-1509.5965859	-1506.6828519	-1509.5952394	-1506.6791067	-1506.6796313
R(N-Al$_2$)	2.391	2.355	1.931	1.930	1.945
R(N-Al$_4$)	2.004	2.004	2.333	2.340	2.296
R(N-Al$_5$)			2.094	2.078	2.019
R(N-Al$_7$)					2.193
R(Al$_2$-Al$_3$)	2.614	2.616	2.795	2.826	2.771
R(Al$_2$-Al$_4$)	2.672	2.683	2.726	2.723	2.698
R(Al$_4$-Al$_5$)	3.010	2.975	2.634	2.637	2.648
R(Al$_4$-Al$_7$)					2.607
R(Al$_5$-Al$_6$)	2.615	2.628			
w$_1$, cm^{-1}	a$_1$, 367 (17)	385	a$_1$, 561 (198)	573	
w$_2$, cm^{-1}	a$_1$, 323 (82)	349	a$_1$, 339 (4)	350	
w$_3$, cm^{-1}	a$_1$, 291 (2)	297	a$_1$, 253 (3)	259	
w$_4$, cm^{-1}	a$_1$, 259 (17)	271	a$_1$, 216 (7)	225	
w$_5$, cm^{-1}	a$_1$, 204 (5)	212	a$_1$, 117 (11)	120	
w$_6$, cm^{-1}	a$_2$, 245 (0)	252	a$_1$, 115 (0)	104	
w$_7$, cm^{-1}	a$_2$, 185 (0)	181	a$_2$, 286 (0)	287	
w$_8$, cm^{-1}	a$_2$, 63 (0)	48	a$_2$, 64 (0)	52i	
w$_9$, cm^{-1}	b$_1$, 536 (77)	536	b$_1$, 332 (12)	360	
w$_{10}$, cm^{-1}	b$_1$, 272 (10)	276	b$_1$, 229 (18)	232	
w$_{11}$, cm^{-1}	b$_1$, 188 (8)	183	b$_1$, 30 (0)	113i	
w$_{12}$, cm^{-1}	b$_2$, 526 (131)	542	b$_2$, 550 (150)	564	
w$_{13}$, cm^{-1}	b$_2$, 250 (13)	242	b$_2$, 278 (2)	282	
w$_{14}$, cm^{-1}	b$_2$, 109 (12)	101	b$_2$, 194 (0)	193	
w$_{15}$, cm^{-1}	b$_2$, 80 (1)	56	b$_2$ 108 (30)	84	

[a] Values in parentheses represent relative absorbance intensities in the IR spectrum (km/mol).

Table 5-4. The molecular properties of the Al_6N species calculated at B3LYP/6-311+G*.

Molecular Parameter	XVIII(C_{2v}, $^2A_1$)	XIX (C_2, ^2A)	XX(C_{2v}, $^2B_1$)
E, a.u.	-1509.5109768	-1509.5148164	-1509.5095013
R(N-Al$_2$)	1.894	3.749	2.443
R(N-Al$_4$)	2.832	1.886	2.003
R(N-Al$_5$)	2.030	1.965	
R(Al$_2$-Al$_3$)	3.499	2.579	2.712
R(Al$_2$-Al$_4$)	2.724	2.767	2.698
R(Al$_2$-Al$_7$)	3.078	2.997	
R(Al$_4$-Al$_5$)	2.700	2.730	2.934
R(Al$_5$-Al$_6$)		2.742	2.689
R(Al$_4$-Al$_7$)		2.694	
w_1, cm^{-1}	a$_1$, 434 (13)	a, 714 (321)	a$_1$, 351 (3)
w_2, cm^{-1}	a$_1$, 360 (1)	a, 408 (31)	a$_1$, 271 (3)
w_3, cm^{-1}	a$_1$, 256 (1)	a, 301(5)	a$_1$, 228(0)
w_4, cm^{-1}	a$_1$, 203 (1)	a, 288 (0)	a$_1$, 212 (35)
w_5, cm^{-1}	a$_1$, 127 (0)	a, 243(4)	a$_1$, 193(8)
w_6, cm^{-1}	a$_1$, 53 (0)	a, 172 (1)	a$_2$, 226 (0)
w_7, cm^{-1}	a$_2$, 233 (0)	a, 70 (0)	a$_2$, 162 (0)
w_8, cm^{-1}	a$_2$, 93 (0)	a, 63 (0)	a$_2$, 59 (0)
w_9, cm^{-1}	b$_1$, 364 (4)	b, 639 (48)	b$_1$, 509 (95)
w_{10}, cm^{-1}	b$_1$, 207 (12)	b, 250 (5)	b$_1$, 222 (4)
w_{11}, cm^{-1}	b$_1$, 119 (1)	b, 221 (4)	b$_1$, 162 (5)
w_{12}, cm^{-1}	b$_2$, 697 (108)	b, 195 (0)	b$_2$, 537 (160)
w_{13}, cm^{-1}	b$_2$, 278 (0)	b, 123 (1)	b$_2$, 229 (4)
w_{14}, cm^{-1}	b$_2$, 187 (0)	b, 70 (1)	b$_2$, 111 (5)
w_{15}, cm^{-1}	b$_2$, 127 (0)	b, 34 (0)	b$_2$, 51 (6)

[a] Values in parentheses represent relative absorbance intensities in the IR spectrum (km/mol).
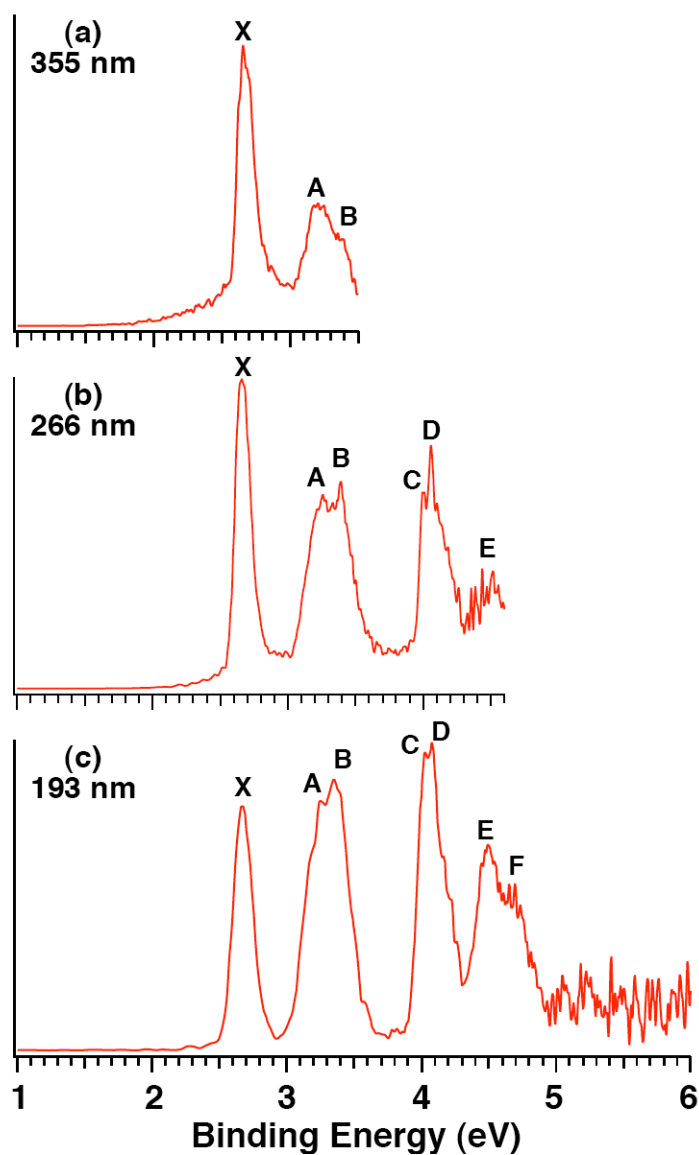
Figure 5-1. Photoelectron spectra of Al_6N^- at (a) 355 nm (3.496 eV, (b) 266 nm (4.661 eV), and (c) 193 nm (6.424 eV).
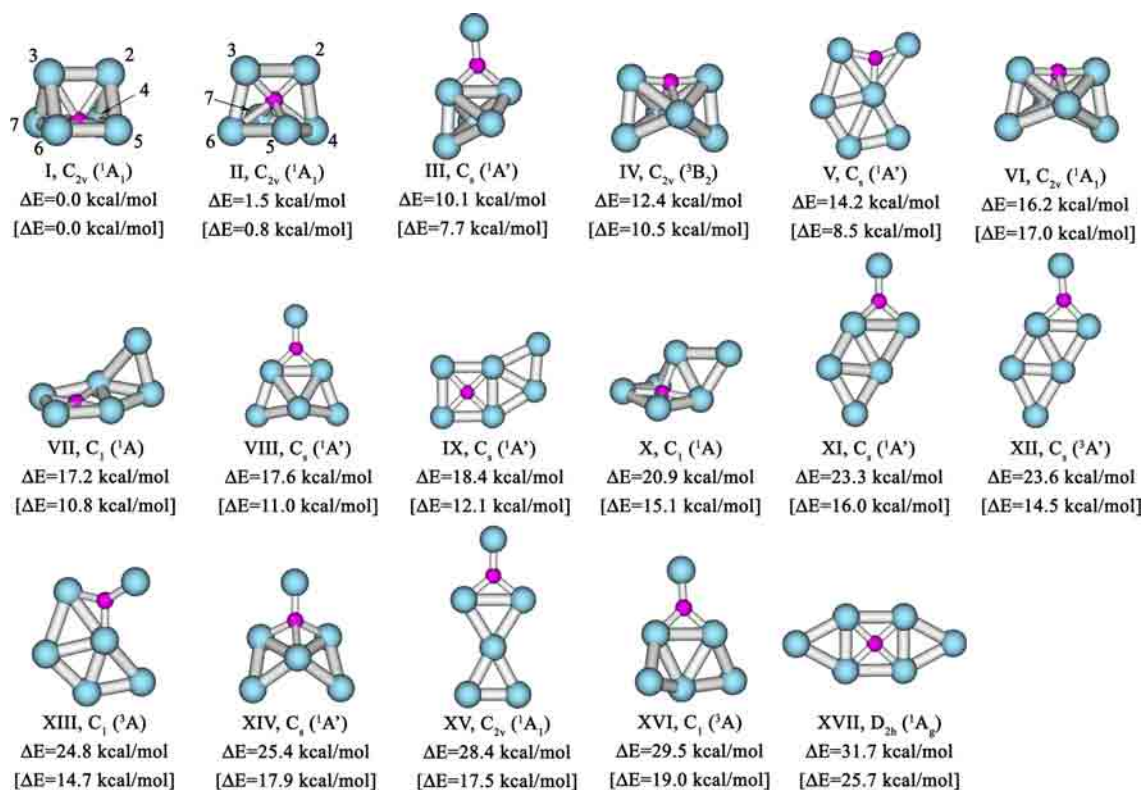
Figure 5-2. Computationally found isomers for Al_6N^-. Relative energies are given at CCSD(T)/6-311+G(2df)//B3LYP/6-311+G* and at B3LYP/6-311+G* in parenthesis.
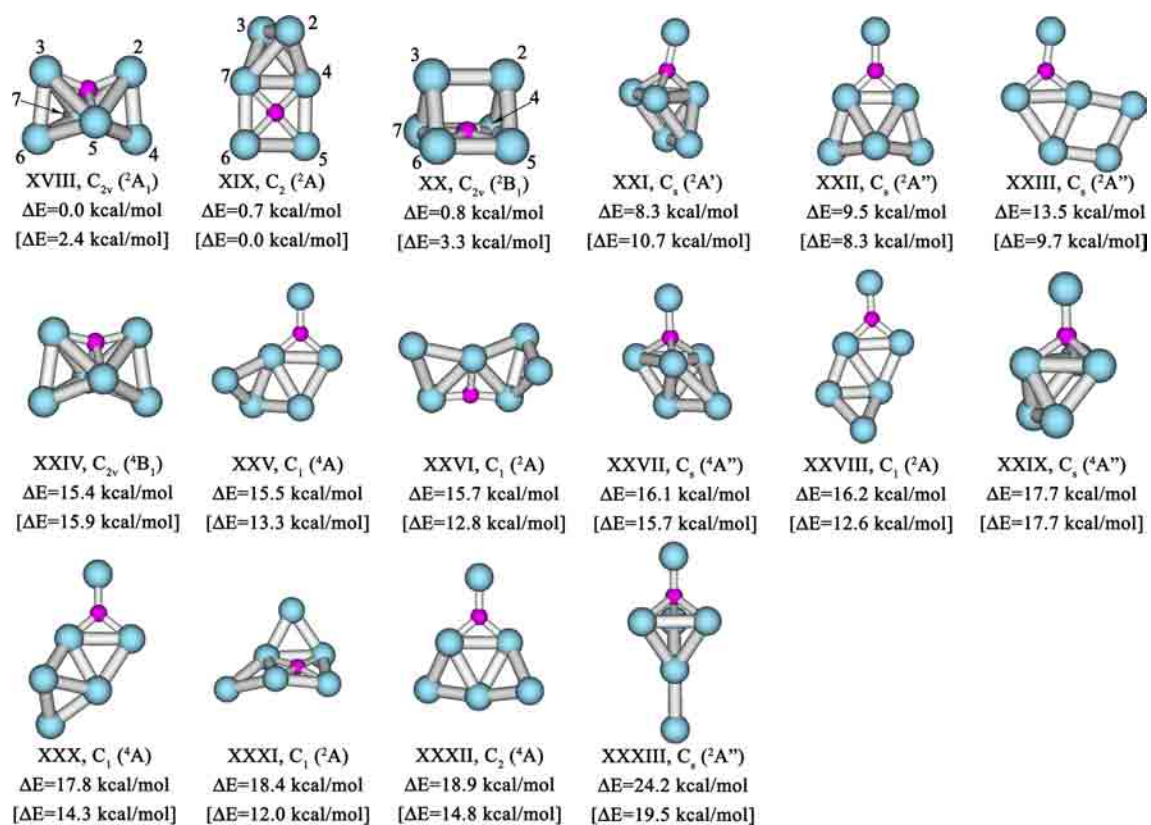
Figure 5-3. Computationally found isomers for Al_6N. Relative energies are given at CCSD(T)/6-311+G(2df)//B3LYP/6-311+G* and at B3LYP/6-311+G* in parenthesis.
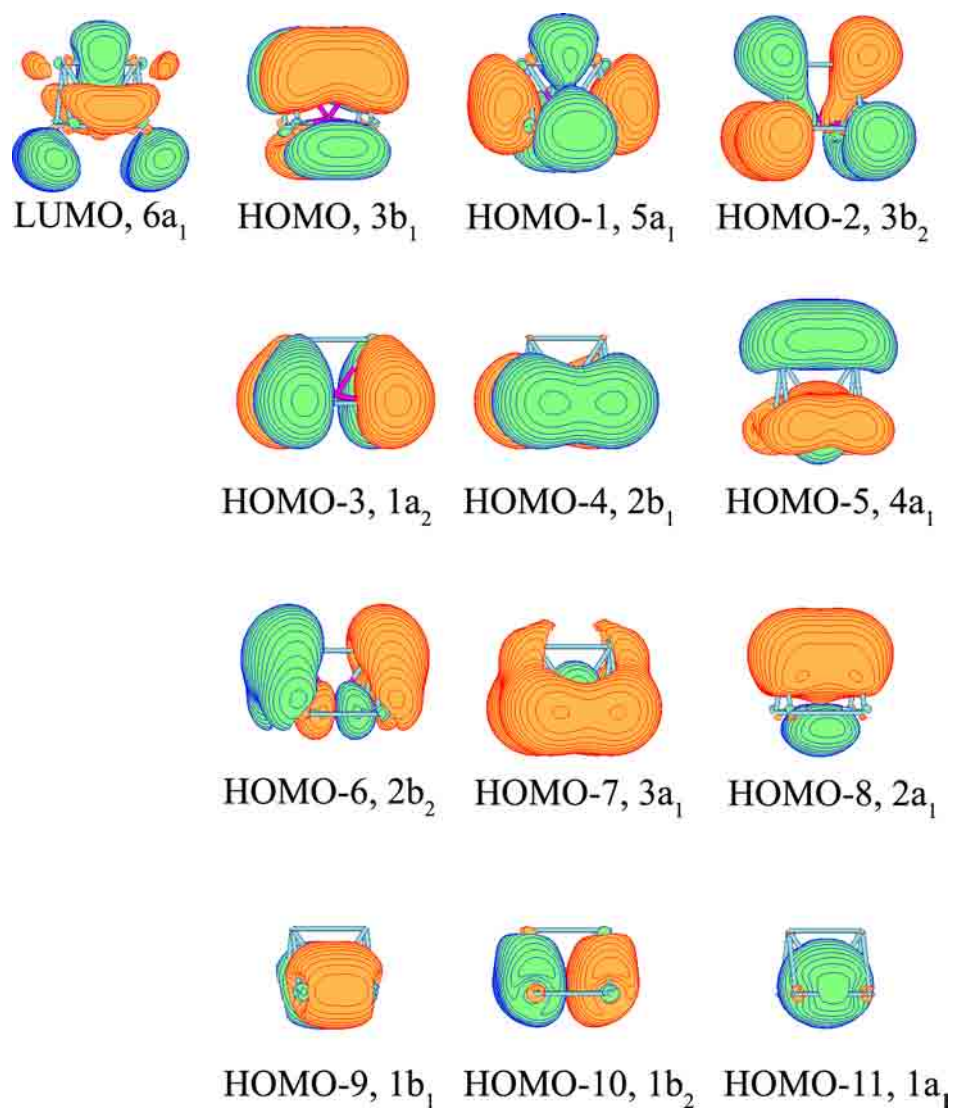
Figure 5-4. Molecular orbital for Al_6N^- (structure I) calculated at RHF/6-311+G*.
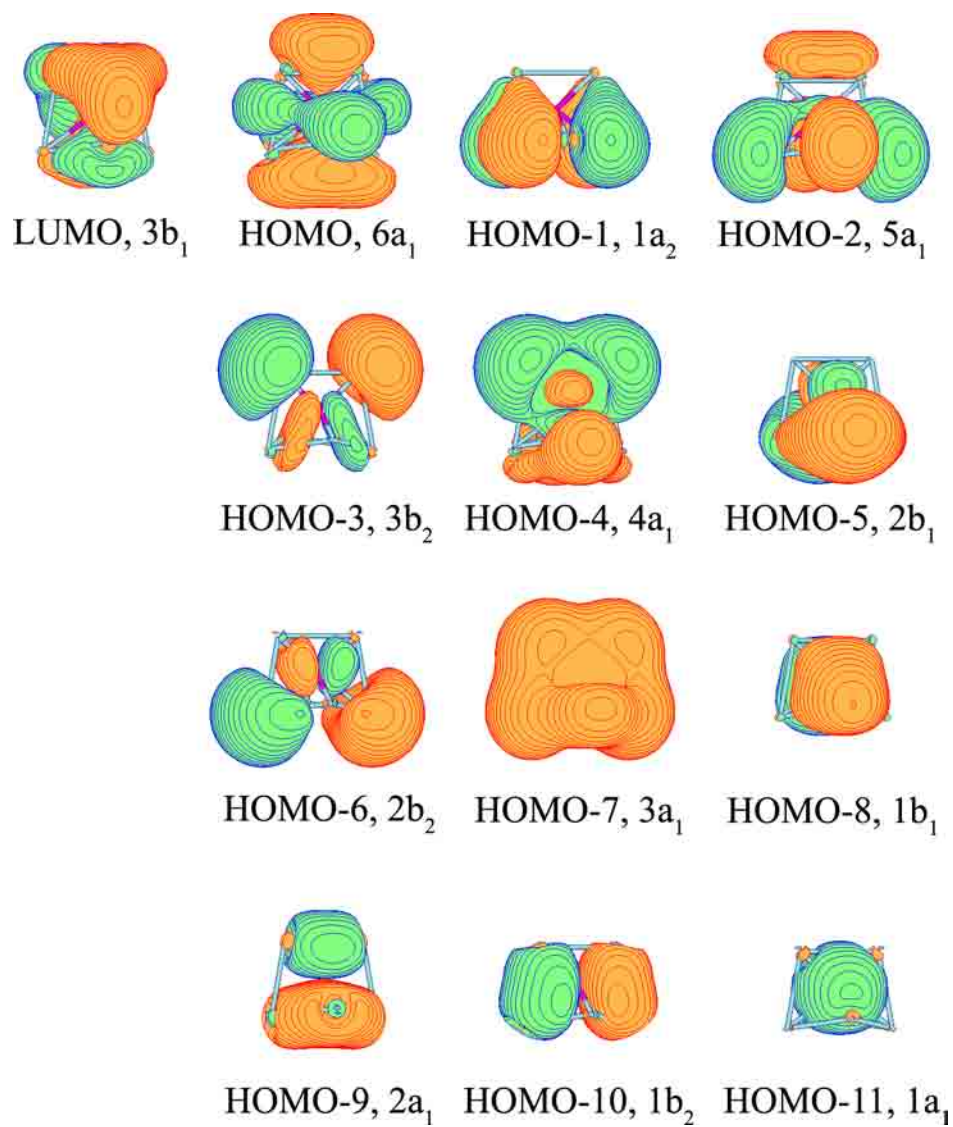
Figure 5-5. Molecular orbital for Al_6N^- (structure II) calculated at RHF/6-311+G*.
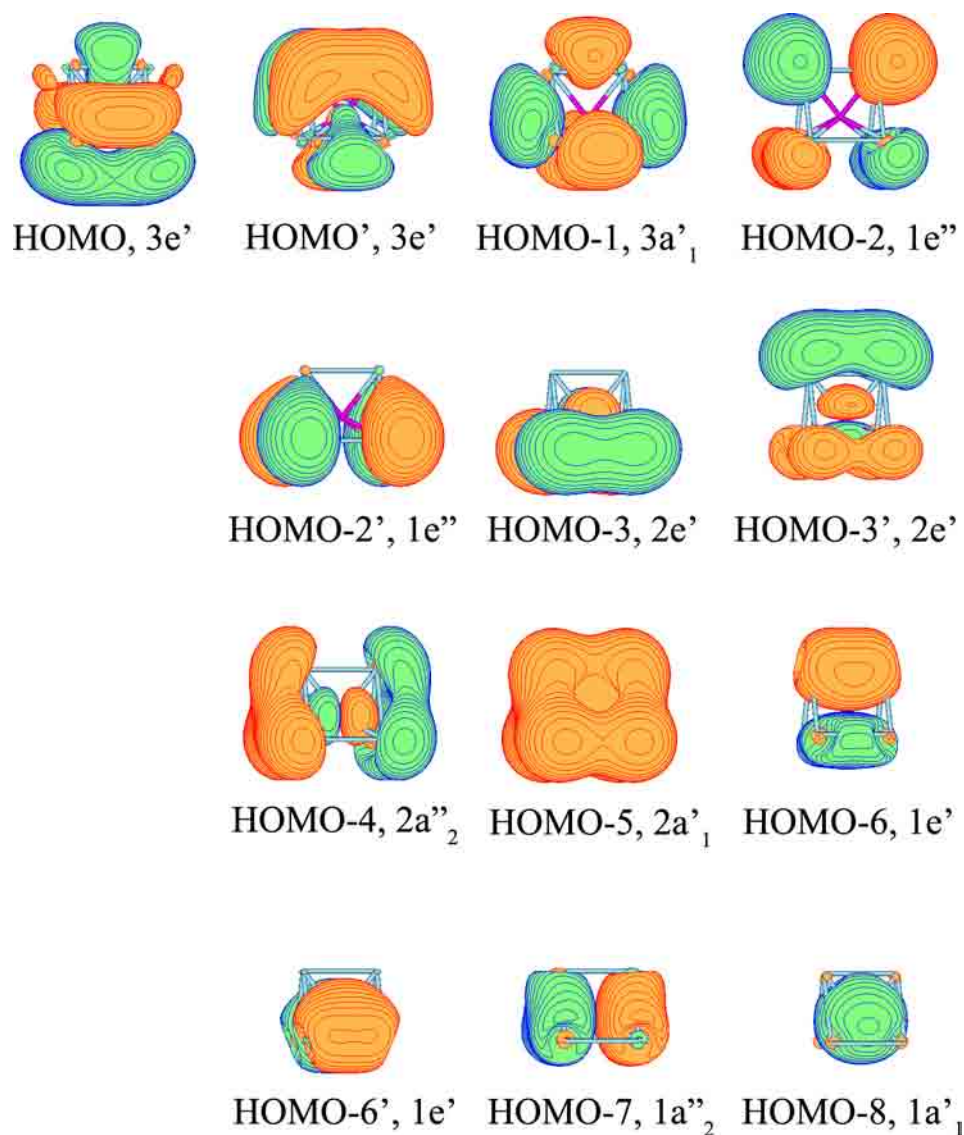
Figure 5-6. Molecular orbital for Al_6N^{3-} (structure D_{3h}, $^1A_1$') calculated at RHF/6-311+G*.

HOMO, $1t_{2g}$ HOMO', $1t_{2g}$ HOMO", $1t_{2g}$ HOMO-1, $1e_g$

HOMO-1', $1e_g$ HOMO-2, $2t_{1u}$ HOMO-2', $2t_{1u}$

HOMO-2", $2t_{1u}$ HOMO-3, $2a_{1g}$ HOMO-4, $1t_{1u}$

HOMO-4', $1t_{1u}$ HOMO-4", $1t_{1u}$ HOMO-5, $1a_{1g}$
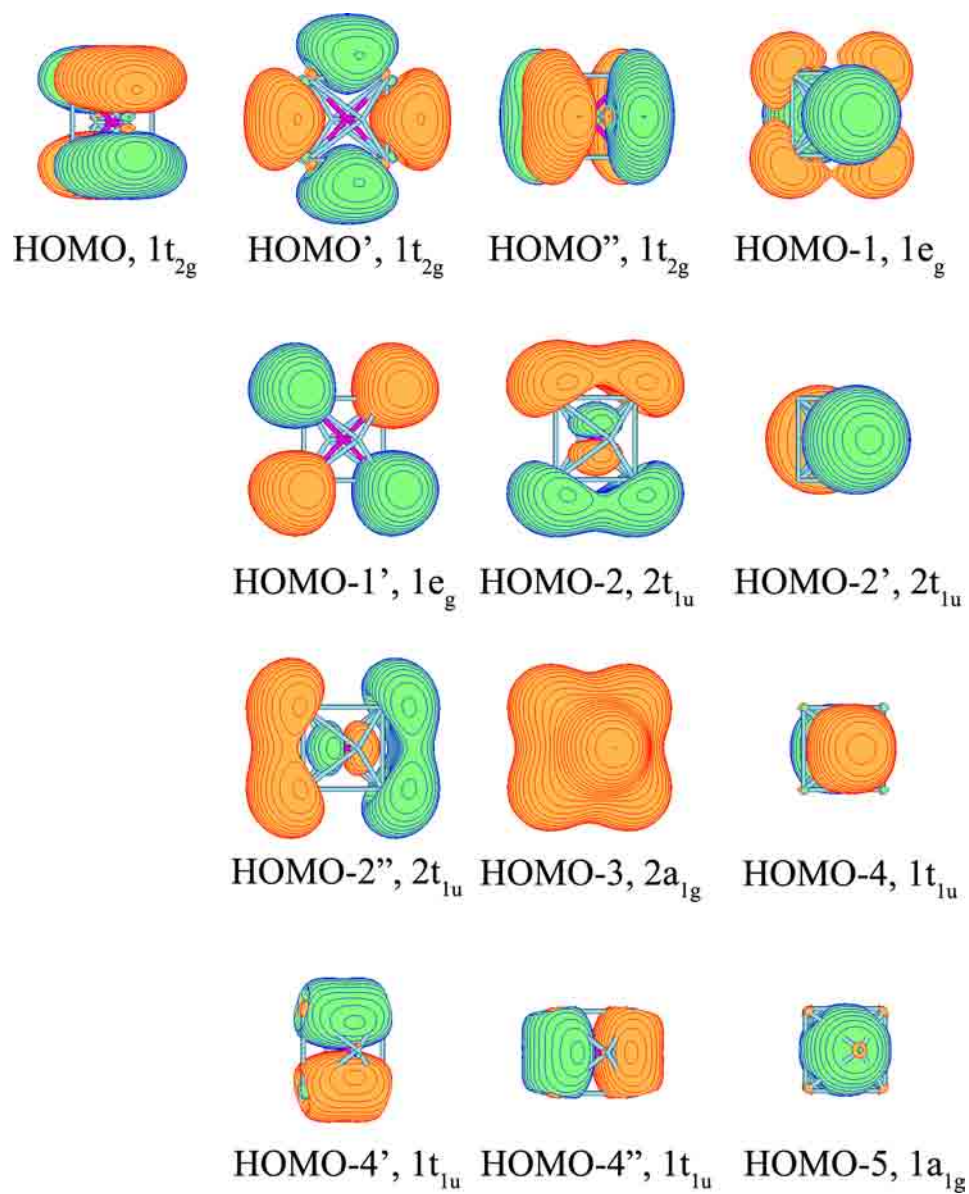
Figure 5-7. Molecular orbital for Al_6N^{3-} (structure O_h, $^1A_{1g}$) calculated at RHF/6-311+G*.

Al_6N^-

I

-2.30   -0.05

0.35

II

-2.38   0.51

0.23   -0.05

Al_6N

XX

0.19

-2.40

0.51

XVIII

0.78

-2.38

0.24

0.17
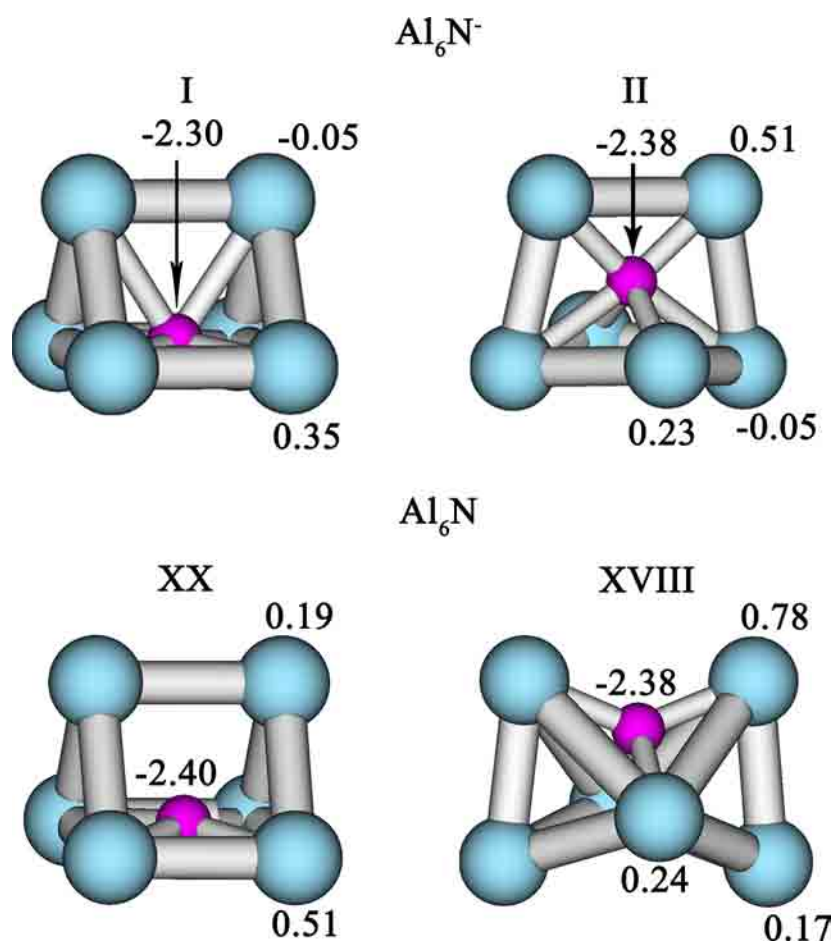
Figure 5-8. Effective NBO atomic charges (in |e|) for Al_6N^- (structures I and II) and Al_6N (structures XX and XVIII) at B3LYP/6-311+G*.

CHAPTER 6

PHOTOELECTRON SPECTROSCOPY AND AB INITIO STUDY OF THE

STRUCTURE AND BONDING OF Al_7N^- AND Al_7N[1]

Abstract

The electronic and geometrical structures of Al_7N^- are investigated using photoelectron spectroscopy and ab initio calculations. Photoelectron spectra of Al_7N^- have been obtained at three photon energies with six resolved spectral features at 193 nm. The spectral features of Al_7N^- are relatively broad, in particular for the ground state transition, indicating a large geometrical change from the ground state of Al_7N^- to that of Al_7N. The ground state vertical detachment energy is measured to be 2.71 eV, whereas only an upper limit of ~1.9 eV can be estimated for the ground state adiabatic detachment energy due to the broad detachment band. Global minimum searches for A_7N^- and Al_7N are performed using several theoretical methods. Vertical electron detachment energies are calculated using three different methods for the lowest energy structure and compared with the experimental data. Calculated results are in excellent agreement with the experimental data. The global minimum structure of Al_7N^- is found to possess C_{3v} symmetry, which can be viewed as an Al atom capping a face of a N-centered Al_6N octahedron. In the ground state of Al_7N, however, the capping Al atom is pushed inward

with the three adjacent Al-Al distances being stretched outward. Thus, even though Al_7N still possesses C_{3v} symmetry, it is better viewed as a N coordinated by seven Al atoms in a cage-like structure. The chemical bonding in Al_7N^- is discussed on the basis of molecular orbital and natural bond analysis.

6-1. Introduction

Metal clusters doped with one or more heteroatoms provide a new approach to manipulate the physical and chemical properties of clusters. Doped clusters are interesting chemical species with novel modes of chemical bonding. Understanding the structures and chemical bonding of such clusters may lead to rational designs of structurally and electronically stable clusters for applications in cluster-assembled nanomaterials or catalysis.

Aluminum nitride is an important semiconductor material. However, there have been relatively few experimental and theoretical studies on aluminum nitride clusters.[1-15] Experimentally, it is difficult to produce $(AlN)_x$ type clusters due to the overwhelming thermodynamic stability of the N_2 molecule. In an attempt to produce $(AlN)_x^-$ clusters, Li and Wang were able to observe only aluminum clusters doped with only one N atom, Al_xN^-.[10] Photoelectron spectra for a series of Al_xN^- clusters ($x = 2$-22) at 193 nm have been reported and compared to those of pure Al_x^- clusters.[10] The N-doped aluminum clusters are interesting and in larger sizes the Al_xN^- clusters are observed to exhibit similar electronic structures as pure $Al_{(x-1)}^-$ clusters. Recently we have performed joint photoelectron spectroscopic and ab initio studies on a series of Al_xN^- ($x = 3$-6) clusters in

order to elucidate their electronic and structural evolution as a function of size.[12,13] We have found that the global minimum structures of Al_xN^- ($x = 3$-5) are planar. The 2D to 3D structural transition occurs at x=6. We have shown that Al_6N^- possesses two closely-lying low-energy structures, which can be described as Jan-Teller distortions from the corresponding symmetric D_{3h} and O_h anions of Al_6N^{3-}, respectively.

In the current work, we report a joint photoelectron spectroscopy (PES) and ab initio study on Al_7N^- and its neutral counterpart Al_7N. The neutral Al_7N cluster is an intriguing species because it is valence-isoelectronic to Al_7C^-, which has been reported to be a particularly stable cluster that can be used as a building block for cluster-assembled materials.[16,17] The stability of Al_7C^- has been predicted due to its stable 18-electron shell closing. It would be interesting to compare the structure and bonding between Al_7N and Al_7C^-. There are several previous theoretical studies on the Al_7N cluster.[7-9,14,15] We performed a detailed PES study on Al_7N^- and measured its PES spectra at three photon energies 355, 266, and 193 nm. Extensive calculations have been carried out to search for the global minimum structures for Al_7N^- and Al_7N. The calculated Al_7N^- global minimum structure was confirmed by comparing the calculated vertical detachment energies (VDEs) with the experimental PES spectra. We found that the global minimum of Al_7N^- is a N-centered Al_6N octahedron capped by one Al atom with C_{3v} symmetry. The global minimum structure of Al_7N also has C_{3v} symmetry, but undergoes a significant geometry change relative to the anion. It can be viewed as a N atom coordinated by seven Al atoms in a cage-like structure, similar to Al_7C^-.

6-2. Experimental Method

The experiment was performed using a magnetic-bottle PES apparatus with a laser vaporization cluster source; details of the experimental apparatus have been published elsewhere.[18] Briefly, the Al_7N^- clusters were produced by laser vaporization of a disk target compressed from mixed powders of Al and AlN using pure helium as the carrier gas. A 10-cm long and 3-mm diameter extender tubing was used in the cluster source to allow adequate thermerlization of the nascent clusters. This was found to produce relatively cold clusters even under room temperature source conditions, which were important to yield well-resolved PES spectra.[19,20] The anion clusters were extracted from the cluster beam perpendicularly and were analyzed using a time-of-flight mass spectrometer. We showed previously that only Al_xN^- clusters with one N impurity atom could be observed under this condition.[10] The anion clusters of interest were mass-gated and decelerated before being photodetached by a laser beam. Photoelectrons were collected at near 100% collecting efficiency by the magnetic bottle and analyzed in a 3.5 m long electron flight tube. In the current experiment, three photon energies were used for photodetachment, 355 nm (3.496 eV) and 266 nm (4.661 eV) from a Nd:YAG laser and 193 nm (6.424 eV) from an ArF excimer laser. The electron energies were calibrated by the known spectrum of Rh^-. The electron energy resolution (DEk/Ek) was about 2.5%, i.e. ~ 25 meV for 1 eV electrons.

6-3. Theoretical Methods

We performed initial computational searches for the global minimum of Al_7N^- and Al_7N using our gradient embedded genetic algorithm (GEGA) program written by A. N. Alexandrova[21,22] and our simulated annealing program written by S. Call. In our simulated annealing Monte Carlo search for the global minimum, we used a population of 20 randomly generated structures at an initial temperature of 10,000 K with an effective Boltzmann constant of 10.0 Hartree K^{-1}, which allowed us to have the initial percentage of accepted transitions above 90%. After each iteration the temperature decreased according to $T_n=0.9995T_{n-1}$. The atomic coordinate perturbation P started at 0.3 Å and decreased according to $P_n=0.9995^{1/2}P_{n-1}$. The maximum allowed interatomic distance was 3.0 Å. The minimum interatomic distances were 1.7 Å between N and Al and 2.5 Å between Al and Al. The Monte Carlo simulation continued until the percentage of accepted transitions decreased to 10% and the final temperature decreased to 25 K. We used a hybrid method known as B3LYP[23-25] with the small split-valence basis sets (3-21G) for energy, gradient and force calculations, with simulated annealing performing single-point energy calculations and GEGA performing gradient optimizations. We reoptimized geometries and calculated frequencies for the lowest structures using the B3LYP method with the polarized split-valence basis sets (6-311+G*).[26-28] Total energies of the lowest structures were also calculated using the CCSD(T)[29-31] method with the extended 6-311+G(2df) basis sets at the B3LYP/6-311+G* geometries.

The vertical electron detachment energies were calculated using the R(U)CCSD(T)/6-311+G(2df) method, the outer valence Green Function method

(R(U)OVGF/6-311+G(2df))[32-36] as well as the time-dependent DFT method[37,38] (TD

B3LYP/6-311+G(2df)) all at the B3LYP/6-311+G* geometry. In the last approach, the

first vertical electron detachment energies were calculated at the B3LYP level of theory

as the lowest transitions from the doublet state of the anion into the final lowest singlet or

triplet states of the neutral species. Then the vertical excitation energies in the neutral

species (at the TD-B3LYP level) were added to the lowest singlet and triplet VDEs in

order to get the second and higher VDEs. Core electrons were frozen in treating the

electron correlation at the R(U)CCSD(T) and R(U)OVGF levels of theory.

The B3LYP, R(U)CCSD(T), R(U)OVGF calculations were performed using the

Gaussian 03 program.[39] Molecular orbital visualization was done using the MOLDEN3.4

program.[40]

6-4. Experimental Results

Figure 6-1 shows the PES spectra of Al_7N^- at three different photon energies. A

total of six distinct detachment bands can be identified in the 193 nm spectrum (Figure 6-

1c), where the C and D bands overlap. All the PES bands seem to be intrinsically broad,

i.e. the band widths do not seem to change with photon energies (the instrumental

resolution is better at lower photon energies). The apparent sharper band A in the 355

nm spectrum (Figure 6-1a) is due to a spectral cutoff at ~3.3 eV. The broad spectral

widths suggest either a large geometry change upon photodetachment and/or overlapping

electronic states. The ground state band X is particularly broad with a long, low energy

tail, making it very difficult to evaluate the adiabatic detachment energy (ADE). This

observation implies that there is a major geometry change between the ground state of Al_7N^- and that of neutral Al_7N, meaning that there may be a negligible Franck-Condon factor for the 0-0 transition. We note that there appears to be a step in the low binding energy side in the 355 nm spectrum (see inset of Figure 6-1a). This step at ~1.9 eV is taken as an upper limit for the ADE for the X band. The VDE of the X band is measured to be 2.71 eV. VDEs for all the six PES bands are given in Table 6-1 and are compared with theoretical calculations.

6-5. Theoretical Results

Al_7N^-. We initially performed simulated annealing and GEGA searches for the global minimum of Al_7N^- at B3LYP/3-21G level separately for doublet and quartet states. Figure 6-2 displays the first 11 low-lying doublet structures (I-XI) and the lowest quartet structure (XII) from simulated annealing. These isomers were recalculated at the B3LYP/6-311+G* level for geometry and at CCSD(T)/6-311*G(2df)//B3LYP/6-311+G* level for relative total energies.

The structure I ($^2A_1$, $1a_1^2 1e^4 2a_1^2 3a_1^2 4a_1^2 2e^4 3e^4 5a_1^2 4e^4 6a_1^1$) with C_{3v} symmetry was found by both searches to be the global minimum (Figure 6-2 and Table 6-2). It is a face-capped Al_6N octahedron. A similar structure was reported previously by Leskiw et al.,[7] who did not specify the point group symmetry. The Al-capped octahedral structure for Al_7N^- is quite stable; the closest-lying isomer (II) is 10.2 kcal/mol higher at CCSD(T)/6-311+G(2df)//B3LYP/6-311+G* level of theory. This isomer can be described as square-face-capped trigonal prism and is related to the global minimum of Al_6N^-.[13] The lowest

quartet structure (XII) is 34.3 kcal/mol (at CCSD(T)/6-311+G(2df)//B3LYP/6-311+G*) higher than the global minimum structure.

Al$_7$N. As with the anion, we performed simulated annealing and GEGA searches for the global minimum structure of neutral Al$_7$N at the B3LYP/3-21G level separately for singlet and triplet states. The geometries for all the low-lying structures were then recalculated at B3LYP/6-311+g* level, and relative energies were recalculated at the CCSD(T)/6-311*G(2df)//B3LYP/6-311+G* level. Both searches found structure XIII as the global minimum (Figure 6-2 and Table 6-2). The structure XIII ($^1A_1$, $1a_1^2 1e^4 2a_1^2 3a_1^2 4a_1^2 2e^4 3e^4 5a_1^2 4e^4$) with C$_{3v}$ symmetry, can be generated from the global minimum of Al$_7$N$^-$ by removing one electron from the singly occupied HOMO. Even though they have the same point group symmetry, there is a significant structural change from the global minimum of Al$_7$N$^-$ to that of neutral Al$_7$N. In the ground state of Al$_7$N, the capping Al atom is pushed inward with the three adjacent Al-Al distances being stretched outward. Thus, neutral Al$_7$N can be viewed as a N atom coordinated by the seven Al atoms in a cage-like structure, whereas in Al$_7$N$^-$ the N atom is only coordinated by six Al atom, and the capping atom is in the second coordination shell. A similar Al$_7$N structure was obtained previously by several authors.[7-9,14,15] It can be seen from Figure 6-2 that the global minimum structure of Al$_7$N is highly stable and that all the alternative structures (XIV-XX) are significantly higher in energy.

6-6. Comparison between the Calculated VDEs and Experiment and Interpretations of the Experimental PES Spectra

Our extensive structural search for Al_7N^- did not locate any isomers close in energy to the global minimum; the closest isomer is 10.2 kcal/mol higher at UCCSD(T)/6-311+G(2df)// B3LYP/6-311+G* (Figure 6-2). Therefore only the global minimum structure should be responsible for the photoelectron spectra. Indeed, the experimental PES spectra exhibit no hints of the presence of another isomer, which sometimes gives weak features in the low-binding energy side.[41] The calculated VDEs for the global minimum structure I of Al_7N^- at the TD-B3LYP/6-311+G(2df), ROVGF/6-311+G(2df) and CCSD(T)/6-311+G(2df) levels of theory are compared with the experimental data in Table 6-1.

The Ground State PES Band X. The ground state of Al_7N^- is a doublet ($^2A_1$) with an electron configuration of $1a_1^2 1e^4 2a_1^2 3a_1^2 4a_1^2 2e^4 3e^4 5a_1^2 4e^4 6a_1^1$. According to our calculation the first PES band (X) of Al_7N^- corresponds to removal of the electron from the singly occupied $6a_1$ orbital. The calculated VDE for this detachment channel is 2.67 eV at the UCCSD(T)/6-311+G(2df) level of theory, 3.04 eV at the UOVGF/6-311+G(2df) level of theory, and 2.56 eV at the TD-B3LYP/6-311+G(2df) level of theory (Table 6-1). The pole strength in the UOVGF calculation was found to be 0.87, indicating that the detachment channel can be primarily described by a one-electron detachment process. The UCCSD(T) result is in excellent agreement with the experimental VDE of 2.71 eV (Table 6-1). Surprisingly, the VDE at UOVGF/6-

311+G(2df) is significantly overestimated (by 0.33 eV) compared to the experimental value, whereas TD-B3LYP underestimated the VDE by 0.15 eV.

The calculated ADE for the ground state transition is 1.86 eV at UCCSD(T)/6-311+G(2df), which is significantly smaller than the VDE (2.67 eV) at the same level of theory. The large relaxation energy (VDE – ADE) of 0.81 eV reflects the large geometry change between the ground states of the anion and the neutral structure; this is in good agreement with the observed broad ground state PES band (X). The calculated ADE at 1.86 eV is in excellent agreement with the estimated upper limit of 1.9 eV from the 355 nm PES spectrum, indicating that there is a finite Franck-Condon factor for the 0-0 transition and that the 1.9 eV value may be taken as representing the true ADE or the electron affinity for neutral Al_7N.

Higher Binding Energy Detachment Bands (A to E). Because of the ground state of Al_7N^- is open shell with a single electron occupying the $6a_1$ HOMO, detachment from any other fully-occupied orbitals results in triplet and singlet final states, as shown in Table 6-1. Unfortunately, the singlet excited states cannot be calculated using the OVGF or the CCSD(T) methods. The TD-B3LYP method yields triplet-singlet splittings ranging from 0.22 to 0.26 eV (Table 6-1). The second detachment channel is from the HOMO-1 4e orbital. The calculated VDE to the ^3E final state is 3.36 eV at CCST(T) level, which is in excellent agreement with the measured VDE of the A band at 3.34 eV. The OVGF VDE for this channel is 3.24 eV, which is in reasonable agreement with the experimental value. TD-B3LYP appears to underestimate this VDE by ~0.3 eV. Because of the broad spectral width (i.e. Franck-Condon envelope) associated with the

anion to neutral geometry change, as well as the expected Jahn-Teller effect for the ^3E final state, the transition to the singlet state cannot be resolved in the current PES spectra even under the slightly higher resolution at 266 nm (Figure 6-1b). In addition, the intensity for the singlet detachment channel is expected to be lower than the triplet channel, and it is likely to be buried on the higher binding energy side of the A band. This appears to be the case for all the higher energy detachment channels (B to E), where the singlet states are not explicitly resolved.

The next detachment channel is from the nondegenerate HOMO-2 $5a_1$ orbital. The calculated VDEs from both CCSD(T) (3.69 eV) and OVGF (3.75 eV) are in excellent agreement with the experimental VDE of the B band at 3.77 eV. TD-B3LYP again underestimates the VDE for this detachment channel by ~0.2 eV. The relatively lower intensity of the B band is consistent with the nondegenerate nature of the $5a_1$ orbital.

The next two detachment channels are from the degenerate HOMO-3 3e and HOMO-4 2e orbitals, which should correspond to the C and D bands, respectively. The calculated VDEs for these two channels at OVDF are 4.33 and 4.54 eV, which are fairly close to each other. The calculated data are again in excellent agreement with the experimental PES spectra, in which the C and D bands overlap (Figure 6-1c). The final detachment channel comes from the HOMO-5 $4a_1$ orbital, corresponding to the E band. Surprisingly, both TD-B3LYP (5.40 eV) and OVGF (5.43 eV) yield VDEs, which are in excellent agreement with the experimental value of 5.45 eV. The $4a_1$ orbital is nondegenerate, again consistent with the relatively weak intensity of the E band.

The overall agreement between the theoretical results and the experimental data is truly excellent, leaving no ambiguity about the C_{3v} global minimum structure (I, Figure 6-2) for Al_7N^-. It is also interesting to note that the single particle MO picture works extremely well for Al_7N^-; there is a precise one-to-one correspondence between the MOs and the observed PES bands, as labeled in Figure 6-1c. The pole strengths in the OVGF calculations for all the detachment channels are >0.80, which also provides good indications for the validity for the single particle MO picture for the detachment processes from Al_7N^-. We have found previously that OVGF works well for Al-based clusters.[12,13,42-56] However, in the current case, the first VDE was severely overestimated by OVGF, although the overall spectral pattern predicted by OVGF is in excellent agreement with experiment, especially for the high binding energy features. Although slightly less accurate, the TD-B3LYP method also yields a quite good spectral pattern in comparison with experiment. In particular, the ability to compute both triplet and singlet final states is a distinct advantage of the TD-DFT method. The CCSD(T) method is the most accurate, but it can only be used to calculate the first three detachment channels. Therefore, the combination of the three theoretical methods is very powerful, providing a quantitative interpretation of the PES spectra of Al_7N^- and unequivocally establishing its global minimum structure.

6-7. Chemical Bonding in Al_7N and Al_7N^-

Al_7N. The Al_7N neutral cluster is isoelectronic to the so-called "magic" cluster Al_7C^-, which is quite prominent in the Al_nC^- mass spectra.[17] Both Al_7N and Al_7C^- have

similar global minimum structures, and we expect that Al_7N should also be a very stable cluster. Enhanced stability of Al_7C^- has already been discussed in the literature.[15,17,57] Initially Leskiw and Castleman[57] suggested that the stability of Al_7C^- could be reconciled within a jellium model framework where Al_7C^- could be viewed as a compound jellium cluster formed from Al_6 with a closed shell of 18 electrons AlC^- unit. However, this bonding picture does not agree with the global minimum structure of Al_7C^- because the C atom is located inside the Al_7 cage and one cannot identify an AlC unit. Thus, it seems that the stability of Al_7C^- is more complicated than the jellium model predicts. Indeed, the total number of valence electrons in Al_7C^- is 26, and according to the jellium model, one should have the following electronic configuration $1s^2 1p^6 1d^{10} 2s^2 1f^6$, which is not a closed-shell system and should not have any special stability. Later on, Reveles et al.[17] proposed an alternative explanation, in which the closed-shell $1s^2 1p^6 1d^{10} 2s^2 2p^6$ electronic configuration is used instead of $1s^2 1p^6 1d^{10} 2s^2 1f^6$. The earlier appearance of the 2p subshell instead of the 1f subshell was explained on the basis of the higher stability of the $2s^2 2p^6$ subshell. Sun et al.[15] explained the "magic" behavior of Al_7C^- on the basis of a large HOMO-LUMO gap. However, we can better understand the structure and bonding in the Al_7N^- anion using an alternative interpretation based on the stability of the highly stable octahedral Al_6N^{3-} unit, which we used to understand the structure and bonding in Al_6N^-.[13]

The ground electronic state of Al_7N^- is a doublet $^2A_1$ with an electron configuration of $1a_1^2 1e^4 2a_1^2 3a_1^2 4a_1^2 2e^4 3e^4 5a_1^2 4e^4 6a_1^1$. In order to simplify our chemical bonding analysis, we fill up the singly occupied HOMO in Al_7N^- by one more electron.

The geometry of the resulting Al_7N^{2-} structure was reoptimized at the B3LYP/6-311+G* level of theory (Figure 6-3a and Table 6-2). The final geometry of the structure of Al_7N^{2-} is very similar to the optimized structure I of Al_7N^- (Figure 6-2). From a purely geometrical perspective, one can formally view the structure of Al_7N^{2-} as a salt between an octahedral Al_6N^{3-} anion and a face-capping Al^+ cation. The octahedral structure and chemical bonding in the Al_6N^{3-} anion were discussed in detail previously.[13] Even though an isolated Al_6N^{3-} triply charged anion is not electronically stable, it has a repulsive Coulomb barrier on the electron ejection pathway[58-60] and therefore it has a finite lifetime at the optimized O_h geometry.

Before discussing the chemical bonding in Al_7N^{2-}, let us briefly review the chemical bonding in Al_6N^{3-}, which is closed shell ($^1A_{1g}$) with an electron configuration of $1a_{1g}^2 1t_{1u}^6 2a_{1g}^2 2t_{1u}^6 1e_g^4 1t_{2g}^6$.[13] The lowest valence MO $1a_{1g}$ is primarily the 2s-AO of the central nitrogen atom. The next triply degenerate $1t_{1u}$ MO can be assigned to three $2p_x$-, $2p_y$-, and $2p_z$-AOs of the central N atom. The next six valence MOs ($2a_{1g}$, $2t_{1u}$, and $1e_g$) are primarily formed by the 3s-AOs of the aluminum atoms and they can be viewed as six lone pairs located on the Al atoms. Finally, the completely-bonding and triply-degenerate $1t_{2g}$-HOMO is formed by the tangential 3p-AOs of the Al atoms, and it is responsible for the delocalized tangential bonding between the Al atoms. In order to test our interpretation of the bonding in Al_6N^{3-}, we performed NBO analysis of the Al_6N^{3+} cation (at the geometry of Al_6N^{3-}), in which the delocalized $1t_{2g}$-HOMO was empty. The NBO analysis reveals four lone pairs of N with occupation numbers on the order of 1.95 |e| (2s) and 1.98 |e| (2p), and one lone pair at every Al with the occupation number of 1.75

|e| (99.5% composed of 3s-AOs). Thus, in the O_h Al_6N^{3-} the chemical bonding can be approximately described as the central atom carrying an effective charge -3 (N^{3-}), which is ionically bonded to an octahedral Al_6 cluster, with every Al carrying a lone pair. The $1t_{2g}$-HOMO is the only orbital responsible for delocalized bonding and tangential aromaticity. The Al_6 cluster keeps its octahedral structure in Al_6N^{3-}, because N^{3-} can fit perfectly in the cavity of the octahedron and because the closed shell N^{3-} unit substitutes a completely bonding pair of electrons in the $2a_{1g}$-MO in Al_6^{2-}.[56]

All valence MOs of the Al_7N^{2-} anion are presented in Figure 6-3b. The HOMO ($6a_1$) and HOMO-1 ($4e$) are responsible for the delocalized bonding, as in the case with $1t_{2g}$-HOMO in Al_6N^{3-}. To understand bonding in the Al_7N^{2-} anion, we performed an analogous NBO analysis for the putative Al_7N^{4+} cation at the geometry of the Al_7N^{2-} anion, but with the $6a_1$-HOMO and $4e$-HOMO-1 empty. The NBO analysis of Al_7N^{4+} revealed four lone pairs of N with occupation numbers from 1.90 |e| to 1.97 |e| and one lone pair at every Al with the occupation number from 1.57 |e| (97.6% composed out of 3s-AOs) to 1.64 |e| (99.4% composed out of 3s-AOs). On the basis of this analysis, we conclude that indeed there is a formal building block in the Al_7N^{2-} cluster $\{Al^+[Al_6N^{3-}]\}$, though the bonding between Al^+ and Al_6N^{3-} is more covalent than ionic. One can see in Figure 6-3b that the 3p-AOs of the capping Al atom participate in the delocalized bonding between the aluminum atoms. The question now is, could the building block Al_6N^{3-} be a part of the larger doped Al_xN^- clusters, and could it even be a part of a N-doped solid aluminum? These questions are worth pursuing in future studies of larger Al_xN^- clusters.

6-8. Summary

The Al_7N^- cluster has been investigated by a combined photoelectron spectroscopy and *ab initio* study. Well-resolved, albeit broad, spectral features were used to compare with the calculated VDEs. The global minimum structures of Al_7N and Al_7N^- were located using both a genetic algorithm and stimulated annealing. The structure of Al_7N^- is found to possess C_{3v} symmetry, which can be viewed as an Al capping an octahedron Al_6N unit. In the neutral Al_7N, significant geometry relaxation is observed, consistent with the broad PES spectral features. The calculated VDEs for the C_{3v} Al_7N^- global minimum structure are in excellent agreement with the PES spectra. The structure and chemical bonding of Al_7N^- are understood using the closed-shell Al_7N^{2-}, which possesses similar C_{3v} structure as Al_7N^-. Al_7N^{2-} can be viewed as an Al^+ capping the face of a highly stable octahedral Al_6N^{3-} building block. The stability of the octahedral Al_6N^{3-} was used previously to understand the structures of Al_6N an Al_6N^-.[13] It would be interesting to discover if the N-centered Al_6N^{3-} octahedron is a building block in larger Al_xN^- clusters.

References

(1) Schleyer, P. v. R.; Boldyrev, A. I. *J. Chem. Soc. Chem. Comm.* **1991**, 1536.

(2) Zakrzewski, V. G.; Niessen, W. v.; Boldyrev, A. I.; Schleyer, P. v. R. *Chem. Phys.* **1993**, *174*, 167.

(3) Nayak, S. K.; Khana, S. N.; Jena, P. *Phys. Rev.* B, **1998**, *57*, 3787.

(4) Nayak, S. K.; Rao, B. K.; Jena, P.; Li, X.; Wang, L. S. *Chem. Phys. Lett.* **1999**, *301*, 379.

(5) Boo, B. H.; Liu, Z. *J. Phys. Chem.* A, **1999**, *103*, 1250.

(6) Andrews, L.; Zhou, M.; Chertihin, G. V.; Bare, W. D.; Hannachi, Y. *J. Phys. A*, **2000**, *104*, 1656.

(7) Leskiw, B. R.; Castleman, A. W. Jr., Ashman, C.; Khanna, S. N. *J. Chem. Phys.* **2001**, *114*, 1165.

(8) Ling, L.; Song, B.; Cao, P.-L. *J. Mol. Struct. (Theochem)* **2005**, *728*, 215.

(9) Gou, L.; Wu, H.-S. *Int. J. Quant. Chem.* **2006**, *106*, 1250.

(10) Li, X.; Wang, L. S. *Eur. Phys. J. D*, **2005**, *34*, 9.

(11) Meloni, G.; Sheehan, S. M.; Parsons, B. F.; Neumark, D. M. *J. Phys. Chem. A*, **2006**, *110*, 3527.

(12) Averkiev, B. B.; Boldyrev, A. I.; Li, X.; Wang, L. S. *J. Chem. Phys.* **2006**, *125*, 124305.

(13) Averkiev, B. B.; Boldyrev, A. I. ; Li, X.; Wang, L. S. *J. Phys. Chem. A.* **2007**, *111*, 34.

(14) Wang, B.; Shi, D.; Chen, X.; Wang, G.; Zhao, J. *Int. J. Modern Phys. B*, **2005**, *19*, 2380.

(15) Sun, Q.; Wang, Q.; Gong, X. G.; Kumar, V.; Kawazoe, Y. *Eur. Phys. J. D*, **2002**, *18*, 77.

(16) Aschman, C.; Khanna, S. N.; Pederson, M. R.; Kortus, J. *Phys. Rev. B*, **2000**, *62*, 16956.

(17) Reveles, J. U.; Khanna, S. N.; Roach, P. J.; Castleman, A. W. Jr. *Proc. Natl. Acad. Sci. (USA)* **2006**, *103*, 18405.

(18) Wang, L. S.; Cheng, H. S.; Fan, J. *J. Chem. Phys.* **1995**, *102*, 9480.

(19) Li, X.; Wu, H.; Wang, X. B.; Wang, L. S. *Phys. Rev. Lett.* **1998**, *81*, 1909.

(20) Akola, J.; Manninen, M.; Hakkinen, H.; Landman, U.; Li, X.; Wang, L. S. *Phys. Rev.* B **1999**, *60*, R11297.

(21) Alexandrova, A. N.; Boldyrev, A. I.; Fu, Y-J.; Wang, X. B.; Wang, L. S. *J. Chem. Phys.* **2004**, *121*, 5709.

(22) Alexandrova, A. N.; Boldyrev, A. I. *J. Chem. Theory and Comput.* **2005**, *1*, 566.

(23) Becke, A. D. *J. Chem. Phys.* **1993**, *98*, 5648.

(24) Vosko, S. H.; Wilk, L.; Nusair, M. *Can. J. Phys.* **1980**, *58*, 1200.

(25) Lee, C.; Yang, W.; Parr, R. G. *Phys. Rev. B*, **1988**, *37*, 785.

(26) (a) Binkley, J. S.; Pople, J. A.; Hehre, W. J. *J. Am. Chem. Soc.* **1980**, *102*, 939; (b) Gordon, M. S.; Binkley, J. S.; Pople, J. A.; Pietro, W. J.; Hehre, W. J. *J. Am. Chem. Soc.* **1982**, *104*, 2797; (c) Pietro, W. J.; Francl, M. M.; Hehre, W. J.; Defrees, D. J.; Pople, J. A.; Binkley, J. S. *J. Am. Chem. Soc.* **1982**, *104*, 5039.

(27) McLean, A. D.; Chandler, G. S. *J. Chem. Phys.* **1980**, *72*, 5639.

(28) Clark, T.; Chandrasekhar, J.; Spitznagel, G. W.; Schleyer, P. v. R. *J. Comput. Chem.* **1983**, *4*, 294.

(29) Cizek, J. *Adv. Chem. Phys.* **1969**, *14*, 35.

(30) Knowles, P. J.; Hampel, C.; Werner, H.-J. *J. Chem. Phys.* **1993**, *99*, 5219.

(31) Raghavachari, K.; Trucks, G. W.; Pople, J. A.; Head-Gordon, M. *Chem. Phys. Lett.* **1989**, *157*, 479.

(32) Cederbaum, L. S. *J. Phys B*, **1975**, *8*, 290.

(33) (a) Ortiz, J. V. *Int. J. Quant. Chem., Quant. Chem. Symp.* **1989,** 23, 321; (b) Lin, J. S.; Ortiz, J. V. *Chem. Phys. Lett.* **1990**, *171*, 197.

(34) Zakrzewski, V. G.; Ortiz, J. V.; Nichols, J. A.; Heryadi, D.; Yeager, D. L.; Golab, J. T. *Int. J. Quant. Chem.* **1996**, *60*, 29.

(35) Dahnovsky, Y. *J. Chem. Phys.* **2007**, 126, 234111.

(36) Kletsov, A. Dahnovsky, Y. *Phys. Rev. B*, **2007**, 76, 035304.

(37) Bauernshmitt, R.; Alrichs, R. *Chem. Phys. Lett.* **1996**, *256*, 454.

(38) Casida, M. E.; Jamorski, C.; Casida, K. C.; Salahub, D. R. *J. Chem. Phys.* **1998,** *108*, 4439.

(39) Gaussian 03, Revision D.01, Frisch, M. J.; Trucks, G. W.; Schlegel, H. B.; Scuseria, G. E.; Robb, M. A.; Cheeseman, J. R.; Montgomery, Jr., J. A.; Vreven, T.; Kudin, K. N.; Burant, J. C.; Millam, J. M.; Iyengar, S. S.; Tomasi, J.; Barone, V.; Mennucci, B.; Cossi, M.; Scalmani, G.; Rega, N.; Petersson, G. A.; Nakatsuji, H.; Hada, M.; Ehara, M.; Toyota, K.; Fukuda, R.; Hasegawa, J.; Ishida, M.; Nakajima, T.; Honda, Y.; Kitao, O.; Nakai, H.; Klene, M.; Li, X.; Knox, J. E.; Hratchian, H. P.; Cross, J. B.; Bakken, V.; Adamo, C.; Jaramillo, J.; Gomperts, R.; Stratmann, R. E.; Yazyev, O.; Austin, A. J.; Cammi, R.; Pomelli, C.; Ochterski, J. W.; Ayala, P. Y.; Morokuma, K.; Voth, G. A.; Salvador, P.; Dannenberg, J. J.; Zakrzewski, V. G.; Dapprich, S.; Daniels, A. D.; Strain, M. C.; Farkas, O.; Malick, D. K.; Rabuck, A. D.; Raghavachari, K.;

Foresman, J. B.; Ortiz, J. V.; Cui, Q.; Baboul, A. G.; Clifford, S.; Cioslowski, J.; Stefanov, B. B.; Liu, G.; Liashenko, A.; Piskorz, P.; Komaromi, I.; Martin, R. L.; Fox, D. J.; Keith, T.; Al-Laham, M. A.; Peng, C. Y.; Nanayakkara, A.; Challacombe, M.; Gill, P. M. W.; Johnson, B.; Chen, W.; Wong, M. W.; Gonzalez, C.; and Pople, J. A.; Gaussian, Inc., Wallingford CT, 2004

(40) MOLDEN3.4. Schaftenaar, G. MOLDEN3.4, CAOS/CAMM Center, The Netherlands (1998).

(41) Zhai, H. J.; Kiran, B.; Li, J.; Wang, L. S. *Nature Materials* **2003**, *2*, 827 (2003).

(42) Boldyrev, A. I.; Simons, J.; Li, X.; Chen, W.; Wang, L. S. *J. Chem. Phys.* **1999**, *110*, 8980.

(43) Li, X.; Wang, L. S.; Boldyrev, A. I.; Simons, J. *J. Am. Chem. Soc.* **1999**, *121*, 6033.

(44) Boldyrev, A. I.; Simons, J.; Li, X.; Wang, L. S. *J. Chem. Phys.* **1999**, *111*, 4993.

(45) Boldyrev, A. I.; Simons, J.; Li, X.; Wang, L. S. *J. Am. Chem. Soc.* **1999**, *121*, 10193.

(46) Boldyrev, A. I.; Li, X.; Wang, L. S. *J. Phys. Chem. A* **2000**, *104*, 5358.

(47) Cannon, N. A.; Boldyrev, A. I.; Li, X.; Wang, L. S. *J. Chem. Phys.* **2000**, *113*, 2671.

(48) Wang, L. S.; Boldyrev, A. I.; Li, X.; Simons, J. *J. Am. Chem. Soc.* **2000**, *122*, 7681.

(49) Boldyrev, A. I.; Li, X.; Wang, L. S. *Angew. Chem. Int. Ed.* **2000**, *39*, 3307.

(50) Geske, G. D.; Boldyrev, A. I.; Li, X.; Wang, L. S. *J. Chem. Phys.* **2000**, *113*, 5130.

(51) Li, X.; Zhang, H. F.; Wang, L. S.; Geske, G. D.; Boldyrev, A. I. *Angew. Chem. Int. Ed.* **2000**, *39*, 3630.

(52) Li, X.; Kuznetsov, A. E.; Zhang, H. F.; Boldyrev, A. I.; Wang, L. S. *Science* **2001**, *291*, 859.

(53) Li, X.; Zhang, H. F.; Wang, L. S.; Kuznetsov, A. E.; Cannon, N. A.; Boldyrev, A. I. *Angew. Chem. Int. Ed.* **2001,** *40*, 1867.

(54) Li, X.; Wang, L. S.; Cannon, N. A.; Boldyrev, A. I. *J. Chem. Phys.* **2002**, *116*, 1330.

(55) Kuznetsov, A. E.; Birch, K. A.; Boldyrev, A. I.; Li, X.; Zhai, H. J.; Wang, L. S. *Science* **2003**, *300*, 622.

(56) Kuznetsov, A. E.; Boldyrev, A. I.; Zhai, H. .J.; Li, X.; Wang, L. S. *J. Am. Chem. Soc.* **2002**, *124*, 11791.

(57) Leskiw, B. D.; Castleman, A. W. Jr. *Chem. Phys. Lett.* **2000**, *316*, 31.

(58) Wang, X. B.; Ding, C. F.; Wang, L. S. *Phys. Rev. Lett.* **1998**, *81*, 3351.

(59) Wang, L. S.; Ding, C. F.; Wang, X. B.; Nicholas, J. B. *Phys. Rev. Lett.* **1998**, *81*, 2667.

(60) Wang X. B.; Wang, L. S. *Nature* **1999**, *400*, 245.

Table 6-1. The experimental vertical detachment energies (VDE) compared to calculated VDEs from the global minimum structure I of Al_7N^- at three levels of theory. All energies are in eV.

Feature	VDE (exp.)	Final State and the Electronic Configuration	VDE (theo.)		
			TD-B3LYP	OVGF[b]	ΔCCSD(T)
X	2.71 (4)	$^1A_1$, $3a_1^2 4a_1^2 2e^4 3e^4 5a_1^2 4e^4 6a_1^0$	2.56	3.04 (0.87)	2.67
A	3.34 (4)	^3E, $3a_1^2 4a_1^2 2e^4 3e^4 5a_1^2 4e^3 6a_1^1$	3.06	3.24 (0.86)	3.36
		^1E, $3a_1^2 4a_1^2 2e^4 3e^4 5a_1^2 4e^3 6a_1^1$	3.32	c	c
B	3.77 (4)	$^3A_1$, $3a_1^2 4a_1^2 2e^4 3e^4 5a_1^1 4e^4 6a_1^1$	3.56	3.75 (0.86)	3.69
		$^1A_1$, $3a_1^2 4a_1^2 2e^4 3e^4 5a_1^1 4e^4 6a_1^1$	3.82	c	c
C	4.35 (5)	^3E, $3a_1^2 4a_1^2 2e^4 3e^3 5a_1^2 4e^4 6a_1^1$	4.19	4.33 (0.85)	c
		^1E, $3a_1^2 4a_1^2 2e^4 3e^3 5a_1^2 4e^4 6a_1^1$	4.41	c	c
D	~4.6	^3E, $3a_1^2 4a_1^2 2e^3 3e^4 5a_1^2 4e^4 6a_1^1$	4.58	4.54 (0.83)	c
		^1E, $3a_1^2 4a_1^2 2e^3 3e^4 5a_1^2 4e^4 6a_1^1$	4.81	c	c
E	5.45 (4)	$^3A_1$, $3a_1^2 4a_1^1 2e^4 3e^4 5a_1^2 4e^4 6a_1^1$	5.40	5.43 (0.81)	c

[a] Numbers in the parentheses represent the uncertainty in the last digit.
[b] Values in parentheses represent the pole strength of the OVGF calculation.
[c] This value cannot be calculated at this level of theory.

Table 6-2. The molecular properties of the Al_7N, Al_7N^-, and Al_7N^{2-} species calculated at B3LYP/6-311+G*.

	Al_7N, XIII, C_{3v} ($^1A_1$)	Al_7N^-, I, C_{3v} ($^2A_1$)	Al_7N^{2-}, C_{3v} ($^1A_1$)
E, a. u.	-1752.0019598	-1752.0661946	-1752.0192342
R(N-Al_1), Å	2.137	3.003	3.515
R(N-Al_2), Å	2.106	1.986	1.996
R(N-Al_5), Å	2.123	2.074	2.041
R(Al_1-Al_2), Å	2.613	2.722	2.840
R(Al_2-Al_3), Å	3.540	3.045	2.794
R(Al_2-Al_5), Å	2.649	2.742	2.840
R(Al_5-Al_6), Å	2.811	2.918	2.943
ω_1 (a_1), cm^{-1}	490 (291)[a]	511 (158)[a]	535 (225)[a]
ω_2 (a_1), cm^{-1}	343 (1)	357 (5)	364 (16)
ω_3 (a_1), cm^{-1}	287 (14)	280 (0)	272 (4)
ω_4 (a_1), cm^{-1}	232 (1)	188 (5)	226 (60)
ω_5 (a_1), cm^{-1}	116 (1)	162 (9)	150 (3)
ω_6 (a_2), cm^{-1}	201 (0)	131 (0)	94 (0)
ω_7 (e), cm^{-1}	488 (260)	553 (173)	532 (163)
ω_8 (e), cm^{-1}	297 (2)	253 (5)	238 (2)
ω_9 (e), cm^{-1}	259 (7)	223 (0)	232 (0)
ω_{10} (e), cm^{-1}	226 (15)	193 (4)	159 (29)
ω_{11} (e), cm^{-1}	166 (0)	146 (22)	118 (12)
ω_{12} (e), cm^{-1}	51 (0)	63 (1)	73 (0)

[a] Values in parentheses represent relative absorbance intensities in the IR spectrum (km/mol).
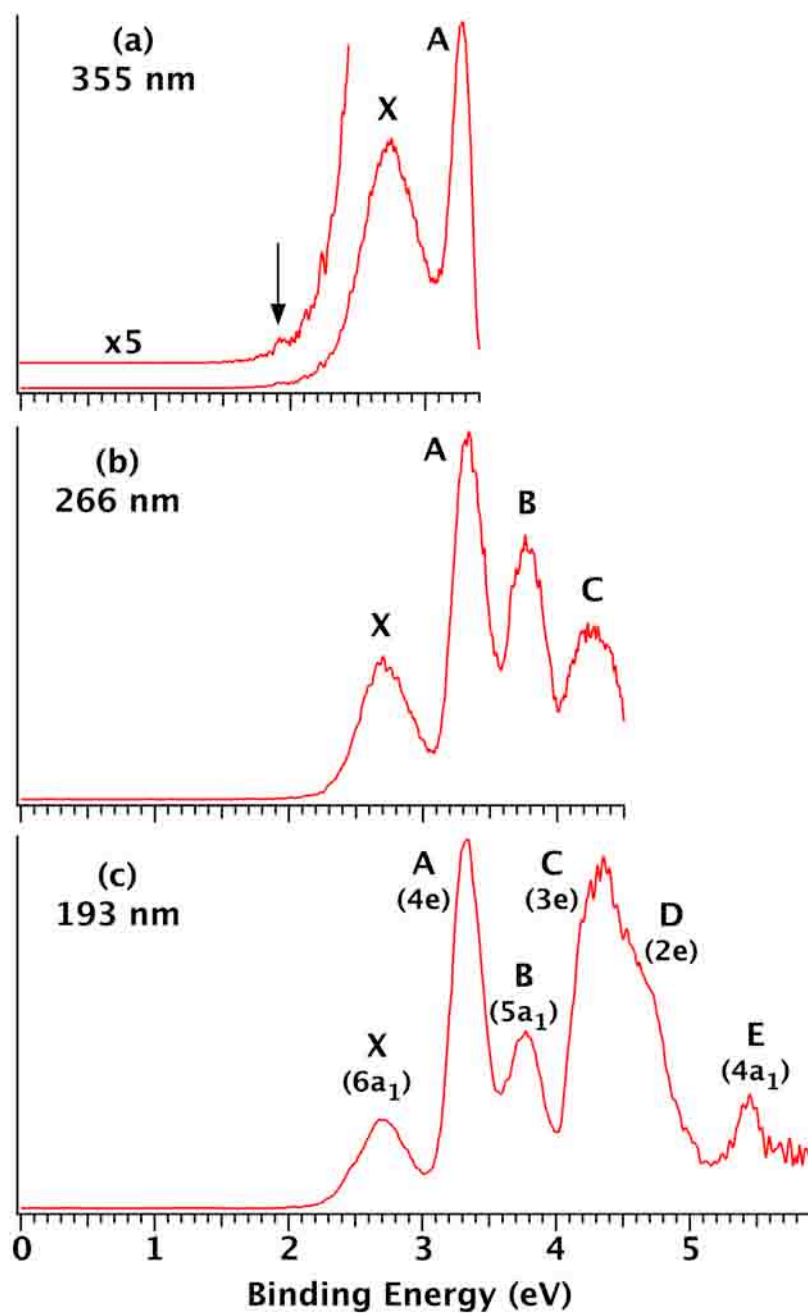
Figure 6-1. Photoelectron spectra of Al_7N^- at (a) 355 nm (3.496 eV), (b) 266 nm (4.661 eV), and (c) 193 nm (6.424 eV). The molecular orbital origin of each band is labeled in (c) according to theoretical calculations in Table 1 for the global minimum C_{3v} structure.
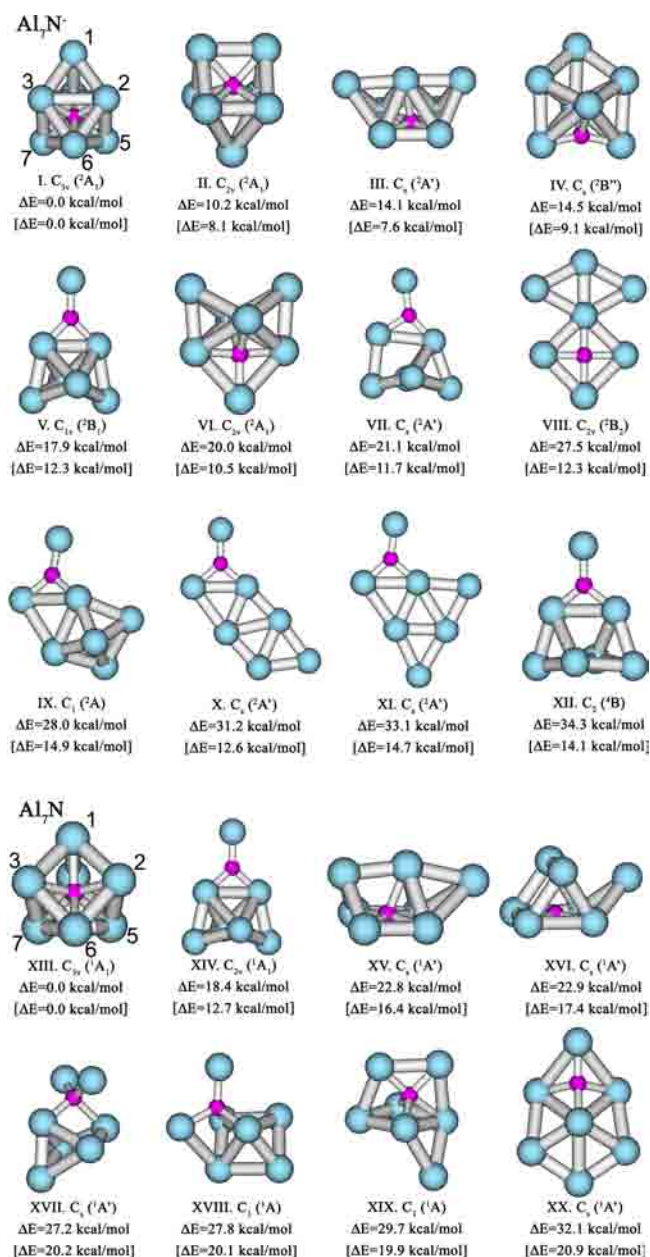
Figure 6-2. Computationally found low-lying isomers for Al₇N⁻ and Al₇N. Relative energies are given at CCSD(T)/6-311+G(2df)//B3LYP/6-311+G* and at B3LYP/6-311+G* in brackets.
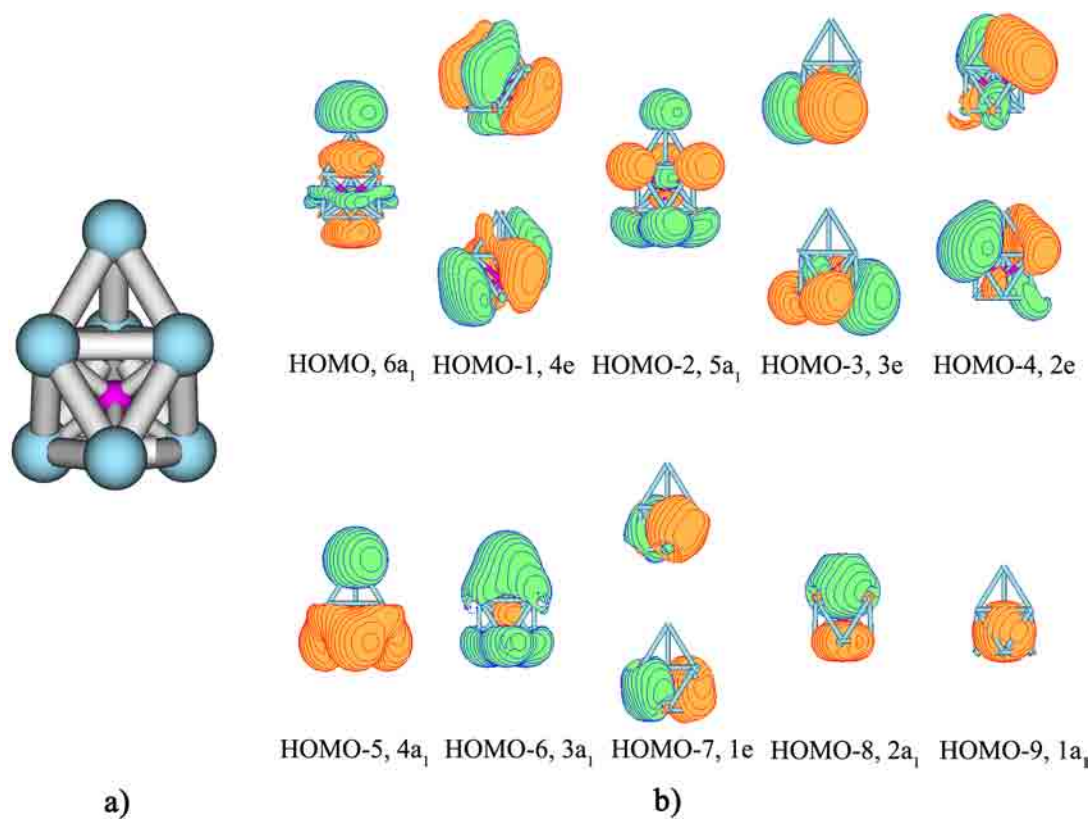
Figure 6-3. The optimized structure (a) and molecular orbital pictures (b) for Al_7N^{2-} calculated at B3LYP/6-311+G*.

CHAPTER 7

EXPERIMENTAL AND THEORETICAL INVESTIGATION OF 3-DIMENSIONAL

NITROGEN-DOPED ALUMINUM CLUSTER Al_8N^- AND Al_8N[1]

Abstract

The structure and electronic properties of the Al_8N^- and Al_8N clusters were investigated by combined photoelectron spectroscopy and ab initio studies. Congested photoelectron spectra were observed and experimental evidence was obtained for the presence of multiple isomers for Al_8N^-. Global minimum searches revealed several structures for Al_8N^- with close energies. The calculated vertical detachment energies of the two lowest-lying isomers, which are of C_{2v} and C_s symmetry, respectively, were shown to agree well with the experimental data. Unlike the 3-dimesional structures of Al_6N^- and Al_7N^-, in which the dopant N atom has a high coordination number of 6, the dopant N atom in the two low-lying isomers of Al_8N^- has a lower coordination number of 4 and 5, respectively. The competition between the Al-Al and Al-N interactions are shown to determine the global minimum structures of the doped aluminum clusters and results in the structural diversity for both Al_8N^- and Al_8N.

7-1. Introduction

Doped clusters are interesting because they can exhibit specific properties tailored with the dopant. Understanding the structures and chemical bonding of such clusters may lead to rational design of structurally and electronically stable clusters for applications in cluster–assembled nanomaterials or catalysis. While aluminum nitride is an important semiconductor material, there have been relatively few experimental and theoretical studies on small aluminum nitride clusters.[1-16] Li and Wang reported a set of photoelectron spectra of Al_xN^- ($x = 2$–22) clusters at 193 nm and compared them to those of pure Al_x^- clusters.[10] They found spectral similarity between Al_xN^- and Al_{x-1}^- clusters and suggested that there is a strong charge transfer to form formally N^{3-} centers in the nitrogen–doped aluminum clusters. In a series of recent studes,[12,13,16] we have combined photoelectron spectroscopy (PES) with global minimum structural search, using a gradient-embedded genetic algorithm followed by high-level *ab initio* calculations, to elucidate the detailed atomic structures and chemical bonding for several small nitrogen-doped aluminum clusters, Al_xN^- ($x = 3$–7). It was shown that Al_xN^- clusters are planar for $x = 3$–5, whereas their global minimum structures become 3-dimensional (3D) for $x = 6$ and 7 with the nitrogen atom having coordination number of six.

In the current work, we continue our research on Al_xN^- clusters and report the atomic and electronic structures of the Al_8N^- cluster using PES and *ab initio* calculations. Congested PES spectra were observed and interpreted by the *ab initio* data. A few different structures have been suggested theoretically for Al_8N and Al_8N^- in previous studies,[7-9] but they have not been confirmed experimentally. We found that there are

several low-lying isomers for Al_8N^- which are all 3D and very close in energy. Photoelectron spectra of Al_8N^- have been obtained at different experimental conditions, confirming the presence of close-lying isomers that contribute to the experiment. The coordination numbers of the nitrogen atom in these low-lying isomers of Al_8N^- vary from 4 to 6. Unlike the 3D clusters of Al_6N^- and Al_7N^-, the N-centered $[Al_6N]^{3-}$ octahedron is no longer found as a building block in the two lowest energy structures of Al_8N^-.

7-2. Experimental Method

The experiment was performed on a magnetic-bottle PES apparatus with a laser vaporization cluster source, details of which have been published elsewhere.[17] Briefly, the Al_8N^- clusters were produced by laser vaporization of an Al/AlN composite disk target using a pure helium carrier gas. The cluster/He gas mixture passed through a 10 cm-long, 3 mm-diameter tube extension to allow adequate thermalization of the clusters. This was found to produce relatively cold clusters, which were shown to be important to yield well-resolved PES spectra.[18,19] The anion clusters were extracted from the cluster beam perpendicularly and were analyzed using a time-of-flight mass spectrometer. Only Al_xN^- clusters with one N impurity atom could be observed under the experimental condition, as was shown before.[10] The Al_8N^- cluster was mass-selected and decelerated before being photodetached by a 193 nm laser beam from an ArF excimer laser, or by a 355 nm or 266 nm beam from a Nd:YAG laser. Photoelectrons were collected at near 100% collecting efficiency by the magnetic bottle and analyzed using a 3.5 m long electron flight tube. The electron energies were calibrated by the known spectrum of Au^-

(193 nm) or Rh$^-$ (355 and 266 nm). The resolution ($\Delta E_k/E_k$) of the apparatus was about 2.5%, i.e. ~25 meV for 1 eV kinetic energy electrons.

7-3. Theoretical Methods

We performed initial computational search for the global minima of Al$_8$N$^-$ and Al$_8$N using both our gradient embedded genetic algorithm (GEGA) program written by A. Alexandrova[20,21] and our simulated annealing program written by S. Call.[16] We used a hybrid method known as B3LYP[22-24] with the small split-valence basis set (3-21G) for energy, gradient and force calculations, with simulated annealing performing single-point energy calculations and GEGA performing gradient optimizations and frequency calculations. We reoptimized geometries and calculated frequencies for the lowest isomers using the B3LYP and CCSD(T)[25-27] methods with the polarized split-valence basis set (6-311+G*).[28-30] Total energies of the lowest isomers were also calculated using the CCSD(T) method with the extended 6-311+G(2df) basis set at the optimized CCSD(T)/6-311+G* geometries.

The vertical electron detachment energies (VDEs) were calculated using the RCCSD(T)/ 6-311+G(2df) method, the restricted outer valence Green Function method (ROVGF/6-311+ G(2df))[31-35] as well as the time-dependent DFT method[36,37] (TD-B3LYP/6-311+G(2df)) all at the optimized B3LYP/6-311+G* geometries. In the last approach, the first VDE was calculated at the B3LYP level of theory as the lowest transition from the singlet state of the anion into the final lowest doublet state of the neutral. Then the vertical excitation energies of the neutral species (at the TD-B3LYP

level) were added to the first VDE to obtain the second and higher VDEs. Core electrons were frozen in treating the electron correlation at the RCCSD(T) and ROVGF levels of theory. The B3LYP, RCCSD(T), ROVGF, and TD-B3LYP calculations were performed using the Gaussian 03 and Molpro programs.[38,39] Molecular structure visualization was done using the MOLDEN 3.4 program.[40]

7-4. Experimental Results

Figure 7-1 shows the PES spectra of Al_8N^- at three different photon energies. At 355 nm (Fig. 7-1a), two relatively sharp bands (X and A) were observed at VDEs of 2.86 and 3.16 eV, respectively. The adiabatic detachment energy (ADE) was evaluated from the relatively sharp onset of the X band to be 2.75 ± 0.05 eV. A shoulder (X') on the high binding energy side of band X was discernible, which became more obvious in the 266 nm (Fig. 7-1b). In addition, the 266 nm spectrum revealed several new bands: B, C, D, E, F. The A band seems to show some fine features on its high binding energy side around ~3.3 eV, which could be due to vibrational structures and/or additional electronic transitions. However, the pattern of the fine features seemed to depend on experimental conditions, indicating that they may be from different isomers. At 193 nm (Fig. 7-1c), a new band G was observed at ~4.6 eV, but featureless and continuous signals were observed beyond 4.8 eV. The overall PES spectral pattern was quite congested and complicated, probably due to contributions from more than one isomer. The VDEs of all observed bands are listed in Table 7-1 and compared to the theoretical data in Table 7-2.

To confirm the presence of low-lying isomers, we also measured PES spectra under "hot" condition without using the tube extension in the cluster source, as shown in Fig. 7-2. These spectra all show a long tail at the low binding energy side due to hot band transitions, consistent with hot source conditions. More importantly, the relative intensity of the X' band was indeed enhanced in the hot spectra, providing definitive experimental evidence that it came from contributions by another isomer. As will be shown below, this is born out by our theoretical calculations.

7-5. Theoretical Results

Al_8N^-. We initially performed simulated annealing and GEGA searches for the global minimum of Al_8N^- at the B3LYP/3-21G level of theory separately for singlet and triplet states. Both methods revealed an identical global minimum structure II (C_s, $^1A'$) (Fig. 7-3). The geometries and frequencies for the low-lying structures of Al_8N^- were then recalculated at the B3LYP/6-311+G* level of theory. Finally, single point calculations for the seven lowest-lying isomers were calculated at RCCSD(T)/6-311+G(2df) at the optimized CCSD(T)/6-311+G* structures. Geometries, symmetry, electronic state, and relative energies at B3LYP/6-311+G* and at CCSD(T)/6-311+G(2df)//CCSD(T)/6-311+G* for the first seven low-lying singlet and the lowest triplet isomers of Al_8N^- are displayed in Fig. 7-3. We found that previously reported global minimum Al_8N^- structure by Leskiw et al.[7] is 15.5 kcal/mol higher in energy than the structure II at CCSD(T)//6-311+G(2df)//B3LYP/6-311+G*+ZPE// B3LYP/6-311+G*.

The structure II (^{1}A',
$1a'^2 2a'^2 1a''^2 3a'^2 4a'^2 2a''^2 5a'^2 6a'^2 7a'^2 3a''^2 8a'^2 4a''^2 9a'^2 5a''^2 10a'^2$) (the MOs are arranged according to its VDEs) of C_s symmetry was found to be the global minimum (Figure 7-3) at both the B3LYP/3-21G and the B3LYP/6-311+G* levels of theory. However, at the CCSD(T)/6-311+G(2df)/CCSD(T)/6-311+G* level of theory the structure I (^{1}A$_1$, $1a_1^2 2a_1^2$ $1b_2^2 1b_1^2 3a_1^2 2b_2^2 2b_1^2 4a_1^2 5a_1^2 3b_2^2 6a_1^2 1a_2^2 3b_1^2 7a_1^2 4b_2^2$) of C_{2v} symmetry is lower than structure II by 1.9 kcal/mol. It should be stressed that from the theoretical point of view, such a small energy difference is beyond our ability to determine the global minimum structure of this anion with certainty. Unlike the 3D global minimum structures of Al$_6$N$^-$ and Al$_7$N$^-$, in which the nitrogen atom has a high coordination number of 6,[13,16] in both low-lying isomers of Al$_8$N$^-$ (I and II) the nitrogen atom has low coordination numbers of 4 and 5, respectively. Structure I can be described as an Al$_6$ octahedron bonded by an Al-N-Al motif. On the basis of Natural Population Analysis the Al-N-Al motif carries formal negative charge of –1. The structure II can be considered as originated from structure I by moving one bottom aluminum atom from the Al$_6$ octahedron to the top to bond with the N atom. Both isomers I and II seem to have been missed in a previous study by Leskiw *et al.*[7]

The next five low-lying isomers of Al$_8$N$^-$ were found to be 3.1 kcal/mol (isomer III), 4.4 kcal/mol (isomer IV), 5.2 kcal/mol (isomer V), 6.0 kcal/mol (isomer VI), and 9.9 kcal/mol (isomer VII) higher in energy than the global minimum (isomer I) at the CCSD(T)/6-311+G(2df)//CCSD(T)/6-311+G* + ZPE//B3LYP/6-311+G* level of theory. The structures III-VII have the following symmetry, electronic state, and configuration:

III – C_{2v}, $^1A_1$, $1a_1^2 1b_2^2 2a_1^2 1b_1^2 3a_1^2 2b_2^2 4a_1^2 2b_1^2 5a_1^2 1a_2^2 6a_1^2 3b_2^2 3b_1^2 7a_1^2 4b_2^2$;

IV – C_{2v}, $^1A_1$, $1a_1^2 2a_1^2 1b_2^2 1b_1^2 3a_1^2 2b_2^2 4a_1^2 2b_1^2 5a_1^2 3b_1^2 3b_2^2 6a_1^2 1a_2^2 7a_1^2 4b_2^2$;

V – C_{3v}, $^1A_1$, $1a_1^2 2a_1^2 3a_1^2 1e^4 2e^4 4a_1^2 5a_1^2 3e^4 6a_1^2 4e^4 7a_1^2$;

VI – D_{3d}, $^1A_{1g}$, $1a_{1g}^2 1a_{2u}^2 1e_u^4 2a_{1g}^2 2a_{2u}^2 3a_{1g}^2 2e_u^4 1e_g^4 3a_{2u}^2 2e_g^4 4a_{1g}^2$;

VII – D_{3h}, $^1A_1{}'$, $1a_1'^2 1a_2''^2 1e'^4 2a_1'^2 2a_2''^2 3a_1'^2 2e'^4 1e''^4 3a_2''^2 4a_1'^2 3e'^4$.
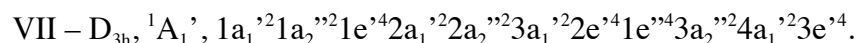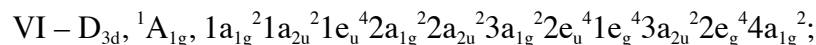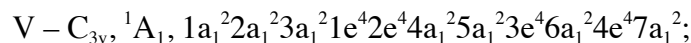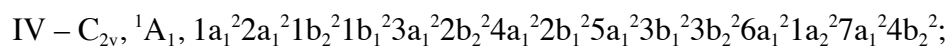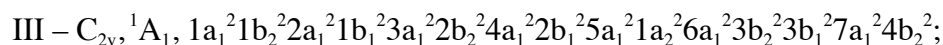
Isomers III, IV, and VI can all be considered as possible combinations of the Al_6N^{3-} octahedron bi-capped by two formal Al^+ cations. We have discussed the structure and bonding of the perfect octahedral Al_6N^{3-} previously.[13] Structure V can be viewed as a distorted aluminum octahedron bi-capped with an Al and an Al-N fragment to opposite sides. Finally, structure VII is formally a trigonal prism Al_6N^{3-} bi-capped by two Al^+ cations.

Al_8N. We also performed simulated annealing and GEGA searches for the global minimum structure of neutral Al_8N at the B3LYP/3-21G level of theory for both doublet and quartet states. The geometries and frequencies for low-lying structures were then recalculated at B3LYP/6-311+G* level. Finally, single point calculations for the low-lying isomers were calculated at RCCSD(T)/6-311+G(2df) at the optimized B3LYP/6-311+G* geometries. The structures of the eleven lowest-lying doublet isomers and one lowest quartet isomer of Al_8N are shown in Fig. 7-4.

There have been three different structures of Al_8N proposed to be a global minimum structure. Guo and Wu[9] reported the structure XI (Fig. 7-4) as the global minimum with the structure X being just 0.07 eV higher in energy than the structure XI. Liskiw et al.[7] reported the structure XII as the global minimum of Al_8N. Though Ling et

al.[8] reported another global minimum structure, which converged into the structure XIII in our calculations. In the current work we found a global minimum structure of Al_8N that is different from all the previously published.

According to our GEGA search, isomer IX was found to be the global minimum structure (Fig. 7-4). This structure (C_{3v}, $^2A_1$, $1a_1^2 2a_1^2 3a_1^2 1e^4 2e^4 4a_1^2 5a_1^2 3e^4 6a_1^2 4e^4 7a_1^1$) can be viewed as generated from structure V of the anion by removing one electron from its doubly occupied HOMO. The next lowest structure is structure X (C_s, $^2A'$, $1a'^2 2a'^2 1a''^2 3a'^2 4a'^2 5a'^2 6a'^2 7a'^2 2a''^2\ 3a''^2 8a'^2 9a'^2 4a''^2 10a'^2 11a'^1$), which is only 1.1 kcal/mol higher in energy at RCCSD(T)/6-311+G*//B3LYP/6-311+G* + ZPE//B3LYP/6-311+G* level, and thus they are degenerate from our point of view. The isomers X, XI, XIII, XV, XIX can be viewed as derived from the anionic isomers III, II, IV, I, and VIII, respectively, by removing one electron from the HOMO and some subsequent bond relaxation. It is more difficult to find parental anionic isomers for the neutral isomers XII, XIV, XVI, XVII, XVIII, and XX. We notice that similar structures as isomer X, XI and XII have been reported previously for Al_8N by several groups.[7-9] Similar to the case of the anionic isomers, the potential energy surface of the neutral Al_8N cluster is found to have many low-lying local minima.

7-6. Interpretation of the PES spectra

Our extensive structural search for Al_8N^- revealed five low-lying isomers within about less than 5 kcal/mol at the CCSD(T)/6-311+G(2df)//CCSD(T)/6-311+G*+ZPE//B3LYP/6-311+G* level of theory (Fig. 7-3). Those isomers are so close

in energies that potentially they could all contribute to the experimentally observed PES spectra. Indeed, the congested spectral pattern of Al_8N^- suggested potential complications due to the presence of more than one isomer, as evidenced experimentally (Figs. 7-1 and 7-2). The calculated VDE patterns for these five low-lying isomers of Al_8N^- at the ROVGF/6-311+G(2df) level of theory (or the CCSD(T) level if available) are compared to the 266 nm PES spectrum in Fig. 7-5, where the calculated VDEs are plotted as vertical bars. To aid the assignments, the spectra taken with and without the tube extension are both presented in Fig. 7-5. Clearly, isomer V ($^1A_1$, C_{3v}) can be ruled out immediately, because its first VDE is very low at 2.53 eV (Fig. 7-5b), which is absent in the experimental data. Similarly, the third VDE of isomer IV ($^1A_1$, C_{3v}) occurs in the gap region of the PES spectra, and it is expected to have negligible contributions to the observed spectrum. Both isomers IV and V are relatively high in energy, and it is reasonable that they are not present in our experiment.

The first VDE of isomer I ($^1A_1$, C_{2v}) and II ($^1A'$, C_s) agrees well with the X and X' band, respectively (Fig. 7-5a). Higher energy detachment channels of these two isomers are also consistent with the PES data quite well. Thus, they should be the major carriers of the PES spectra. Isomer III ($^1A_1$, C_{2v}) also gives detachment transitions, which are within the observed PES pattern (Fig. 7-5b). While we cannot assign this isomer definitively, we also cannot completely rule it out. The calculated VDEs for isomers I, II and III of Al_8N^- at the TD-B3LYP/6-311+G(2df), ROVGF/6-311+G(2df) and RCCSD(T)/6-311+G(2df) levels of theory are presented in Table 7-2, as well as tentative spectral assignments.

Overall, the experimental data are in excellent agreement with the combined detachment transitions calculated for the two lowest isomers (I and II), indicating that these structures are competing for the global minimum of Al_8N^-. The slightly higher energy of the isomer II is consistent with its enhanced population under hotter experimental conditions, indicating that isomer I should be the true global minimum for Al_8N^- and confirming the accuracy of the current level of theory.

7-7. Discussion

One of the most striking results found in the current experimental and theoretical study of Al_8N^- and Al_8N is the presence of structurally diverse isomers with close energies. This is likely a result of increasing competition between Al-Al and Al-N interactions in the doped cluster. In the smaller doped clusters, Al_xN^- and Al_xN ($x = 3–5$),[12] the Al-N interactions are more important. For example, in the Al_3N^- (C_{2v}) and Al_4N^- (D_{4h}) clusters, all aluminum atoms are located in the first coordination layer of the central nitrogen atom in planar geometries, which optimize the Al-N interactions.[12] We started to encounter low-lying isomers in Al_5N^- due to the competition between Al-Al and Al-N interactions. The global minimum structure of Al_5N^- (C_{2v}) is built upon the square-planar Al_4N^- structure with the additional Al atom boned to one of its four edges outside the first coordination layer. However, a 3D structure, which can be viewed as a tetrahedral Al_4 cluster bound to an AlN unit, was found to be a low-lying isomer and was also present in the PES spectra of Al_5N^-.[12] Thus, the Al-Al interactions start to be important structure-forming factors in Al_5N^-. For Al_6N^-, we found two close low-lying isomers, which

appear to optimize both the Al-Al and Al-N interactions.[13] For Al_7N^- and Al_7N, our study found only one dominating isomer in which the N atom has high coordination number of 6 and 7, respectively. Particularly for Al_7N, the seven Al atoms are all in the first coordination sphere and bound to the N atom, which seems to optimize Al-N interactions.[16] We have also shown that the global minimum structures of the Al_6N^- and Al_7N^- can be viewed as being evolved from the N-centered Al_6N^{3-} octahedron. The chemical bonding in the Al_6N^{3-} octahedron can be approximately rationalized as the central N atom carrying an effective charge of -3 (N^{3-}), which is ionically bound to an octahedral Al_6 cluster, thus optimizing both Al-Al and Al-N interactions.

For Al_8N^-, this Al_6N^{3-} octahedron is no longer found as a building block in the two lowest-lying isomers (Fig. 7-3). Instead, the two lowest isomers (I and II) of Al_8N^- can both be viewed as a distorted Al_4N^- square bound to four additional Al atoms. Unlike the 3D structures of Al_6N^- and Al_7N^-, the Al-Al interactions seem to be dominating in Al_8N^-, although isomers III and IV do contain the Al_6N^{3-} octahedron units and they are not too high in energy. Thus, the more complicated Al-Al and Al-N interactions in the larger Al_8N^- cluster are responsible for its structural diversity. It should also be pointed out that in all the low-lying isomers for Al_8N^- we found that the effective atomic charges on the N atom (calculated using natural bond analysis at B3LYP/6-311+G*) vary from -2.1 |e| to -2.5 |e|, indicating the formation of the nearly complete shell $2s^2 2p^6$ in the ionic limit (N^{3-}), which is consistent with the previous experimental observations.[10]

7-8. Summary

We investigated the structural properties of the Al_8N^- cluster in a combined photoelectron spectroscopy and ab initio study. The calculated VDEs were compared to the complicated PES spectral features and confirmed the presence of multiple isomers in the experiment for Al_8N^-. The global minimum structures of Al_8N and Al_8N^- were located using both genetic algorithm and stimulated annealing. We found that at least two low-lying isomers of Al_8N^- were populated experimentally and contribute to the observed PES spectra. Unlike the 3-dimesional structures of Al_6N^- and Al_7N^-, where the N atom has a high coordination number of 6, in the two low-lying isomers of Al_8N^- the N atom has low coordination numbers of 4 and 5. The competition between Al-Al and Al-N interactions are found to dictate the structures of the N-doped aluminum clusters and results in the diverse low-lying structures for Al_8N^- and Al_8N.

References

[1] P. v. R. Schleyer and A. I. Boldyrev, J. Chem. Soc., Chem. Commun. 1536 (1991).

[2] V. G. Zakrzewski, W. v. Niessen, A. I. Boldyrev, and P. v. R. Schleyer, Chem. Phys. **174**, 167 (1993).

[3] S. K. Nayak, S. N. Khana, and P. Jena, P. Phys. Rev. B **57**, 3787 (1998).

[4] S. K. Nayak, B. K. Rao, P. Jena, X. Li, and L. S. Wang, Chem. Phys. Lett. **301**, 379 (1999).

[5] B. H. Boo and Z. Liu, J. Phys. Chem. A **103**, 1250 (1999).

[6] L. Andrews, M. Zhou, G. V. Chertihin, W. D. Bare, and Y. Hannachi, J. Phys. A, **104**,

1656 (2000).

[7] B. R. Leskiw, A. W. Castleman, Jr., C. Ashman, and S. N. Khanna, J. Chem. Phys. **114**, 1165 (2001).

[8] L. Ling, B. Song, and P.-L. Cao, J. Mol. Struct.: THEOCHEM **728**, 215 (2005).

[9] L. Guo and H.-S. Wu, Int. J. Quantum Chem. **106**, 1250 (2006).

[10] X. Li and L. S. Wang, Eur. Phys. J. D **34**, 9 (2005).

[11] G. Meloni, S. M. Sheehan, B. F. Parsons, and D. M. Neumark, J. Phys. Chem. A **110**, 3527 (2006).

[12] B. B. Averkiev, A. I. Boldyrev, X. Li, and L. S. Wang, J. Chem. Phys. **125**, 124305 (2006).

[13] B. B. Averkiev, A. I. Boldyrev, X. Li, and L. S. Wang, J. Phys. Chem. A **111**, 34 (2007).

[14] B. Wang, D. Shi, X. Chen, G. Wang, and J. Zhao, Int. J. Modern Phys. B **19**, 2380 (2005).

[15] Q. Sun, Q. Wang, X. G. Gong, V. Kumar, and Y. Kawazoe, Eur. Phys. J. D **18**, 77 (2002).

[16] B. B. Averkiev, S. Call, A. I. Boldyrev, L. M. Wang, W. Huang, and L. S. Wang, J. Phys. Chem. A, **112**, 1873 (2008).

[17] L. S. Wang, H. S. Cheng, and J. Fan, J. Chem. Phys. **102**, 9480 (1995).

[18] X. Li, H. Wu, X. B. Wang, and L. S. Wang, Phys. Rev. Lett. **81**, 1909 (1998).

[19] J. Akola, M. Manninen, H. Hakkinen, U. Landman, X. Li, and L. S. Wang, Phys. Rev. B **60**, 11297 (1999).

[20] A. N. Alexandrova, A. I. Boldyrev, Y-J. Fu, X. B. Wang, and L. S. Wang, J. Chem. Phys. **121**, 5709 (2004).

[21] A. N. Alexandrova and A. I. Boldyrev, J. Chem. Theory Comput. **1**, 566 (2005).

[22] A. D. Becke, J. Chem. Phys. **98**, 5648 (1993).

[23] S. H. Vosko, L. Wilk, and M. Nusair, Can. J. Phys. **58**, 1200 (1980).

[24] C. Lee, W. Yang, and R. G. Parr, Phys. Rev. B **37**, 785 (1988).

[25] J. Cizek, Adv. Chem. Phys. **14**, 35 (1969).

[26] P. J. Knowles, C. Hampel, and H.–J. Werner, J. Chem. Phys. **99**, 5219 (1993).

[27] K. Raghavachari, G. W. Trucks, J. A. Pople, and M. Head-Gordon, Chem. Phys. Lett. **157**, 479 (1989).

[28] J. S. Binkley, J. A. Pople, and W. J. Hehre, J. Am. Chem. Soc. **102**, 939 (1980); M. S. Gordon, J. S. Binkley, J. A. Pople, W. J. Pietro, and W. J. Hehre, J. Am. Chem. Soc. **104**, 2797 (1982); W. J. Pietro, M. M. Francl, W. J. Hehre, D. J. Defrees, J. A. Pople, and J. S. Binkley, J. Am. Chem. Soc. **104**, 5039 (1982).

[29] A. D. McLean and G. S. Chandler, J. Chem. Phys. **72**, 5639 (1980).

[30] T. Clark, J. Chandrasekhar, G. W. Spitznagel, and P. v. R. Schleyer, J. Comput. Chem. **4**, 294 (1983).

[31] L. S. Cederbaum, J. Phys. B **8**, 290 (1975).

[32] J. V. Ortiz, Int. J. Quantum Chem., Quantum Chem. Symp. **23**, 321 (1989); J. S. Lin and J. V. Ortiz, Chem. Phys. Lett. **171**, 197 (1990).

[33] V. G. Zakrzewski, J. V. Ortiz, J. A. Nichols, D. Heryadi, D. L. Yeager, and J. T. Golab, Int. J. Quantum Chem. **60**, 29 (1996).

[34] Y. Dahnovsky, J. Chem. Phys. **126**, 234111 (2007).

[35] A. Kletsov and Y. Dahnovsky, Phys. Rev. B **76**, 035304 (2007).

[36] R. Bauernshmitt and R. Alrichs, Chem. Phys. Lett. **256**, 454 (1996).

[37] M. E. Casida, C. Jamorski, K. C. Casida, and D. R. Salahub, J. Chem. Phys. **108**, 4439 (1998).

[38] M. J. Frisch, G. W. Trucks, H. B. Schlegel *et al*, Gaussian 03, revision D.01; Gaussian, Inc.: Wallingford, CT, 2004.

[39] H.-J. Werner, P. J. Knowles, R. Lindh, F. R. Manby, M. Schütz *et al*, MOLPRO, version 2006.1, a package of ab initio programs, see http://www.molpro.net.

[40] MOLDEN3.4. G. Schaftenaar, CAOS/CAMM Center, The Netherlands, 1998.

Table 7-1. Experimentally observed vertical (VDE) and adiabatic (ADE) detachment

energies of Al_8N^- from its photoelectron spectra.[a]

Observed features	VDE (eV)	ADE (eV)
X	2.86 (4)	2.75 (5)
X'	2.99 (5)	
A	3.16 (3)	
B	3.45 (5)	
C	~ 4.0	
D	4.09 (3)	
E	4.26 (5)	
F	4.40 (5)	
G	~4.6	

[a] The numbers in the parentheses represent the experimental uncertainties in the last digit.

Table 7-2. The calculated VDEs of Al_8N^- for isomers I, II, and III at different levels of theory, and comparisons to the experimental data.

isomer	final states and configuration	VDE (Theo.) (eV)			PES assignments	
		TD-DFT	ROVGF[a]	RCCSD(T)	features	VDE (exp.) (eV)[b]
I	$^2B_2$, $5a_1^2 3b_2^2 6a_1^2 1a_2^2 3b_1^2 7a_1^2 4b_2^1$	2.64	2.79 (0.87)	2.89	X	2.86 (4)
	$^2A_1$, $5a_1^2 3b_2^2 6a_1^2 1a_2^2 3b_1^2 7a_1^1 4b_2^2$	2.96	3.09 (0.87)	3.25	A	3.16 (3)
	$^2B_1$, $5a_1^2 3b_2^2 6a_1^2 1a_2^2 3b_1^1 7a_1^2 4b_2^2$	3.28	3.09 (0.86)	3.33	A tail	~ 3.3
	$^2A_2$, $5a_1^2 3b_2^2 6a_1^2 1a_2^1 3b_1^2 7a_1^2 4b_2^2$	3.17	3.34 (0.86)	3.42	B	3.45 (5)
	$^2A_1$, $5a_1^2 3b_2^2 6a_1^1 1a_2^2 3b_1^2 7a_1^2 4b_2^2$	3.86	3.92 (0.86)		C	~ 4.0
	$^2B_2$, $5a_1^2 3b_2^1 6a_1^2 1a_2^2 3b_1^2 7a_1^2 4b_2^2$	3.89	4.23 (0.86)		E	4.26 (5)
	$^2A_1$, $5a_1^1 3b_2^2 6a_1^{22} 1a_2^2 3b_1 7a_1^2 4b_2^2$	4.32	4.38 (0.85)		F	4.40 (5)
II	$^2A'$, $6a'^2 7a'^2 3a''^2 8a'^2 4a''^2 9a'^2 5a''^2 10a'^1$	2.73	2.77 (0.87)	2.93	X'	2.99 (5)
	$^2A''$, $6a'^2 7a'^2 3a''^2 8a'^2 4a''^2 9a'^2 5a''^1 10a'^2$	2.95	3.16 (0.86)	3.28	A	3.16 (3)
	$^2A'$, $6a'^2 7a'^2 3a''^2 8a'^2 4a''^2 9a'^1 5a''^2 10a'^2$	3.24	3.30 (0.86)		A tail	~ 3.3
	$^2A''$, $6a'^2 7a'^2 3a''^2 8a'^2 4a''^1 9a'^2 5a''^2 10a'^2$	3.18	3.35 (0.86)		A tail	~ 3.3
	$^2A'$, $6a'^2 7a'^2 3a''^2 8a'^1 4a''^2 9a'^2 5a''^2 10a'^2$	4.04	4.11 (0.84)		D	4.09 (3)
	$^2A''$, $6a'^2 7a'^2 3a''^1 8a'^2 4a''^2 9a'^2 5a''^2 10a'^2$	4.15	4.38 (0.83)		F	4.40 (5)
	$^2A'$, $6a'^2 7a'^1 3a''^2 8a'^2 4a''^2 9a'^2 5a''^2 10a'^2$	4.52	4.88 (0.81)		G	~ 4.6
	$^2A'$, $6a'^1 7a'^2 3a''^2 8a'^2 4a''^2 9a'^2 5a''^2 10a'^2$	5.24	5.18 (0.77)			
III	$^2B_2$, $2b_1^2 5a_1^2 1a_2^2 6a_1^2 3b_2^2 3b_1^2 7a_1^2 4b_2^1$	2.83	3.17 (0.87)	3.12	A	3.16 (3)
	$^2A_1$, $2b_1^2 5a_1^2 1a_2^2 6a_1^2 3b_2^2 3b_1^2 7a_1^1 4b_2^2$	2.98	3.22 (0.86)	3.24	A tail	~ 3.3
	$^2B_1$, $2b_1^2 5a_1^2 1a_2^2 6a_1^2 3b_2^2 3b_1^1 7a_1^2 4b_2^2$	3.25	3.47 (0.85)	3.49	B	3.45 (5)
	$^2B_2$, $2b_1^2 5a_1^2 1a_2^2 6a_1^2 3b_2^1 3b_1^2 7a_1^2 4b_2^2$	3.92	3.96 (0.85)		C	~ 4.0
	$^2A_1$, $2b_1^2 5a_1^2 1a_2^2 6a_1^1 3b_2^2 3b_1^2 7a_1^2 4b_2^2$	4.12	4.32 (0.84)		E	4.26 (5)

$^2A_2$, $2b_1^2 5a_1^2 1a_2^1 6a_1^2 3b_2^2 3b_1^2 7a_1^2 4b_2^2$	4.74	4.92 (0.84)	4.92		
$^2A_1$, $2b_1^2 5a_1^1 1a_2^2 6a_1^2 3b_2^2 3b_1^2 7a_1^2 4b_2^2$	4.79	4.98 (0.84)			
$^2B_1$, $2b_1^1 5a_1^2 1a_2^2 6a_1^2 3b_2^2 3b_1^2 7a_1^2 4b_2^2$	4.64	4.94 (0.82)			

[a] Numbers in the parentheses represent the pole strength of the OVGF calculation.

[b] Numbers in the parentheses represent the experimental uncertainties in the last digit
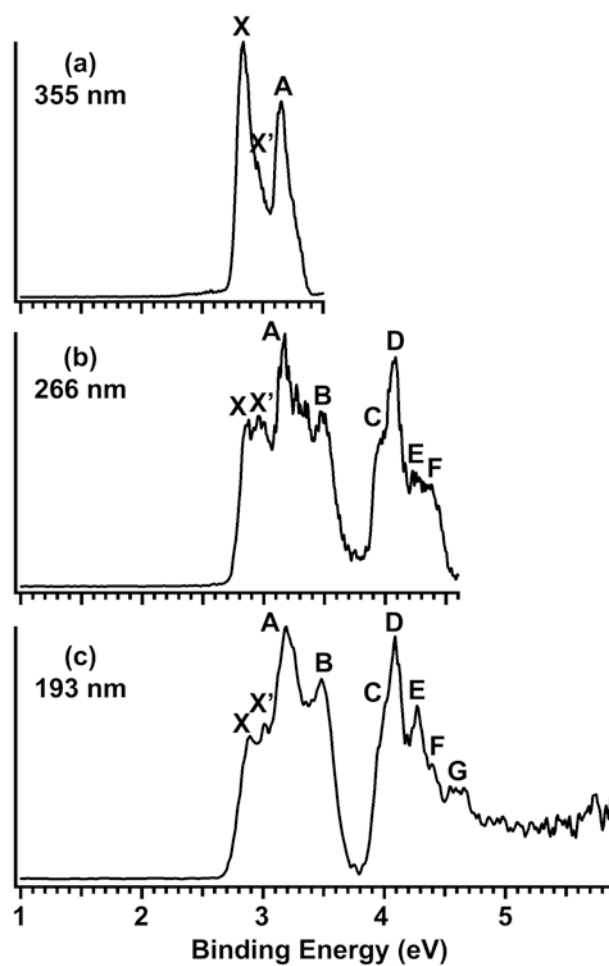
Figure 7-1. Photoelectron spectra of Al_8N^- at (a) 355 nm (3.496 eV), (b) 266 nm (4.661 eV), and (c) 193 nm (6.424 eV).
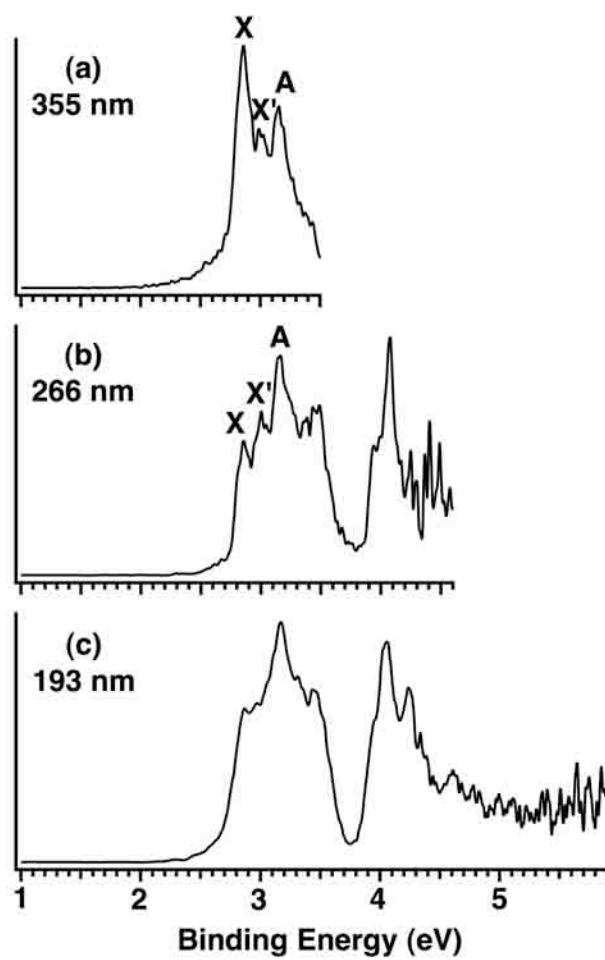
Figure 7-2. Same as figure 7-1, but taken under hotter source conditions.

I C$_{2v}$ (^{1}A$_1$)
0.0 kcal/mol
4.0 kcal/mol

II C$_s$ (^{1}A')
1.9 kcal/mol
0.0 kcal/mol

III C$_{2v}$ (^{1}A$_1$)
3.1 kcal/mol
3.2 kcal/mol

IV C$_{2v}$ (^{1}A$_1$)
4.4 kcal/mol
5.2 kcal/mol

V C$_{3v}$ (^{1}A$_1$)
5.2 kcal/mol
1.3 kcal/mol

VI D$_{3d}$ (^{1}A$_{1g}$)
6.0 kcal/mol
6.9 kcal/mol

VII D$_{3h}$ (^{1}A$_1'$)
9.9 kcal/mol
3.0 kcal/mol

VIII C$_s$ (^{3}A'')

10.3 kcal/mol
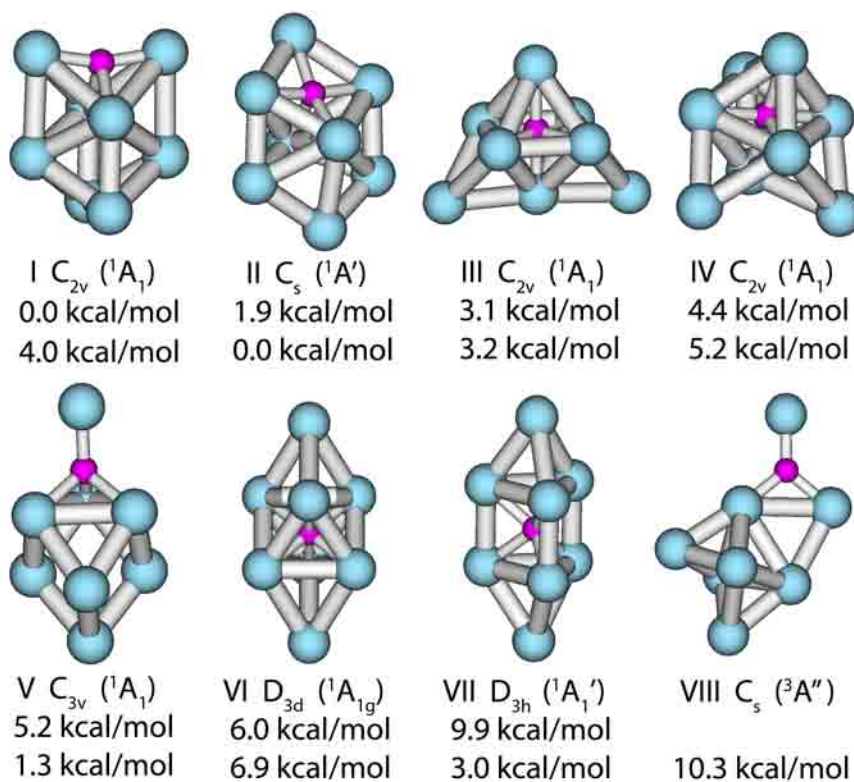
Figure 7-3. The first seven low-lying singlet isomers and the lowest triplet isomer of Al$_8$N$^-$. Upper and lower numbers are relative energies calculated at the CCSD(T)/6-311+G(2df)//CCSD(T)/6-311+G*+ZPE//B3LYP/6-311+G* and B3LYP/6-311+G*+ZPE//B3LYP/6-311+G* levels of theory, respectively.

IX C_{3v} ($^2A_1$)
0.0 kcal/mol
0.0 kcal/mol

X C_s ($^2A'$)
1.1 kcal/mol
3.7 kcal/mol

XI C_{2v} ($^2A_1$)
3.1 kcal/mol
1.9 kcal/mol

XII C_s ($^2A'$)
3.4 kcal/mol
5.1 kcal/mol

XIII C_s ($^2A'$)
4.1 kcal/mol
7.1 kcal/mol

XIV C_s ($^2A''$)
4.3 kcal/mol
3.5 kcal/mol

XV C_s ($^2A'$)
4.4 kcal/mol
7.6 kcal/mol

XVI C_s ($^2A'$)
6.3 kcal/mol
6.7 kcal/mol

XVII C_s ($^2A'$)
7.9 kcal/mol
7.2 kcal/mol

XVIII C_s ($^2A'$)
11.4 kcal/mol
6.4 kcal/mol

XIX C_1 (^2A)
12.6 kcal/mol
7.4 kcal/mol

XX C_s ($^4A''$)
16.5 kcal/mol
13.1 kcal/mol
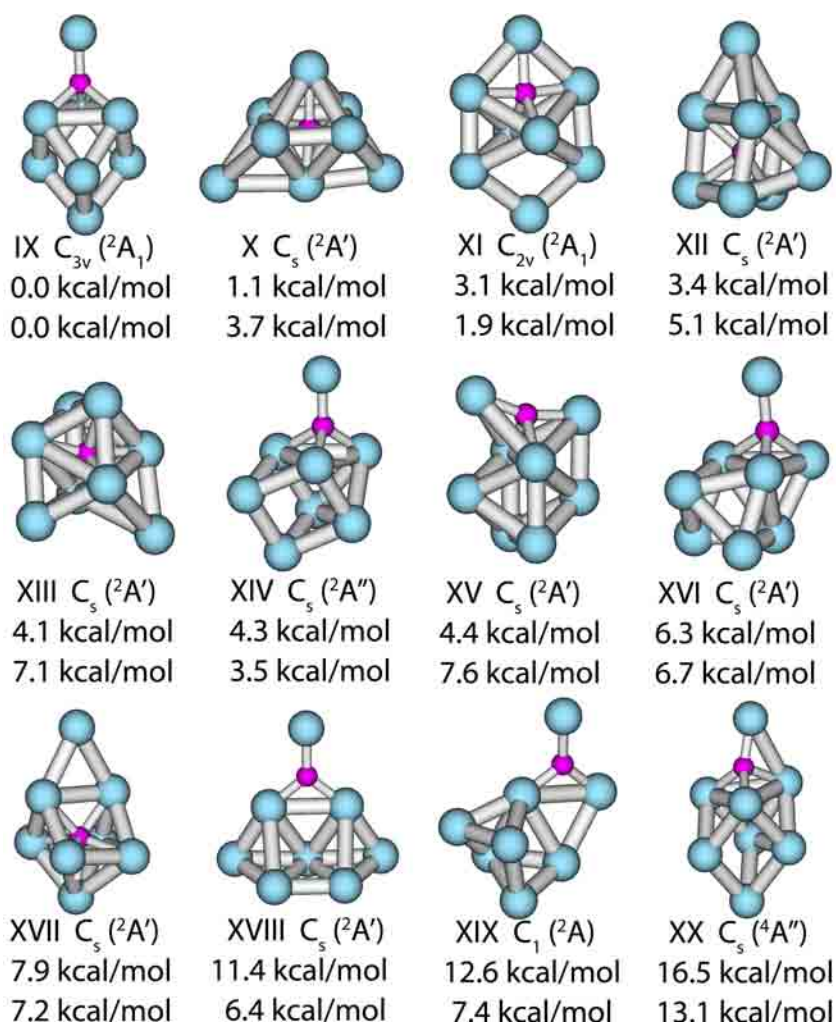
Figure 7-4. The first eleven low-lying doublet isomers and the lowest quartet isomer of Al_8N. Upper and lower numbers are relative energies calculated at the CCSD(T)/6-311+G(2df)//B3LYP/6-311+G* + ZPE//B3LYP/6-311+G* and B3LYP/6-311+G* + ZPE//B3LYP/6-311+G* levels of theory, respectively.
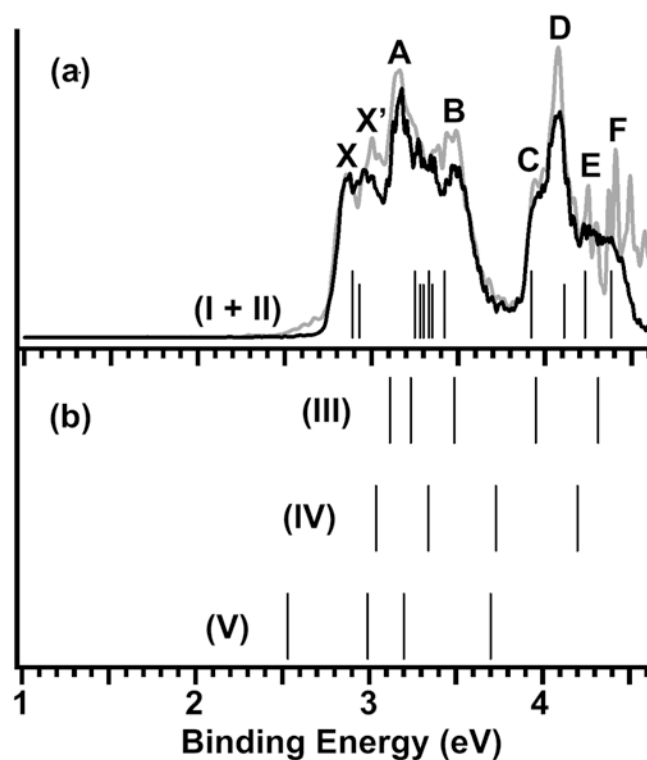
Figure 7-5. Comparison between the 266 nm PES spectra and the calculated VDEs (shown as vertical bars) at the ROVGF/6-311+G(2df) level of theory (or the CCSD(T) level if available) for (a) isomer I (longer bars) and isomer II (shorter bars), (b) isomers III , IV and V of Al_8N^-. PES spectra taken under both cold (dark) and hot (light gray) source conditions are shown for comparison.

CHAPTER 8

CB$_7^-$: EXPERIMENTAL AND THEORETICAL EVIDENCE AGAINST

HYPERCOORDINATED PLANAR CARBON[1]

Abstract

The B$_8^{2-}$ cluster was previously shown to possess a planar molecular wheel structure with a heptacoordinated boron. Substitution of one B$^-$ by C in B$_8^{2-}$ is expected to yield a closed shell CB$_7^-$ molecular wheel, which has been produced experimentally in a cluster beam and probed by photoelectron spectroscopy. Ab initio calculations show that the CB$_7^-$ cluster possesses an extremely stable planar C_{2v} structure, in which the C atom substitutes a B$^-$ atom at the edge of the B$_8^{2-}$ molecular wheel, whereas the D_{7h} structure with a heptacoordinated C is a high-lying isomer 63.2 kcal/mol (CCSD(T)/6-311+G(2df)//CCSD(T)/6-311+G*) above the global minimum.

8-1. Introduction

In organic chemistry, saturated carbon is known to bond to four ligands tetrahedrally, as first recognized independently by J. H. van't Hoff and J. A. LeBel in 1874. However, after the proposal by Hoffmann and co-workers about tetracoordinated planar carbon in 1970,[1] there were extensive experimental and theoretical efforts to search for the so-called anti-van't Hoff/anti-Lebel molecules (for recent reviews see

---

references 2-4). In particular, the first experimental and theoretical realization of penta-atomic planar coordinated carbon species in 1999 and 2000,[5-8] which confirmed earlier theoretical predictions,[9,10] has stimulated renewed interest in designing new tetracoordinated[11,12] and even hypercoordinated planar carbon molecules.[13-16] Notably, a series of hypercoordinated planar carbon species with boron ligands have been proposed.[13-15, 16a,c,e] Although none of these species is the global minimum on the potential energy surfaces, it has been suggested that they might be viable experimentally. The two proposed hexa- and hepta-coordinated carbon species are the D_{6h} CB_6^{2-} [13a,b,d,14c,15] and D_{7h} CB_7^-,[13b,14c] respectively. The CB_7^- species is isoelectronic to B_8^{2-}, which we have shown previously to possess a global minimum D_{7h} structure with a heptacoordinated boron.[17-20] The D_{7h} CB_7^- can be viewed as replacing the center B^- ion in B_8^{2-} by a C atom. In the current Communication, we report a serendipitous observation of CB_7^- experimentally. It is investigated by photoelectron spectroscopy (PES) and ab initio calculations, which show that the observed species is a C_{2v} CB_7^-, in which the C atom replaces a B^- ion from the edge of the D_{7h} B_8^{2-} molecular wheel.

8-2. Experimental Method

The experiment was performed using a laser vaporization cluster source and a magnetic bottle photoelectron spectrometer (see Experimental Section).[21] We have recently modified our cluster source by adding a 10 cm long and 0.2 cm diameter stainless steel tubing to enhance cluster cooling.[22] We were using boron clusters, which we have investigated previously extensively,[17-20,23-28] to test the new cluster source

conditions. A [10]B-enriched disk target containing a small amount of Au was used as the laser vaporization target.[23] Under certain conditions, when the vaporization laser was not perfectly aligned, we noted that in addition to the pure boron clusters we were also able to produce clusters containing one or two carbon atoms, as shown in Figure 8-1. The carbon source was most likely coming from the stainless steel tubing hit by the slightly misaligned vaporization laser beam. The trace amount of carbon contamination was ideal to produce the boron clusters doped with only one or two carbon atoms and the beam condition was stable and reproducible.

The CB_7^- cluster is particularly intense with abundance as strong as the nearby pure B_x^- clusters (Figure 8-1). Its photoelectron spectra are shown in Figure 8-2 at two detachment laser wavelengths. The 193 nm spectrum reveals five well-separated bands (X, A-D) and the B band exhibits a short vibrational progression with a frequency of 1050 ± 60 m^{-1}. The 355 nm spectrum shows a much better resolved X band, which seems to also display a short vibraitonal progression. However, the broad line width suggests that more than one low frequency modes may also be involved in the X band. The onset of the X band yields an adiabatic detachment energy or electron affinity for CB_7 as 2.99 ± 0.03 eV. The vertical detachment energies (VDE's) are given in Table 8-1, in comparison with theoretical results from several levels of theory.

8-3. Theoretical Methods

In our theoretical calculations, we first tested the two planar wheel structures of CB_7^- with the C substituting a central B (D_{7h}) and an edge B (C_{2v}) in the B_8^{2-} molecular

wheel. We found that the C_{2v} structure is overwhelmingly favored and is more stable than the D_{7h} heptacoordinated carbon structure by 63.9 kcal/mol at the B3LYP/6-311+G* level and 63.1 kcal/mol at the CCSD(T)/6-311+G(2df)//CCSD(T)/6-311+G* level. We further searched the potential energy surface for other low-lying structures using the GEGA method[29,30] and the top twelve low-lying isomers are shown in Figure 8-3. The C_{2v} wheel structure **I** was found to be the global minimum and the closest-lying isomer (**II**, C_s) is 37.6 kcal/mol (CCSD(T)/6-311+G(2df)//B3LYP/6-311+G*) higher in energy.

The VDE's from the C_{2v} global minimum and the D_{7h} isomer were calculated using three theoretical methods (Table 8-1), which are consistent with each other. We found that the calculated VDE's for the first five detachment channels from the C_{2v} global minimum are in excellent agreement with the experimental PES data, whereas those from the D_{7h} isomer totally disagree with the experiment. The excellent agreement between experiment and theory confirmed unequivocally the C_{2v} molecular wheel global minimum for CB_7^-.

8-4. Results and Discussion

To understand the difference in stability and chemical bonding in the two different molecular wheel structures of CB_7^-, we analyzed their valence molecular orbitals, as shown in Figure 8-4. The MOs of the D_{7h} CB_7^- (Figure 8-4b) are identical to those of the B_8^{2-} molecular wheel,[17-19] i.e., it is doubly aromatic with 6 totally delocalized π electrons (HOMO 1e''$_2$ and HOMO-3 1a''$_2$) and 6 totally delocalized σ electrons (HOMO-1 2e'$_1$ and HOMO-4 2a'$_1$), as well as 7 MOs (HOMO-2 1e'$_3$, HOMO-5 1e'$_2$,

HOMO-6 $1e'_1$, and HOMO-7 $1a'_1$) which can be localized into seven two-center two-electron (2c-2e) B-B peripheral bonds. The MOs of the C_{2v} global minimum (Figure 8-4a) are rather similar to those of the D_{7h} isomer; it is also π aromatic with 6 totally delocalized π electrons (HOMO $1a_2$, HOMO-1 $2b_1$, and HOMO-5 $1b_1$). There are also 7 MOs (HOMO-4 $5a_1$, HOMO-7 $3b_2$, HOMO-8 $3a_1$, HOMO-9 $2b_2$, HOMO-10 $1b_2$, HOMO-11 $2a_1$, and HOMO-12 $1a_1$), which could be localized into five 2c-2e peripheral B-B and two 2c-2e C-B peripheral bonds, similar to those in the D_{7h} isomer. The only major difference between MOs in the C_{2v} and D_{7h} isomers comes from the HOMO-6 $4a_1$ orbital, in which the peripheral electron delocalization is broken between the two boron atoms located on the opposite side to the carbon atom; the corresponding HOMO-4 $2a'_1$ orbital in the D_{7h} isomer is a completely delocalized s bonding orbital. One can also see that there is an enhancement in the area between those two boron atoms in the HOMO-3 $6a_1$ (Figure 8-3). Hence, the σ-aromaticity in the C_{2v} isomer of CB_7^- is less pronounced, though we think that this structure is still s-aromatic from the HOMO-2 $4b_2$, HOMO-3 $6a_1$, and HOMO-6 $4a_1$. In the D_{7h} isomer the bonding between the central carbon atom and the peripheral boron ring is completely delocalized (doubly σ- and π- aromaticity), while in the C_{2v} global minimum structure, the carbon atom is involved in the two 2c-2e B-C peripheral bonds, in addition to the participation in the delocalized σ- and π-bonding. Carbon is known to form strong 2c-2e σ-bonds because of its high valence charge that makes the peripheral position of carbon atom significantly more preferable compared to the central position. On the other hand, boron is known to participate in delocalized σ-bonding because of its relatively low valence charge, making the doubly

aromatic C_{2v} structure I the most stable. The current experimental and theoretical study shows that the heptacoordinated carbon in the C-B system is extremely unfavorable.

The low symmetry of the global minimum structure of CB_7^- leads to a dipole moment (1.4 D at B3LYP/6-311+G*) and this makes it possible to use the CB_7^- cluster for a rotary motion, similar to the rotary motion experimentally observed in metallocarboranes[31] by Hawthorne and co-workers, if the CB_7^- anion is incorporated into a sandwich like structure.

8-5. Experimental Section

Photoelectron spectroscopy: The $C_yB_x^-$ clusters were produced by laser vaporization of a ^{10}B-enriched disk target containing 60% ^{10}B and 40% Au by atom for mass calibration. The carbon source came from the long stainless steel tubing in the source due to a slight misalignment. Subsequently we also prepared a ^{10}B/C mixed target containing 5% C and produced $C_yB_x^-$ clusters similar to that shown in Figure 8-1. Negatively charged clusters were extracted from the cluster beam and were analyzed using a time-of-flight mass spectrometer (Figure 8-1).[21] The CB_7^- clusters of interest were mass selected and decelerated before being intercepted by a 193 nm laser beam from an ArF excimer laser and 355 nm from Nd:YAG laser for photodetachment. Photoelectron time-of-flight spectra were calibrated using the known spectra of Au$^-$ and Rh$^-$ and converted to the binding energy spectra by subtracting the kinetic energy spectra

from the photon energies. The resolution of the magnetic-bottle PES spectrometer was DE/E ~ 2.5%, i.e., about 25 meV for 1 eV electrons.

8-6. Theoretical Section

Calculations: We performed the search for the global minimum of CB_7^- using a gradient embedded genetic algorithm (GEGA) program,[29,30] using the B3LYP/3-21G method for energy, gradient and force calculations. We reoptimized geometries and calculated frequencies for the lowest 12 isomers at the B3LYP/6-311+G* level of theory. We also recalculated geometries of the two C_{2v}, $^1A_1$ and D_{7h}, $^1A'_1$ structures of CB_7^- using the CCSD(T)/6-311+G* method. Total energies of the twelve local minimum structures were also recalculated at the CCSD(T)/6-311+G(2df)//B3LYP/6-311+G* level of theory.

The CB_7^- vertical electron detachment energies (VDE's) were calculated using the R(U)CCSD(T)/6-311+G(2df), the outer valence Green Function method (ROVGF/6-311+G(2df)) at the RCCSD(T)/6-311+G* geometries, and the time-dependent DFT method (TD B3LYP/6-311+G(2df)) at the B3LYP/6-311+G* geometries. All calculations were performed using the Gaussian 03 program.[32] Molecular orbital visualization has been done using the MOLDEN3.4 program.[33]

References

[1] a) R. Hoffmann, R. W. Alder, C. F. Wilcox, Jr. *J. Am. Chem. Soc.* **1970**, *92*, 4992; b) R. Hoffmann, *Pure Appl. Chem.* **1971**, *28*, 181.

[2] R. Keese, *Chem. Rev.* **2006**, *106*, 4787.

[3] G. Merino, M. A. Mendez-Rojas, A. Vela, T. Heine, *J. Comput. Chem.* **2007**, *28*, 362.

[4] B. Sateesh, A. S. Reddy, G. N. Sastry, *J. Comput. Chem.* **2007**, *28*, 335.

[5] X. Li, L. S. Wang, A. I. Boldyrev, J. Simons, *J. Am. Chem. Soc.* **1999**, *121*, 6033.

[6] L. S. Wang, A. I. Boldyrev, X. Li, J. Simons, *J. Am. Chem. Soc.* **2000**, *122*, 7681.

[7] X. Li, H. F. Zhang, L. S. Wang, G. D. Geske, A. I. Boldyrev, *Angew. Chem. Int. Ed.* **2000**, *39*, 3630; *Angew. Chem.* **2000**, *112*, 3776.

[8] X. Li, H. J. Zhai, L. S. Wang, *Chem. Phys. Lett.* **2002**, *357*, 415.

[9] P. v. R. Schleyer, A. I. Boldyrev, *J. Chem. Soc. Chem. Comm.* **1991**, 1536.

[10] A. I. Boldyrev, J. Simons, *J. Am. Chem. Soc.* **1998**, *120*, 7967.

[11] a) G. D. Geske, A. I. Boldyrev, *Inorg. Chem.* **2002**, *41*, 2795; b) S.-D. Li, G.-M. Ren, C.-Q. Miao, Z.-H. Jin, *Angew. Chem. Int. Ed.* **2004**, *43*, 1371; *Angew. Chem.* **2004**, *116*, 1395; c) L.-M. Yang, Y.-H. Ding, C.-C. Sun, *J. Am. Chem. Soc.* **2007**, *129*, 658; d) V. A. Starodub, D. V. Ziolkovskii, *J. Struct. Chem.* **2006**, *47*, 8; e) L.-M. Yang, Y.-H. Ding, C.-C. Sun, *J. Am. Chem. Soc.* **2007**, *129*, 1900.

[12] a) G. Merino, M. A. Mendez-Rojas, A. Vela, *J. Am. Chem. Soc.* **2003**, *125*, 6026. b) G. Merino, M. A. Mendez-Rojas, H. I. Beltran, C. Corminboeuf, T. Heine, A. Vela, *J. Am. Chem. Soc.* **2004**, *126*, 16160; c) N. Perez, T. Heine, R. Barthel, G. Seifert, A. Vela, M. A. Mendez-Rojas, G. Merino, *Org. Lett.* **2005**, *7*, 1509; d) M.-D. Su, *Inorg. Chem.* **2005**, *44*, 4829; e) P. M. Esteves, N. B. P. Ferreira, R. J. Correa, *J. Am. Chem. Soc.* **2006**, 127, 8680; f) M.-D. Su, *Inorg. Chem.* **2005**, *44*, 4829.

[13] a) K. Exner, P. v. R. Schleyer, *Science*, **2000**, *290*, 1937; b) Z.-X. Wang, P. v. R. Schleyer, *Science*, **2001**, *292*, 2465; c) S. Erhardt, G. Frenking, Z. Chen, P. v. R. Schleyer, *Angew. Chem. Int. Ed.* **2005**, *44*, 1078; *Angew. Chem.* **2005**, *117*, 1102; d)

K. Ito, Z. Chen, C. Corminboeuf, C. S. Wannere, X. H. Zhang, Q. S. Li, P. v. R. Schleyer, *J. Am. Chem. Soc.* **2007**, *129*, 1510.

[14] a) R. M. Minyaev, T. N. Gribanova, A. G. Starikov, V. I. Minkin, *Mendeleev Comm.* **2001**, *11*, 213; b) T. N. Gribanova, R. M. Minyaev, V. I. Minkin, *Russ. J. Inorg. Chem.* **2001**, *46*, 1207; c) R. M. Minyaev, T. N. Gribanova, A. G. Starikov, V. I. Minkin, *Dokl. Chem.* **2002**, *382*, 41; V. I. Minkin, R. M. Minyaev, *Mendeleev Comm.* **2004**, *14*, 43.

[15] R. W. A. Havenith, P. W. Fowler, E. Steiner, *Chem. Eur, J.* **2002**, *8*, 1068.

[16] a) S.-D. Li, C.-Q. Miao, J.-C. Guo, G.-M. Ren, *J. Am. Chem. Soc.* **2004**, *126*, 16227; b) S.-D. Li, C.-Q. Miao, G.-M. Ren, *Eur. J. Inorg. Chem.* **2004**, 2232; c) S.-D. Li, J.-C. Guo, C.-Q. Miao, G.-M. Ren, *J. Phys. Chem. A*, **2005**, *109*, 4133; d) S.-D. Li, C.-Q. Miao, *J. Phys. Chem. A*, **2005**, *109*, 7594; e) S.-D. Li, C.-Q. Miao, G.-M. Ren, J.-C. Guo, *Eur. J. Inorg. Chem.* **2006**, 2567.

[17] H. J. Zhai, A. N. Alexandrova, K. A. Birch, A. I. Boldyrev, L. S. Wang, *Angew. Chem. Int. Ed.* **2003**, *42*, 6004; *Angew. Chem.* **2003**, *115*, 6186.

[18] A. N. Alexandrova, H. J. Zhai, L. S. Wang, A. I. Boldyrev, *Inorg. Chem.* **2004**, *43*, 3552.

[19] A. N. Alexandrova, A. I. Boldyrev, H. J. Zhai, L. S. Wang, *Coord. Chem. Rev.* **2006**, *250*, 2811.

[20] D. Yu. Zubarev, A. I. Boldyrev, *J. Comput. Chem.* **2007**, *28*, 251.

[21] L. S. Wang, H. S. Cheng, J. Fan, *J. Chem. Phys.* **1995**, *102*, 9480.

[22] L. S. Wang, X. Li in *Clusters and Nanostructure Interfaces* (Eds.: by P. Jena, S. N. Khanna, B. K. Rao), World Scientific, River Edge, NJ, **2000**, pp. 293-300.

[23] H. J. Zhai, B. Kiran, J. Li, L. S. Wang, *Nature Materials* **2003**, *2*, 827.

[24] H. J. Zhai, L. S. Wang, A. N. Alexandrova, A. I. Boldyrev, V. G. Zakrzewski, *J. Phys. Chem. A* **2003**, *107*, 9319.

[25] H. J. Zhai, L. S. Wang, A. N. Alexandrova, A. I. Boldyrev, *J. Chem. Phys.* **2002**, *117*, 7917.

[26] A. N. Alexandrova, A. I. Boldyrev. H. J. Zhai, L. S. Wang, E. Steiner, P. W. Fowler, *J. Phys. Chem. A* **2003**, *107*, 1359.

[27] A. N. Alexandrova, A. I. Boldyrev, H. J. Zhai, L. S. Wang, *J. Phys. Chem. A* **2004**, *108*, 3509.

[28] A. N. Alexandrova, A. I. Boldyrev, H. J. Zhai, L. S. Wang, *J. Chem. Phys.* **2005**, *122*, 054313.

[29] A. N. Alexandrova, A. I. Boldyrev, Y. J. Fu, X. B. Wang, L. S. Wang, *J. Chem. Phys.* **2004**, *121*, 5709.

[30] A. N. Alexandrova and A. I. Boldyrev, *J. Chem. Theory and Comput.* **2005**, *1*, 566.

[31] M. F. Hawthorne, J. I. Zink, J. M. Skelton, M. J. Bayer, C. Liu, E. Livshits, R. Baer, D. Neuhauser, *Science,* **2004**, *303*, 1849.

[32] Gaussian 03, Revision D.01, M. J. Frisch, G. W. Trucks, H. B. Schlegel, G. E. Scuseria, M. A. Robb, J. R. Cheeseman, J. A. Montgomery, Jr., T. Vreven, K. N. Kudin, J. C. Burant, J. M. Millam, S. S. Iyengar, J. Tomasi, V. Barone, B. Mennucci, M. Cossi, G. Scalmani, N. Rega, G. A. Petersson, H. Nakatsuji, M.

Hada, M. Ehara, K. Toyota, R. Fukuda, J. Hasegawa, M. Ishida, T. Nakajima, Y. Honda, O. Kitao, H. Nakai, M. Klene, X. Li, J. E. Knox, H. P. Hratchian, J. B. Cross, V. Bakken, C. Adamo, J. Jaramillo, R. Gomperts, R. E. Stratmann, O. Yazyev, A. J. Austin, R. Cammi, C. Pomelli, J. W. Ochterski, P. Y. Ayala, K. Morokuma, G. A. Voth, P. Salvador, J. J. Dannenberg, V. G. Zakrzewski, S. Dapprich, A. D. Daniels, M. C. Strain, O. Farkas, D. K. Malick, A. D. Rabuck, K. Raghavachari, J. B. Foresman, J. V. Ortiz, Q. Cui, A. G. Baboul, S. Clifford, J. Cioslowski, B. B. Stefanov, G. Liu, A. Liashenko, P. Piskorz, I. Komaromi, R. L. Martin, D. J. Fox, T. Keith, M. A. Al-Laham, C. Y. Peng, A. Nanayakkara, M. Challacombe, P. M. W. Gill, B. Johnson, W. Chen, M. W. Wong, C. Gonzalez, J. A. Pople, Gaussian, Inc., Wallingford, CT, **2004**.

[33]   MOLDEN3.4. Schaftenaar, G. MOLDEN3.4, CAOS/CAMM Center, The Netherlands, **1998**.

Table 8-1. Comparison of the experimental vertical detachment energies (VDE) of CB_7^- to the calculated values for the global minimum C_{2v} structure and the high-lying D_{7h} isomer. All energies are in eV.

Feature	VDE (exp.) [a]	Final State and Electronic Configuration	VDE (theo.)		
			TD-B3LYP	OVGF [b]	DCCSD(T) [c]
		CB_7^- (C_{2v}, $^1A_1$)			
X [d]	3.03 (2)	$^2A_2$, $4a_1^2 1b_1^2 5a_1^2 6a_1^2 4b_2^2 2b_1^2 1a_2^1$	2.90	2.94 (0.89)	3.04
A	3.80 (3)	$^2B_1$, $4a_1^2 1b_1^2 5a_1^2 6a_1^2 4b_2^2 2b_1^1 1a_2^2$	3.79	3.81 (0.88)	3.86
B [e]	4.73 (3)	$^2B_2$, $4a_1^2 1b_1^2 5a_1^2 6a_1^2 4b_2^1 2b_1^2 1a_2^2$	4.66	4.80 (0.89)	4.78
C	5.28 (3)	$^2A_1$, $4a_1^2 1b_1^2 5a_1^2 6a_1^1 4b_2^2 2b_1^2 1a_2^2$	5.17	5.24 (0.88)	5.35
D	6.2 (1)	$^2A_1$, $4a_1^2 1b_1^2 5a_1^1 6a_1^2 4b_2^2 2b_1^2 1a_2^2$	6.10	6.29 (0.87)	
		CB_7^- (D_{7h}, $^1A_1$)			
		$^2E_2''$, $2a_1'^2 1a_2''^2 1e_3'^4 2e_1'^4 1e_2''^3$	2.86	2.86 (0.89)	2.98
		$^2E_1'$, $2a_1'^2 1a_2''^2 1e_3'^4 2e_1'^3 1e_2''^4$	5.40	5.29 (0.89)	5.51
		$^2E_3'$, $2a_1'^2 1a_2''^2 1e_3'^3 2e_1'^4 1e_2''^4$	6.18	6.34 (0.87)	
		$^2A_2''$, $2a_1'^2 1a_2''^1 1e_3'^4 2e_1'^4 1e_2''^3$	7.04	6.77 (0.65)	

[a] Numbers in parentheses represent the uncertainty in the last digit.
[b] VDEs were calculated at ROVGF/6-311+G(2df)//RCCSD(T)/6-311+G* level of theory. Values in parentheses represent the pole strength of the OVGF calculation.
[c] VDEs were calculated at UCCSD(T)/6-311+G(2df)//RCCSD(T)/6-311+G* level of theory.
[d] The adiabatic detachment energy of the X band or the electron affinity of CB_7 is 2.99 ± 0.03 eV.
[e] The vibrational frequency observed for this band is 1050 ± 60 cm^{-1}.
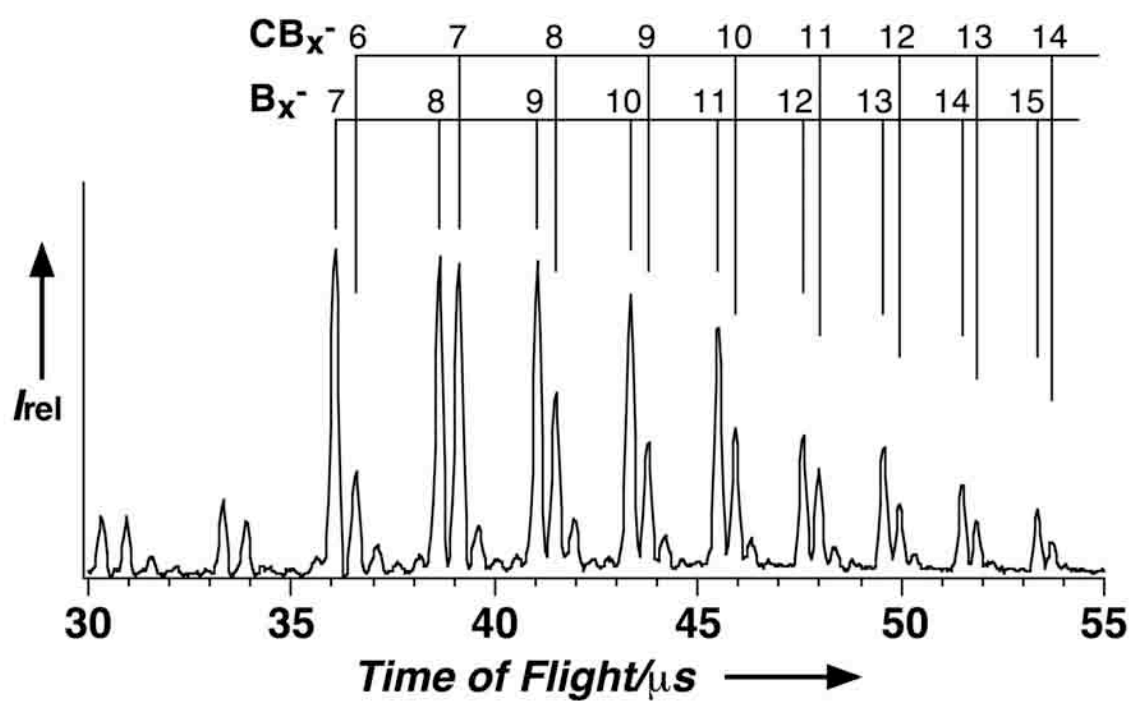
Figure 8-1. Mass spectrum of B_x^- and $C_yB_x^-$ clusters by using a ^{10}B-enriched boron target. The B_x^- and CB_x^- series are marked. Weaker masses for the $C_2B_x^-$ and $C_3B_x^-$ series can also be seen.
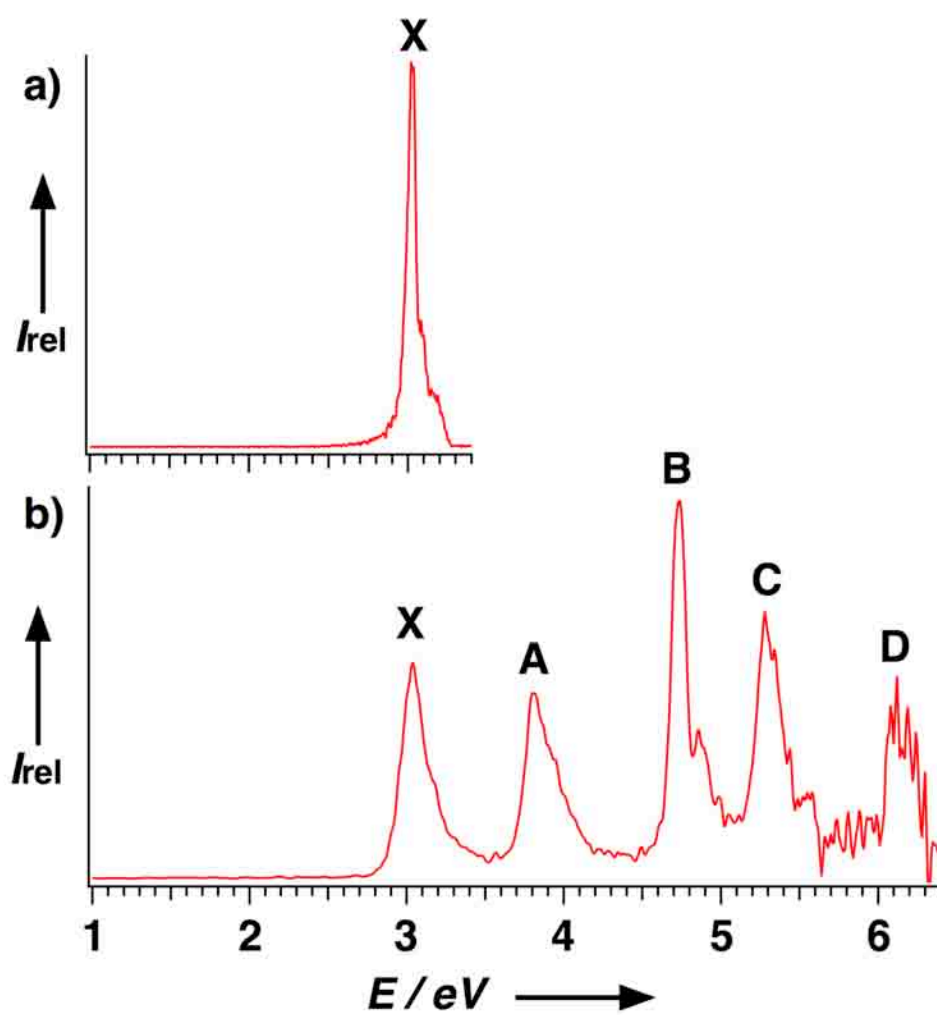
Figure 8-2. Photoelectron spectra of CB_7^- at a) 355 nm (3.496 eV) and b) 193 nm (6.424 eV).
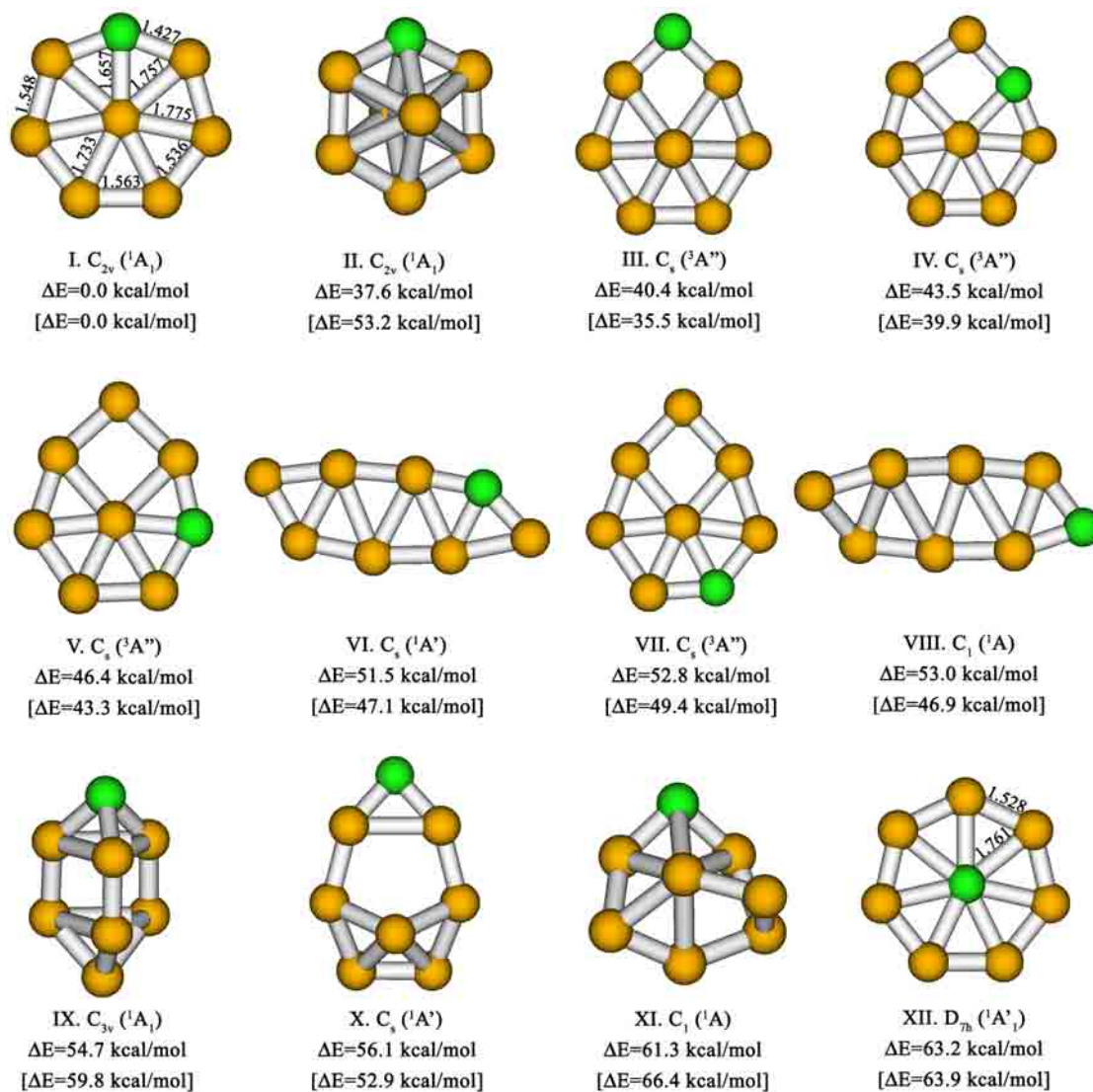
Figure 8-3. Optimized structures (at B3LYP/6-311+G*) and relative energies of CB_7^- (at CCST(D)/6-311+G(2df)//B3LYP/6-311+G*). The relative energies in the brackets are from B3LYP/6-311+G*.

a) *C*$_{2v}$ b) *D*$_{7h}$

HOMO, 1a$_2$ HOMO-1, 2b$_1$ HOMO-2, 4b$_2$ HOMO-3, 6a$_1$

HOMO-4, 5a$_1$ HOMO-5, 1b$_1$ HOMO-6, 4a$_1$

HOMO-7, 3b$_2$ HOMO-8, 3a$_1$ HOMO-9, 2b$_2$

HOMO-10, 1b$_2$ HOMO-11, 2a$_1$ HOMO-12, 1a$_1$

HOMO, 1e"$_2$ HOMO', 1e"$_2$ HOMO-1, 2e'$_1$ HOMO-1', 2e'$_1$

HOMO-2, 1e'$_3$ HOMO-2', 1e'$_3$ HOMO-3, 1a"$_2$

HOMO-4, 2a'$_1$ HOMO-5, 1e'$_2$ HOMO-5', 1e'$_2$

HOMO-6, 1e'$_1$ HOMO-6', 1e'$_1$ HOMO-7, 1a'$_1$
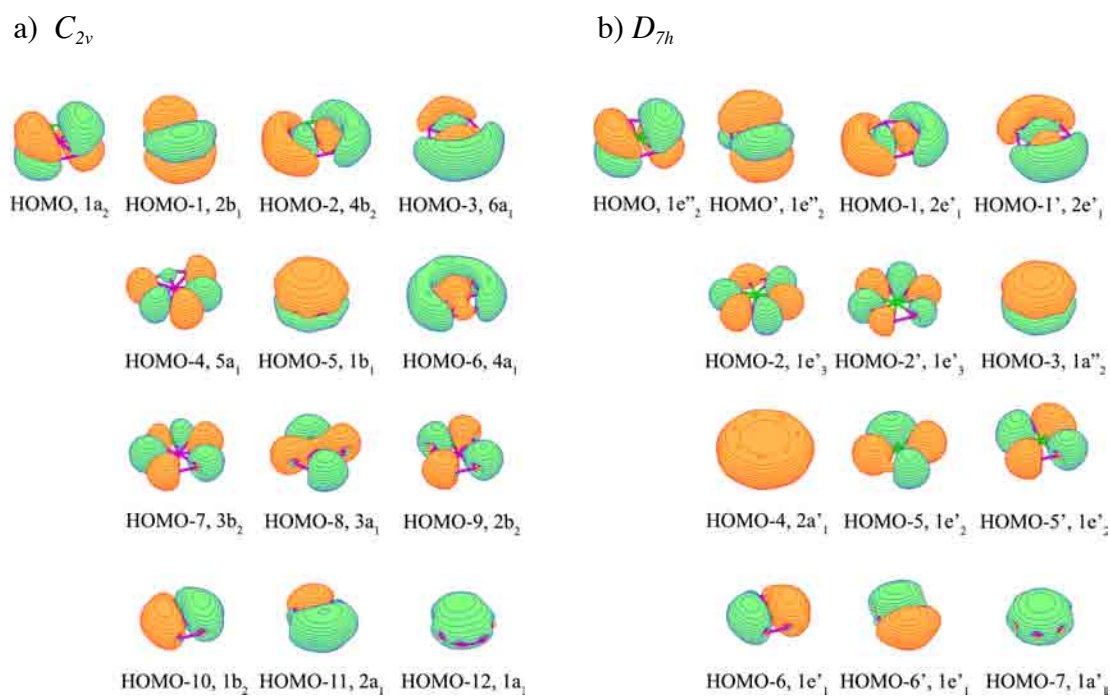
Figure 8-4. Comparison of the valence molecular orbitals of the global minimum *C*$_{2v}$ CB$_7^-$ and the high-lying *D*$_{7h}$ isomer.

CHAPTER 9

CARBON AVOIDS HYPERCOORDINATION IN CB_6^-, CB_6^{2-}, AND $C_2B_5^-$

PLANAR CARBON-BORON CLUSTERS[1]

Abstract

The structures and bonding of CB_6^-, $C_2B_5^-$, and CB_6^{2-} are investigated by photoelectron spectroscopy and ab initio calculations. It is shown that the global minimum structures for these systems are distorted hepta-cyclic structures. The previously reported hexa-cyclic structures with a hypercoordinate central carbon atom are found to be significantly higher in energy and were not populated under current experimental conditions. The reasons why carbon avoids hyper-coordination in these planar carbon-boron clusters are explained through detailed chemical bonding analyses.

9-1. Introduction

In the past two decades computational chemistry has made dramatic advances, making it possible to predict novel molecules that often contradict chemical intuition. Many theoretical chemists have participated in this endeavor, proposing myriads of unusual molecules. However, very often the predicted species are not the global minima and it is difficult if not impossible to observe them experimentally. Molecules with hyper-coordinated carbons in planar boron-carbon clusters are vivid examples of such

---

[1] Coauthored by Boris B. Averkiev, Dmitry Yu. Zubarev, Lei-Ming Wang, Wei Huang, Lai-Sheng Wang, and Alexander I. Boldyrev. Reproduced with permission from *J. Am. Chem. Soc.* **2008**, 130, 9248-9250. Copyright 2008 American Chemical Society.

predictions. Here we aim to show, via a joint experimental and theoretical investigation, that such species are too high in energy to be experimentally observed.

Since Hoffmann and co-workers proposed the idea of tetracoordinate planar carbon (tpC) molecules,[1] there have been numerous computational predictions of such unusual species.[2-5] Ab initio predictions of thought-to-be outlandish pentaatomic tpC molecules[6] were experimentally confirmed in 1999 and 2000.[7] These experimental advances have stimulated further searches for even higher coordination in planar carbon species.[8-10] In particular, a series of C/B binary clusters with hypercoordinate planar carbons,[8a] has been proposed which have attracted significant attention.[11,12] The planar CB_6^{2-} cluster with a hexacoordinate carbon has been touted as a "divining molecule" highlighted on the cover of *Chem. & Eng. News*.[11] In this article we show that in the systems containing boron atoms as ligands, such as CB_6^{2-}, the central position with high coordination number should be favored for atoms with low electronegativity and strong tendency to participate in delocalized bonding. The key point here is the presence of two-center two-electron bonds between peripheral atoms. The higher electronegativity of C compared to B clearly disfavors the hexacoordinate C isomers of CB_6^- and $C_2B_5^-$. It should be pointed out that in Ref. 8a an extensive survey of the isoelectronic C_3B_4 also revealed that the hexacoordinate isomer is higher in energy.

Heptacoordinated planar carbon in the D_{7h} CB_7^- cluster was initially computationally predicted by Schleyer and co-workers.[8b] We recently observed a highly stable CB_7^- cluster serendipitously during laser vaporization experiments. Using photoelectron spectroscopy (PES) and *ab initio* calculations, we found that the global

minimum planar structure CB_7^- has C_{2v} symmetry with the C atom in a peripheral position.[13] The planar D_{7h} CB_7^- structure may be kinetically stable but it is much higher in energy than the C_{2v} global minimum. In principle, kinetically stable but thermodynamically unfavorable isomers can be observed under some special conditions, but they were not populated under the experimental conditions of the previous study. Here we present both experimental and *ab initio* results demonstrating that the most stable isomers for CB_6^{2-} and its isoelectronic $C_2B_5^-$, as well as CB_6^-, are not the previously proposed planar structures containing a hexacoordinate carbon. Instead, the latter are found to be extremely high energy isomers and cannot be made through atom self-assembly in the gas phase.

9-2. Experimental Methods

The experiment was done using a laser vaporization cluster source and a magnetic-bottle PES analyzer, details of which can be found elsewhere.[14] The target used to produce CB_6^- and $C_2B_5^-$ was compressed from a 98%-isotopically-enriched ^{10}B powder mixed with ~5% graphite. The PES resolution was $\Delta E/E \sim 2.5\%$, i.e., about 25 meV for 1 eV electrons. The spectra of CB_6^- and $C_2B_5^-$ at three different photon energies are presented in Figure 9-1. The spectra of both species are rather broad and complicated, indicating either large geometry changes between the anions and the neutrals, and/or presence of multiple isomers. The observed vertical detachment energies (VDE) for the main PES bands are given in Tables 9-1, and 9-2 and 9-3, where they are compared to theoretical data.

9-3. Computational Methods

Computationally we first searched for the global minima of CB_6^{2-}, CB_6^-, and $C_2B_5^-$ using the genetic algorithm program GEGA[15] at the B3LYP/3-21G level of theory. We then recalculated geometries of low-lying isomers and two hexagonal structures for each species at the B3LYP/6-311+G* and for the two lowest isomers of CB_6^- and $C_2B_5^-$ at the CCSD(T)/6-311+G* levels of theory. Total energies of the twelve local minimum structures were recalculated at the CCSD(T)/6-311+G(2df)//B3LYP/6-311+G* level of theory.

VDEs for CB_6^- and $C_2B_5^-$ were calculated using the R(U)CCSD(T)/6-311+G(2df) method, the outer valence Green Function method [ROVGF/6-311+G(2df)] at the RCCSD(T)/ 6-311+G* geometries, and the time-dependent DFT method [TD-B3LYP/6-311+G(2df)] at the B3LYP/6-311+G* geometries. All calculations were done using the Gaussian 03 program.[16a] Molecular orbital visualization was done using the MOLDEN3.4 program.[16b]

9-4. Results and Discussion

According to our GEGA search, the structure **I** (C_s) is the global minimum for CB_6^{2-} (Figure 9-2). Though the isolated CB_6^{2-} dianion is not electronically stable as Exner pointed out,[8a] we used compact (6-311+G*) basis to model this unit in the electronically stable $NaCB_6^-$ or Na_2CB_6 species. This modeling is adequate for the description of the part of the potential surface within the Coulomb barrier. The previously discussed[8a] structure **IV** (D_{6h}) with a hexacoordinate C is 34.4 kcal/mol higher in energy [here and

elsewhere the relative energies are given at CCSD(T)/6-311+G(2df)//B3LYP/6-311+G*] than the global minimum. Similarly, for CB_6^- and $C_2B_5^-$, the structures with a hexacoordinate C, **VIII** (D_{2h}) and **XII** (C_{2v}), are also significantly higher in energy than the corresponding global minimum structures (Figure 9-2).

For all three clusters, we found a low-lying isomer very close to the global minimum. In the cases of CB_6^- and $C_2B_5^-$, both of the low-lying isomers may be present experimentally, giving rise to the complicated PES patterns. Indeed, comparison of the theoretical VDEs with the experimental data (Tables 9-1, 9-2 and 9-3) clearly shows that the two lowest isomers are almost equally populated for both CB_6^- and $C_2B_5^-$. For CB_6^-, the first VDEs for the two lowest isomers **V** (2.95 eV) and **VI** (2.75 eV) calculated at the CCSD(T) level are close to each other, and both should contribute to the observed ground state band X, Figure 9-1a-c). The first VDE of isomer **VI** is slightly lower, corresponding to the main X band, whereas that of isomer **V** corresponds to the higher binding energy tail of the X band. The second calculated VDEs for isomers **V** (3.68 eV) and **VI** (3.14 eV) are very different, corresponding to the observed PES bands B and A, respectively, and providing the most critical spectral signatures for the presence of both isomers. Spectral features beyond 4 eV can all be assigned to the two isomers (Table 9-2).

For $C_2B_5^-$, the first four observed PES bands (Figure 9-1d-f) can be unambiguously assigned to the first two detachment channels of each of the two lowest isomers, as shown in Table 9-1. Higher PES bands can all be assigned to the higher binding energy detachment channels from the two isomers (the peak labeled * is likely due to a vibrational feature of the A band or contribution from a third low-lying isomer),

as given in Table 9-3. All the observed PES bands are relatively broad without vibrational resolution, consistent with the low symmetries of the two isomers of each cluster and suggesting that these structures are relatively floppy. Overall the agreement between the observed PES features and the theoretical data is quite satisfying, providing considerable credence for the obtained lowest structures for CB_6^- (**V** and **VI**) and $C_2B_5^-$ (**IX** and **X**). Clearly, the isomers with a hexacoordinate C (**VIII** for CB_6^- and **XII** for $C_2B_5^-$) are too high in energy. Though hypercoordinated isomers **IV** and **XII** are true local minima and kinetically stable, we were only able to observe the global minimum and low-lying isomers.

To understand why the structures with a hexacoordinate C for CB_6^{2-}, CB_6^- and $C_2B_5^-$ are higher in energy than the global minima, we analyzed their chemical bonding using the recently developed Adaptive Natural Density Partitioning (AdNDP) method.[17] This approach leads to partitioning of the charge density into elements with the highest possible degree of localization of electron pairs: n center – two electron (nc-2e) bonds. If some part of the density cannot be localized in this manner, it is represented using completely delocalized objects, similar to canonical MOs, naturally incorporating the idea of completely delocalized (globally aromatic) bonding. Thus, AdNDP achieves seamless description of different types of chemical bonds.

According to our AdNDP analyses (see Figures 9-3 and 9-4 for details) the hexagonal structures of CB_6^{2-} and $C_2B_5^-$ are doubly (σ and π) aromatic systems (6 delocalized σ-electrons and 6 delocalized π-electrons) with six peripheral two-center two-electron (2c-2e) B-B or B-C bonds. This bonding picture explains why the hexagonal

isomers (**IV** and **XII**) with a central C atom are higher in energy than the hexagonal structures (**III** and **XI**) with the C atoms located on the periphery. The central C atoms in the hexagonal isomers **IV** and **XII** are involved in delocalized bonding only, while in the isomers **III** and **XI** the C atoms are involved in 2c-2e peripheral bonding in addition to the delocalized bonding. The lower electronegativity of B compared to C clearly favors the hexacoordinate B isomers of CB_6^{2-} and $C_2B_5^{-}$.

The lowest energy structures **I** and **II** for CB_6^{2-} and **IX** and **X** for $C_2B_5^{-}$ originate from hepta-cyclic structures. These four structures are all σ-aromatic (6 delocalized σ-electrons) and π-antiaromatic (4 π-electrons) with seven peripheral 2c-2e B-B/ B-C bonds. There are no "internal" 2c-2e B-B or B-C bonds; in Figure 9-2 the internal lines connecting atoms do not represent 2c-2e B-B or B-C bonds. In order to prove that these low symmetry structures are indeed related to seven-membered rings we performed additional calculations for the CB_6 cluster. We started at the geometry of the CB_6^{2-} global minimum structure **I** and removed two electrons from its HOMO-10a' (Figure 9-5). In the neutral CB_6 structure we switched σ-HOMO (9a') and π-LUMO+2 (3a") thus making this structure doubly aromatic (2 σ-electrons, 6 π-electrons) preserving seven 2c-2e peripheral B-B and B-C bonds. Subsequent geometry optimization for the doubly aromatic structure led to almost perfect heptagonal ring for CB_6 (C_{2v}, $^1A_1$) (Figure 9-5). The MOs of the latter now clearly confirm our initial assignment of this cluster as doubly aromatic (2 σ-electrons, 6 π-electrons) with seven 2c-2e peripheral B-B and B-C bonds. Hence, the stable low-lying structures **I** and **II** for CB_6^{2-} and **IX** and **X** for $C_2B_5^{-}$ are derived from distortions of the hepta-cyclic structures due to p antiaromaticity. There

might be more than one deformation for the C_{2v} CB_6 after the addition of two electrons. We selected the above-mentioned one for illustrative purpose.

9-5. Conclusion

Our chemical bonding analyses suggest that in theoretical designs of chemical systems with planar hyper-coordination the peripheral ring size, the electronegativity and size of the central atom have all to be considered.[6a] So far the highest coordination number observed in a planar environment is 8 in the B_9^- molecular wheel.[18] A similar molecular wheel has been predicted for AlB_9 with a nona-coordinated Al,[19] which represents the highest coordination number in the planar environment predicted so far as a low energy isomer.

Supporting Information Available: Complete VDE Tables, complete reference 16a, alternative structure of CB_6^{2-}, CB_6^-, and $C_2B_5^-$, pictures of n-centered two-electron localized bonds for the CB_6^{2-} and $C_2B_5^-$ species, correlation MO diagram, absolute energies and Cartesian coordinates of all calculated structures. This information is available free of charge via Internet at http://pubs.acs.org.

References

(1) (a) R. Hoffmann, R. W. Alder, C. F. Wilcox, Jr. *J. Am. Chem. Soc.* **1970**, *92*, 4992; (b) R. Hoffmann, *Pure Appl. Chem.* **1971**, *28*, 181.

(2) Keese, R. *Chem. Rev.* **2006**, *106*, 4787 and references therein.

(3) Merino, G; Mendez-Rojas, M. A.; Vela, A.; Heine, T. *J. Comput. Chem.* **2007**, *28*, 362 and references therein.

(4) Sateesh, B.; Reddy, A. S.; Sastry,G. N. *J. Comput. Chem.* **2007**, *28*, 335.and references therein.

(5) Siebert, W.; Gunale, A. *Chem. Soc. Rev.* **1999**, *28*, 367 and references therein.

(6) (a) Schleyer, P. v. R.; Boldyrev, A. I. *J. Chem. Soc. Chem. Comm.* **1991**, 1536; (b) Boldyrev, A. I.; Simons, J. *J. Am. Chem. Soc.* **1998**, *120*, 7967.

(7) (a) Li, X.; Wang, L. S.; Boldyrev, A. I.; Simons, J. *J. Am. Chem. Soc.* **1999**, *121*, 6033; (b) Wang, L. S.; Boldyrev, A. I.; Li, X.; Simons, J. *J. Am. Chem. Soc.* **2000**, *122*, 7681; (c) Li, X.; Zhang, H. F.; Wang, L. S.; Geske, G. D.; Boldyrev, A. I. *Angew. Chem. Int. Ed.* **2000**, *39*, 3630; (d) Li, X.; Zhai, H. J.; Wang, L. S. *Chem. Phys. Lett.* **2002**, *357*, 415.

(8) (a) Exner, K.; Schleyer, P. v. R. *Science*, **2000**, *290*, 1937; (b) Wang, Z.-X.; Schleyer, P. v. R. *Science*, **2001**, *292*, 2465; (c) Erhardt, S.; Frenking, G. Z. Chen,; Schleyer, P. v. R. *Angew. Chem. Int. Ed.* **2005**, *44*, 1078;; (d) Ito, K.; Chen, Z.; Corminboeuf, C.; Wannere, C. S.; Zhang, X. H.; Li, Q. S.; Schleyer, P. v. R. *J. Am. Chem. Soc.* **2007**, *129*, 1510; (e) Islas, R. Heine, T.; Ito, K.; Schleyer, P. v. R.; Merino, G. *J. Am. Chem. Soc.* **2007**, *129*, 14767.

(9) (a) Minyaev, R. M.; Gribanova, T. N.; Starikov, A. G.; Minkin, V. I. *Mendeleev Comm.* **2001**, *11*, 213; (b) Gribanova, T. N.; Minyaev, R. M.; Minkin, V. I. *Russ. J. Inorg. Chem.* **2001**, *46*, 1207; (c) Minyaev, R. M.; Gribanova, T. N.; Starikov, A. G.;

Minkin, V. I. *Dokl. Chem.* **2002**, *382*, 41; Minkin, V. I.; Minyaev, R. M. *Mendeleev Comm.* **2004**, *14*, 43.

(10) (a) Li, S.-D.; Miao, C.-Q.; Ren, G.-M. *Eur. J. Inorg. Chem.* **2004**, 2232; (b) Li, S.-D.; Guo, J.-G.; Miao, C.-Q.; Ren, G.-M. *J. Phys. Chem. A*, **2005**, *109*, 4133; (c) Li, S.-D.; Miao, C.-Q.; *J. Phys. Chem. A*, **2005**, *109*, 7594; (d) Li, S.-D.; Miao, C.-Q.; Ren, G.-M.; Guo, J.-C. *Eur. J. Inorg. Chem.* **2006**, 2567; (e) Shahbazian, S.; Sadjadi, A.; *J. Mol. Struct. Theochem*, **2007**, *822*, 116.

(11) Kemsley, J. *Chem. & Eng. News*, **2007**. *85 (N33)*, 17.

(12) (a) Luo, Q.; Zhang, X. H.; Huang, L. K.; Liu, S. Q.; Yu, Z. H.; Li, Q. S. *J. Phys. Chem. A*, **2007**, *111*, 2930; (b) Li, S.-D.; Miao, C.-Q.; Guo, J.- C. *J. Phys. Chem. A*, **2007**, *111*, 12069.

(13) Wang, L. M.; Huang, W.; Averkiev, B. B.; Boldyrev, A. I.; Wang, L. S. *Angew. Chem., Int. Ed.* **2007**, *46*, 4550.

(14) Wang, L. S.; Cheng, H. S.; Fan, J. *J. Chem. Phys.* **1995**, *102*, 9480.

(15) (a) Alexandrova, A. N.; Boldyrev, A. I.; Fu, Y-J.; Wang, X. B.; Wang, L. S. *J. Chem. Phys.* **2004**, *121*, 5709. (b) Alexandrova, A. N.; Boldyrev, A. I. *J. Chem. Theory and Comput.* **2005**, *1*, 566.

(16) (a) Gaussian 03, Revision D.01, Frisch, M. J. et al. Gaussian, Inc., Wallingford CT, 2004; (b) MOLDEN3.4. Schaftenaar, G. MOLDEN3.4, CAOS/CAMM Center, The Netherlands (1998).

(17) Zubarev, D. Y.; Boldyrev, A. I. *Phys. Chem. Chem. Phys.* accepted for publication.

(18) (a) H. J. Zhai, A. N. Alexandrova, K. A. Birch, A. I. Boldyrev, L. S. Wang, *Angew. Chem. Int. Ed.* **2003**, *42*, 6004; (b) Alexandrova, A. N.; Boldyrev, A. I.; Zhai, H.-J.; Wang, L. S. *Coord. Chem. Rev.* **2006**, *250*, 2811; (c) Zubarev, D. Y.; A. I. Boldyrev, *J. Comput. Chem.* **2007**, *28*, 251.

(19) Averkiev, B. B.; Boldyrev, A. I. *Russ. Chem. J.* **2007**, *51*, 87.

Table 9-1. Comparison of Experimental Vertical Detachment Energies (VDE) of CB_6^- and $C_2B_5^-$ to Theoretical values. All energies are in eV

	Feature	VDE (exp.) [a]	Final State and Electronic Configuration	VDE (theo.)		
				TD-B3LYP	OVGF [b]	ΔCCSD(T) [c]
CB_6^-, V	X tail	~ 2.9	$^1A'$, $1a''^2 7a'^2 8a'^2 2a''^2 9a'^2 10a'^0$	3.20	3.19 (0.88)	2.95
	B	3.62 (3)	$^3A'$, $1a''^2 7a'^2 8a'^2 2a''^2 9a'^1 10a'^1$	3.65	3.56 (0.88)	3.68
	C	4.21 (3)	$^3A''$, $1a''^2 7a'^2 8a'^2 2a''^1 9a'^2 10a'^1$	4.14	4.11 (0.88)	4.22
	D	~ 4.5	$^1A''$, $1a''^2 7a'^2 8a'^2 2a''^1 9a'^2 10a'^1$	4.55		
	E	4.71 (5)	$^3A'$, $1a''^2 7a'^2 8a'^1 2a''^2 9a'^2 10a'^1$	4.81	4.88 (0.86)	
CB_6^-, VI	X [d]	2.78 (3)	$^1A'$, $1a''^2 7a'^2 8a'^2 2a''^2 9a'^2 10a'^0$	3.14	3.58 (0.88)	2.75
	A	3.17 (2)	$^3A'$, $1a''^2 7a'^2 8a'^2 2a''^2 9a'^1 10a'^1$	3.12	2.86 (0.88)	3.14
	C	4.21 (3)	$^3A''$, $1a''^2 7a'^2 8a'^2 2a''^1 9a'^2 10a'^1$	4.13	4.07 (0.88)	4.19
	D	~ 4.5	$^1A''$, $1a''^2 7a'^2 8a'^2 2a''^1 9a'^2 10a'^1$	4.52		
	E	4.71 (5)	$^3A'$, $1a''^2 7a'^2 8a'^1 2a''^2 9a'^2 10a'^1$	4.74	4.78 (0.86)	
$C_2B_5^-$, IX	A	2.95 (6)	$^2A_1$, $1b_1^2 4a_1^2 5a_1^2 1a_2^2 4b_2^2 6a_1^1$	3.00	3.08 (0.88)	3.13
	C	4.36 (4)	$^2B_2$, $1b_1^2 4a_1^2 5a_1^2 1a_2^2 4b_2^1 6a_1^2$	4.42	4.73 (0.84)	4.49
	D	4.93 (3)	$^2A_2$, $1b_1^2 4a_1^2 5a_1^2 1a_2^1 4b_2^2 6a_1^2$	4.79	4.90 (0.88)	4.97
$C_2B_5^-$, X	X [d]	2.61(5)	$^2A'$, $7a'^2 8a'^2 2a''^2 9a'^2 10a'^1$	2.54	2.74 (0.86)	2.69
	B	4.06 (3)	$^2A'$, $7a'^2 8a'^2 2a''^2 9a'^1 10a'^2$	4.13	4.47 (0.83)	

[a] Numbers in parentheses represent the uncertainty in the last digit.
[b] VDEs were calculated at OVGF/6-311+G(2df)//CCSD(T)/6-311+G* level of theory. Values in parentheses represent the pole strength of the OVGF calculation.
[c] VDEs were calculated at CCSD(T)/6-311+G(2df)//CCSD(T)/6-311+G* level of theory.
[d] ADEs were estimated from the X band to be 2.71 ± 0.02 eV (CB_6^-) and 2.40 ± 0.05 eV ($C_2B_5^-$). Calculated ADE are 2.65 eV (CB_6^-, V), 2.63 eV (CB_6^-, VI), 2.82 eV ($C_2B_5^-$, IX), and 2.39 eV ($C_2B_5^-$, X) at CCSD(T)/6-311+G(2df)//CCSD(T)/6-311+G*.

Table 9-2. Comparison of the experimental vertical detachment energies (VDE) of CB_6^- to the calculated values for two lowest isomers: C_s, V, $^2A_1$ and C_s, VI, ^{1}A'. All energies are in eV.

Feature	VDE (exp.) [a]	Final State and Electronic Configuration	VDE (theo.)		
			TD-B3LYP	OVGF [b]	ΔCCSD(T) [c]
		CB_6^- (C_s, V, ^{2}A')			
X [d] tail	~ 2.9	^{1}A', 1a"²7a'²8a'²2a"²9a'²10a'⁰	3.20	3.19 (0.88)	2.95
B	3.62 (3)	^{3}A', 1a"²7a'²8a'²2a"²9a'¹10a'¹	3.65	3.56 (0.88)	3.68
C	4.21 (3)	^{3}A", 1a"²7a'²8a'²2a"¹9a'²10a'¹	4.14	4.11 (0.88)	4.22
D	~ 4.5	^{1}A", 1a"²7a'²8a'²2a"¹9a'²10a'¹	4.55		
E	4.71 (5)	^{3}A', 1a"²7a'²8a'¹2a"²9a'²10a'¹	4.81	4.88 (0.86)	
E tail	~ 5	^{1}A', 1a"²7a'²8a'¹2a"²9a'²10a'¹	5.00		
F tail	~ 5.5	^{3}A', 1a"²7a'¹8a'²2a"²9a'²10a'¹	5.41	5.53 (0.83)	
F tail	~ 5.5	^{1}A', 1a"²7a'²8a'¹2a"²9a'²10a'¹	5.50		
G	~ 6.1	^{3}A", 1a"¹7a'²8a'²2a"²9a'²10a'¹	6.12	6.20 (0.84)	
		CB_6^- (C_s, VI, ^{2}A')			
X [d]	2.78 (3)	^{1}A', 1a"²7a'²8a'²2a"²9a'²10a'⁰	3.14	3.58 (0.88)	2.75
A	3.17 (2)	^{3}A', 1a"²7a'²8a'²2a"²9a'¹10a'¹	3.12	2.86 (0.88)	3.14
C	4.21 (3)	^{3}A", 1a"²7a'²8a'²2a"¹9a'²10a'¹	4.13	4.07 (0.88)	4.19
D	~ 4.5	^{1}A", 1a"²7a'²8a'²2a"¹9a'²10a'¹	4.52		
E	4.71 (5)	^{3}A', 1a"²7a'²8a'¹2a"²9a'²10a'¹	4.74	4.78 (0.86)	
E tail	~ 5	^{3}A', 1a"²7a'¹8a'²2a"²9a'²10a'¹	5.03	5.46 (0.84)	
E tail	~ 5	^{1}A', 1a"²7a'²8a'²2a"²9a'¹10a'¹	5.04		
F	5.27 (5)	^{1}A', 1a"²7a'²8a'¹2a"²9a'²10a'¹	5.27		

[a] Numbers in parentheses represent the uncertainty in the last digit.

[b] VDEs were calculated at OVGF/6-311+G(2df)//CCSD(T)/6-311+G* level of theory. Values in parentheses represent the pole strength of the OVGF calculation.

[c] VDEs were calculated at CCSD(T)/6-311+G(2df)//CCSD(T)/6-311+G* level of theory.

[d] ADEs were estimated from the X band to be 2.71 ± 0.02 eV. Calculated ADE are 2.65 eV (V) and 2.63 eV (VI) at CCSD(T)/6-311+G(2df)//CCSD(T)/6-311+G*.

Table 9-3. Comparison of the experimental vertical detachment energies (VDE) of $C_2B_5^-$ to the calculated values for two lowest isomers: C_{2v}, IX, $^1A_1$ and C_s, X, $^1A'$. All energies are in eV.

Feature	VDE (exp.) [a]	Final State and Electronic Configuration	VDE (theo.)		
			TD-B3LYP	OVGF [b]	ΔCCSD(T) [c]
$C_2B_5^-$ (C_{2v}, IX, $^1A_1$)					
A	2.95 (6)	$^2A_1$, $1b_1^2 4a_1^2 5a_1^2 1a_2^2 4b_2^2 6a_1^1$	3.00	3.08 (0.88)	3.13
C	4.36 (4)	$^2B_2$, $1b_1^2 4a_1^2 5a_1^2 1a_2^2 4b_2^1 6a_1^2$	4.42	4.73 (0.84)	4.49
D	4.93 (3)	$^2A_2$, $1b_1^2 4a_1^2 5a_1^2 1a_2^1 4b_2^2 6a_1^2$	4.79	4.90 (0.88)	4.97
G	~ 6	$^2A_1$, $1b_1^2 4a_1^2 5a_1^1 1a_2^2 4b_2^2 6a_1^2$	5.74	5.97 (0.88)	
G	~ 6	$^2A_1$, $1b_1^2 4a_1^1 5a_1^2 1a_2^2 4b_2^2 6a_1^2$	6.08	6.24 (0.85)	
		$^2B_1$, $1b_1^1 4a_1^2 5a_1^2 1a_2^2 4b_2^2 6a_1^2$	6.42	6.57 (0.83)	6.65
$C_2B_5^-$ (C_s, X, $^1A'$)					
X [d]	2.61(5)	$^2A'$, $7a'^2 8a'^2 2a''^2 9a'^2 10a'^1$	2.54	2.74 (0.86)	2.69
B	4.06 (3)	$^2A'$, $7a'^2 8a'^2 2a''^2 9a'^1 10a'^2$	4.13	4.47 (0.83)	
E	5.09 (3)	$^2A''$, $7a'^2 8a'^2 2a''^1 9a'^2 10a'^2$	5.08	5.30 (0.86)	5.42
F	5.62 (3)	$^2A'$, $7a'^2 8a'^1 2a''^2 9a'^2 10a'^2$	5.57	5.86 (0.83)	
G	~ 6	$^2A'$, $7a'^1 8a'^2 2a''^2 9a'^2 10a'^2$	6.03	6.41 (0.84)	

[a] Numbers in parentheses represent the uncertainty in the last digit.

[b] VDEs were calculated at OVGF/6-311+G(2df)//CCSD(T)/6-311+G* level of theory. Values in parentheses represent the pole strength of the OVGF calculation.

[c] VDEs were calculated at CCSD(T)/6-311+G(2df)//CCSD(T)/6-311+G* level of theory.

[d] ADEs were estimated from the X band to be 2.40 ± 0.05 eV. Calculated ADE are 2.82 eV (IX) and 2.39 eV (X) at CCSD(T)/6-311+G(2df)//CCSD(T)/6-311+G*.
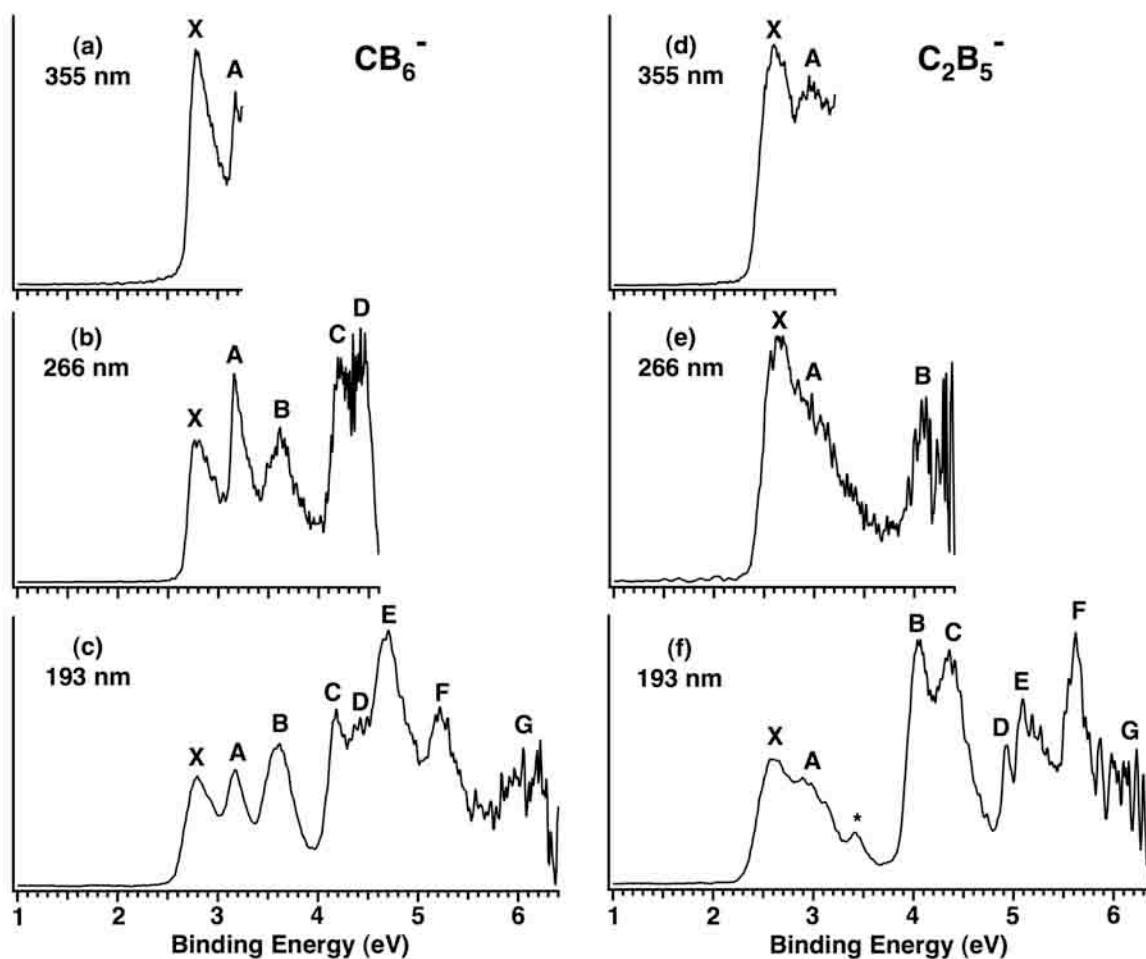
Figure 9-1. Photoelectron spectra of CB_6^- (left) and $C_2B_5^-$ (right) at 355 nm (3.496 eV), 266 nm (4.661 eV), and 193 nm (6.424 eV).

CB_6^{2-}

I C_s, $^1A'$	II C_s, $^1A'$	III C_s, $^1A'$	IV D_{6h}, $^1A_{1g}$
0.0 kcal/mol	1.1 kcal/mol	12.7 kcal/mol	34.4 kcal/mol
0.0 kcal/mol	0.8 kcal/mol	20.7 kcal/mol	42.4 kcal/mol

CB_6^-

V C_s, $^2A'$	VI C_s, $^2A'$	VII, C_s, $^2A''$	VIII D_{2h}, $^2B_{2g}$
0.0 kcal/mol	2.9 kcal/mol	6.0 kcal/mol	26.9 kcal/mol
0.0 kcal/mol	2.2 kcal/mol	11.3 kcal/mol	34.2 kcal/mol

$C_2B_5^-$

IX C_{2v}, $^1A_1$	X C_s, $^1A'$	XI C_s, $^1A'$	XII, C_{2v}, $^1A_1$
0.0 kcal/mol	0.7 kcal/mol	15.1 kcal/mol	40.2 kcal/mol
0.0 kcal/mol	1.7 kcal/mol	24.4 kcal/mol	50.8 kcal/mol

Figure 9-2. Calculated structures and relative energies (upper line at CCSD(T)/6-311+G(2df)//B3LYP/6-311+G* and bottom line at B3LYP/6-311+G*) for CB_6^{2-}, CB_6^-, and $C_2B_5^-$.
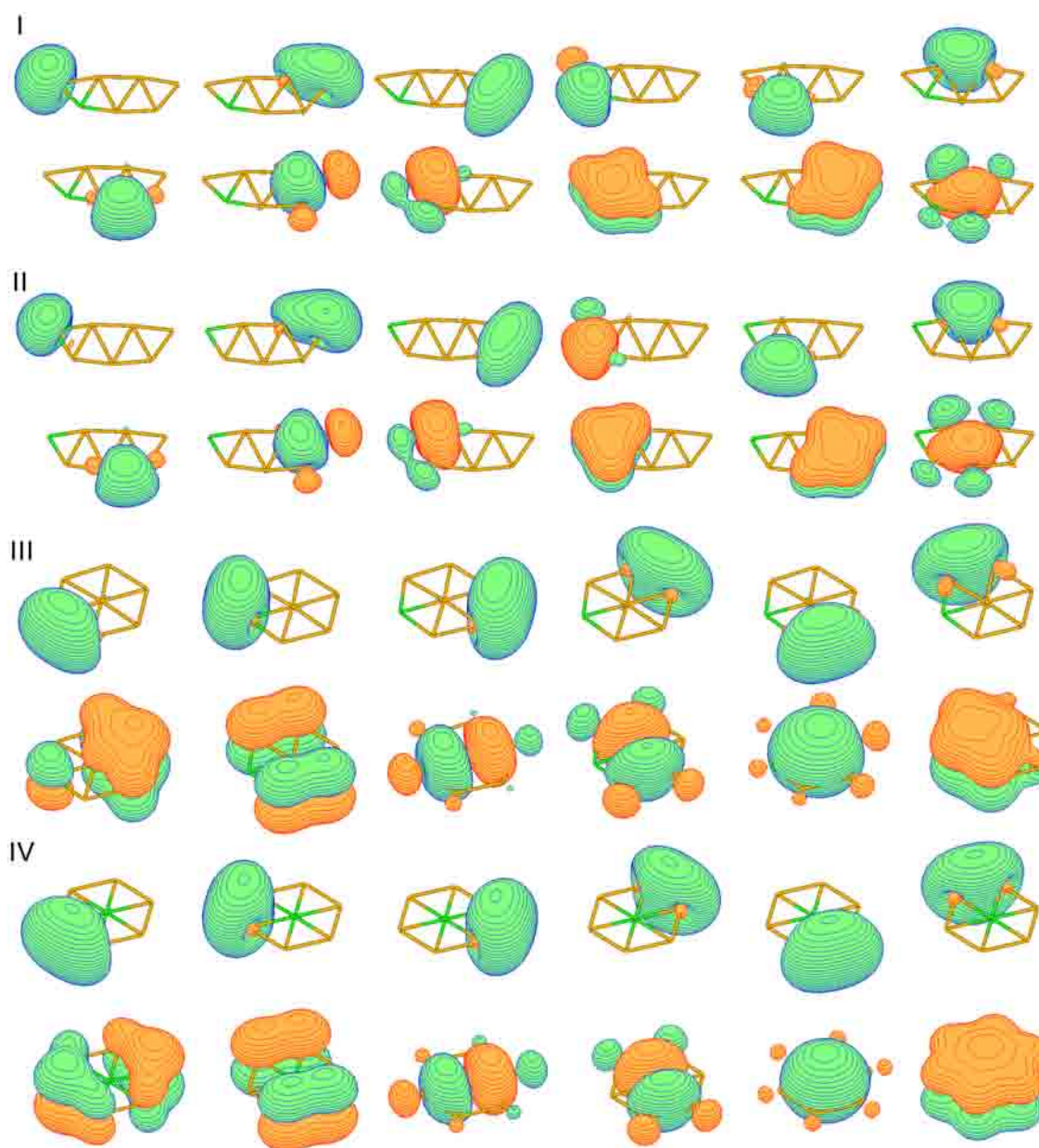
Figure 9-3. Orbitals calculated according to the Adaptive Natural Density Partitioning (AdNDP) method of structures of CB_6^{2-} (number of structures are given according to Figure 9-1)
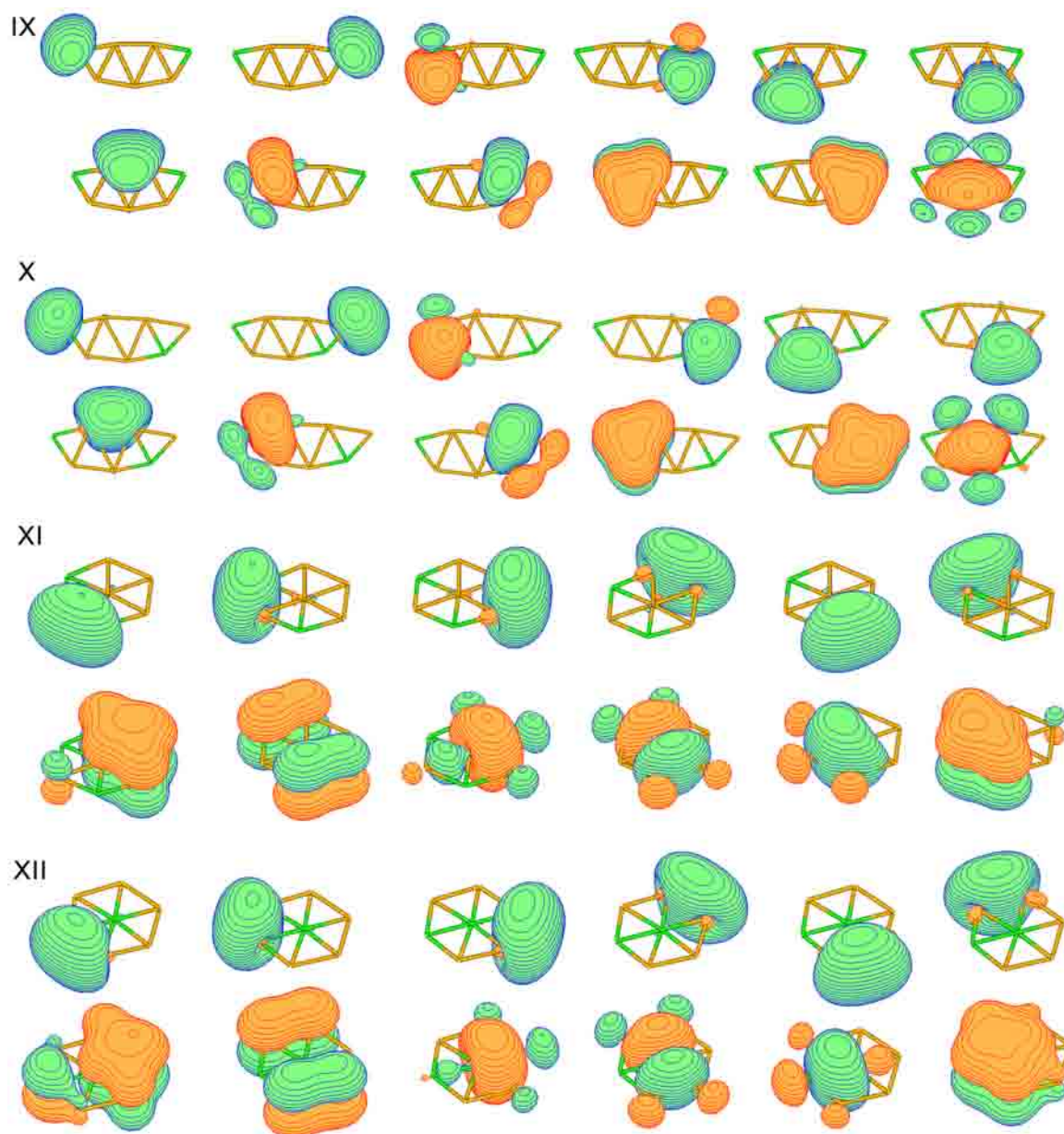
Figure 9-4. Orbitals calculated according to the Adaptive Natural Density Partitioning (AdNDP) method of structures of $C_2B_5^-$ (number of structures are given according to Figure 9-1)
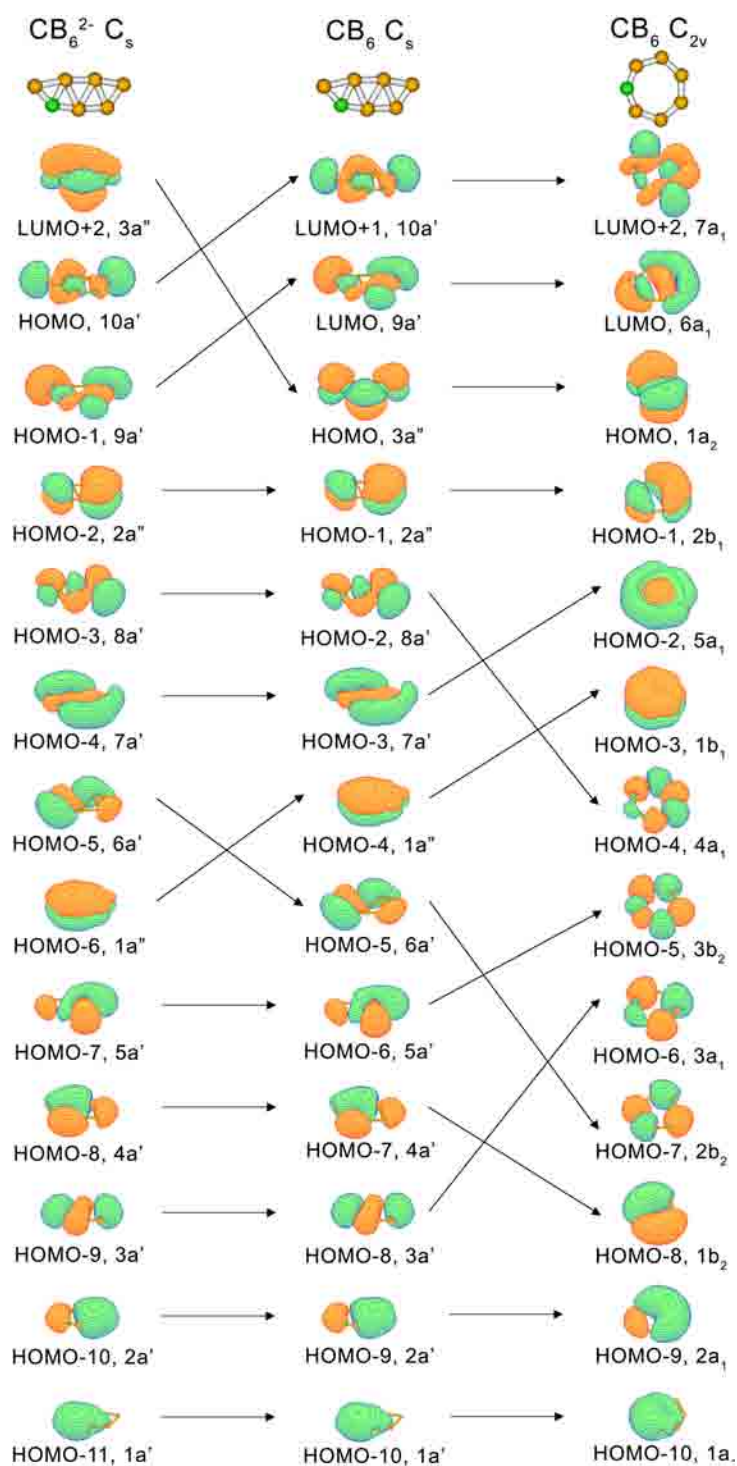
Figure 9-5. Correlation diagram for the geometric transformation of CB_6 (C_s, $^1A'$) (initially at the optimal geometry of the global minimum) into CB_6 (C_{2v}, $^1A_1$).

CHAPTER 10

THEORETICAL DESIGN OF PLANAR MOLECULES WITH A NONA- AND

DECACOORDINATE CENTRAL ATOM[1]

Abstract

The maximum coordination number of the central atom in planar molecules generated by now in mole-cular beams was 8. We made use of the chemical bond model developed for planar boron clusters to check the possibility of existence of planar molecules with coordination numbers 9 and 10. The objects of our study were the AlB_9 and AlB_{10}^+ clusters, which have local minima corresponding to highly symmetrical D_{9h} and D_{10h} structures, respectively. According to our calculations, the highly symmetrical structure of AlB_9 is a global minimum or a low-lying isomer, and, therefore, it holds promise as a new ligand for coordination chemistry. The energy of the highly symmetrical structure of AlB_{10}^+ with the coordination number 10 is too high, and this structure is hardly synthetically feasible. Thus, 9 is presently the maximum coordination number of an atom in a planar molecule.

10-1. Introduction

---

[1] Coauthored by B. B. Averkiev and A. I. Boldyrev. Reproduced with kind permission from Springer Science+Business Media: *Russian Journal of General Chemistry* **2008**, 78, 769-773.

The progress of quantum chemistry over the past two decades has made it possible to predict new molecules. An example is the successful quantumchemical prediction in 1991 of a series of five-atomic clusters with a tetracoordinate central carbon atom: *cis*-CSi_2Al_2, *trans*-CSi_2Al_2, *cis*-CSi_2Ga_2, *trans*- CSi_2Ga_2, *cis*-CGe_2Al_2, and *trans*-CGe_2Al_2 [1]. These molecules are unusual: They contain planar tetracoordinate carbon, even though a four-bond carbon atom has long, since van't Hoff and Le Bel (1874), been considered to have invariably a tetrahedral environment. In 1970 Hoffmann, Alder, and Wilcox published a fundamental work in which they suggested several approaches to constructing molecules with a planar tetracoordinate carbon atom [2]. However, even these researchers expressed certain skepticism as to the possibility of existence of pentaatomic molecules with planar tetracoordinate carbon. In particular, they considered it too optimistic to believe that carbon in a simple compound will prefer a planar structure over tetrahedral. Therefore**,** the theoretical prediction of the above molecules was met with a great deal of skepticism.

In 1999 Lee et al. [3] showed in their combined theoretical and experimental study that the structure of the negatively charged ion CAl_4^- is a planar square with the carbon atom in the center [3]. A year later the same researchers discovered that the anions CAl_3Si^- and CAl_3Ge^- and their corresponding neutral molecules CAl_3Si and CAl_3Ge, too, contain a tetracoordinate planar carbon atom [4]. The above five-atomic molecules all are planar, since they have a purely bonding ligand–ligand highest occupied molecular orbital (for details, see [1, 3, 4]). This successful prediction of unusual planar molecules stimulated further theoretical design of other planar molecules with even higher

coordinate carbon and other main group atoms [5–21]. In particular, Exner and Schleyer [5] predicted planar molecules with hexacoordinate carbon, and Wang and Schleyer [6] predicted planar molecules with penta- and heptacoordinate carbon [6]. Minkin et al. suggested planar molecules with a heptacoordinate carbon or nitrogen atom, based on quantum-chemical calculations [11]. They also predicted a series of planar octacoordinate carbon, silicon, and phosphorus structures: CB_8, SiB_8, and PB_8^+ [9]. Minyaev et al. [19, 20] showed in their combined theoretical and experimental study that B_8^{2-} and B_9^- are planar structures containing a hepta- and an octacoordinate central boron atom. The maximum coordination number of the central atom in planar molecules presently generated in molecular beams is eight.

Here we present a quantum-chemical research into the possibility of existence of planar molecules in which the coordination number of the central atom is 9 and 10. As potential candidates we chose the neutral molecule AlB_9 and cation AlB_{10}^+. These systems, according to the chemical bond theory developed for boron clusters [21, 22], are doubly aromatic structures with a ring formed by two-electron two-centered ($2e$–$2c$) B–B bonds (formed by sp hybrid orbitals). The first of these systems (AlB_9) has 30 valence electrons, of which 18 are involved in nine $2e$–$2c$ B–B bonds of the outer ring, 6 form a delocalized π bond between the central aluminum atom and the ring, and the rest 6 electrons form a delocalized σ bond of the central aluminum atom with the ring. Analogous analysis for AlB_{10}^+ shows that this cation should have ten $2e$–$2c$ B–B bonds in the outer ring, 6 delocalized π and 6 delocalized σ electrons. The six delocalized π and σ electrons correspond to the Huckel ($4n+2$) rule which makes both molecules doubly

aromatic. Therefore, they would be expected to be planar nona- and decahedral structures.

10-2. Procedure and Results of Calculations of
Molecular Systems with Nona- and
Decacoordinate Central Atoms

We started with search for a global energy minimum for the AlB_9 molecule using the Gradient-Embedded Genetic Algorithm (GEGA) software developed at our group by A. N. Alexandrova [23, 24]. The energies, gradients, and force constants were calculated using B3LYP–DFT with the small 3-21G basis set. The five lowest energy isomers found by GEGA were reoptimized with the subsequent calculation of vibration frequencies by means of B3LYP/6-311+G*. The full energies of these isomers were recalculated using CCSD(T)/6-311+G(2df) with the B3LYP/6-311+G* geometries.

With AlB_{10}^+, we restricted ourselves to two isomers. The geometric parameters and vibration frequencies of these isomers were calculated by the B3LYP/6-311+G* method, and their full energies were recalculated by the CCSD(T)/6-311+G(2df) method with the B3LYP/6-311+G* geometry. The calculations were performed using the Gaussian03 program [25]. The structures and molecular orbitals were drawn using the MOLDEN3.4 program [26].

The five lowest energy isomers of AlB_9, found by GEGA, are depicted in Fig. 10-1a. Isomer **II** with a nonacoordinate aluminum atom in the center corresponds to a global minimum on the PES calculated by means of B3LYP/6-311+G*.

Isomer **I** which can be considered as a structure obtained by substitution of one peripheral boron atom by aluminum in the global minimum structure of the B_{10} cluster [21, 22] is 6.1 kcal mol^{-1} higher in energy than isomer **II** obtained by B3LYP/6-311+G* calculations However, according to CCSD(T)/6-311+G(2df) calculations with the B3LYP/6-311+G* geometry, isomer **I** is a global minimum structure. Isomer **II** at the latter level of theory is as little as 1.0 kcal mol^{-1} higher in energy than isomer **I**. Therefore, these results allow us to draw no conclusions as to which of the isomers corresponds to a global minimum, and we are inclined to consider them energetically degenerate.

Isomers **III** and **V** are also derivatives of the global minimum structure of the B_{10} cluster, with peripheral boron atoms substituted in two other possible positions. These isomers are both higher in energy than isomers **I** and **II**. Geometry optimization of the structure in which one of the two central boron atoms in the B_{10} cluster is substituted by aluminum leads to structure **IV** with an ionic bond between Al^+ and B_9^-.

For the cluster AlB_{10}^+ we only compared the two structures depicted in Fig. 10-1b. Isomer **VII** with a decacoordinate planar aluminum center is much higher in energy than isomer **VI** which can be considered as a complex of Al^+ with the B_{10} cluster. Even though the global minimum structure of the AlB_{10}^+ cluster is unknown, the fact that isomer **VII** is much higher in energy than isomer **VI** allows us to rule out isomer **VII** from possible candidate decacoordinate planar structures.

Thus, as follows from our calculations, nine is a maximum coordination number of the central atom in a planar molecule where it surrounded by a ring of boron atoms.

Structure **VII** for the AlB_{10}^+ cluster, while being a local minimum, has a too high energy for this structure to be realized in practice in any chemical compound. The energy gap is also too low for isomer **VII** to form in any appreciable amounts in experiments with molecular beams or under matrix isolation conditions.

Our choice of the AlB_9 and AlB_{10}^+ clusters as possible candidate molecules with a nona- or decacoordinate atom in a planar structure is motivated by unique features of chemical bonds in boron clusters. Even though the crystal lattice of boron is formed by three-dimensional fragments (icosahedrons),isolated boron clusters, at least those containing up to 15 atoms, are either planar or quasiplanar [21, 22]. The planar or quasiplanar structure of boron clusters is explained by the fact that they have an outer ring of $2e$–$2c$ B–B bonds. Additional bonding in boron is provided by delocalized σ and π bonds. Clusters in which the number of delocalized σ and π electrons is $4n+2$ are double aromatic and, therefore, highly symmetrical, which makes them suitable candidate planar molecules with a high-coordinate central atom.

Aluminum was chosen for the central atom, since it is less electronegative than boron. This is important, because the central atom is only involved in delocalized bonds with peripheral atoms, whereas ring atoms are additionally involved in the formation of ring $2e$–$2c$ bond; as a result, electronegative atoms will prefer to reside in the ring rather than in the molecular center.

Molecular orbital analysis of AlB_9 and AlB_{10}^+ (Figs. 10-2a and 10-2b) points to the same nature of bonding as in purely boron clusters. The HOMO-4 through HOMO-8 in AlB_9 can be localized by the NBO method on two-center B–B bonds with effective

filling numbers of 1.95 e, which is quite close to the classical number 2 for a 2*e*–2c

bond. The NBO analysis showed that the peripheral boron atoms in these bonds are *sp*-

hybridized. The HOMO – HOMO-3 are impossible to localize, which means that they are

responsible for the delocalized bond between the central aluminum atom and the

peripheral ring. The HOMO and HOMO-2 are π orbitals (they are similar in structure to

benzene π orbitals), i.e. they provide π-aromaticity of the molecule. The HOMO-1 and

HOMO-3 are σ orbitals, and they provide σ-aromaticity of the cluster. The HOMO-4

through HOMO-9 in AlB_{10}^+ can be localized by the NBO method on two-center B–B

bonds with effective filling numbers of 1.96 e. The NBO analysis showed that the

peripheral boron atoms in these bonds are *sp*-hybridized. The HOMO – HOMO-3 cannot

be localized; which means that they are responsible for the delocalized bond between the

central aluminum atom and the peripheral ring. The HOMO and HOMO-2 in AlB_{10}^+ are π

orbitals, i.e. they make the molecule π-aromatic. The HOMO-1 and HOMO-3 are σ

orbitals responsible for σ-aromaticity of the cluster.

The above-described chemical bonding in the AlB_9 and AlB_{10}^+ clusters explains

the planar structure and high symmetry of isomers **II** and **VII**. Isomer **VII** of AlB_{10}^+ is

much less stable than isomer **VI**, since the radius of the outer boron ring is too large for a

single central atom to maintain 12 delocalized electrons. Substitution of aluminum by

gallium or indium in the ring center fails to make the decacoordinate structure much more

stable, despite the larger atomic radius of gallium or indium.

10-3. Conclusion

The chemical bond model developed for planar boron clusters was used to check the possibility of existence of planar molecules with the coordination numbers 9 and 10. The objects for study were the AlB_9 and AlB_{10}^+ clusters which have local energy minima corresponding to highly symmetrical D_{9h} and D_{10h} structures. The highly symmetrical structure of the AlB_9 molecule is a global minimum or a low-lying isomer, and, therefore, it holds promise as a new ligand for coordination chemistry. The highly symmetrical structure of AlB_{10}^+ with the coordination number 10 has a too high energy and is hardly interesting for synthetic chemistry. Thus, at present 9 is the maximum coordination number of atoms in a planar molecule.

References

1. Schleyer, P.v.R. and Boldyrev, A.I., *J. Chem. Soc., Chem. Commun.*, 1991, p. 1536.

2. Hoffmann, R, Alder, R.W., and Wilcox, C.F.Jr., *J. Am. Chem. Soc.*, 1970, vol. 92, p. 4992.

3. Li X., Wang L.S., Boldyrev A.I., and Simons J., *Ibid.*, 1999, vol.. 121, p. 6033.

4. Wang L.S., Boldyrev A.I., Li X., and Simons J., *Ibid.*, 2000, vol. 122, p. 7681.

5. Exner, K. and Schleyer, P.v.R., Science, 2000, vol. 290, p. 1937.

6. Wang, Z.-X. and Schleyer, P.v.R., *Ibid.*, 2001, vol. 292, p. 2465.

7. Erhardt, S., Frenking, G., Chen, Z., and Schleyer, P.v.R., *Angew. Chem. Int. Ed.*, 2005, vol. 44, p. 1078.

8. Ito, K., Chen, Z., Corminboeuf, C., Wannere, C.S., Zhang, X.H., Li, Q.S., and

Schleyer, P.v.R., *J. Am. Chem. Soc.*, 2007, vol. 129, p. 1510.

9. Minyaev, R.M., Gribanova, T.N., Starikov, A.G., and Minkin, V.I., *Mendeleev Comm.*, 2001, vol. 11, p. 213.

10. Gribanova, T.N., Minyaev, R.M., and Minkin, V.I., *Zh. Neorg. Khim.*, 2001, vol. 46, p. 1340.

11. Minyaev, R.M., Gribanova, T.N., Starikov, A.G., and Minkin, V.I., *Dokl. Ross. Akad. Nauk, Ser. Khim.*, 2002, vol. 382, p. 785.

12. Minkin, V.I. and Minyaev, R.M., *Mendeleev Comm.*, 2004, vol. 14, p. 43.

13. Havenith, R.W.A., Fowler, P.W., and Steiner, E., *Chem. Eur. J.*, 2002, vol. 8, p. 1068.

14. Li, S.-D., Miao, C.-Q., Guo, J.-C., and Ren, G.-M., *J. Am. Chem. Soc.*, 2004, vol. 126, p. 16227.

15. Li, S.-D., Miao, C.-Q., and Ren, G.-M., *Eur. J. Inorg. Chem.*, 2004, p. 2232.

16. Li, S.-D., Guo, J.-C., Miao, C.-Q., and Ren, G.-M., *J. Phys. Chem. A*, 2005, vol. 109, p. 4133.

17. Li, S.-D. and Miao, C.-Q., *Ibid.*, 2005, vol. 109, p. 7594.

18. Li, S.-D., Miao, C.-Q., Ren, G.-M., and Guo, J.-C., *Eur. J. Inorg. Chem.*, 2006, p. 2567.

19. Zhai, H.-J., Alexandrova, A.N., Birch, K.A., Boldyrev, A.I., and Wang, L.S., *Angew. Chem. Int. Ed.*, 2003, vol. 42, p. 6004.

20. Alexandrova, A.N., Zhai, H.-J., Wang, L.S., and Boldyrev, A.I., *Inorg. Chem.*, 2004, vol. 43, p. 3552.

21. Alexandrova, A.N., Boldyrev, A.I., Zhai, H.-J., and Wang, L.S., *Coord. Chem. Rev.*, 2006, vol. 250, p. 2811.

22. Zubarev, D.Yu. and Boldyrev, A.I., *J. Comput. Chem.*, 2007, vol. 28, p. 251.

23. Alexandrova, A.N., Boldyrev, A.I., Fu, Y-J., Wang, X.-B., and Wang, L.S., *J. Chem. Phys.*, 2004, vol. 121, p. 5709.

24. Alexandrova, A.N. and Boldyrev, A.I., *J. Chem. Theory Comput.*, 2005, vol. 1, p. 566.

25. Frisch, M.J., et al. *GAUSSIAN 03*, Rev. C. 02, Pittsburgh, PA: Gaussian, 2003.

26. Schaftenaar, G., MOLDEN3.4, the Netherlands: CAOS/ CAMM Center, 1998.

I, C_1 (^1A)
ΔE=0.0 kcal/mol
[ΔE=6.1 kcal/mol]

II, D_{9h} ($^1A'_1$)
ΔE=1.0 kcal/mol
[ΔE=0.0 kcal/mol]

III, C_2 (^1A)
ΔE=5.7 kcal/mol
[ΔE=11.3 kcal/mol]

IV, C_{8v} ($^1A_{1g}$)
ΔE=6.3 kcal/mol
[ΔE=11.7 kcal/mol]

V, C_s ($^1A'$)
ΔE=8.0 kcal/mol
[ΔE=12.8 kcal/mol]

a)

VI, C_s ($^1A'$)
ΔE=0.0 kcal/mol
[ΔE=0.0 kcal/mol]

VII, D_{10h} ($^1A_{1g}$)
ΔE=38.2 kcal/mol
[ΔE=23.0 kcal/mol]

b)
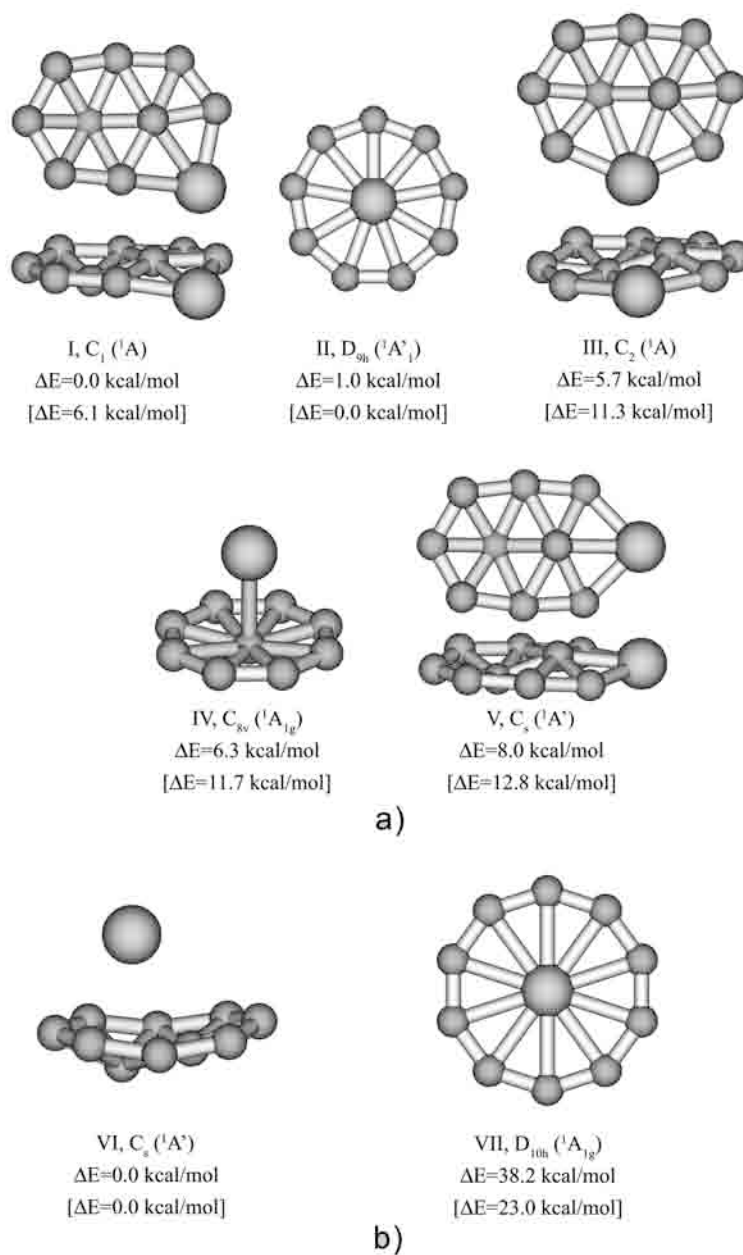
Figure 10-1. Calculated structures and relative energies for (a) AlB_9 and (b) AlB_{10}^+.

HOMO, 1e"$_1$ HOMO', 1e"$_1$ HOMO-1, 2e'$_1$ HOMO-1', 2e'$_1$

HOMO-2, 1a"$_2$ HOMO-3, 2a$_1$ HOMO-4, 1e'$_4$ HOMO-4', 1e'$_4$

HOMO-5, 1e'$_3$ HOMO-5', 1e'$_3$ HOMO-6, 1e'$_2$ HOMO-6', 1e'$_2$

HOMO-7, 1e'$_1$ HOMO-7', 1e'$_1$ HOMO-8, 1a'$_1$

a)

HOMO, 1e$_{1g}$ HOMO', 1e$_{1g}$ HOMO-1, 2e$_{1u}$ HOMO-1', 2e$_{1u}$

HOMO-2, 1a$_{2u}$ HOMO-3, 2a$_{1g}$ HOMO-4, 1b$_{2u}$ HOMO-5, 1e$_{4g}$

HOMO-5', 1e$_{4g}$ HOMO-6, 1e$_{3u}$ HOMO-6', 1e$_{3u}$ HOMO-7, 1e$_{2g}$

HOMO-7', 1e$_{2g}$ HOMO-8, 1e$_{1u}$ HOMO-8', 1e$_{1u}$ HOMO-9, 1a$_{1g}$
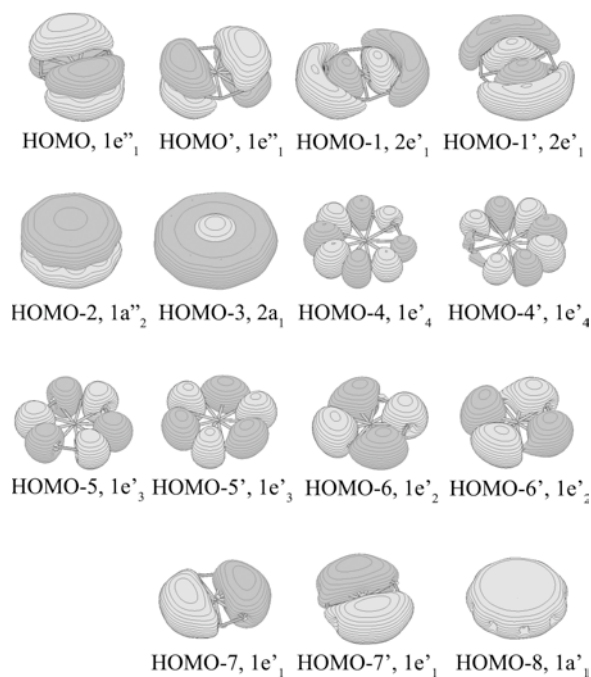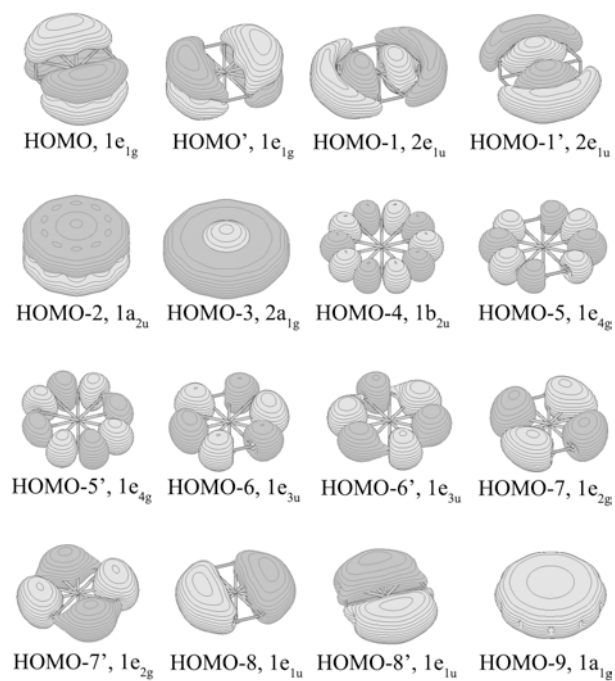
b)

Figure 10-2. Molecular orbitals for (a) AlB$_9$ and (b) AlB$_{10}^+$ clusters.

CHAPTER 11

EXPERIMENTAL AND THEORETICAL INVESTIGATIONS OF CB_8^-: TOWARDS

RATIONAL DESIGN OF HYPERCOORDINATED PLANAR CHEMICAL SPECIES[1]

Abstract

We demonstrated in our joint photoelectron spectroscopic and ab initio study that wheel-type structures with a boron ring are not appropriate for designing planar molecules with a hypercoordinate central carbon on the example of CB_8, and CB_8^- clusters. We presented a chemical bonding model, derived from the Adaptive Natural Density Partitioning analysis, capable of rationalizing and predicting planar structures either with a boron ring or with a carbon atom occupying central hypercoordinate position. According to our chemical bonding model, in the wheel type structures the central atom is involved in delocalized bonding, while peripheral atoms are involved in both delocalized bonding and two center two electron (2c-2e) σ-bonding. Since carbon is more electronegative than boron it favors peripheral positions where it can participate in 2c-2e σ–bonding. To design a chemical species with a central hypercoordinate carbon atom, one should consider electropositive ligands, which would have lone pairs instead of 2c-2e peripheral bonds. Using our extensive chemical bonding model that considers both σ- and π-bonding we also discussed why the AlB_9 and FeB_9^- species with octacoordinate Al and Fe are the global minima or low-lying isomers, as well as why carbon atom fits

---

well into the central cavity of CAl_4^{2-} and CAl_5^+. This represents the first step toward rational design of nano- and subnano-structures with tailored properties.

11-1. Introduction

Continuous miniaturization in electronic devices requires rational design of nano- and subnano-structures. However, there are no simple chemical rules, such as the Lewis model in organic chemistry, for designing novel nano-structures with tailored properties. One attempt has been made recently to develop a simple structural model for boron and mixed carbon-boron clusters.[1-4] This model assumes that there is a peripheral ring of boron atoms bonded by classical two-center two-electron (2c-2e) bonds with interior atoms bonded to the peripheral ring through delocalized bonding, which can be understood in terms of σ - and π -aromaticity (double aromaticity), σ - and π - antiaromaticity (double antiaromaticity), σ -aromaticity and π -antiaromaticity, and σ - antiaromaticity and π -aromaticity (conflicting aromaticity). We assess aromaticity in chemical species on the basis of the presence of delocalized bonding in cyclic structures. We have recently developed a new tool Adaptive Natural Density Partitioning (AdNDP) method[5] for assessing delocalized bonding in chemical species. This method leads to partitioning of the charge density into elements with the highest possible degree of localization of electron pairs. If some part of the density cannot be localized in this manner, it is represented using completely delocalized objects, similar to canonical MOs, naturally incorporating the idea of delocalized bonding, i.e., n center - two electron (nc-2e) bonds. Thus, AdNDP achieves seamless description of different types of chemical

bonds and has been applied recently to representative aromatic organic molecules,[6] as well as boron and gold clusters.[5,7] If we encounter a molecule or a cluster in which AdNDP analysis reveals that σ- or π- electrons cannot be localized into lone pairs or 2c-2e bonds, we consider such a species from the aromaticity/antiaromaticity point of view. If delocalization occurs over the whole molecule and corresponding bonds satisfy the 4n+2 rule we consider such species to be globally aromatic.

The B_9^- molecular wheel $(D_{8h}, {}^1A_{1g})$[8] is a good example of probing aromaticity using AdNDP analysis (Fig. 1). The B_9^- cluster has 28 valence electrons that form eight 2c-2e peripheral bonds with occupation numbers (ON) 1.96|e| that are close to the ideal 2.00|e| values and six delocalized bonds between the central boron atom and the B_8 ring. The six delocalized bonds are evenly divided between the σ- and π-systems, giving rise to double aromaticity (the delocalized σ-system has 6 electrons satisfying the $4n+2$ rule for σ-aromaticity and similarly for the delocalized π- system) and nicely explaining the high symmetry wheel structure of B_9^-.

There is a temptation to substitute isoelectronically the central boron atom in B_9^- by a carbon atom to make a CB_8 wheel structure with the highest coordination number for the central C atom yet known in a planar arrangement. The search for high-coordinate planar carbon species started in 1999 and 2000 when we first presented experimental and theoretical evidence of penta-atomic planar coordinated carbon species,[9-11] which confirmed earlier theoretical predictions.[12,13] These studies have stimulated renewed interests in designing new tetracoordinate[14-15] and even hypercoordinate planar carbon molecules.[16-36] Although none of these species is the global minimum on the potential

energy surfaces, it has been suggested that they might be viable experimentally. The three proposed hexa-, hepta-, and octa-coordinated carbon species are the D_{6h} CB_6^{2-},[19] D_{7h} CB_7^-,[20] and C_{2v} (effectively D_{8h}) CB_8,[24] respectively. The planar CB_6^{2-} cluster with a hexacoordinate carbon has been touted as a "divining molecule" highlighted on the cover of *Chem. & Eng. News*.[14] We have shown in previous joint experimental and theoretical investigations that the hypercoordinate D_{6h} CB_6^{2-} (ref. 4) and D_{7h} CB_7^- (ref. 3) clusters are highly unstable and that carbon avoids the central position and therefore hypercoordination in those species as well. Pei and Zeng[37] computed the planar tetra-, penta-, hexa-, hepta-, and octa-coordinated structures in carbon-boron mixed clusters and again found that in all the species tested carbon avoids hypercoordination. However, up to now there is no experimental proof that there exists a planar global minimum or planar low-lying isomer of the CB_8 cluster with a hypercoordinated carbon atom.

In the current article, we report a joint experimental and theoretical study of CB_8^- and CB_8. Photoelectron spectroscopy (PES) is used to probe the electronic structure of the CB_8^- anion and compared with *ab initio* studies for both the anion and the neutral cluster. We show that the experimentally observed species is a C_s CB_8^- cluster, in which the C atom replaces a B atom from the edge rather than at the center of the D_{8h} B_9^- molecular wheel. We present a simple chemical bonding explanation why carbon avoids hypercoordination in the mixed B/C clusters. We further propose a method on how to use pencil and paper chemical bonding models for designing hypercoordinate planar carbon molecules and planar chemical species with other hypercoordinated atoms.

11-2. Experimental section

The experiment was performed using a magnetic-bottle PES analyzer equipped with a laser vaporization cluster source, details of which can be found elsewhere.[38,39] The target used to produce CB_8^- was compressed from a mixed powder of 98%-isotopically-enriched ^{10}B with ~3% graphite and about 40% gold (to enhance the compressibility). The cluster anions from the source were analyzed using time-of-flight mass spectrometry. The CB_8^- cluster was mass-selected and decelerated before being photodetached by a 193 nm laser beam from an ArF excimer laser. The photoelectron spectra were calibrated by the known spectrum of Au^-. The energy resolution of the apparatus was $\Delta E/E \sim 2.5\%$, i.e., about 25 meV for 1 eV electrons.

The photoelectron spectrum of CB_8^- (Fig. 11-2) is rather broad and complicated, suggesting either large geometry changes between the anion and the neutral or a cluster with low symmetry. Numerous spectral features are resolved and are labeled in Fig. 11-2. The experimental vertical detachment energies (VDEs) of the resolved PES bands are given in Table 11-1 and compared with theoretical values to be discussed below. The calculated VDEs (at TD-B3LYP level) of the first few detachment channels for the lowest energy structure V (Fig. 11-4) are plotted as vertical bars in Fig. 11-2 for comparison.

11-3. Theoretical calculations of CB_8 and CB_8^-

and comparison with experiment

We initially performed searches for the global minimum structure of CB_8 and CB_8^- using a gradient-embedded genetic algorithm (GEGA) program[40,41] with the B3LYP/3-21G method for energy, gradient, and force calculations. We then reoptimized geometries and calculated frequencies for the lowest four (CB_8) and eight (CB_8^-) structures at the B3LYP/6-311+G* level of theory.[42-44] We also performed single point energy calculations of the four structures of CB_8 and eight structures of CB_8^- at the CCSD(T)/6-311+G(2df) level of theory[45-47] using the B3LYP/6-311+G* optimized geometries and then corrected the obtained energy values for zero-point energy at B3LYP/6-311+G* (CCSD(T)/6-311+G(2df)//B3LYP/6-311+G* + ZPE//B3LYP/6-311+G*). We found that isomer I (Fig. 11-3) is the global minimum, in agreement with the result by Pei and Zeng.[37] The closest isomer II was found to be 20.4 kcal/mol (here and thereafter the relative energies in the text refer to CCSD(T)/6-311+G(2df)//B3LYP/6-311+G*+ZPE//B3LYP/6-311+G*). We found that the high symmetry structure IV with the putative octa-coordinate carbon is a second-order saddle point consistent with previous calculations by Minkin *et al.*[24] Optimization following the imaginary frequencies led to isomer III, which is significantly higher (71.2 kcal/mol) than the global minimum. The GEGA search for the doublet CB_8^- anion revealed that isomer V (Fig. 11-4) is the global minimum, in agreement with the results reported by Pei and Zeng.[37] There are two low-lying isomers VI and VII, whereas other isomers (VIII-XI) are found to be significantly higher in energy. Again, the high symmetry structure XII with an octa-

coordinate carbon is unstable with five imaginary frequencies and it was found to be 116.8 kcal/mol higher than the global minimum structure.

The CB_8^- VDEs for the lowest three isomers were calculated using the R(U)CCSD(T)/6-311+G(2df) method, the outer-valence Green Function method[48-51] (ROVGF/6-311+G(2df)), and the time-dependent DFT method[52,53] (TD B3LYP/6-311+G(2df)) at the B3LYP/6-311+G* geometries. VDEs for isomer V are found to be in excellent agreement with the experimental ones (Table 11-1). The large geometry changes between the lowest CB_8^- structure V and the neutral CB_8 structure I are consistent with the broad spectrum observed (Fig. 11-2). As shown in Table 11-1, all the calculated VDEs are in good agreement with the experimental data. The CCSD(T) values for the X, A, and C channels are in quantitative agreement with the experimental values. VDEs for isomers VI and VII do not agree well with the experimental data. However, due to the broad nature of the experimental spectrum, we could not completely rule out the presence of isomers VI and VII. But their contributions to the observed spectrum, if any, were expected to be small.

All calculations were performed via the Gaussian03 program.[54] Molecular structures were visualized using MOLDEN3.4 program[55] and the AdNDP bonds visualizion was performed using MOLEKEL, Version 4.3.[56]

11-4. Chemical bonding analysis

To understand why the structures with an octacoordinate C for CB_8 and CB_8^- are unstable we performed the AdNDP analysis of chemical bonding in these species at the

HF/3-21G level of theory. It was shown previously that the results of the AdNDP analysis similar to that of the Natural Bonding Orbital analysis do not depend on the choice of the basis set.[6]

According to our AdNDP analysis, the chemical bonding in the D_{8h} CB_8 structure IV is identical to that of B_9^- (Fig. 11-1): they both are doubly ($\sigma-$ and $\pi-$) aromatic systems (6 delocalized $\sigma-$electrons and 6 delocalized $\pi-$electrons) with eight peripheral 2c-2e B-B bonds (Fig. 11-5a). However, unlike B_9^-, the D_{8h} CB_8 is not even a minimum because the carbon atom is too small to make a perfect fit into the B_8 ring. Therefore, it is important to take into account the geometric factors in designing highly coordinated planar molecules. The bonding pattern in isomer III (Fig. 11-5c) that is obrtained by following the imaginary frequency mode of the structure IV is somewhat different from the bonding pattern of the high-symmetry structure IV (Fig. 11-5a).

Although the eight peripheral 2c-2e B-B bonds (Fig. 11-5a-1 and 11-5c-1) are very similar in both structures, their delocalized $\sigma-$ and $\pi-$bonds are different. The $\pi-$bonds in structure IV (Fig. 11-5a-5-7) are delocalized over the whole cluster, while in isomer III they become one 3c-2e (Fig. 11-5c-5) and two 4c-2e $\pi-$bonds (Fig. 11-5c-6 and 7). Despite these changes, the partially localized π-bonds in isomer III are simply linear combinations of the completely delocalized $\pi-$bonds in structure IV. This was confirmed by calculating a slightly distorted structure IV* (Fig. 11-5b), in which the central carbon atom was shifted by 0.004 Å from the central position. Neither the total energy nor the orbital energies of IV* change significantly from those of IV, but the shape of the $\pi-$bonds (Fig. 11-5b-5-7) in this distorted structure now looks exactly like

there in isomer III (Fig. 5c-5-7). Hence, isomer III can be still viewed as a π–aromatic system. However, isomer III is no longer a σ–aromatic system, even though it has three partially delocalized σ–bonds. We found that the σ–bonding pattern of the slightly distorted structure IV* (Fig. 11-5b-2-4) is different from that of isomer III (Fig. 11-5c-2-4). The slightly distorted structure IV* is still σ–aromatic, even though the σ–bonds are now partially localized, analogous to the π–bonds discussed above. However, upon further distortion towards isomer III one of the "aromatic" σ–bond (Fig. 11-5b-4) is transformed into a new σ–bond (Fig. 11-5c-4). The three σ–bonds in III (Fig 11-5c-2-4) are now localized on the bottom part of the cluster, with the three upper peripheral atoms not participating in the delocalized σ–bonding. Therefore, isomer III is no longer σ–aromatic, while clusters IV and IV* are with all the atoms being involved in delocalized bonding.

This conclusion is confirmed by calculation of $NICS_{zz}$ indices for structures IV and III. In structure IV we found that NICS values are highly negative just above the central carbon atom and they slowly decrease with the height of the probe charge. In structure III, NICS values are highly positive just above the carbon atom, but they become negative with increasing the height of the probe charge. However, III and IV are not low-lying structures. Structure I is the global minimum structure for CB_8. The reason why isomer I is significantly more stable than structure III and IV can be understood from the bonding patterns. The central C atom in structures III and IV is involved in delocalized bonding with the peripheral atoms only, while in isomer I the C atom is also

involved in 2c-2e peripheral bonding with two neighboring boron atoms, in addition to the delocalized bonding. The lower electronegativity of B compared to C clearly favors structures with the peripheral position for the carbon atom. The bonding pattern (Fig. 11-5d) is almost identical to the bonding pattern of the slightly distorted structure IV* (Fig. 11-5b) and thus, isomer I is also doubly (σ– and π–) aromatic.

We further performed the AdNDP analysis for the doubly charged CB_8^{2-} anion at the geometry of the global minimum structure V of CB_8^- by adding an electron to the singly occupied HOMO (Fig. 11-6a). The AdNDP analysis revealed that there are six 2c-2e B-B and two C-B peripheral σ–bonds (Fig. 11-6a-1), three 3c-2e σ–bonds (Fig. 11-6a-2-4), one 4c-2e σ–bond (Fig. 11-6a-5), and two 4c-2e and one 3c-2e π–bonds (Fig. 11-6a-6-8). The three 3c-2e σ–bonds in structure V of CB_8^{2-} are similar to the three 4c-2e σ–bonds in the slightly distorted octagonal structure of CB_8 (Fig. 11-5b-2-4). The π-bonds in structure V of CB_8^{2-} are similar to those in the slightly distorted octagonal structure of CB_8 (Fig. 11-5b-5-7). Finally, 4c-2e σ–bond (Fig. 11-6a-5) is similar to the 4c-2e σ–bond in the structure III of CB_8 (Fig. 11-5c-4). As we have already mentioned above, the slightly distorted octagonal structure is still doubly aromatic. The appearance of the extra σ–bond (Fig. 11-6a-5) makes structure V of CB_8^{2-} σ-antiaromatic with eight σ-electrons participating in the delocalized bonding. We confirmed this conclusion by calculation of NICS over the central boron atom and found that NICS values at low height (0.2 Å and 0.4 Å) are positive and at higher position (0.6 Å, 0.8 Å, 1.0 Å, and 1.2

Å) become negative. These results imply a system with conflicting aromaticity, i.e., σ–antiaromatic and π–aromatic.

11-5. Rational design of hypercoordinate planar species with an external boron ring

Our previous studies on pure boron clusters[1,59-61] revealed that in planar structures there is always a peripheral ring of 2c-2e B-B σ -bonds with additional delocalized bonding between peripheral atoms or peripheral atoms and atoms located inside of the ring. The presence of this peripheral ring gives us an opportunity to design planar molecules with hypercoordinate central atoms. In order to obtain planar boron clusters with a hypercoordinate central atom, the wheel type structure has to be a minimum (geometric fit, i.e., structural factor) and the system has also to be doubly aromatic (electronic factor). As we mentioned above, the B_9^- cluster has a D_{8h} wheel structure and it is σ- and π-aromatic. Apparently, the central boron atom fits well into the octagonal B_8 ring. It was shown that ten atomic boron cluster favors the structure in which two boron atoms occupy central positions[59] and the wheel structure with one central atom located inside the nine-member ring is significantly higher in energy.[1,2] B_9^- is a system with the highest yet experimentally observed coordination number of 8.

In the CB_6^-, $C_2B_5^-$, CB_6^{2-}, CB_7^-, and CB_8^- clusters, we found that the carbon atom avoids the central position in wheel type structures. Chemical bonding analysis performed by the AdNDP method revealed that the atom in the central position in the wheel type structures is involved in delocalized bonding only, while atoms at the

periphery are involved in both delocalized bonding and 2c-2e peripheral σ-bonding. The carbon atom, being more electronegative than the boron atom, favors peripheral positions, where it can participate in 2c-2e σ-bonding. Thus, the boron ring wheel-type structures are not suitable for designing planar molecules with a hypercoordinate central carbon atom.

This observation suggests that atoms, which are more electropositive than boron, may be more viable candidates to sit in a boron ring for hypercoordinate structures. Indeed, we recently demonstrated[62] that an aluminum atom can be placed into a B_9 ring to result in a high-symmetry and stable D_{9h} structure, which according to high-level theoretical calculations was shown to be either the global minimum or a low-lying isomer on the potential energy surface. We can readily apply our chemical bonding model described above to the AlB_9 cluster: it possesses 30 valence electrons with 18 electrons participating in nine 2c-2e peripheral B-B σ -bonds, 6 electrons participating in delocalized σ-bonding and 6 electrons participating in delocalized π-bonding (Fig. 11-7). Thus, AlB_9 is doubly (σ- and π-) aromatic system and Al atom is a good geometric fit for the B_9 ring. AlB_9 is the first computationally found system with a nine-coordinate central atom. We tried to use this approach to design a ten-coordinated atom in the AlB_{10}^+ cluster. However, we found that the isomer with Al at the central position of the B_{10} ring is significantly higher in energy than an alternative isomer, in which the Al^+ cation is located above the B_{10} cluster. We believe that the central cavity for B_{10} is too big to fit favorably the Al^+ cation at the center. Nevertheless, suitable atoms may exist to make ten-coordinated planar clusters.

Recently, Ito et al.[63] reported a calculation of the global minimum wheel-type FeB_9^- structure with a nine-coordinate Fe atom. This structure can be easily rationalized using our chemical bonding model. The FeB_9^- cluster has 36 valence electrons with 18 electrons participating in nine 2c-2e peripheral B-B σ-bonds, 6 electrons participating in delocalized σ–bonding and 6 electrons participating in delocalized π–bonding, and three pairs of localized 3d electrons on Fe (Fig. 11-7). Thus, the FeB_9^- cluster is doubly (σ– and π–) aromatic and similar to AlB_9 the central atom is an electropositive element in agreement with our conclusion that only electropositive (relative to boron) atoms can have high symmetry global minimum structures or at least to be a low-lying isomer.

11-6. Rational design of hypercoordinate planar carbon species

In spite of the unfavorable location of a carbon atom in boron rings, it has been shown theoretically and experimentally that carbon occupies the central position in the square of four aluminum atoms in the CAl_4^- (ref. 6) and $NaCAl_4^-$ (ref. 8) species. At first glance, these findings may seem to contradict the previously discussed chemical bonding model. However, our AdNDP analysis performed for the CAl_4^{2-} dianion (Fig. 11-9) showed that bonding between the peripheral boron atoms in planar wheel structures and those of aluminum atoms in CAl_4^{2-} is quite different. One can see that there are no 2c-2e peripheral Al-Al σ-bonds in CAl_4^{2-}. Instead, there is a lone pair at every aluminum atom (Fig. 11-9a). There are also two delocalized bonds: one is a 4c-2e peripheral σ-bond composed out of 3p tangential aluminum AOs (Fig. 11-9f) and another one is a 5c-2e π-

bonds composed of mainly $2p_z$-AO of carbon with small contributions from the $3p_z$-AOs of Al atoms (Fig. 11-9e). The other three bonds are essentially 2s-AO on C (Fig. 11-9d) and $2p_x$- and $2p_y$-AOs on C (Fig. 11-9b,c). Thus, bonding in CAl_4^{2-} can be approximately considered as being due to ionic bonding between a central carbon C^{4-} anion and an Al_4^{2+} cation (with significant covalent contribution) and due to the delocalized σ-bonding and weakly delocalized π-bonding. Therefore, in order to design a chemical species with a central hypercoordinate carbon atom, one should consider electropositive ligands, which tend to form lone pairs instead of 2c-2e peripheral bonds. Aluminum is a good example of such a ligand, but it is conceivable that there may exist a class of such atoms to design hypercoordinate carbon species. A recent theoretical prediction of a planar pentacoordinate carbon in the CAl_5^+ cation[64] provides another example for our design principle.

The considered in our article hypercoordinate chemical species CB_8, CB_8^-, CAl_5^+, AlB_9 and FeB_9^- belong to electron deficient hypervalent chemical species.[65,66] This conclusion can be supported by results of the Natural Bond Analysis (at B3LYP/6-311+G*) that revealed that the charges at the central atoms are the following: Q(C)=-0.45 |e| with the atomic occupations $2s^{1.28}2p^{3.15}$ in CB_8 , Q(C)=-2.65 |e| with the atomic occupations $2s^{1.65}2p^{4.97}$ in CAl_5^+, Q(Al)=1.46 |e| with the atomic occupations $3s^{0.44}3p^{1.05}$ in AlB_9, and Q(Fe)=0.02 |e| with atomic occupations $4s^{0.21}3d^{7.65}$ in FeB_9^-. The hypervalency in these hypercoordinate species is due to delocalized bonding revealed by our AdNDP analysis and not due to the formation of extra 2c-2e radial bonds.

11-7. Summary

From our joint photoelectron spectroscopic and ab initio study we have demonstrated that carbon avoids central positions in CB_6^{2-}, CB_7^-, CB_8, and CB_8^-. We have developed a chemical bonding model (using AdNDP analysis), which explains why carbon avoids the central position in those species. According to this model, in the wheel type structures the central atom is involved in delocalized bonding only, while atoms at the periphery of the wheel structure are involved in both delocalized bonding and 2c-2e peripheral σ-bonding. The carbon atom is more electronegative than boron atoms and favors peripheral positions where it can participate in 2c-2e σ-bonding. Thus, wheel-type structures with a boron ring are not appropriate for designing planar molecules with a hypercoordinate central carbon. However, if the central atom is more electropositive than boron, then the wheel type structures are stable and can be either global minimum or low-lying isomers. The results of the AdNDP analysis of the chemical bonding in the CAl_4^{2-} dianion showed that in this case, the favorable central position of the carbon atom is due to essentially ionic bonding between a central carbon C^{4-} anion and an Al_4^{2+} cation with contributions from delocalized σ-bonding and weakly delocalized π-bonding. In order to design a chemical species with a central hypercoordinate carbon atom, one should consider electropositive ligands, which would have lone pairs instead of forming 2c-2e peripheral bonds. The same is true for the pentacoordinate carbon atom inside of the Al_5^+ ring (CAl_5^+ cluster). We used our extensive chemical bonding model, which considers both σ- and π-electrons to explain why the AlB_9 and FeB_9^- species with octacoordinate Al and Fe are the global minima or low-lying isomers. Though the global minimum structure

of FeB_9^- was established by Ito et al,[63] they considered in their chemical bonding analysis only π-electron. We have shown that σ-electrons are also important for rationalizing high symmetry and high coordination number of Fe in FeB_9^-. Hence, we presented a comprehensive chemical bonding model capable of rationalizing and predicting structures either with a boron ring or a central planar carbon. This represents the first step towards rational design of nano- and subnano-structures with tailored properties.

References

1. A. N. Alexandrova, A. I. Boldyrev, H.-J. Zhai and L. S. Wang, *Coord. Chem. Rev.*, 2006, **250**, 2811.

2. D. Yu. Zubarev and A. I. Boldyrev, *J. Comput. Chem.*, 2007, **28**, 251.

3. L.-M. Wang, W. Huang, B. B. Averkiev, A. I. Boldyrev and L. S. Wang, *Angew. Chem. Int. Ed.*, 2007, **46**, 4550.

4. B. B. Averkiev, D. Yu. Zubarev, L.-M. Wang, W. Huang, L. S. Wang and A. I. Boldyrev, *J. Am. Chem. Soc.*, 2008, **130**, 9248.

5. D. Yu. Zubarev and A. I. Boldyrev, *Phys. Chem. Chem. Phys.*, 2008, **10**, 5207.

6. D. Yu. Zubarev and A. I. Boldyrev, *J. Org. Chem.*, 2008, **73**, 9251.

7. D. Yu. Zubarev and A. I. Boldyrev, *J. Phys. Chem. A*, 2009, **113**, 866.

8. H.-J. Zhai, A. N. Alexandrova, A. I. Boldyrev and L. S. Wang, *Angew. Chem. Int. Ed.*, 2003, **42**, 6004. See also a recent study on the low-lying isomers of B_9^-: L. L. Pan, J. Li and L. S. Wang, *J. Chem. Phys.*, 2008, **129**, 024302.

9. X. Li, W. Chen, L. S. Wang, A. I. Boldyrev and J. Simons, *J. Am Chem. Soc.*, 1999, **121**, 6033.

10. L. S. Wang, A. I. Boldyrev, X. Li, and J. Simons. *J. Am. Chem. Soc.*,2000, **122**, 7681.

11. X. Li, H-F. Zhang, L. S. Wang, G. D. Geske, and A. I. Boldyrev, *Angew. Chem. Int. Ed.*, 2000, **39**, 3630.

12. P. v. R. Schleyer and A. I. Boldyrev, *J. Chem. Soc. Chem. Comm.*, 1991, 1536.

13. A. I. Boldyrev and J. Simons, *J. Am. Chem. Soc.,* 1998, **120**, 7967.

14. J. Kemsley, *Chem. & Eng. News*, 2007, **85**, 17.

15. R. Keese, *Chem. Rev.*, 2006, **106**, 4787, and references there in.

16. G. Merino, M. A. Mendez-Rojas, A. Vela, T. Heine, *J. Comput. Chem.*, 2007, **28**, 362, and references there in.

17. B. Sateesh, A. S. Reddy, G. N. Sastry, *J. Comput. Chem.*, 2007, **28**, 335, and references there in.

18. W. Siebert, A. Gunale, *Chem. Soc. Rev.*, 1999, **28,** 367, and references there in.

19. K. Exner, P. v. R. Schleyer, *Science*, 2000, **290**, 1937.

20. Z.-X. Wang, P. v. R. Schleyer, *Science*, 2001, **292**, 2465.

21. S. Erhardt, G. Frenking, Z. Chen, P. v. R. Schleyer, *Angew. Chem. Int. Ed.*, 2005, **44**, 1078.

22. K. Ito, Z. Chen, C. Corminboeuf, C. S. Wannere, X. H. Zhang, Q. S. Li, P. v. R. Schleyer, *J. Am. Chem. Soc.*, 2007, **129**, 1510.

23. R. Islas, T. Heine, K. Ito, P. v. R. Schleyer and G. Merino, *J. Am. Chem. Soc.*, 2007, **129**, 14767.

24. R. M. Minyaev, T. N. Gribanova, A. G. Starikov and V. I. Minkin, *Mendeleev Comm.*, 2001, **11**, 213.

25. T. N. Gribanova, R. M. Minyaev and V. I. Minkin, *Russ. J. Inorg. Chem.*, 2001, **46**, 1207.

26. R. M. Minyaev, T. N. Gribanova, A. G. Starikov and V. I. Minkin, *Dokl. Chem.*, 2002, **382**, 41.

27. V. I. Minkin and R. M. Minyaev, *Mendeleev Comm.*, 2004, **14**, 43.

28. S.-D. Li, C.-Q. Miao and G.-M. Ren, *Eur. J. Inorg. Chem.*, 2004, 2232.

29. S.-D. Li, J.-G. Guo, C.-Q. Miao and G.-M. Ren, *J. Phys. Chem. A,* 2005, **109,** 4133.

30. S.-D. Li, C.-Q and Miao, *J. Phys. Chem. A*, 2005, **109**, 7594.

31. S.-D. Li, C.-Q. Miao, G.-M. Ren and J.-C. Guo, *Eur. J. Inorg. Chem.*, 2006, 2567.

32. S. Shahbazian and A. Sadjadi, *J. Mol. Struct. Theochem.*, 2007, **822**, 116.

33. L.-M. Yang, H.-P. He, Y.-H. Ding and C.-C. Sun, *Organometallics*, 2008, **27**, 1727.

34. S. Shahbazian and A. Sadjadi, *J. Phys. Chem. A*, 2008, **112**, 10365.

35. Q. Luo, X. H. Zhang, K. L. Huang, S. Q. Liu, Z. H. Yu and Q. S. Li, *J. Phys. Chem. A*, 2007, **111**, 2930.

36. S.-D. Li, C.-Q. Miao and J.-C. Guo, *J. Phys. Chem. A*, 2007, **111**, 12069.

37. Y. Pei and X. C. Zeng, *J. Am. Chem. Soc.*, 2008, **120**, 2580.

38. L. S. Wang, H. S. Cheng and J. Fan, *J. Chem. Phys.*, 1995, **102**, 9480.

39. L. S. Wang and X. Li, in *Clusters and Nanostructure Interfaces*, ed. by P. Jena, S. N. Khanna, and B. K. Rao, World Scientific, River Edge, New Jersey, 2000, pp. 293-300.

40. A. N. Alexandrova, A. I. Boldyrev, Y.-J. Fu, X. Yang, X.-B. Wang and L. S. Wang, *J. Chem. Phys.*, 2004, **121**, 5709.

41. A. N. Alexandrova and A. I. Boldyrev, *J. Chem. Theory and Comput.*, 2005, **1**, 566.

42. A. D. Becke, *J. Chem. Phys.*, 1993, **98**, 5648.

43. S. H. Vosko, L. Wilk and M. Nusair, *Can. J. Phys.*, 2008, **58**, 1200.

44. C. Lee, W. Yang and R. G. Parr, *Phys. Rev. B*, 1988, **37**, 785.

45. J. Cizek, *Adv. Chem. Phys.*, 1969, **14**, 35.

46. P. J. Knowles, C. Hampel and H.-J. Werner, *J. Chem. Phys.*, 1993, **99**, 5219.

47. K. Raghavachari, G. W. Trucks, J. A. Pople and M. Head-Gordon, *Chem. Phys. Lett.*, 1989, **157**, 479.

48. L. S. Cederbaum, *J. Phys. B*, 1975, **8**, 290.

49. J. V. Ortiz, *Int. J. Quant. Chem., Quant. Chem. Symp.*, 1989, **23**, 321.

50. J. S. Lin and J. V. Ortiz, *Chem. Phys. Lett.*, 1990, **171**, 197.

51. V. G. Zakrzewski, J. V. Ortiz, J. A. Nichols, D. Heryadi, D. L. Yeager and J. T. Golab, *Int. J. Quant. Chem.*, 1996, **60**, 29.

52. R. Bauernshmitt and R. Alrichs, *Chem. Phys. Lett.*, 1996, **256**, 454.

53. M. E. Casida, C. Jamorski, K. C. Casida and D. R. Salahub, *J. Chem. Phys.*, 1998, **108**, 4439.

54. M. J. Frisch, G. W. Trucks, H. B. Schlegel, G. E. Scuseria, M. A. Robb, J. R. Cheeseman, J. A. Montgomery, Jr., T. Vreven, K. N. Kudin, J. C. Burant, J. M. Millam, S. S. Iyengar, J. Tomasi, V. Barone, B. Mennucci, M. Cossi, G. Scalmani, N. Rega, G. A. Petersson, H. Nakatsuji, M. Hada, M. Ehara, K. Toyota, R. Fukuda, J.

Hasegawa, M. Ishida, T. Nakajima, Y. Honda, O. Kitao, H. Nakai, M. Klene, X. Li, J. E. Knox, H. P. Hratchian, J. B. Cross, V. Bakken, C. Adamo, J. Jaramillo, R. Gomperts, R. E. Stratmann, O. Yazyev, A. J. Austin, R. Cammi, C. Pomelli, J. Ochterski, P. Y. Ayala, K. Morokuma, G. A. Voth, P. Salvador, J. J. Dannenberg, V. G. Zakrzewski, S. Dapprich, A. D. Daniels, M. C. Strain, O. Farkas, D. K. Malick, A. D. Rabuck, K. Raghavachari, J. B. Foresman, J. V. Ortiz, Q. Cui, A. G. Baboul, S. Clifford, J. Cioslowski, B. B. Stefanov, G. Liu, A. Liashenko, P. Piskorz, I. Komaromi, R. L. Martin, D. J. Fox, T. Keith, M. A. Al-Laham, C. Y. Peng, A. Nanayakkara, M. Challacombe, P. M. W. Gill, B. G. Johnson, W. Chen, M. W. Wong, C. Gonzalez and J. A. Pople, GAUSSIAN 03 (Revision D.01), Gaussian, Inc., Wallingford, CT, 2004.

55. G. Schaftenaar, MOLDEN 3.4, CAOS/CAMM Center, The Netherlands, 1998.

56. S. Portmann, MOLEKEL, Version 4.3., CSCS/ETHZ, 2002.

57. J. Li, X. Li, H. J. Zhai and L. S. Wang, *Science*, 2003, **299**, 864.

58. S. Bulusu, X. Li, L. S. Wang and X. C. Zeng, *Proc. Natl. Acad. Sci.* U.S.A., 2006, **103**, 8326.

59. H. J. Zhai, B. Kiran, J. Li and L. S. Wang, *Nature Materials*, 2003, **2**, 827.

60. B. Kiran, S. Bulusu, H. J. Zhai, S. Yoo, X. C. Zeng and L. S. Wang, *Proc. Natl. Acad. Sci.* U.S.A., 2005, **102**, 961.

61. A. P. Sergeeva, D. Yu. Zubarev, H. J. Zhai, A. I. Boldyrev and L. S. Wang, *J. Am. Chem. Soc.*, 2008, **130**, 7244.

62. B. B. Averkiev and A. I. Boldyrev, *Russ. J. Gen. Chem.*, 2008, **78**, 769.

63. K. Ito, Z. Pu, Q.-S. Li and P. v. R. Schleyer, *Inorg. Chem.*, 2008, **47**, 10906.

64. Y. Pei, W. An, K. Ito, P. v. R. Schleyer and X. C. Zeng, *J. Am. Chem. Soc.*, 2008, **130**, 10394.

65. K.-y. Akiba, Chemistry of Hypervalent Compounds, Wiley-VCH, New York, 1999.

66. I. Fernandes, E. Uggerud, and G. Frenking, *Chem. Eur. J.* 2007, **13**, 8620.

Table 11-1 Comparison of the experimental vertical detachment energies (VDE) of CB_8^- with the calculated values for the global minimum C_S structure. All energies are in eV.

Feature	VDE (exp.) [a]	Final State and Electronic Configuration	VDE (theo.) TD-B3LYP[b]	OVGF [c]	DCCSD(T) [d]
X [e]	~ 3.45	$^1A'$, $9a'^2 10a'^2 11a'^2 2a''^2 3a''^2 12a'^0$	3.45	3.69 (0.89)	3.41
A	3.70 (5)	$^3A''$, $9a'^2 10a'^2 11a'^2 2a''^2 3a''^1 12a'^1$	3.58	3.57 (0.89)	3.72
A tail	~ 4.0	$^1A''$, $9a'^2 10a'^2 11a'^2 2a''^2 3a''^1 12a'^1$	4.02	[f]	[f]
B	4.23 (4)	$^3A''$, $9a'^2 10a'^2 11a'^2 2a''^1 3a''^2 12a'^1$	4.17	4.27 (0.88)	[f]
B tail	~ 4.5	$^1A''$, $9a'^2 10a'^2 11a'^2 2a''^1 3a''^2 12a'^1$	4.43	[f]	[f]
C	4.75 (5)	$^3A'$, $9a'^2 10a'^2 11a'^1 2a''^2 3a''^2 12a'^1$	4.71	4.93 (0.88)	4.80
D	~ 5	$^3A'$, $9a'^2 10a'^1 11a'^2 2a''^2 3a''^2 12a'^1$	5.06	5.17 (0.87)	[f]
E	5.16 (5)	$^1A'$, $9a'^2 10a'^2 11a'^1 2a''^2 3a''^2 12a'^1$	5.48	[f]	[f]
F	5.35 (5)	$^3A'$, $9a'^1 10a'^2 11a'^2 2a''^2 3a''^2 12a'^1$	5.66	5.80 (0.86)	[f]

[a] Numbers in the parentheses represent uncertainties in the last digit.

[b] The first two VDEs were calculated at the B3LYP/6-311+G(2df)//B3LYP/6-311+G* level of theory as the lowest transition from the doublet state of the anion into the final lowest singlet and triplet states of the neutral species. Then the vertical excitation energies of the neutral species in the lowest singlet and triplet states (at the TD-B3LYP level) were added to the first two VDEs, respectively, in order to obtain higher VDEs.

[c] UOVGF/6-311+G(2df)//B3LYP/6-311+G*. Pole strength is given in parenthesis.

[d] UCCSD(T)/6-311+G(2df)//B3LYP/6-311+G*.

[e] The adiabatic detachment energy (ADE) was estimated to be 3.2±0.1 eV.

[f] This VDE cannot be calculated at this level of theory.
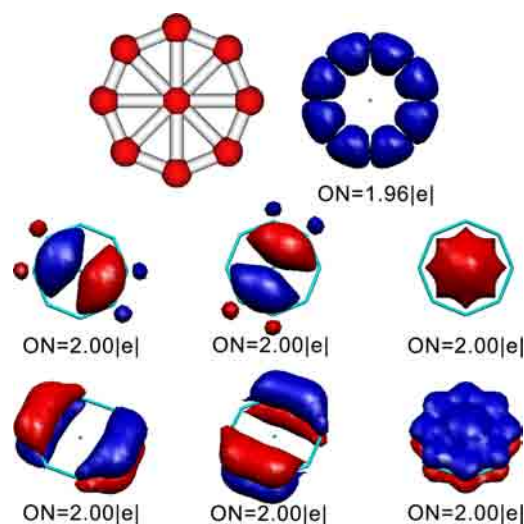
Fig. 11-1 The global minimum structure of B_9^- (upper left), the eight 2c-2e B-B σ-bonds superimposed over the B_9^- structure (upper right), the three 9c-2e delocalized σ-bonds (middle row), and the three 9c-2e delocalized π-bonds (bottom row), all recovered by the AdNDP analysis.
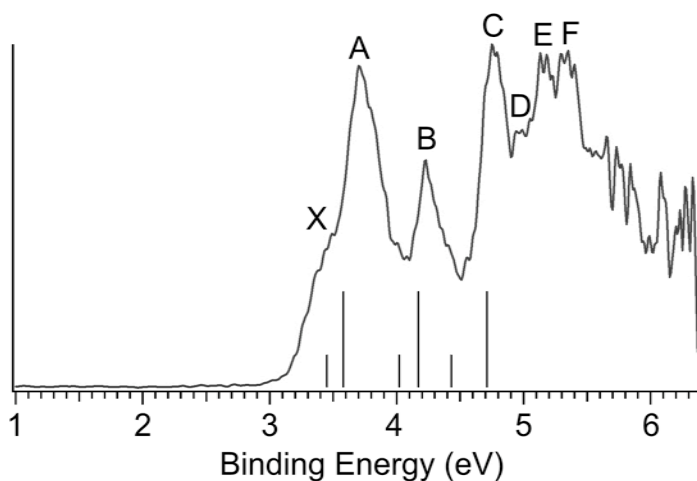
Fig. 11-2 Photoelectron spectrum of CB_8^- at 193 nm. The vertical bars represent the calculated VDEs (at TD-B3LYP level) for the lowest anion structure. The short bars represent the detachment transitions to singlet neutral states while the longer ones represent transitions to triplet final states.
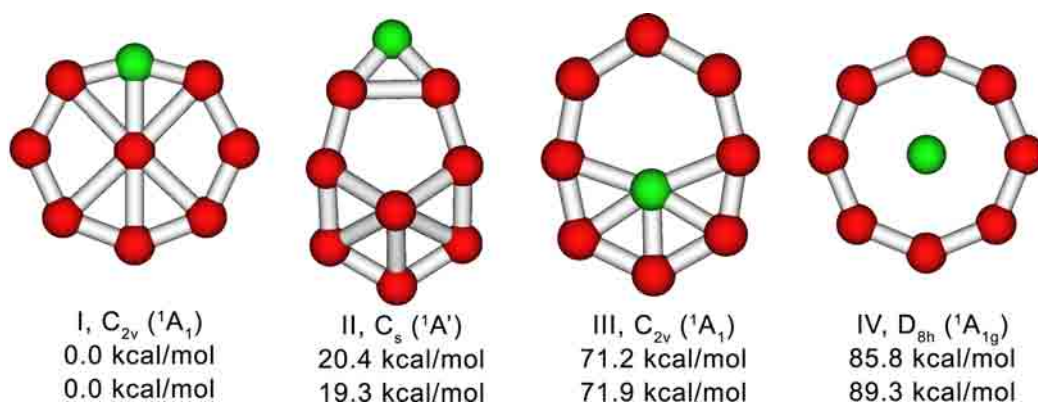
Fig. 11-3 Selected optimized structures of CB_8. Upper and lower numbers are relative energies calculated at the CCSD(T)/6-311+G(2df)//B3LYP/6-311+G*+ZPE//B3LYP/6-311+G* and B3LYP/6-311+G*+ZPE//B3LYP/6-311+G* levels of theory, respectively.
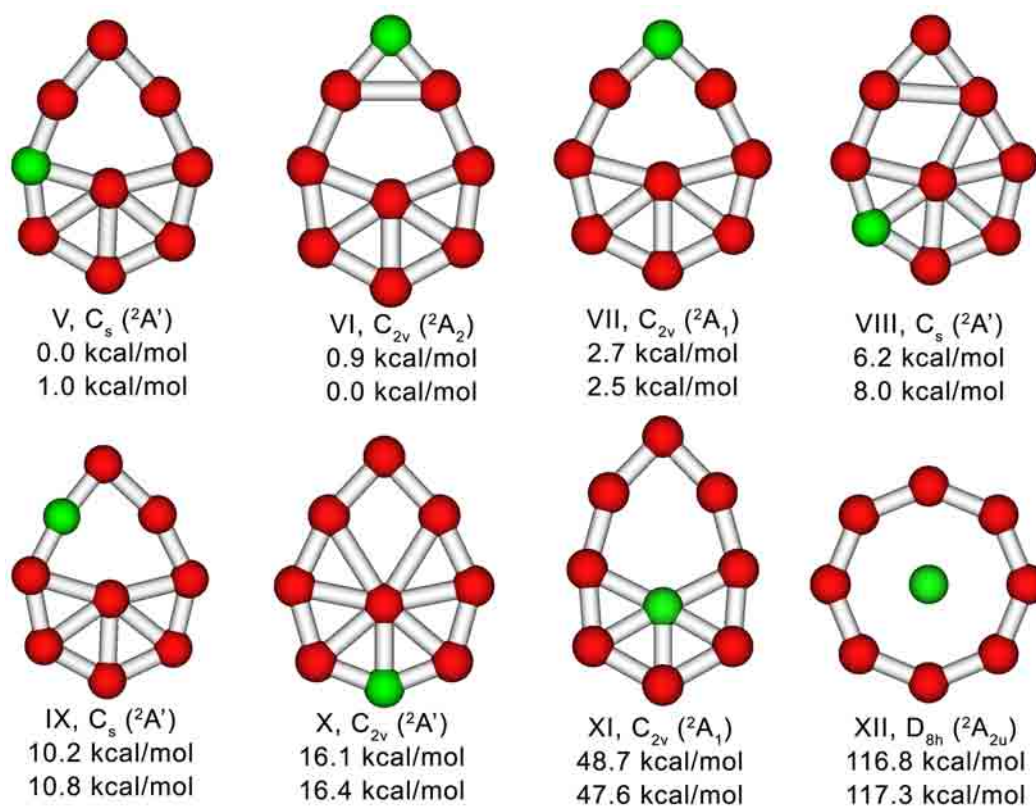
Fig. 11-4 Selected optimized structures of CB_8^-. Upper and lower numbers are relative energies calculated at the CCSD(T)/6-311+G(2df)//B3LYP/6-311+G*+ZPE//B3LYP/6-311+G* and B3LYP/6-311+G*+ZPE//B3LYP/6-311+G* levels of theory, respectively.
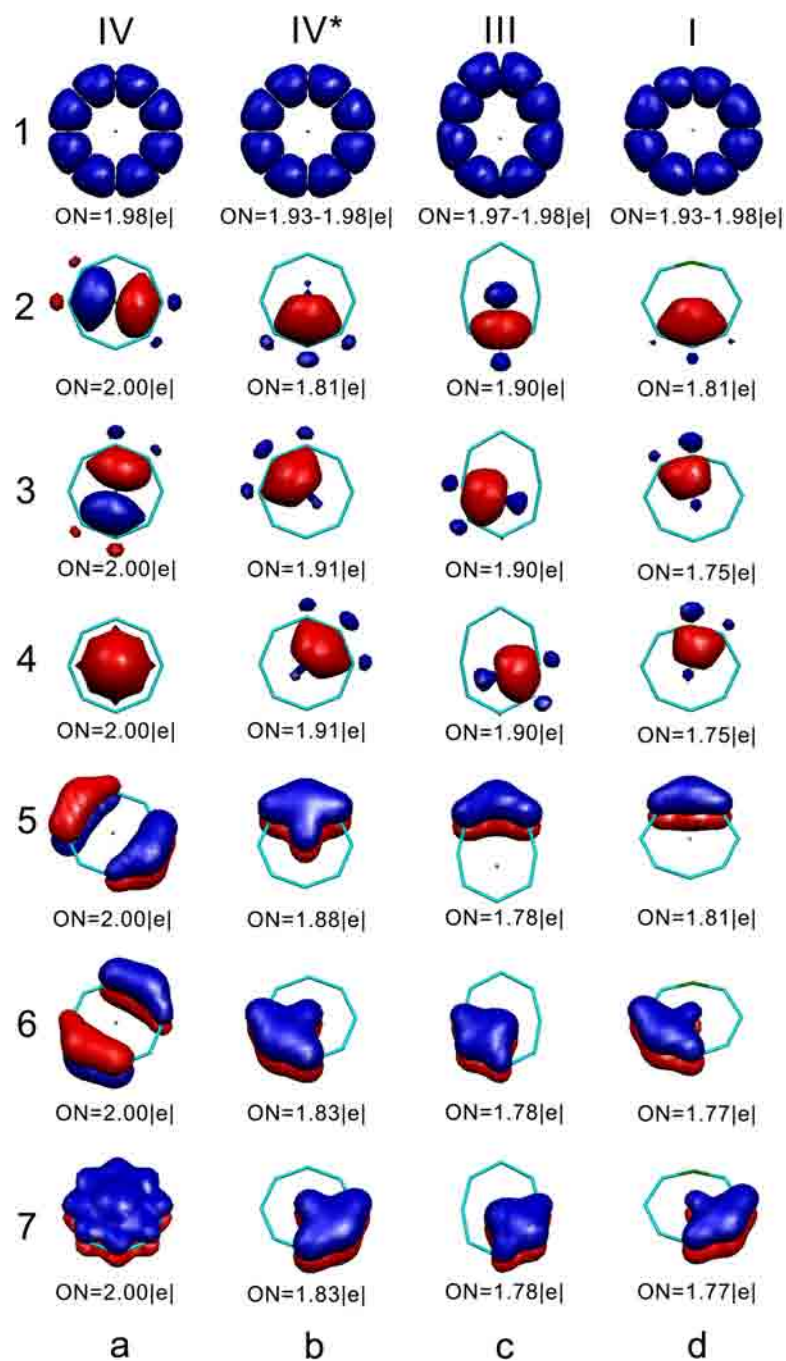
Fig. 11-5 The eight 2c-2e B-B σ-bonds superimposed over the CB_8 structures (first row), the three delocalized σ-bonds (second to fourth rows), and the three delocalized π-bonds (fifth to seventh rows), recovered by the AdNDP analysis (see text for details).
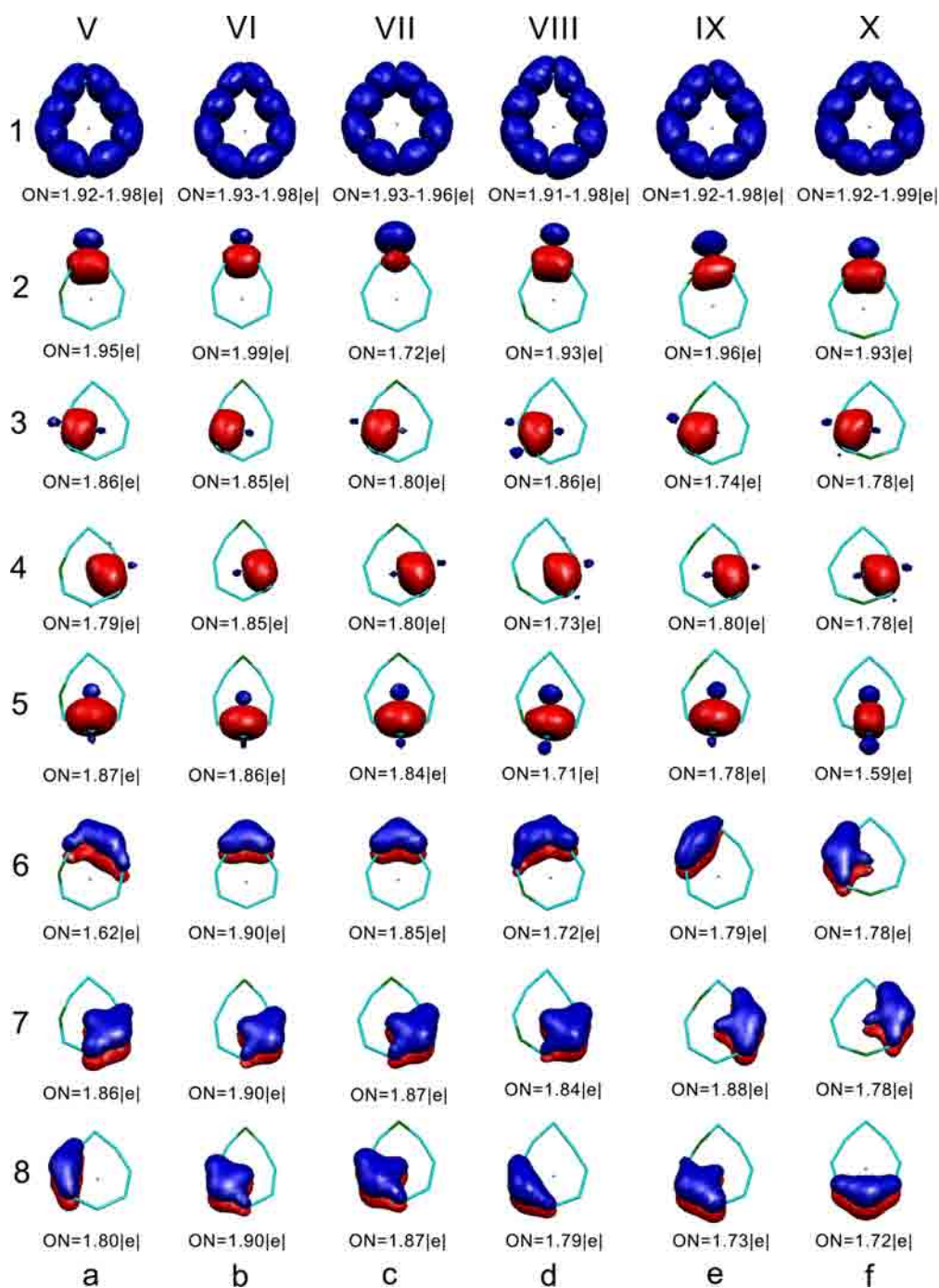
Fig. 11-6 The eight 2c-2e B-B σ-bonds superimposed over the CB$_8^{2-}$ structures (first row), the four delocalized σ-bonds (second to fifth rows), and the three delocalized π-bonds (sixth to eighth rows), recovered by the AdNDP analysis (see text for details).
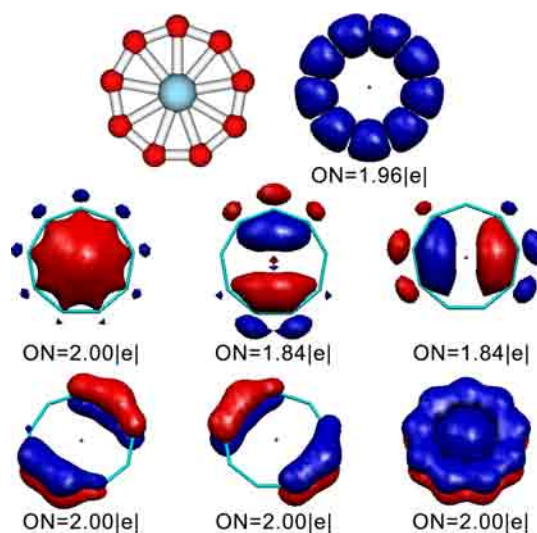
Fig. 11-7 One of the lowest energy structures of AlB$_9$ (upper left), its nine 2c-2e B-B σ-bonds superimposed over the AlB$_9$ structure (upper right), the three 10c-2e delocalized σ-bonds (middle row), and the three 10c-2e delocalized π -bonds (bottom row), all recovered by the AdNDP analysis.
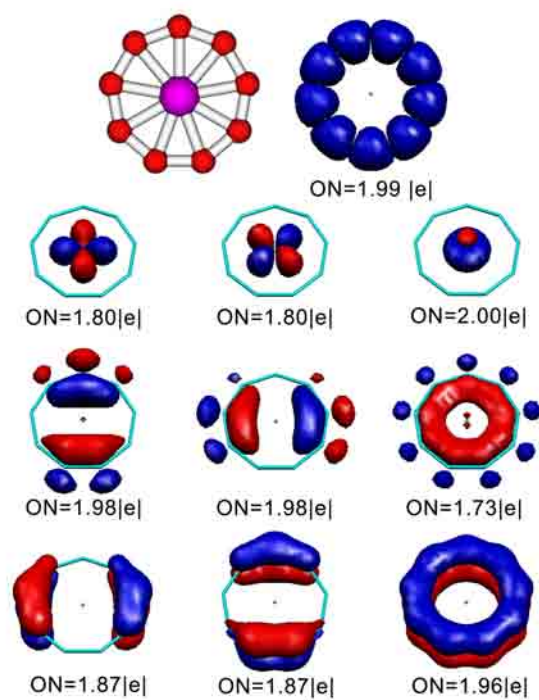
Fig. 11-8 The global minimum structure of FeB$_9$ (upper left), its nine 2c-2e B-B σ-bonds superimposed over the FeB$_9$ structure (upper right), the three pairs of localized 3d electrons (second row), the 9c-2e delocalized σ-bonds (third row), and the three 9c-2e delocalized π-bonds (fourth row), all recovered by the AdNDP analysis.
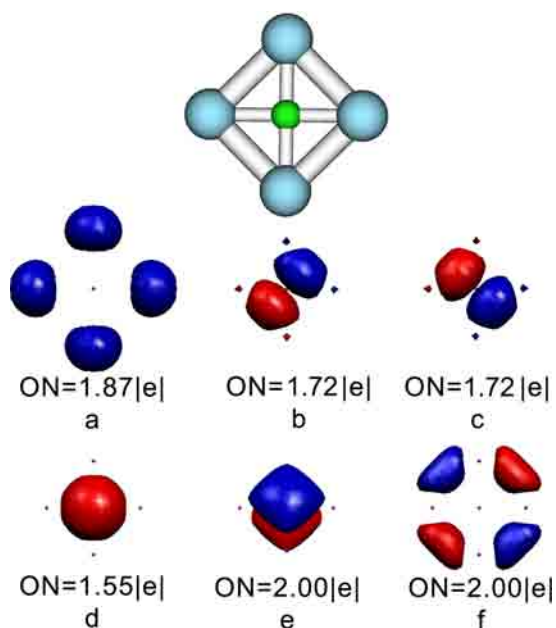
Fig. 11-9 The structure of CAl_4^{2-} (top), (a) the four Al lone pairs superimposed over the CAl_4^{2-} structure, (b and c) the $2p_x$- and $2p_y$-AOs of the carbon atom, (d) the 2s-AO of the carbon atom, (e) 5c-2e delocalized π-bond, and (f) 4c-2e σ-tangential bond (all recovered by AdNDP analysis).

CHAPTER 12

δ-AROMATICITY IN Ta$_3$O$_3^-$: A NEW MODE OF CHEMICAL BONDING[1]

Abstract

We report experimental and theoretical evidence of δ-aromaticity, which is discovered in the Ta$_3$O$_3^-$ cluster via a combined photoelectron spectroscopy and *ab initio* study. Well-resolved low-lying electronic transitions are observed in the photoelectron spectra of Ta$_3$O$_3^-$ and are compared with *ab initio* calculations, which show that the Ta$_3$O$_3^-$ cluster possesses a planar D_{3h} triangular structure. Chemical bonding analyses reveal that among the five valence molecular orbitals responsible for the multi-center metal-metal bonding there is a completely bonding δ and π orbital from the 5d atomic orbitals of Ta. The totally delocalized multi-center δ bond renders δ-aromaticity for Ta$_3$O$_3^-$ and represents a new mode of chemical bonding. Ta$_3$O$_3^-$ is the first δ-aromatic molecule confirmed experimentally and theoretically, suggesting that δ-aromaticity may exist in many multi-nuclear, low oxidation state transition-metal compounds.

12-1. Introduction

Aromaticity was introduced in organic chemistry to describe delocalized p-bonding in planar, cyclic and conjugate molecules possessing (4n + 2) p-electrons.[1] In recent years the concept of aromaticity has been advanced into main group molecules

---

including organometallic compounds with cyclic cores of metal atoms[2] and in particular all-metal clusters.[3] It has been shown that main group clusters may possess multiple aromaticity (σ and π), multiple antiaromaticity (σ and π), and conflicting aromaticity (σ-aromaticity and π-antiaromaticity or σ-antiaromaticity and π-aromaticity).[4-6]   Here we report experimental and theoretical evidence of d-aromaticity, which is only possible in transition metal systems. It is discovered in the $Ta_3O_3^-$ cluster via a combined photoelectron spectroscopy and *ab initio* study. Well-resolved low-lying electronic transitions are observed in the photoelectron spectra of $Ta_3O_3^-$ and are compared with *ab initio* calculations, which show that the $Ta_3O_3^-$ cluster possesses a planar D_{3h} triangular structure. Chemical bonding analyses reveal that among the five valence molecular orbitals responsible for the multi-center metal-metal bonding there is a completely bonding δ and π orbital from the 5d atomic orbitals of Ta. The totally delocalized multi-center δ bond renders δ-aromaticity for $Ta_3O_3^-$ and represents a new mode of chemical bonding. $Ta_3O_3^-$ is the first δ-aromatic molecule confirmed experimentally and theoretically, suggesting that δ-aromaticity may exist in many multi-nuclear, low oxidation state transition-metal compounds.

In 1964, Cotton and co-workers published a milestone work on the $K_2[Re_2Cl_8].2H_2O$ compound,[7] in which they showed the presence of a new type of chemical bond – δ-bond between the two Re atoms. Since then, a new branch of inorganic chemistry has been developed involving multiple metal-metal bonding[8] with bond orders higher than three, the maximum allowed for main group molecules. Power and co-workers recently reported the synthesis of Ar'CrCrAr' [where Ar' is the bulky

aryl group C_6H_3-2,6(C_6H_3-2,6-Pr^i_2)$_2$] with a quintuple bond ($\sigma^2\pi^4\delta^4$) between the two Cr atoms.[9] This work, along with the quantum chemical prediction of a quintuple bond in U_2 by Galiardi and Roos,[10a] and in $Re_2Cl_8^{2-}$ by Galiardi and Roos,[10b] and by Saito et al.[10c] has generated renewed interest into metal-metal multiple bonding.[11-13] The presence of δ-bonds between two transition metal atoms suggests that there may exist multi-center transition metal species with completely delocalized cyclic δ-bond, thus raising the possibility of δ-aromaticity analogous to π- or σ-aromaticity in main group systems. We have been interested in understanding the electronic structure and chemical bonding of early transition metal oxide clusters as a function of size and composition and using them as potential molecular models for oxide catalysts.[14-16] During our investigation of tantalum oxide clusters, we found serendipitously the presence of δ-aromaticity in the $Ta_3O_3^-$ cluster, in which each Ta is in a low-oxidation state of Ta(II) and still possesses three electrons for Ta-Ta bonding.

12-2. Experimental Method

The experiment was conducted using a magnetic-bottle-type photoelectron spectroscopy apparatus equipped with a laser vaporization cluster source, details of which have been described elsewhere.[17] $Ta_mO_n^-$ clusters with various compositions were produced by laser vaporization of a pure tantalum disk target in the presence of a helium carrier gas seeded with O_2 and were size-separated by time-of-flight mass spectrometry. The $Ta_3O_3^-$ species of current interest was mass-selected and decelerated before photodetachment by a pulsed laser beam. Photoelectron spectra were obtained at two

relatively high photon energies, 193 nm (6.424 eV) and 157 nm (7.866 eV), to guarantee access to all valence electronic transitions, as shown in Figure 12-1. Three well-resolved bands (X, A, and B) were observed at the lower binding energy side. The X band is much more intense and shows a discernible splitting at 193 nm (Figure 12-1a). Surprisingly, no well-defined electronic transitions were observed beyond 3.7 eV, where continuous signals were present, probably due to multi-electron transitions. The vertical detachment energies (VDEs) of the observed transitions at the low binding energy side are given in Table 12-1, where they are compared with theoretical calculations using two different methods.

12-3. Theoretical Methods

We initially performed an extensive search for the $Ta_3O_3^-$ global minimum for the singlet, triplet, and quintet states at the B3LYP/LANL2DZ level of theory and then recalculated the global minimum structure and the three lowest isomers at three other levels of theory.

12-4. Results and Discussion

We found that the $Ta_3O_3^-$ global minimum has a perfect D_{3h} ($^1A_1'$) planar triangular structure I (Figure 12-2). The closest isomer II is 6.6 (B3LYP/Ta/Stuttgart+2f1g/O/aug-cc-pvTZ) and 1.7 kcal/mol (B3PW91/Ta/Stuttgart+2f1g/O/aug-cc-pvTZ) higher in energy than the D_{3h} ground state. The theoretical VDEs of the global minimum at the two highest levels of theory are compared with the experimental data in Table 12-1. One can see that the calculated

VDEs for the global minimum structure I agree well with the experimental results, while those for the three low-lying isomers are completely off, lending considerable credence to the theoretical methods and the D_{3h} structure for $Ta_3O_3^-$. The highest occupied molecular orbital (HOMO, 4e') of the D_{3h} $Ta_3O_3^-$ is doubly degenerate, consistent with the intense X band observed experimentally. The splitting of the X band could be due to either a Jahn-Teller effect or spin-orbit coupling.

To help understand the structure and bonding in $Ta_3O_3^-$ we performed a detailed molecular orbital analysis. Out of the 34 valence electrons in $Ta_3O_3^-$, 24 belong to either pure oxygen lone pairs or those polarized towards Ta (responsible for the covalent contributions to Ta-O bonding). The remaining 10 valence electrons are primarily Ta-based and are responsible for direct metal-metal bonding, as shown in Figure 12-3. Among the five MOs, three are responsible for σ-bonding of the triangular Ta_3 framework. They include the partially bonding/antibonding doubly degenerate 4e' HOMO and the completely bonding $3a_1$' HOMO-3. The antibonding nature of the HOMO significantly reduces the σ-bonding contribution to the Ta_3 framework.[18] In the $Ta_3O_3^-$ anion, the HOMO-2 ($2a_2$") is a completely bonding π orbital composed primarily of the 5d orbitals of Ta, giving rise to π-aromatic character according to the $(4n + 2)$ Hückel rule for π-aromaticity.[19]

The most interesting MO is HOMO-1 ($4a_1$'), which is a completely bonding orbital mainly coming from the overlap of the d_z^2 orbital on each Ta atom. This orbital has the "appearance" of a π orbital with major overlaps above and below the molecular plane, but it is not a π-type MO because it is symmetric with respect to the molecular

plane. However, perpendicular to the molecular C_3 axis, this MO possesses two nodal surfaces, and thus it is a δ orbital.[20] In fact, a similar δ-bonding MO exists in the recently synthesized quintuple bond Cr_2 complex,[9] where it is a two-center bond formed from a d_z^2 orbital on each Cr atom.[13] Analogous to the circularly delocalized p-MO over the three carbon atoms in $C_3H_3^+$, which renders $C_3H_3^+$ p-aromatic,[6] the circular delocalization and the bonding nature of the $4a_1$' MO gives rise to δ-aromaticity in $Ta_3O_3^-$, which is also consistent with the $(4n + 2)$ Hückel rule.[19] In the $Ta_3O_3^-$ cluster, the δ-MO is a three-center bond, but similar types of MOs are possible in planar tetraatomic, pentaatomic, or larger transition metal systems.

Therefore, the $Ta_3O_3^-$ cluster possesses an unprecedented multiple (δ and π) aromaticity, which is responsible for the metal-metal bonding and the perfect triangular Ta_3 framework. The stability of the Ta_3 triangular kernel can be seen in all the low-lying isomers of $Ta_3O_3^-$ (Figure 12-2), which differ only in the coordination of the oxygen atoms to the aromatic Ta_3 framework. It is also noteworthy that the energy ordering of σ (HOMO-3) < π (HOMO-2) < δ (HOMO-1) (Table 12-1 and Figure 12-3) indicates that the strength of the metal-metal bonding increases from δ to π to σ, in agreement with the intuitive expectation that σ-type overlap is greater than π-type overlap, and δ-type overlap is expected to be the weakest, as is also the case in the multiple bonding of diatomic transition metal compounds including classical $Re_2Cl_8^{2-}$ dianion.[7-13] Despite the expected weaker overlap in the δ MO, it makes important contributions to the overall metal-metal bonding, as shown in the quintuple bonds in the new Cr_2 complex[9,11-13] or in

the U_2 dimer.[10] The three center delocalization in the aromatic δ MO in $Ta_3O_3^-$ is expected to provide even more bonding contributions than in the cases of the metal dimers, even though it is difficult to quantify them. The three center delocalization in the aromatic $W_3O_9^{2-}$ molecule due to a d-d σ bond was estimated previously to provide about 1 eV additional resonance energy, similar to that estimated for benzene.[21]

12-5. Conclusion

Aromaticity in transition metal systems has been discussed in the literature,[4,5,21-30] in particular, since the discovery of aromaticity in all-metal clusters.[3] King[22] and Li[23] have considered aromaticity in transition metal oxides due to metal-metal interactions via M-O-M bridges. The Hg_4^{6-} cluster, which is a building block of the Na_3Hg_2 amalgam, has been shown by Kuznetsov *et al.*[24] to be aromatic similar to that of the all-metal Al_4^{2-} unit.[3] Tsipis *et al.*[25,26] explained the planar structure of cyclic hydro-coinage compounds on the basis of their aromatic character. Aromaticity in square-planar coinage metal clusters was discussed by Wannere *et al.*[27] and Lin *et al.*[28] Alexandrova *et al.*[29] suggested the presence of aromaticity in the $Cu_3C_4^-$ cluster. Datta *et al.*[30] used d-orbital aromaticity to explain the metal ring structure in tiara nickel thiolates. Recently, Huang *et al.*[21] demonstrated the presence of d-orbital aromaticity in 4d and 5d transition metal oxide clusters, $Mo_3O_9^{2-}$ and $W_3O_9^{2-}$. The claim of d-aromaticity in the square-planar coinage metal clusters[27] was questioned by Lin *et al.*,[28] who showed that the completely filled d orbitals do not play any significant role in the bonding in these clusters. Instead, aromaticity in these systems comes primarily from σ-bonding

interactions of the valence s electrons. Thus, today the $Mo_3O_9^{2-}$ and $W_3O_9^{2-}$ clusters are the only examples, where aromaticity comes from d bonding interactions, albeit it has σ character.[21]

In the $Ta_3O_3^-$ cluster, we in fact found two new types of d bonding interactions leading to π- and δ-aromaticity. The δ-aromaticity found in this cluster is a new mode of chemical bonding, which can only occur in multi-nuclear transition metal systems. The current finding suggests that δ-aromaticity may exist in many cyclic transition metal systems containing metal atoms in low oxidation states. The next challenge is to find ϕ aromaticity, which may occur in multi-nuclear and cyclic f-metal systems.

References

1.   V. I. Minkin, M. N. Glukhovtsev, B. Ya. Simkin, *Aromaticity and Antiaromaticity*, Wiley, New York, 1994. Also see special issues: *Chem. Rev.* **2001**, *101*(5), and *Chem. Rev.* **2005**, *105*(10).

2.   G. H. Robinson, *Acc. Chem. Res.* **1999**, *32*, 773.

3.   X. Li, A. E. Kuznetsov, H. F. Zhang, A. I. Boldyrev, L. S. Wang, *Science* **2001**, *291*, 859.

4.   A. I. Boldyrev, L. S. Wang, *Chem. Rev.* **2005**, *105*, 3716 and references therein.

5.   C. A. Tsipis, *Coord. Chem. Rev.* **2005**, *249*, 2740.

6.   M. Hofmann, A. Berndt, *Heteroatom Chem.* **2006**, *17*, 224.

7.   F. A. Cotton, N. F. Curtis, C. B. Harris, B. F. G. Johnson, S. J. Lippard, J. T. Mague, W. R. Robinson, J. S. Wood, *Science* **1964**, *145*, 1305.

8. F. A. Cotton, C. A. Murillo, R. A. Walton, *Multiple Bonds Between Metal Atoms*, 3rd ed., Springer, New York, 2005.

9. T. Nguyen, A. D. Sutton, M. Brynda, J. C. Fettiger, G. J. Long, P. P. Power, *Science* **2005**, *310*, 844.

10. (a) L. Gagliardi, O. B. Roos, *Nature* **2005**, *433*, 848; (b) L. Gagliardi, O. B. Roos, *Inorg. Chem.* **2003**, *42*, 1599; (c) K. Saito, Y. Nakao, H. Sato, S. Sakaki, *J. Phys. Chem. A*, **2006**, *110*, 9710.

11. G. Frenking, *Science* **2005**, *310*, 796.

12. U. Radius, F. Breher, *Angew. Chem. Int. Ed.* **2006**, *45*, 3006. *Angew. Chem.* **2006**, *118*, 3072.

13. M. Brynda, L. Gagliardi, P.-O. Widmark, P. P. Power, B. O. Roos, *Angew. Chem. Int. Ed.* **2006**, *45*, 3804. *Angew. Chem.* **2006**, *118*, 3888.

14. H. J. Zhai, B. Kiran, L. F. Cui, X. Li, D. A. Dixon, L. S. Wang, *J. Am. Chem. Soc.* **2004**, *126*, 16134.

15. X. Huang, H. J. Zhai, J. Li, L. S. Wang, *J. Phys. Chem. A* **2006**, *110*, 85.

16. X. Huang, H. J. Zhai, T. Waters, J. Li, L. S. Wang, *Angew. Chem. Int. Ed.* **2006**, *45*, 657. *Angew. Chem.* **2006**, *118*, 673.

17. L. S. Wang, H. Wu, in *Advances in Metal and Semiconductor Clusters. IV. Cluster Materials* (Ed.: M. A. Duncan), JAI, Greenwich, CT, **1998**, pp 299-343.

18. If the HOMO (4e') and the HOMO-3 ($3a_1$') were composed of the same s-d hybrid functions, they would cancel each other, resulting in negligible metal-metal σ-bonding. However, the hybridization in the 4e' and $3a_1$' orbitals is

somewhat different. Therefore, we cannot rule out some σ-bonding contribution in the Ta_3 framework, i.e., there should be some σ-aromatic character in $Ta_3O_3^-$.

19. In the case of multiple aromaticity, the $(4n + 2)$ counting rule should be applied separately for each type of aromaticity encountered in a particular planar system, i. e. separately for σ-, π-, δ-, and ϕ-type molecular orbitals.[4]

20. Strictly speaking, the σ-, π-, δ-, and ϕ-notations for molecular orbitals are only appropriate for linear systems, where they are irreducible representations of the $C_{\infty v}$ and $D_{\infty h}$ point groups. However, it is customary in chemistry to use p-notation in planar molecules for molecular orbitals that are formed by the p_z atomic orbitals and are perpendicular to the molecular plane, even though they do not belong to the p-irreducible representation. For example, the orbitals responsible for the aromaticity in the prototypical aromatic C_6H_6 molecule are called p orbitals. Following this tradition in chemistry, one can introduce d- or f-type molecular orbitals in planar molecules formed from appropriate atomic orbitals.

21. X. Huang, H. J. Zhai, B. Kiran, L. S. Wang, *Angew. Chem. Int. Ed.* **2005**, *44*, 7251. *Angew. Chem.* **2005**, *117*, 7417.

22. R. B. King, *Inorg. Chem.* **1991**, *30*, 4437.

23. J. Li, *J. Cluster Sci.* **2002**, *13*, 137.

24. A. E. Kuznetsov, J. D. Corbett, L. S. Wang, A. I. Boldyrev, *Angew. Chem. Int. Ed.* **2001**, *40*, 3369. *Angew. Chem.* **2001**, *113*, 3473.

25. A. C. Tsipis, C. A. Tsipis, , *J. Am. Chem. Soc.* **2003**, *125*, 1136.

26. C. A. Tsipis, E. E. Karagiannis, P. F. Kladou, A. C. Tsipis, *J. Am. Chem. Soc.* **2004**, *126*, 12916.

27. C. S. Wannere, C. Corminboeuf, Z.-X. Wang, M. D. Wodrich, R. B. King, P. v. R. Schleyer, *J. Am. Chem. Soc.* **2005**, *127*, 5701.

28. Y.-C. Lin, D. Sundholm, J. Juselius, L. F. Cui, H. J. Zhai, L. S. Wang, *J. Phys. Chem. A* **2006**, *110*, 4244.

29. A. N. Alexandrova, A. I. Boldyrev, H. J. Zhai, L. S. Wang, *J. Phys. Chem. A* **2005**, *109*, 562.

30. A. Datta, N. S. John, G. U. Kulkarni, S. K. Pati, *J. Phys. Chem. A* **2005**, *109*, 11647.

Table 12-1: Experimental vertical electron detachment energies (VDE in eV) for $Ta_3O_3^-$, compared with those calculated for the D_{3h} global minimum.

Observed Feature	VDE (exp.)	Final State and Configuration	VDE (B3LYP)[a]	VDE (B3PW91)[a]
X	2.25 ± 0.03^b	$^2E'$ ($3a_1'^2 2a_2''^2 4a_1'^2 4e'^3$)	2.27	2.25
A	2.89 ± 0.02	$^2A_1'$ ($3a_1'^2 2a_2''^2 4a_1'^1 4e'^4$)	2.93	2.96
B	3.44 ± 0.03	$^2A_2''$ ($3a_1'^2 2a_2''^1 4a_1'^2 4e'^4$)	3.27	3.36

[a]Using the Ta/Stuttgartt+2f1g/O/aug-cc-pvTZ basis set.

[b]Adiabatic electron detachment energy was measured to be 2.22 ± 0.03 eV.
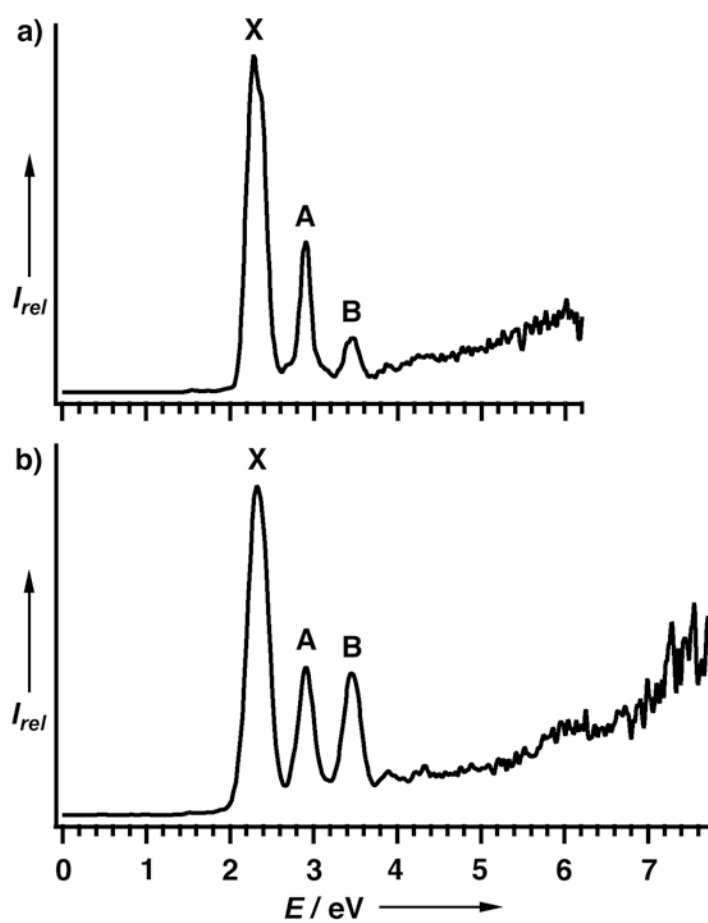
Figure 12-1. Photoelectron spectra of $Ta_3O_3^-$. a) 193 nm (6.424 eV). b) 157 nm (7.866 eV).
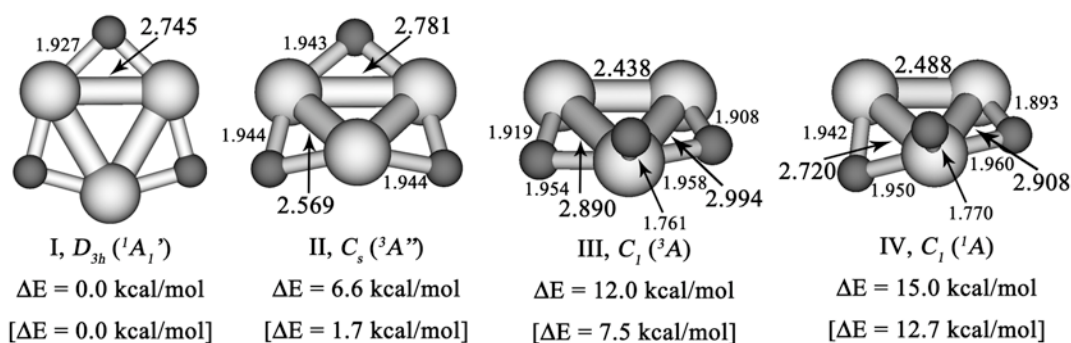
Figure 12-2. Optimized structures for the global minimum of $Ta_3O_3^-$ (D_{3h}, $^1A_1$') and selected low-lying isomers. The relative energies (ΔE_{total} in kcal/mol at B3LYP/Ta/Stuttgart+2f1g/O/aug-cc-pvTZ and at B3PW91/Ta/Stuttgart+2f1g/O/aug-cc-pvTZ in brackets) and interatomic distances (Å) were calculated at the B3LYP/Ta/Stuttgart+2f1g/O/aug-cc-pvTZ level of theory.
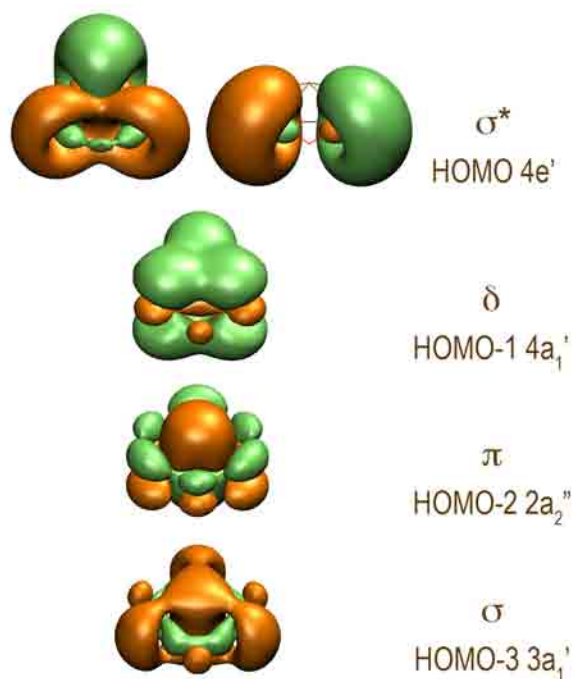
Figure 12-3. The five valence molecular orbitals responsible for the metal-metal bonding in $Ta_3O_3^-$ (D_{3h}, $^1A_1$').

CHAPTER 13

Hf$_3$ CLUSTER IS TRIPLY (σ-, π-, AND δ-) AROMATIC IN THE D$_{3h}$, ^{1}A$_1$' STATE[1]

Abstarct

The extensive search for the global minimum structure of Hf$_3$ at the B3LYP/LANL2DZ level of theory revealed that the D$_{3h}$ ^{3}A$_2$' (1a$_1$'^{2}1a$_2$"^{2}1e'^{4}2a$_1$'^{2}1e"^{2}) and the D$_{3h}$ ^{1}A$_1$' (1a$_1$'^{2}2a$_1$'^{2}1e'^{4}1a$_2$"^{2}3a$_1$'^{2}) are the lowest triplet and singlet states, respectively, with the triplet state being the lowest one. However, at the CASSCF(10,14)/Stuttgart+2f1g level of theory these two states are degenerate, indicating that at higher level of theory the singlet state could be in fact the global minimum structure. The triplet D$_{3h}$ ^{3}A$_2$' (1a$_1$'^{2}1a$_2$"^{2}1e'^{4}2a$_1$'^{2}1e"^{2}) structure is doubly (σ- and π-) aromatic and the singlet D$_{3h}$ ^{1}A$_1$' (1a$_1$'^{2}2a$_1$'^{2}1e'^{4}1a$_2$"^{2}3a$_1$'^{2}) structure is the first reported triply (σ-, π-, and δ-) aromatic system.

13-1. Introduction

In recent years the concepts of aromaticity and antiaromaticity have been advanced beyond the framework of organic chemistry. In particular, aromaticity and antiaromaticity have been extended into organometallic compounds with cyclic cores of metal atom[1] and into all-metal clusters.[2] It has been shown that main group metal clusters, in which the chemical bonding involves only s-AOs and p-AOs, may possess multiple

---

[1] Coauthored by B. B. Averkiev and A. I. Boldyrev. Reproduced with permission from *J. Phys. Chem. A*, **2007**, 111, 12864-12866. Copyright 2007 American Chemical Society.

aromaticity (σ- and π-), multiple antiaromaticity (σ- and π-), and conflicting aromaticity (σ-aromaticity and π-antiaromaticity or σ-antiaromaticity and π-aromaticity).[2c] In the transition metal clusters in which d-orbitals are involved in chemical bonding σ-tangential (σ_t-), σ-radial (σ_r-), π-tangential (π_t-), π-radial (π_r-), and δ-aromaticity/antiaromaticity could occur. In this case, there can be triple (σ-, π-, and δ-) aromaticity, triple (σ-, π-, and δ-) antiaromaticity, and a variety of conflicting aromaticities (simultaneous σ-aromaticity, π-aromaticity, and δ-antiaromaticity; σ-aromaticity, π-antiaromaticity, and δ-aromaticity; σ-antiaromaticity, π-aromaticity, and δ-aromaticity; σ-aromaticity, π-antiaromaticity, and δ-antiaromaticity; σ-antiaromaticity, π-aromaticity, and δ-antiaromaticity; σ-antiaromaticity, π-antiaromaticity, and δ-aromaticity).

Aromaticity in transition metal systems have been already discussed in the literature.[2-12] King[3] and Li[4] have considered aromaticity in transition metal oxides due to metal-metal interactions via M-O-M bridges. Kuznetsov *et al.*[5] have shown that the Hg_4^{6-} cluster, which is a building block of the Na_3Hg_2 amalgam, is aromatic similarly to the all-metal aromatic Al_4^{2-} unit.[2a] Tsipis *et al.*[6] explained the planar structures of cyclic hydro-coinage compounds on the basis of their aromatic character. Alexandrova *et al.*[7] suggested the presence of aromaticity in the $Cu_3C_4^-$ cluster. Datta *et al.*[8] used d-orbital aromaticity to explain the metal ring structure in tiara-like nickel thiolates. Aromaticity in square-planar coinage metal clusters was discussed by Wannere *et al.*[9] and Lin *et al.*[10] The claim of δ−aromaticity in the square-planar coinage metal clusters[9] was questioned by

Lin *et al.*,[10] who showed that the completely filled d orbitals do not play any significant role in the bonding in these clusters. Instead, aromaticity in these systems comes primarily from σ bonding interactions of the valence s electrons. Recently, Huang *et al.*[11] demonstrated in the joint experimental and theoretical study the presence of d-orbital aromaticity in 4d and 5d transition metal oxide clusters, $Mo_3O_9^{2-}$ and $W_3O_9^{2-}$. In these clusters d-orbitals form σ-aromatic canonical molecular orbital. It was recently shown by Zhai *et al.*[12] that the $Ta_3O_3^-$ cluster possesses an unprecedented multiple (π and δ) aromaticity, which is responsible for the metal-metal bonding and the perfect triangular Ta_3 framework. However, this cluster does not possess σ-aromaticity, because the bonding from the delocalized $3a_1$'-HOMO-3 is canceled by the antibonding contributions from the $4e$'-HOMO.[12] So far, there are no any reported systems in the literature, that would have all three (σ-, π-, and d-) types of aromaticity/antiaromaticity.

We conjectured that the Hf_3 cluster could possess triple (σ-, π-, and δ-) aromaticity, because Hf has the most diffuse valence orbitals out of all triatomic clusters of group IV thus providing good orbital overlap. Also, in the singlet D_{3h}, $^1A_1$' state this cluster may use all its six d-electrons to populate completely bonding delocalized σ-MO $(2a_1')$, π-MO $(1a_2'')$, and δ-MO $(3a_1')$ in the $1a_1'^2 2a_1'^2 1e'^4 1a_2''^2 3a_1'^2$ electronic configuration. These three MOs would render σ-, π-, and δ-aromaticity just like the completely bonding π-delocalized MO in $C_3H_3^+$ renders π-aromaticity in $C_3H_3^+$. However, this triply aromatic electronic state might not necessarily be the lowest state. It is known in chemistry, that usually several σ-MO should be occupied, before π-bonding orbitals

start to fill up. For example, in $C_3H_3^+$ (valence electronic configuration $1a_1'^2 1e'^4 2a_1'^2 2e'^4 1a_2''^2$), the completely bonding π-MO ($1a_2''^2$) is occupied after the entire set of σ-MOs ($2a_1'^2 2e'^4$). Thus, completely bonding d-MO in Hf_3 could be occupied after the sets of σ- and π-MOs, and the triply aromatic state might not be among low-lying states.

13-2. Theoretical Methods

To test our conjecture we initially performed an extensive search for the Hf_3 global minimum for singlet, triplet, and quintet states at the B3LYP level of theory using the LANL2DZ pseudo-potential and basis set (B3LYP/LANL2DZ). All calculations have been performed with the Gaussian 03 program.[13] We recalculated the global minimum structure and the seven lowest isomers at the B3LYP level of theory using the Stuttgart+2f1g pseudo-potential and basis set (B3LYP/ Stuttgart+2f1g) (see Supporting Information for additional results and details of theoretical calculations). At this level of theory we found that the lowest isomer of Hf_3 has the triangular D_{3h} $^3A_2'$ structure with the $1a_1'^2 1a_2''^2 1e'^4 2a_1'^2 1e''^2$ valence electronic configuration. The lowest singlet state with the triangular D_{3h} $^1A_1'$ structure with the $1a_1'^2 2a_1'^2 1e'^4 1a_2''^2 3a_1'^2$ valence electronic configuration was found to be 9.2 kcal/mol (B3LYP/Stuttgart+2f1g) higher in energy than the triplet D_{3h} $^3A_2'$ structure. The B3LYP/CEP-121G calculations of Hf_3 cluster have been reported by Jin *et al*.[14] They concluded that the singlet D_{3h} $^1A_1'$ state is the global minimum for Hf_3 in contradiction to our B3LYP results. We recalculated the D_{3h} $^3A_2'$ and D_{3h} $^1A_1'$ structures of Hf_3 at the B3LYP/CEP-121G level of theory and found the triplet

state to be more stable than the singlet state by 8.2 kcal/mol. Apparently Jin *et al.*[14] missed the lowest triplet state. However, the B3LYP method could overestimate stability of triplet states over singlet states. In order to test this, we performed a series of CASSCF calculations at the B3LYP/Stuttgart+2f1g geometries. Because the CASSCF calculations are based on the restricted open shell Hartee-Fock (ROHF) method, we first calculated both D_{3h} $^3A_2$' and D_{3h} $^1A_1$' structures at the ROHF/Stuttgart+2f1g level of theory. The D_{3h} $^3A_2$' triplet state was found to be 31.3 kcal/mol lower in energy than the D_{3h} $^1A_1$' singlet state. However, the energy difference dramatically decreased to 7.2 kcal/mol at the CASSCF(8,8)/Stuttgart+2f1g level of theory and even further to 0.5 kcal/mol at CASSCF(10,14)/Stuttgart+2f1g. Thus, the singlet state might become the ground state for the Hf_3 cluster, as the number of active electrons and active orbitals is further increased. However, such calculations are beyond our computational abilities. The high level calculations for Hf_3 have been performed by Dai *et al.*[15] According to their MRCISD/4s4p3d calculations the triplet C_{2v}, $^3A_2$ state is the most stable one with the lowest singlet C_{2v}, $^1A_1$ state being 2.5 kcal/mol higher in energy. However these two states were not the lowest triplet and singlet states in our B3LYP/Stuttgart+2f1g calculations (see Supporting Information). When Dai *et al.*[15] included spin-orbit coupling in their calculations they found significant stabilization in the triplet states due to the state mixing. They concluded that after including spin-orbit coupling the ground state appears to be like a closed shell $^1A_1$ state in agreement with the statements by Wang *et al.*[16] based on the observed spectra of Hf_3. It looks like at this point it is difficult to determine with

certainty if the Hf_3 cluster is a singlet or a triplet in its ground electronic state. However, if the singlet state is not a ground state it is certainly a low-lying excited state.

13-3. Results and Discussion

The singlet D_{3h} $^1A_1'$ structure is indeed a triply (σ-, π-, and δ-) aromatic system. The $1a_2''$-MO is a circularly delocalized p-MO (similar to the $1a_2''$-MO in $C_3H_3^+$, that renders π-aromaticity in $C_3H_3^+$), the $2a_1'$-MO is a circularly delocalized σ-MO, and the $3a_1'$-MO is a circularly delocalized δ-MO (Figure 13-1). All these bonding MOs are formed by d-AOs of Hf and thus we have an example of triple d-aromaticity. Pictures of the molecular orbitals are made using Molden 3.4 program.[17]

We also calculated nuclear independent chemical shifts $(NICS_{zz})$[18] in order to probe aromaticity in Hf_3. We found that $NICS_{zz}$ is large and negative at the center of the cluster and quickly diminishing above the plane: $NICS_{zz}$=-41.5 ppm (z=0.0 Å), $NICS_{zz}$=-23.0 ppm (z=0.5 Å), and $NICS_{zz}$=+4.0 ppm (z=1.0 Å), thus providing additional evidence of multiple aromaticity in Hf_3 (D_{3h}, $^1A_1'$). The triangular D_{3h} $^3A_2'$ structure with the $1a_1'^2 1a_2''^2 1e'^4 2a_1'^2 1e''^2$ electronic configuration is a doubly (σ- and π-) aromatic state with two σ-electrons and four π-electrons. Two σ-electrons render σ-aromaticity according to the 4n+2 rule for the singlet coupling of electrons and four π-electrons render π-aromaticity according to the 4n rule for the triplet coupling of electrons. Thus, the competition for being the global minimum in Hf_3 occurs between the singlet triply (σ-, π-, and δ-) aromatic D_{3h} $^1A_1'$ ($1a_1'^2 2a_1'^2 1e'^4 1a_2''^2 3a_1'^2$) state and the triplet doubly (σ- and π-) aromatic D_{3h} $^3A_2'$ ($1a_1'^2 1a_2''^2 1e'^4 2a_1'^2 1e''^2$) state.

In our highest (CASSCF(10,14)/Stuttgart+2f1g) multiconfigurational treatment the occupation numbers were found to be: $1a_1'^{2.00}2a_1'^{1.86}1e'^{3.82}1a_2''^{1.87}3a_1'^{1.74}2e'^{0.30}1e''^{0.13}3e'^{0.14}2e''^{0.13}1a_2'^{0.02}$. One can see that about 0.3 |e| have been promoted from $3a_1'$ δ-HOMO into $2e'$ σ-LUMO. That means that δ-aromaticity is reduced at the multiconfigurational level of theory because the $3a_1'$ δ-HOMO lost some electron density and that σ-aromaticity is reduced too at the same level of theory because bonding/antibonding $2e'$ σ-LUMO gained some electron density compared to the pure one electron treatment. Partial promotion from δ-HOMO into $2e'$ σ-LUMO occurs in order to reduce electron density and electron repulsion at the center of the cluster due to the presence of four electrons on completely bonding HOMO and HOMO-3. In spite of some multiconfigurational nature of the wave function, we believe that our qualitative assignment of the singlet D_{3h} $^1A_1'$ structure of Hf_3 as the triply aromatic is still valid, because rather small amount of electron density was promoted and the Hartree-Fock configuration (with the coefficient 0.842) is still dominant in the CASSCF(10,14)/Stuttgart+2f1g expansion.

13-4. Conclusion

In summary, in the current communication we presented theoretical evidence that the singlet D_{3h} $^1A_1'$ structure of Hf_3 is the first triply (σ-, π-, and δ-) aromatic system. We believe that transition metal systems with triple antiaromaticity and all types of conflicting aromaticity outlined in the introduction will be identified soon. Most importantly we hope that our work would stimulate theoretical analysis of chemical

bonding in numerous known chemical compounds with metal clusters at the center (such as carbonyls of transition metals) with the goal to probe if these systems are in fact aromatic, antiaromatic or they have conflicting aromaticity and how this affects their stability and reactivity.

References

(1)   Robinson, G. H. *Acc. Chem. Res.* **1999**, *32*, 773.

(2)   (a) Li, X.; Kuznetsov, A. E.; Zhang, H. F.; Boldyrev, A. I. Wang, L. S. *Science*, **2001**, *291*, 859. (b) Kuznetsov, A. E.; Birch, K. A.; Boldyrev, A. I.; Li, X.; Zhai, H.-J.; Wang, L. S. *Science*, **2003**, *300*, 622. (c) Boldyrev, A. I. Wang, L. S. *Chem. Rev.* **2005**, *106*, 3716 and references there in. (d) Tsipis, C. A. *Coord. Chem. Rev.* **2005**, *249*, 2740 and references there in.

(3)   King, R. B. *Inorg. Chem.* **1991**, *30*, 4437.

(4)   Li, J. *J. Cluster Sci.* **2002**, *13*, 137.

(5)   Kuznetsov, A. E.; Corbett, J. D.; Wang, L. S.; Boldyrev, A. I. *Angew. Chem. Int. Ed.* **2001**, *40*, 3369.

(6)   Tsipis, A. C.; Tsipis, C. A. *J. Am. Chem. Soc.* **2003**, *125*, 1136.

(7)   Alexandrova, A. N.; Boldyrev, A. I.; Zhai, H.-J.; Wang, L. S. *J. Phys. Chem. A* **2005**, *109*, 562.

(8)   Datta, A.; John, N. S.; Kulkarni, G. U.; Pati, S. K. J. Phys. Chem. A, **2005**, *109*, 11647.

(9)   Wannere, C. S.; Corminboeuf, C.; Wang, Z.-X.; Wodrich, M.D.; King, R. B.; Schleyer, P. v. R. *J. Am. Chem. Soc.* **2005**, *127*, 5701.

(10)   Lin, Y.-C.; Sundholm, D.; Juselius, J.; Cui, L.-F.; Zhai, H.-J.; Wang, L. S. *J. Phys. Chem. A* **2006**, *110*, 4244.

(11)   Huang, X.; Zhai, H.-J.; Kiran, B.; Wang, L. S. *Angew. Chem. Int. Ed.* **2005**, *44*, 7251.

(12)   Zhai, H.-J.; Averkiev, B. B.; Zubarev, D. Yu.; Wang, L. S.; Boldyrev, A. I. *Angew. Chem. Int. Ed.* **2007**, *46*, 4277.

(13)   Frisch, M. J.; Trucks, G. W.; Schlegel, H. B.; Scuseria, G. E.; Robb, M. A.; Cheeseman, J. R.; Montgomery, Jr., J. A.; Vreven, T.; Kudin, K. N.; Burant, J. C.; Millam, J. M.; Iyengar, S. S.; Tomasi, J.; Barone, V.; Mennucci, B.; Cossi, M.; Scalmani, G.; Rega, N.; Petersson, G. A.; Nakatsuji, H.; Hada, M.; Ehara, M.; Toyota, K.; Fukuda, R.; Hasegawa, J.; Ishida, M.; Nakajima, T.; Honda, Y.; Kitao, O.; Nakai, H.; Klene, M.; Li, X.; Knox, J. E.; Hratchian, H. P.; Cross, J. B.; Bakken, V.; Adamo, C.; Jaramillo, J.; Gomperts, R.; Stratmann, R. E.; Yazyev, O.; Austin, A. J.; Cammi, R.; Pomelli, C.; Ochterski, J. W.; Ayala, P. Y.; Morokuma, K.; Voth, G. A.; Salvador, P.; Dannenberg, J. J.; Zakrzewski, V. G.; Dapprich, S.; Daniels, A. D.; Strain, M. C.; Farkas, O.; Malick, D. K.; Rabuck, A. D.; Raghavachari, K.; Foresman, J. B.; Ortiz, J. V.; Cui, Q.; Baboul, A. G.; Clifford, S.; Cioslowski, J.; Stefanov, B. B.; Liu, G.; Liashenko, A.; Piskorz, P.; Komaromi, I.; Martin, R. L.; Fox, D. J.; Keith, T.; Al-Laham, M. A.; Peng, C. Y.; Nanayakkara, A.; Challacombe, M.; Gill, P. M. W.; Johnson, B.; Chen, W.; Wong, M.

W.; Gonzalez, C.; and Pople, J. A. Gaussian 03, Revision D.01; Gaussian, Inc.: Wallingford, CT, 2004

(14)   Jin, P. C.; Han, B.; Dai, Z. W.; Wu, Z. J. *J. Mol. Struct. THEOCHEM*, **2004**, *680*, 1.

(15)   Dai, D.; Roszak, S.; Balasubramanian, K. *Chem. Phys. Lett.* **1999**, *308*, 495.

(16)   Wang, H.; Hu, Z.; Haouari, H.; Craig, R.; Liu, L.; Lambardi, J. R.; Lindsay, D. M. *J. Chem. Phys.* **1997**, *106*, 8339.

(17)   MOLDEN3.4.   Schaftenaar, G. MOLDEN3.4, CAOS/CAMM Center, (The Netherlands, 1998).

(18) (a) Schleyer, P. v. R.; Maerker, C.; Dransfeld, A.; Jiao, H.; Hommes, N. J. v. E. *J. Am. Chem. Soc.* **1996**, *118*, 6317. (b) Fowler, P. W.; Steiner, E. *Mol. Phys.* **2000**, *98*, 945. (c) Steiner, E.; Fowler, P. W.; Jenneskens, L. W. *Angew. Chem. Int. Ed.* **2001**, *40*, 362.
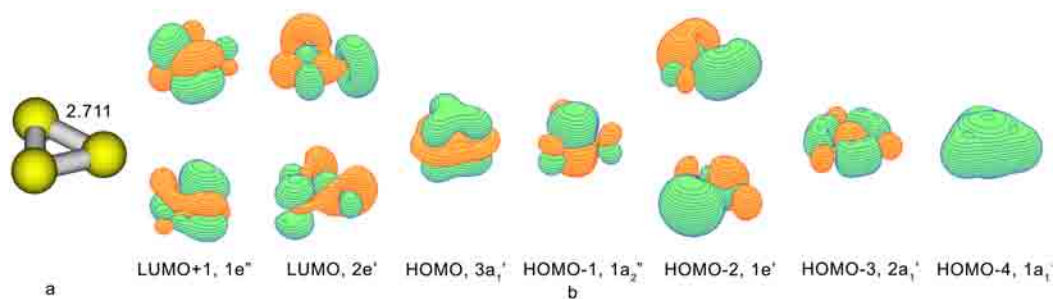
Figure 13-1. (a) Structure of Hf_3 D_{3h}, $^1A_1$' optimized at the B3LYP/ Stuttgart+2f1g level of theory; (b) valence molecular orbitals at the B3LYP/ Stuttgart+2f1g level of theory.

CHAPTER 14

AROMATICITY AND ANTIAROMATICITY IN TRANSITION-METAL SYSTEMS[1]

Abstract

Aromaticity is an important concept in chemistry primarily for organic compounds, but it has been extended to compounds containing transition-metal atoms. Recent findings of aromaticity and antiaromaticy in all-metal clusters have stimulated further researches in describing the chemical bonding, structures, and stability in transition-metal clusters and compounds on the basis of aromaticity and antiaromaticity, which are reviewed here. The presence of d-orbitals endows much more diverse chemistry, structure, and chemical bonding to transition-metal clusters and compounds. One interesting feature is the existence of a new type of aromaticity - δ-aromaticity, in addition to σ- and π-aromaticity that are only possible for main group compounds. Another striking characteristic in the chemical bonding of transition-metal systems is the multi-fold nature of aromaticity, antiaromaticity, or even conflicting aromaticity. Separate sets of counting rules have been proposed for cyclic transition-metal systems to account for the three types of σ-, π-, and δ-aromaticity/antiaromaticity. The diverse transition-metal clusters and compounds reviewed here indicate that multiple aromaticity and antiaromaticity may be much more common in chemistry than one would anticipate.

It is hoped that the current review will stimulate interest in further understanding the structure and bonding, on the basis of aromaticity and antiaromaticity, of other known or unknown transition-metal systems, such as the active sites of enzymes or other biomolecules, which contain transition-metal atoms and clusters.

14-1. Introduction

Aromaticity in compounds containing a transition-metal atom was first considered in a pioneering paper in 1979 by Thorn and Hoffmann[1] on six-membered ring metallocyclic compounds, that are derived from the prototypical aromatic benzene molecule with one C-H moiety replaced by an isolobal transition-metal fragment. Just three years later the first example of a stable, isolable metallobenzene — osmabenzene — was reported by Elliott *et al*.[2] A large family of metallobenzenes — the iridabenzenes — was synthesized by Bleeke and co-workers;[3-5] whereas a series of dimetallobenzenes with two metal atoms incorporated into the benzene ring was synthesized and characterized by Rothweel *et al*.[6,7] Recent advances in metallobenzenes have been reviewed by Bleeke,[8] He *at al*.,[9] Wright,[10] and Landorf and Haley.[11] A thorough chemical bonding analysis of metallobenzene has been recently performed by Fernandez and Frenking.[12] However, aromaticity in transition metal compounds is not restricted to metallobenzene molecules. Other molecules, in which the aromatic cycle composed of transition-metal atoms only and are not based on the prototypical benzene molecule, have also been reported recently, and they are the subjects of the current article.

Before discussing in detail the aromaticity in transition-metal systems, let us briefly review the concept of aromaticity, since it has been rather controversial, despite the fact that it is taught routinely in general chemistry. Many books[13-21] and numerous reviews[22-29] have been published, and several conferences[30-32] have been dedicated to deciphering the concept of aromaticity. We would like to adopt a view of aromaticity, with which we hope that most chemists can agree. Aromaticity was initially introduced into chemistry to describe the lack of reactivity of benzene and its derivatives, in spite of the apparent unsaturated nature of the carbon-carbon bonds in these molecules. Because all these molecules have an aroma, the property of chemical stability of the unsaturated bonds in the cyclic systems was called aromaticity. Nowadays most molecules, which are considered to be aromatic, do not have any aroma and in order to characterize them as aromatic a variety of criteria have been proposed in the literature based on molecular orbitals or other considerations. They are summarized in Table 1 (we adopt a list of the properties proposed by Krygowski *et al*.[33] with some small modifications and additions).

These criteria have been proposed for p-aromatic and p-antiaromatic organic systems, but we will see that many of them are also applicable to s-aromatic and s-antiaromatic systems, as well as to δ-aromatic and δ-antiaromatic systems. We stress that one should not expect that aromaticity/antiaromaticity in transition metal systems will manifest itself exactly the same way as in organic chemistry. Many specific deviations are expected. Nevertheless, we believe that the overall delocalized chemical bonding and most of the molecular properties in certain transition metal species could be understood using the aromaticity/antiaromaticity concepts.

The discovery and experimental generation of the first all-metal aromatic and antiaromatic clusters using photoelectron spectroscopy and ab initio calculations[34,35] have stimulated much interest in extending these ideas to other metal systems, including transition metals.[36,37] It has been understood that aromaticity/antiaromaticity in metal systems has very specific flavors if compared with organic compounds. The striking feature of chemical bonding in metal systems is the possibility of the multi-fold nature of aromaticity, antiaromaticity, and conflicting aromaticity.[36-39] When only s-atomic orbitals (AOs) are involved in chemical bonding, one may expect only σ-aromaticity or σ-antiaromaticity. If p-AOs are involved, σ-tangential (σ_t-), σ-radial (σ_r-), and π-aromaticity/antiaromaticity could occur.[36] In this case, there can be multiple (σ- and π-) aromaticity, multiple (σ- and π-) antiaromaticity, and conflicting aromaticity (simultaneous σ-aromaticity and π-antiaromaticity or σ−antiaromaticity and π-aromaticity). If d-AOs are involved in chemical bonding, σ-tangential (σ_t-), σ-radial (σ_r-), π-tangential (π_t-), π-radial (π_r-), and δ-aromaticity/antiaromaticity could occur. In this case, there can be multiple (σ-, π-, and δ-) aromaticity, multiple (σ-, p-, and δ-) antiaromaticity, and conflicting aromaticity (simultaneous aromaticity and antiaromaticity among the three types of σ, π, and δ bonds).

One would expect that doubly and triply aromatic molecules would be significantly more stable with higher resonance energies, shortened bond lengths, enhanced ring currents, more negative NICS values, and a higher average bifurcation value of the electron localization function (ELF) than in conventional singly aromatic

molecules. Indeed, Boldyrev and Kuznetsov,[40] and Zhan *et al*.[41] showed that the doubly (σ- and π-) aromatic species Al_4^{2-} has a very high resonance energy ~48 kcal/mol[40] and ~73 kcal/mol[41], respectively. For the prototypical singly aromatic benzene molecule the resonance energy is only 20 kcal/mol.[13] The ring-current susceptibilities for the doubly aromatic Al_4^{2-} dianion was also found to be 10 nA T^{-1}, which is higher than 8 nA T^{-1} in benzene.[42] Fowler *et al*. demonstrated that the contribution to the ring current from s-delocalized electrons is significantly higher than from p-electrons.[43,44] According to Chen *et al*.,[45] Al_4^{2-} has significant negative NICS (-30.9 ppm) compared to that in benzene (-9.7 ppm).[46] Santos *et al*.[47] showed that Al_4^{2-} has the highest average bifurcation value of ELF_s and ELF_p among the set of various singly aromatic systems. Establishing the overall aromaticity or antiaromaticity in molecules with conflicting aromaticity is especially challenging task, because of the simultaneous presence of aromaticity and antiaromaticity in different electronic subsystems.[35,45,48] Studies of magnetic properties of systems with conflicting aromaticity such as $Li_3Al_4^-$ and Li_4Al_4 can lead to contradictory conclusions on the overall aromaticity or antiaromaticity of the system.[35,49-51] Conflicting aromaticity also results in floppy geometries of the $Li_3Al_4^-$ and Li_4Al_4 clusters.[50] One of the most interesting features of molecules with conflicting aromaticity is the possibility of large linear and nonlinear optical properties such as linear polarizability, first hyperpolarizability, and second hyperpolarizability.[52]

In the following sections we will consider in details the cases of multiple aromaticity, multiple antiaromaticity and conflicting aromaticity in recent examples of transition metal clusters and compounds, including Cu_3^+,[53] *cyclo*-Cu_nH_n (n = 3-6),[54]

cyclo-M_nH_n (M = Ag, Au; n = 3-6),[55] *cyclo*-$Au_3L_nH_{3-n}$ (L = CH_3, NH_2, OH, and Cl; n = 1-3),[56] *cyclo*-$Cu_nAg_{3-n}H_n$ (n = 1-3), *cyclo*-$Cu_nAg_{4-n}H_n$ (n = 1-4), and *cyclo*-$Cu_nAg_{5-n}H_n$ (n = 1-5),[57] Au_5Zn^+,[58] M_4Li_2 (M = Cu, Ag, Au),[59] M_4L_2 and M_4L^- (M = Cu, Ag, Au; L = Li, Na),[60] Hg_4^{6-},[61] M_3^{2-}, NaM_3^-, and Na_2M_3 (M = Zn, Cd, Hg),[62] M_3^- (M = Sc, Y, La),[63] $M_3O_9^-$ and $M_3O_9^{2-}$ (M = W, Mo),[64] $Ta_3O_3^-$,[65] and Hf_3.[66]

14-2. s-AO based σ-aromaticity and σ-antiaromaticity in transition metal systems

A. s-AO based σ-aromaticity and σ-antiaromaticity in M₃ clusters

The prototypical system with s-AO based σ-aromaticity is the Li_3^+ cluster, which was initially discussed by Alexandrova and Boldyrev,[67] and then by Havenith *et al.*[68] and Yong *et al.*[53] The Cu_3^+ has a similar D_{3h}, $^1A_1'$ ($1a_1'^2 1e'^4 1a_2''^2$ $2a_1'^2 1e''^4 2e'^4 2a_2''^2 3e'^4 2e''^4 3a_2''^2 3a_1'^2$) global minimum structure.[53] As in the case of Li_3^+, the bonding in Cu_3^+ is rooted in 4s-AOs of Cu, because all the bonding and antibonding MOs ($1a_1'^2 1e'^4 1a_2''^2$ $2a_1'^2 1e''^4 2e'^4 2a_2''^2 3e'^4 2e''^4 3a_2''^2$) composed out of 3d-AOs of Cu are occupied, hence the contribution to bonding from 3d-AOs of Cu is negligible. The $3a_1'$-valence HOMO is a sum of the 4s-AOs of three Cu atoms (Fig. 14-1a). It is completely bonding and in this sense similar to the completely bonding p-MO in the prototypical π-aromatic $C_3H_3^+$ cation (Fig. 14-1b). The only difference is that the p-MO is a sum of $2p_z$-AOs of carbons. The delocalized p-MO in $C_3H_3^+$ renders its p-aromaticity according to the famous 4n+2 Huckel rule. On the basis of the analogy between the p-delocalized MO

in $C_3H_3^+$ and the s-delocalized MO in Cu_3^+ it is reasonable to call the latter s-aromatic

(the $4n+2$ rule holds for s-aromatic cyclic systems with valence s-AOs participating in

bonding).[19]

Yong *et al.*[53] considered aromaticity in the Cu_3^+ cation on the basis of nucleus-

independent chemical shift (NICS) indexes.[46]   Their calculations show NICS(0.0) = -

28.22 ppm, NICS(0.5) = -22.59 ppm, and NICS(1.0) = -12.31 ppm at B3LYP/6-311+G*,

clearly confirming the presence of s-aromaticity in this cluster.[53]   Yong *et al.*[53] also

evaluated the resonance energy in the Cu_3^+ D_{3h}, $^1A_1$' using the following equation:

$$Cu_3Cl \ (C_{2v}, {}^1A_1) \rightarrow Cu_2 + CuCl \qquad\qquad (14\text{-}1)$$

where Cu_2 and CuCl are reference classical molecules. According to their calculations,

the energy of reaction (14-1), which is also the resonance energy for Cu_3^+, is 36.8

kcal/mol (B3LYP/6-311+G(3df)). The calculated resonance energy is certainly very high

compared to the Cu_2 dissociation energy (41.7 kcal/mol at the same level of theory).

Thus, the use of the σ-aromaticity for the description of the Cu_3^+ cation is justified.

Apparently, the concept of σ–aromaticity based on the s-AOs should be applicable to

Ag_3^+ and Au_3^+, though in the last case the s-d hybridization may play a more significant

role.

For σ–antiaromatic species (with ns-AOs participating in bonding) the counting

rule is $4n$ (singlet coupling). The Cu_3^- anion is a good example of s-antiaromatic system

with 4s-electrons. The electronic configuration for the singlet state of Cu_3^- at the D_{3h}

symmetry is $1a_1'^2 1e'^2$ (only bonding MOs are included), and the triangular structure with the singlet electronic state must undergo the Jahn-Teller distortion towards linear $D_{\infty h}$ structure with a $1s_g^2 1s_u^2$ valence electronic configuration.

Two σ-delocalized MOs can be approximately localized into two 2c-2e bonds and the linear structure of Cu_3^- can be formally considered as a classical structure. This situation is similar to the antiaromatic cyclobutadiene structure, which can be considered as having two double and two single carbon-carbon bonds, and thus can be described using single a Lewis structure. The antiaromaticity should manifest itself in the reduction of the stability of the molecule. Two reactions below show that the atomization energy of Cu_3^- (reaction 14-2, CCSD(T)/6-311+G(2df)//CCSD(T)6-311+G*+ZPE/CCSD(T)/6-311+G*) is indeed substantially lower than the atomization energy of Cu_3^+ (reaction 3, CCSD(T)/6-311+G(2df)//CCSD(T)6-311+G*+ZPE/CCSD(T)/6-311+G*).

$$Cu_3^- \; (D_{\infty h}, \, {}^1S_g^+) \rightarrow 2Cu \; ({}^2S) + Cu^- \; ({}^1S) \qquad DE = +82.4 \text{ kcal/mol} \qquad (14\text{-}2)$$

$$Cu_3^+ \; (D_{3h}, \, {}^1A_1') \rightarrow 2Cu \; ({}^2S) + Cu^+ \; ({}^1S) \qquad DE = +106.3 \text{ kcal/mol} \qquad (14\text{-}3)$$

B. s-AO based σ-aromaticity in M_4^{2-} clusters

Initially aromaticity in the M_4^{2-} (M = Cu, Ag, Au) dianions as parts of M_4Li_2 (M = Cu, Ag, Au) neutral species was studied by Wannere et al.[59] They found that the Li_2M_4 species have distorted octahedral D_{4h}, ${}^1A_{1g}$ structures (Fig. 14-2) with the M_4^{2-} dianion forming a perfect square with two Li^+ cations located above and below the square on the C_4 axis. The significant charge transfer from Li to M_4 was confirmed by the NPA charges. For example, in Cu_4Li_2, the NPA charge on Li is +0.8 |e|. These authors also

reported the NICS values in the centers of Cu_4Li_2 (-14.5 ppm), Ag_4Li_2 (-14.1 ppm), and Au_4Li_2 (-18.6 ppm) (all at PW91PW91/LANL2DZ) clusters which show the presence of aromaticity in the M_4^{2-} dianions. Wannere *et al.*[59] stated that the participation of p-orbitals in the bonding (and cyclic electron delocalization) in these clusters is negligible. Instead, these clusters benefit strongly from the delocalization of d and to some extent s orbitals. They also pointed out that d-orbital aromaticity of Cu_4Li_2 is indicated by its high (243.2 kcal/mol) atomization energy.

Lin *et al.*[60] reported a joint photoelectron spectroscopy and theoretical study of Cu_4Na^-, Au_4Na^- as well as theoretical results on Cu_4Li^-, Ag_4Li^-, Ag_4Na^-, Au_4Li^-, Cu_4Li_2, Ag_4Li_2, Au_4Li_2, and Cu_4^{2-}. They found that the Cu_4Li^-, Cu_4Na^-, Ag_4Li^-, and Ag_4Na^- anions have a pyramidal structure consistent with the bipyramidal structure reported by Wannere *et al.*, while the Au_4Li^- and Au_4Na^- anions were found to be planar. The pyramidal structure of Cu_4Na^- with the Na^+ cation located above the planar square Cu_4^{2-} dianion was confirmed by good agreement between theoretical and experimental VDEs for this system.

Using the Gauge-Including Magnetically Induced Current (GIMIC) method Lin *et al.*[60] concluded that strong ring currents are sustained mainly by the HOMO derived from the Cu 4s-AOs. Thus, the GIMIC calculations show that the Cu_4^{2-} ring is s-aromatic due to 4s-AOs and that the d orbitals do not play any significant role for the electron delocalization effects. This study did not support the notion by Wannere *et al.*[59] that the square-planar Cu_4^{2-} is the first example of d-orbital aromatic molecules.

If bonding in the Cu_4^{2-} and Ag_4^{2-} rings is primarily due to σ-orbitals, than these systems are examples of systems with six valence σ-electrons and should be regarded as σ-aromatic according to the 4n+2 rule, similar to the Li_4^{2-}, Mg_4^{2+} and Li_2Mg_2 main group clusters with six bonding σ-electrons considered by Alexandrova and Boldyrev.[67]

C. s-AO based σ-aromaticity in the Au_5Zn^+ cluster and Au_6

The Au_5Zn^+ cation was found to be the most abundant cluster in the mass-spectrum of Au_nZn^+ (n = 2-44) by Tanaka et al.[58] The authors performed MP2/Zn/6-311+G*/Au/5s5p4d1f calculations and identified three lowest isomers I, II, and III for Au_5Zn^+ (Fig. 14-3). For the two lowest isomers, Tanaka et al.[58] presented MO pictures (Fig. 14-4) showing that six valence s-electrons are delocalized over the whole cluster. The Au_5Zn^+ cluster is isoelectronic to the Au_6 cluster and its most stable structure is the same as the D_{3h} global minimum structure of Au_6, which possesses a large HOMO-LUMO gap and possesses a very stable electronic configuration.[69,70]

The MO pattern of Au_5Zn^+ depicted in Fig. 14-4 resembles those of prototypical aromatic organic molecules C_6H_6 and $C_5H_5^-$, except for their nodal properties in the molecular plane. The six delocalized electrons with the appropriate nodal pattern in Au_5Zn^+ satisfies the 4n+2 rule for σ-aromaticity. Tanaka et al.[58] also performed NICS calculations for all three structures and concluded the negative NICS indexes are larger than in the prototypical aromatic organic molecules C_6H_6 and $C_5H_5^-$, confirming the presence of aromaticity in Au_5Zn^+. Overall the Au_5Zn^+ cluster can be regarded as a σ-

aromatic bimetallic cluster with six delocalized s-electrons and that the enhanced stability of Au_5Zn^+ may be ascribed to its aromaticity.

D. s-AO based σ-aromaticity in the *cyclo*-M_nH_n
(M = Cu, Ag, Au; *n* = 3-6), *cyclo*-$Au_3L_nH_{3-n}$ (L = CH$_3$, NH$_2$, OH, and Cl; *n* = 1-3),
cyclo-$Cu_nAg_{k-n}H_n$ (*n* = 1-*k*, *k* = 3-5) clusters

Tsipis and Tsipis[54] performed B3LYP/6-311+G* calculations on Cu_nH_n (*n* = 3-6) cyclic species (Fig. 14-5) as models for the well documented cyclic organocopper (I) compounds, such as the square planar four-membered ring Cu_4R_4 (R = CH_2SiMe_3) with short Cu-Cu distances of 2.42 Å.[71] Tsipis and Tsipis[54] calculated also the 3D-structures for Cu_nH_n (*n* = 4-6) and concluded that they are significantly less stable than the planar ones. In follow-up articles,[55-57] Tsipis and co-workers studied *cyclo*-M_nH_n (M = Ag, Au; *n* = 3-6), *cyclo*-$Au_3L_nH_{3-n}$ (L = CH$_3$, NH$_2$, OH, and Cl; *n* = 1-3), *cyclo*-$Cu_nAg_{3-n}H_n$ (*n* = 1-3), *cyclo*-$Cu_nAg_{4-n}H_n$ (*n* = 1-4), and *cyclo*-$Cu_nAg_{5-n}H_n$ (*n* = 1-5). The Cu_nH_n (*n* = 3-6) cyclic species are discussed here and the other species are similar.

All Cu_nH_n (*n* = 3-6) species were found to be cyclic with short Cu-Cu distances (between 2.404 Å in Cu_3H_3 to 2.556 Å in Cu_6H_6). The authors[54] stated that the equivalence of the Cu-Cu and Cu-H bonds in these species is indicative of the aromatic character of the cyclic hydrocoppers (I). In addition, they reported binding energies, NICS values and the electrophilicity index w (Table 14-2), which also support the aromatic nature of these species.

The authors[21] stated that all the metallocycles exhibit a composite bonding mode involving σ, π, and δ components on the basis of their analysis of occupied valence MOs. However, we found a rather different picture. We performed a NBO analysis of the representative Cu_4H_4 (D_{4h}, $^1A_{1g}$) cluster at B3LYP/6-311++G** level of theory. According to our NBO analysis the Cu atoms have $4s^{0.56}3d^{9.91}4p^{0.02}$ valence atomic occupations and a effective atomic charge of +0.50 |e|, while the H atoms have $1s^{1.49}$ atomic occupation and an effective atomic charge of -0.50 |e|. One can see that the 3d-AOs of Cu are almost completely occupied and thus do not significantly contribute to bonding. The bonding from completely delocalized δ-HOMO-11, π-HOMO-17, π-HOMO-18, σ-HOMO-19 and σ-HOMO-20 (Fig. 14-6) will be offset by the effect of antibonding orbitals (Fig. 14-6) composed of d-AOs of Cu atoms. Thus, the net bonding effect from MOs composed of 3d-AOs cannot be significant. Rather, the bonding in the Cu_nH_n cyclic clusters comes from an ionic contribution between $H^{-0.501}$ and $Cu^{+0.501}$ and from delocalized MOs composed out of 4s-AOs on Cu. In fact, NBO analysis in Cu_4H_4 reveals one resonance structure (the same way as NBO produces some of the Kekule resonance structure for benzene), in which there are four Cu-H 2c-2e bonds composed of 1s-AOs of H and 4s-AOs of Cu with the occupation number 1.744 |e| alternated over the Cu_4H_4 distorted planar octahedron. This confirms the aromatic nature of the Cu_nH_n clusters, but the aromaticity is due to delocalization of σ-bonds (composed of 1s-AOs of H and 4s-AOs of Cu) and not due to the delocalized σ-, π-, and δ-MOs composed of 3d-AOs of Cu. Thus, aromaticity in the Cu_nH_n clusters is neither π nor δ but rather σ in nature. Lin *et al.*,[60] however, reported that they did not find any strong magnetically

induced ring current in Cu_4H_4. This might be a sign of the weak aromaticity in Cu_nH_n clusters. Due to relativistic effects, s-d hybridization started to play a bigger role in Ag_nH_n and Au_nH_n clusters, but additional research accounting for the relativistic effects should be performed before making any conclusions on the bonding nature in the these clusters.

14-3. p-AO based aromaticity and antiaromaticity

in transition metal systems

Double aromaticity (simultaneous presence of σ- and π-aromaticity) was introduced in chemistry by Chandrasekhar *et al.* to explain the properties of the 3,5-dehydrophenyl cation.[72] Simultaneous presence of aromaticity and antiaromaticity was first used by Martin-Santamaria and Rzepa[73] to explain chemical bonding in small carbon rings. Präsang *et al.*[74,75] have shown that small carborane molecules containing 3- and 4-membered rings also exhibit both s and p aromaticity. The Hg_4^{6-} cluster was the first transition metal system where double (σ- and π-) aromaticity due to p-AOs was discovered.[73]

A. p-AO based multiple aromaticity in the Hg_4^{6-} cluster

Mercury has a closed shell electron configuration ($6s^2$) and therefore a neutral Hg_4 cluster is expected to be a van der Waals complex. However, it was shown in the solid that one particular sodium-mercury amalgam Na_3Hg_2 contains Hg_4^{6-} square units as its building blocks.[61] The high stability of the Hg_4^{6-} building block was explained once we

recognized that it is isoelectronic to the first all-metal aromatic cluster, Al_4^{2-}.[34] Basically, the bonding in Hg_4^{6-} is due to Hg 6p-AO based MOs and the completely occupied Hg d-AOs do not contribute to bonding.[61] Fig. 14-7 displays the seven valence MOs of the square-planar Hg_4^{6-}, which are very similar to those in Al_4^{2-}.[34]

The HOMO ($1b_{2g}$), HOMO-1 ($1a_{2u}$), and HOMO-2 ($2a_{1g}$) are completely bonding orbitals formed from the Hg 6p-AOs and represent $p_{\sigma-t}$–MOs (tangential MO), p_{π}-MOs, and $p_{\sigma-r}$–MOs (radial MO), respectively. The remaining four MOs are bonding, non-bonding, and antibonding orbitals formed primarily from the filled valence 6s orbitals of Hg and can be viewed as atomic $6s^2$ lone pairs. Thus, the upper three MOs are mainly responsible for the chemical bonding in Hg_4^{6-}. If we split the s- and p-orbitals into two separate sets, we can represent the MOs formed by the Hg 6p-AOs with the MO diagram shown in Fig. 14-8.

The lowest-lying π-MO and the two lowest-lying σ–MOs are completely bonding, whereas the highest-lying ones are completely antibonding. The two MOs in the π-set and the four MOs in the σ-set that are located in between the completely bonding and antibonding MOs are doubly degenerate with bonding/antibonding characters. The $2e_u$- and $3e_u$-MOs are composed of $p_{\sigma-r}$- and $p_{\sigma-t}$-AOs. This is the reason why $p_{\sigma-r}$- and $p_{\sigma-t}$-MOs are presented as one set in Fig. 14-8. On the basis of this mixing in the $p_{\sigma-r}$- and $p_{\sigma-t}$-AOs the counting rule for σ-electrons for cyclic systems with even number of vertices should be $4n+4/4n+6$ for aromaticity/antiaromaticity (in the simplest case of the occupation of just one $p_{\sigma-r}$- or one $p_{\sigma-t}$-MO the system is also aromatic), but

they are $4n+2/4n$ for the cyclic systems with the odd number of vertices. On the basis of two distinct types of MOs, we can introduce one types of aromaticity: π-aromaticity based on the p_π MOs, and two types of σ-aromaticity based on the $p_{\sigma-r}$ and $p_{\sigma-t}$ MOs. The occupation of all three bonding MOs in Hg_4^{6-} makes its shape a perfect square and renders its doubly (σ- and π-) aromatic nature.

The finding of the double aromaticity in Hg_4^{6-} establishes a solid bridge between our gas-phase studies of multiply aromatic clusters and bulk materials containing such species. It is surprising that such an ancient material as amalgams can be rationalized on the basis of multiple aromaticity initially discovered in the gas phase studies of the Al_4^{2-} all-metal aromatic cluster,[34, 41,76,77] produced in the form of MAl_4^- in the gas phase, where $M = Li, Na, Cu$.

B. p-AO based multiple aromaticity in the M_3^{2-}, NaM_3^-, Na_2M_3 (M = Zn, Cd, Hg) clusters

Yong and Chi[62] have recently shown using B3LYP, B3PW91, and CCSD(T) calculations that a series of M_3^{2-}, NaM_3^-, Na_2M_3 (M = Zn, Cd, Hg) clusters all have the M_3^{2-}, D_{3h}, $^1A_1'$ core, which is π-aromatic. Like in Hg_4^{6-}, neither 5d- nor 6s-AOs participate in the bonding in M_3^{2-}. Its bonding is due to the a_2''-HOMO, which is composed of the outer π-AOs of M. This is a completely bonding π-MO similar to the $1a_2''$-HOMO in the $C_3H_3^+$ cation (Fig. 14-1b). Thus, in all the M_3^{2-}, NaM_3^-, Na_2M_3 (M = Zn, Cd, Hg) systems bonding in the M_3^{2-} core is due to π-aromaticity only, without the formation of a σ-framework. Similar bonding pattern was previously reported for Mg_3^{2-},

$NaMg_3^-$ and Na_2Mg_3 systems by Kuznetsov and Boldyrev.[78]   Yong and Chi[62] also

calculated a sizable resonance energy of 24.8 kcal/mol (Zn_3^{2-}), 12.9 kcal/mol (Cd_3^{2-}), and

12.1 kcal/mol (Hg_3^{2-}) (either at CCSD(T)/6-311+G* or CCSD(T)/LANL2DZ), as well as

large negative values of NICS: -24.86 ppm (Zn_3^{2-}), -19.59 ppm (Cd_3^{2-}), and -15.40 ppm

(Hg_3^{2-}), further confirming their π-aromaticity.

14-4. d-AO based aromaticity and antiaromaticity

in transition metal systems

Due to the more complicated nodal structure of d-AOs that can form δ-bond in

addition to σ and π bonds, transition-metal systems can provide a more diverse array of

aromaticity-antiaromaticity combinations. We may expect σ-tangential (σ_t), σ-radial

(σ_r), π-tangential (π_t), π-radial (π_r), and δ-MOs. For σ- and π-MOs, the counting rules

are $4n+4$ (aromaticity) and $4n+6$ (antiaromaticity) for cyclic structures with even number

of atoms and $4n+2$ (aromaticity) and $4n$ (antiaromaticity) for cyclic structures with odd

number of atoms.   For δ-MOs the counting rule is $4n+2/4n$ for

aromaticity/antiaromaticity. In general, there can be multiple (σ-, π-, and δ-) aromaticity,

multiple (σ-, π-, and δ-) antiaromaticity, and conflicting aromaticity (simultaneous

aromaticity and antiaromaticity among the three types of σ, π, and δ MOs). So far only

few transition metal systems with d-AO based aromaticity have been reported.[63-66]

A. d-AO based σ-aromaticity in the $Mo_3O_9^{2-}$ and $W_3O_9^{2-}$ clusters

The first cases of d-orbital aromaticity in 4d and 5d transition metal oxide clusters, $Mo_3O_9^-$ and $W_3O_9^-$, were reported by Huang *et al.* by combining photoelectron spectroscopy and theoretical calculations.[64] They found that the M_3O_9, $M_3O_9^-$, and $M_3O_9^{2-}$ (M = Mo, W) clusters all have D_{3h} structures and each metal atom is bonded to two bridged O atoms and two terminal O atoms (Fig. 14-9).

The attachment of the first and second electrons to the M_3O_9 species reduces the M-M distance significantly (0.25 Å for $Mo_3O_9^-$ and 0.29 Å for $W_3O_9^-$) and (0.20 Å for $Mo_3O_9^{2-}$ and 0.19 Å for $W_3O_9^{2-}$). The large geometry changes induced by addition of one or two electrons to the M_3O_9 species agree with the nature of the HOMO in the singly $M_3O_9^-$ and doubly $M_3O_9^{2-}$ charged anions (Fig. 14-10).

The completely bonding nature of the σ-HOMO in $M_3O_9^-$ and $M_3O_9^{2-}$ species renders their σ-aromaticity. Calculations of NICS at the center of $Mo_3O_9^{2-}$ (-21.5 ppm) and $W_3O_9^{2-}$ (-20.5 ppm) also support the presence of aromaticity. Huang *et al.*[64] also estimated a sizable (7.6 kcal/mol) resonance energy for $W_3O_9^-$. These results provide solid evidence that the anionic $Mo_3O_9^-$, $W_3O_9^-$ $Mo_3O_9^{2-}$ and $W_3O_9^{2-}$ species with the D_{3h} ($^2A_1$' or $^1A_1$') structure are the first experimentally-confirmed δ-orbital aromatic (σ) species.

B. d-AO based σ-and π- double aromaticity

in X_3^- (X = Sc, Y, La) clusters

The first systems with double (σ- and π-) aromaticity have been recently reported by Chi and Liu.[63] They demonstrated using B3LYP, B3PW91, MP2 and CCSD(T) levels of theory with 6-311+G* basis sets for Sc and LANL2DZ basis sets with relativistic effective core potentials for Y and La, that the D_{3h} ($^1A_1'$) structures are the global minimum structures for X_3^- (X = Sc, Y, La). All three species have the same valence electronic configuration $1a_1'^2 1e'^4 1a_2''^2 2a_1'^2$, though the order of the MOs varies (Fig. 14-11). Here the $1a_1'$- and $1e'$-MOs are formed by the ns-AOs and do not contribute to bonding significantly, because all the bonding and antibonding MOs composed of the ns-AOs are occupied and the bonding effect from the $1a_1'$-MO is compensated by the antibonding effect from the $1e'$-MOs. Valence $1a_2''$- and $2a_1'$-MOs are responsible for bonding in the X_3^- anions. The $1a_2''$-MO is a completely bonding p-MO and it renders π-aromaticity. The $2a_1'$-MO is a completely bonding σ-MO and it renders σ-aromaticity in X_3^-. Thus all three anions are d-orbital doubly (σ-and π-) aromatic systems. Chi and Liu[63] also reported large negative NICS values for all three anions, thus supporting the presence of aromaticity in Sc_3^-, Y_3^-, and La_3^-.

C. d-AO based π-and δ- double aromaticity

in the $Ta_3O_3^-$ cluster

It was shown by Zhai *et al.*[65] using photoelectron spectroscopy and theoretical calculations that the $Ta_3O_3^-$ cluster possesses a global minimum with a perfect D_{3h} ($^1A_1'$) planar triangular structure (Fig. 14-12a).

The structure and bonding in $Ta_3O_3^-$ can be understood by analyzing their molecular orbitals (Fig. 14-12b). Out of 34 valence electrons in $Ta_3O_3^-$, 24 belong to either pure oxygen lone pairs or those polarized towards Ta (responsible for the covalent contributions to Ta-O bonding). The other ten valence electrons are responsible for the direct metal-metal bonding, as shown in Fig. 14-12b. Among the five upper MOs, three MOs are of σ-type: the partially bonding/antibonding doubly degenerate 4e' HOMO and the completely bonding $3a_1'$ HOMO-3. The antibonding nature of the completely occupied doubly degenerate HOMO significantly reduces the bonding contribution of completely bonding HOMO-3 to the σ-bonding in the Ta_3 framework. If the HOMO (4e') and the HOMO-3 ($3a_1'$) were composed of the same s-d hybrid functions, bonding due to these MOs would be completely canceled. However, the hybridization in the 4e' and $3a_1'$ orbitals is somewhat different. Therefore, there should remain some σ-aromatic bonding in $Ta_3O_3^-$. In the $Ta_3O_3^-$ anion, the HOMO-2 ($2a_2''$) is a completely bonding π orbital composed primarily out of the 5d orbitals of Ta, giving rise to π-aromatic character according to the (4n + 2) Hückel rule for π-aromaticity for ring molecules with odd numbers of atoms in the ring. Here, we apply the (4n + 2) counting rule (odd

number of atoms in the metal cycle) separately for each type of aromaticity encountered in a particular planar system, i. e. separately for σ-, π-, and δ-type molecular orbitals.

The HOMO-1 ($4a_1$'), which is a completely bonding orbital mainly coming from the overlap of the d_z^2 orbital on each Ta atom is in fact a δ-aromatic orbital. This orbital has the "appearance" of a π orbital with major overlaps above and below the molecular plane, but it is not a π-type MO because it is symmetric with respect to the molecular plane. This MO possesses two nodal surfaces perpendicular to the molecular C_3 axis, and thus it is a d orbital (see detailed discussion in ref. 65). Therefore, the $Ta_3O_3^-$ cluster possesses an unprecedented multiple (δ and π) aromaticity, which is responsible for the metal-metal bonding and the perfect triangular Ta_3 framework. The energy ordering of σ (HOMO-3) $< \pi$ (HOMO-2) $< \delta$ (HOMO-1)[65] molecular orbitals indicates that the strength of the metal-metal bonding increases from δ to π to σ, in agreement with the intuitive expectation that σ-type overlap is greater than π-type overlap, and δ-type overlap is expected to be the weakest.

D. d-AO based σ-, π-and δ- triple aromaticity

in the Hf_3 cluster

Averkiev and Boldyrev[66] theoretically predicted that the Hf_3 cluster in the D_{3h}, $^1A_1$' ($1a_1$'$^2 2a_1$'$^2 1e$'$^4 1a_2$''$^2 3a_1$'^{2}) state possesses triple (σ-, π-, and δ-) aromaticity. The valence $1a_1$'- and $1e$'-MOs are primarily composed out of 6s-AOs of Hf and as in $Ta_3O_3^-$ do not contribute to bonding significantly (Fig. 14-13). The six d-electrons populate

completely bonding delocalized σ-MO (2a$_1$'), π-MO (1a$_2$"), and δ-MO (3a$_1$') (Fig. 14-13b). The former three MOs render σ-, π-, and δ-aromaticity just like the completely bonding π-delocalized MO in C$_3$H$_3^+$ renders π-aromaticity in C$_3$H$_3^+$. Thus the Hf$_3$ cluster in the D$_{3h}$, ^{1}A$_1$' state represents the first example of a chemical system with the triple aromaticity.

14-5. Summary and overview

The goal of this review is to demonstrate that the concepts of aromaticity and antiaromaticity, initially introduced in organic chemistry, can and should be applied to the description of chemical bonding in transition metal systems. At the present, systems containing transition metal clusters are being actively studied both experimentally and theoretically in chemistry and biochemistry. Apparently there is a need for convenient tools that connect electronic structure with molecular properties of such systems. We have shown that aromaticity and antiaromaticity indeed are useful tools for explaining and understanding chemical bonding in transition metal systems.

Aromaticity and antiaromaticity have been established in the gas phase Cu$_3^+$ and Cu$_3^-$ clusters. The aromaticity in Cu$_3^+$ helped to explain its high symmetry (D$_{3h}$) structure, high atomization and resonance energies, and high negative value of NICS. The aniaromaticity of Cu$_3^-$ helped to explain its linear structure and low atomization energy.

Similarly, aromaticity in *cyclo*-Cu$_n$H$_n$ (n = 3-6), *cyclo*-M$_n$H$_n$ (M = Ag, Au; n=3-6), *cyclo*-Au$_3$L$_n$H$_{3-n}$ (L = CH$_3$, NH$_2$, OH, and Cl; n = 1-3), *cyclo*-Cu$_n$Ag$_{3-n}$H$_n$ (n = 1-3), *cyclo*-Cu$_n$Ag$_{4-n}$H$_n$ (n = 1-4), and *cyclo*-Cu$_n$Ag$_{5-n}$H$_n$ (n = 1-5) helped explain the planar

cyclic structure of these species, high binding energies, and negative NICS. Also, aromaticity in these model systems was used to rationilize the planar cyclic organocopper (I) compounds in condense phase. The recognition of aromaticity in the gas phase Au_5Zn^+ cluster helped to understand high abundance observed in the mass spectrum. The presence of aromaticity in gas phase clusters M_4Li_2 (M = Cu, Ag, Au), M_4L_2 and M_4L^- (M = Cu, Ag, Au; L=Li, Na) allowed us to understand the planar square structure of Cu_4^{2-} and Ag_4^{2-} structural units. The presence of double (σ- and π-) aromaticity in the Hg_4^{6-} building block of Na_3Hg_2 amalgam explains the planar square structure as well as stability of it in the stabilizing external field of Na^+ cations. π-Aromaticity in M_3^{2-}, NaM_3^-, Na_2M_3 (M = Zn, Cd, Hg) is responsible for their stability. Double (σ- and π-) aromaticity in gas phase M_3^- (M = Sc, Y, La) clusters is responsible for their high symmetry (D_{3h}) structure, high atomization and resonance energies, and high negative value of NICS.

True d-orbital aromaticity was first observed in $M_3O_9^-$ and $M_3O_9^{2-}$ (M = W, Mo) metal oxide clusters. The presence of σ-aromaticity in these anions is responsible for their high symmetry (D_{3h}) structure, appreciable resonance energies, and high negative value of NICS. The high symmetry (D_{3h}) of $Ta_3O_3^-$ and high first VDE could be explain on the basis of the presence of double (π- and δ-) aromaticity. This oxide cluster is the first example of δ-aromaticity in a transition metal system. Finally, the Hf_3 cluster in the D_{3h}, $^1A_1'$ ($1a_1'^2 2a_1'^2 1e'^4 1a_2''^2 3a_1'^2$) state is the first example of triple (σ-, π-, and δ-) aromaticity.

It is clear that aromaticity and antiaromaticity could be very useful concepts in explaining structure, stability and other molecular properties of isolated and embedded clusters of transition metals and transition metal oxide clusters. The chemical bonding in transition metal clusters can come from s-AOs, p-AOs, and d-AOs, and can be expressed as a variety of multiple aromaticities and antiaromaticities as well as of conflicting aromaticities. We believe that transition metal systems with triple antiaromaticity and all types of conflicting aromaticity outlined in the introduction should all exist and should represent a research frontier. Furthermore, atomic f-AOs in lanthanide and actinide clusters offer additional possibility to form ϕ-bonds and thus could lead to systems with even richer variety of ϕ-aromaticity/antiaromaticity. Such systems have not yet been reported and may suggest new research opportunities both computationally and experimentally.

The counting rules for s-AO based σ-aromaticity are the same as the Huckel $4n+2/4n$ rules for aromaticity/anriaromaticity for all cyclic structures. The counting rules for p-AO based σ-aromaticity are $4n+4$ (aromaticity) and $4n+6$ (antiaromaticity) for cyclic structures with even number of atoms and $4n+2$ (aromaticity) and $4n$ (antiaromaticity) for cyclic structures with odd number of atoms, because there are two types of σ-orbitals: $p_{\sigma-r}$- and $p_{\sigma-t}$-MOs which should be considered together. In the simplest case of the occupation of just one $p_{\sigma-r}$- or one $p_{\sigma-t}$-MO the system is also aromatic. For p-AO based π-aromaticity the counting rule are $4n+2/4n$ for aromaticity/antiaromaticity for all cyclic structures. For d-AO based σ- and π-

aromaticity the counting rules are 4n+4 (aromaticity) and 4n+6 (antiaromaticity) for cyclic structures with even number of atoms and 4n+2 (aromaticity) and 4n (antiaromaticity) for cyclic structures with odd number of atoms, because there two types of σ-orbitals: $d_{\sigma\text{-r}}$- and $d_{\sigma\text{-t}}$-MOs and two types of p-orbitals: $d_{\pi\text{-r}}$- and $d_{\pi\text{-t}}$-MOs. For d-AO based δ-aromaticity the counting rule is 4n+2/4n for aromaticity/antiaromaticity, respectively.

It is hoped that the introduction of the aromatic and antiaromatic concepts would stimulate theoretical analysis of chemical bonding in other known or unknown chemical compounds containing transition metal atoms and clusters in both inorganic compounds and metallo-biomolecules. Such analysis may establish simple and robust rules connecting electronic and molecular structures with stability and reactivity. It may be possible that aromaticity and antiaromaticity may become as useful concepts in deciphering the chemical bonding in transition metal systems as in organic chemistry.

References

1. D. L. Thorn, R. Hoffmann, *Nouv. J. Chim.* 1979, **3**, 39.

2. G. P. Elliot, W. R. Roper, J. M. Waters, *J. Chem. Soc. Chem. Commun.* 1982, 811.

3. J. R. Bleeke, Y.-F. Xie, W.-J. Peng, M. Chiang, *J. Am. Chem. Soc.* 1989, **111**, 4118.

4. J. R. Bleeke, R. Behm, Y.-F. Xie, T. W. Clayton, Jr., K. D. Robinson, *J. Am. Chem. Soc.* 1994, **116**, 4093.

5. J. R. Bleeke, R. Behm, Y.-F. Xie, M. Y. Chiang, K. D. Robinson, A. M. Beatty, *Organometallics* 1997, **16**, 606.

6. R. D. Profilet, P. E. Fanwick, I. P. Rothwell, *Angew. Chem., Int. Ed.* 1992, **31**, 1261.

7. P. N. Riley, R. D. Profilet, M. M. Salberg, P. E. Fanwick, I. P. Rothwell, *Polyhedron* 1998, **17**, 773.

8. J. R. Bleeke, *Chem. Rev.* 2001, **101**, 1205.

9. G. He, H. Xia, G. Jia, *Chin. Sci. Bull.* 2004, **49**, 1543.

10. L. J. Wright, *Dalton Trans.* 2006, 1821.

11. W. C. Landorf, M. M. Haley, *Angew. Chem. Int. Ed.* 2006, **45**, 3914.

12. I. Fernandez, G. Frenking, *Chem. Eur. J.* 2007, **13**, 5873.

13. Minkin, V. I.; Glukhovtsev, M. N.; Simkin, B. Ya. *Aromaticity and Antiaromaticity. Electronic and Structural Aspects,* Wiley & Sons, New York, 1994.

14. R. G. Harvey, *Polycyclic Aromatic Hydrocarbons*, Wiley-VCH, New York, 1997.

15. I. Gutman, S. J. Cyvin, *Introduction to the Theory of Benzenoid Hydrocarbons*, Springer-Verlag, Berlin, 1989.

16. D. Lloyd, *The Chemistry of Conjugate Cyclic Compounds*, Wiley & Sons, Chichester, 1989.

17. S. J. Cyvin, I. Gutman, I. *Kekule Structures in Benzenoid Hydrocarbons*, Springer-Verlag, Berlin, 1988.

18. J. R. Dias, *Handbook of Polycyclic Hydrocarbons. Part A. Benzenoid Hydrocarbons*, Elsevier, Amsterdam, 1987.

19. P. J. Garrat, *Aromaticity*, Wiley & Sons, New York, 1986.

20. D. Lewis, D. Peters, *Facts and Theories of Aromaticity*, Macmillan, London, 1975.

21. E. Clar, *The Aromatic Sexte*, Wiley & Sons, London, 1972.

22. Special edition on delocalization pi and sigma, ed. P. v. R. Schleyer, *Chem. Rev.*, 2005, **105**, No. 10.

23. Special edition on aromaticity, ed. P. v. R. Schleyer, *Chem. Rev.* 2001, **101**, No. 5.

24. Special edition on heterocycles, ed. A. Katrizky, *Chem. Rev.* 2004, **104**, No. 5.

25. M. Randic, *Chem. Rev.* 2003, **103**, 3449.

26. S. Shaik, A. Shurki, D. Danovich, P. C. Hiberty, *J. Mol. Struct. (Theochem)* 1997, **155**, 398.

27. P. v. R. Schleyer, H. Jiao, *Pure & Appl. Chem.* 1996, **38**, 209.

28. J.-I. Aihara, *Pure Appl. Chem.* 1982, **54**, 1115.

29. A. T. Balaban, *Pure Appl. Chem.* 1980, **52**, 1409.

30. 4th Int. Symp. Chem. of Novel Aromatic Compounds, Jerusalem, 1981; Agranat, I., Ed.; *Pure Appl. Chem.* 1982, **54**, 927.

31. Int. Symp. Aromaticity, Dubrovnik, 1979; Graovac, A., Trinajstic, N. Eds.; *Pure Appl. Chem.* 1980, **52**, 1397.

32. *Aromaticity, Pseudoaromaticity, Antiaromaticity*, ed. E. D. Bergman and B. Pullman, Israel Academy of Science and Humanities, Jerusalem, Academic Press, New York, 1971.

33. T. M. Krygowski, M. K. Cyranski, Z. Czarnocki, G. Häfelinger, G. A. R. Katritzky, *Tetrahedron* 2000, **56**, 1783.

34. X. Li, A. E. Kuznetsov, H. F. Zhang, A. I. Boldyrev, L. S. Wang, *Science*, 2001, **291**, 859.

35. A. E. Kuznetsov, K. A. Birch, A. I. Boldyrev, X. Li, H.-J. Zhai, L. S. Wang, *Science*, 2003, **300**, 622.

36. A. I. Boldyrev, L. S. Wang, *Chem. Rev.* 2005, **106,** 3716.

37. C. A. Tsipis, Coord. *Chem. Rev.* 2005, **249**, 2740.

38. A. N. Alexandrova, A. I. Boldyrev, H.-J. Zhai, L. S. Wang, *Coord. Chem. Rev.* 2006, **250**, 2811.

39. D. Yu. Zubarev, A. I. Boldyrev, *J. Comput. Chem.* 2007, **28**, 251.

40. A. I. Boldyrev, A. E. Kuznetsov, *Inorg. Chem.* 2002, **41**, 532.

41. C.-G. Zhan, F. Zheng, D. A. Dixon, *J. Am. Chem. Soc.* 2002, **124**, 14795.

42. J. Juselius, M. Straka, D. Sundholm, *J. Phys. Chem. A,* 2001, **105**, 9939.

43. P. W. Fowler, R. W. A. Havenith, E. Steiner, *Chem. Phys. Lett.* 2001, **342**, 85.

44. P. W. Fowler, R. W. A. Havenith, E. Steiner, *Chem. Phys. Lett.* 2002, **359**, 530.

45. Z. Chen, C. Corminboeuf, T. Heine, J. Bohmann, P. v. R. Schleyer, *J. Am. Chem. Soc.* 2003, **125**, 13930.

46. P. v. R. Schleyer, C. Maerker, A. Dransfeld, H. Jiao, N. J. v. E. Hommes, *J. Am. Chem. Soc.* 1996, **118**, 6317.

47. J. C. Santos, J. Andres, A. Aizman, P. Fuentealba, *J. Chem. Theory Comput.* 2005, **1**, 83.

48. S. K. Ritter, *Chem. & Eng. News*, 2003, **81**, 23.

49. Y.-C. Lin, J. Juselius, D. Sundholm, J. Gauss, *J. Chem. Phys.* 2005, **122**, 214308.

50. R. Islas, T. Heine, G. Merino, *J. Chem. Theory Comput.* 2007, **3**, 775.

51. R. W. A. Havenith, P. W. Fowler, E. Steiner, S. Shetty, D. Kanhere, S. Pal, *Phys. Chem. Chem. Phys.* 2004, **6**, 285.

52. A. Datta, S. S. Mallajosyula, S. K. Pati, *Acc. Chem. Res.* 2007, **40**, 213.

53. L. Yong, S. D. Wu, X. X. Chi, *Int. J. Quant. Chem.* 2007, **107**, 722.

54. A. C. Tsipis, C. A. Tsipis, *J. Am. Chem. Soc.* 2003, **125**, 1136.

55. C. A. Tsipis, E. E. Karagiannis, P. F. Kladou, A. C. Tsipis, *J. Am. Chem. Soc.* 2004, **126**, 12916.

56. A. C. Tsipis, C. A. Tsipis, *J. Am. Chem. Soc.* 2005, **127**, 10623.

57. A. C. Tsipis, A. V. Stalikas, *New. J. Chem.* 2007, **31**, 852.

58. H. Tanaka, S. Neukermans, E. Janssens, R. E. Silverans, P. Lievens, *J. Am. Chem. Soc.* 2003, **125**, 2862.

59. C. S. Wannere, C. Corminboeuf, Z.-X. Wang, M. D. Wodrich, R. B. King, P. v. R. Schleyer, *J. Am. Chem. Soc.* 2005, **127**, 5701.

60 Y.-C. Lin, D. Sundholm, J. Juselius, L.-F. Cui, X. Li, H. J. Zhai, L. S. Wang, *J. Phys. Chem. A*, 2006, **110**, 4244.

61. A. E. Kuznetsov, J. D. Corbett, L.-S. Wang, A. I. Boldyrev, *Angew. Chem. Int. Ed.* 2001, **40**, 3369.

62. L. Yong, C. Chi, J. Mol. Struct. *THEOCHEM*, 2007, 818, 93.

63. X. X. Chi, Y. Liu, *Int. J. Quant. Chem.* 2007, **107**, 1886.

64. X. Huang, H. J. Zhai, B. Kiran, L. S. Wang, *Angew. Chem. Int. Ed.* 2005, **44**, 7251.

65. H. J. Zhai, B. B. Averkiev, D. Yu. Zubarev, L. S. Wang, A. I. Boldyrev, *Angew. Chem. Int. Ed.* 2007, **46**, 4277.

66. B. B. Averkiev, A. I. Boldyrev, *J. Phys. Chem. A*, 2007, **111**, 12864.

67. A. N. Alexandrova, A. I. Boldyrev, J. Phys. Chem. A, 2003, **107**, 554.

68. R. W. A. Havenith, F. De Proft, P. W. Fowler, P. Geerlings, *Chem. Phys. Lett.* 2004, **407**, 391.

69. H. Häkkinen, B. Yoon, U. Landman, X. Li, H. J. Zhai, and L. S. Wang, *J. Phys. Chem. A* 2003, **107**, 6168.

70. H. J. Zhai, B. Kiran, B. Dai, J. Li, and L. S. Wang, *J. Am. Chem. Soc.* 2005, **127**, 12098.

71. J. A. J. Jarvis, B. T. Kilbourn, R. Pearce, M. F. Lappert, *J. Chem. Soc., Chem. Commun.* 1973, 475.

72. J. Chandrasekhar, E. D. Jemmis, P. v. R. Schleyer, *Tetrahedron Lett.* 1979, **39**, 3707.

73. S. Martin-Santamaria , H. S. Rzepa, *Chem. Commun.* 2000, **16**, 1503.

74. C. Präsang, A. Mlodzianowska, Y. Sahin, M. Hofmann, G. Geiseler, W. Massa, A. Berndt, *Angew. Chem. Int. Ed.* 2002, **41**, 3380.

75. C. Präsang, A. Mlodzianowska, G. Geiseler, W. Massa, M. Hofmann, A. Berndt, *Pure Appl. Chem.* 2003, **75**, 1175.

76. A. E. Kuznetsov, A. I. Boldyrev, X. Li, L. S. Wang, *J. Am. Chem. Soc.* 2001**, 123**, 8825.

77. A. I. Boldyrev, A. E. Kuznetsov, *Inorg. Chem.* 2002, **41**, 532.

78. A. E. Kuznetsov, A. I. Boldyrev, *Chem. Phys. Lett.* 2004, **388**, 452.

Table 14-1. Criteria for π-Aromaticity and π-Antiaromaticity.[33]

Property	Aromatic	Olefinic/Classical	Antiaromatic
(i) Electronic nature	$(4n + 2)$ π-electron cyclic conjugation	No cyclic conjugation	$4n$ π-electron cyclic conjugation
(ii) Energy			
Cyclic conjugation	Stabilization	Standard	Destabilization
Delocalization	Enhanced	Standard	Decreased
HOMO-LUMO gap	Large	Standard	Small
(iii) Geometry			
Bond lengths	Equalization	Alternation	Alternation
(iv) Magnetic properties			
Anisotropy of diamagnetic susceptibility	Enhanced		Small
Susceptibility exaltation	High		Low
^{1}H NMR shifts	Diatropic (low-field shift)		Paratropic (high-field shift)
NICS (nucleus independent chemical shift)	Large negative	Close to zero	Large positive
(v) Reactivity			
Chemical example	e.g., benzene	e.g., cyclohexadiene	e.g., cyclooctatetraene
Retention of structure	Electrophilic substitution	Electrophilic addition	Addition
(vi) Spectroscopy			
UV spectra	High energy	Standard	Low energy
IR/Raman spectra	High symmetry		Low symmetry
Photoelectron spectra	High electron detachment energies	Standard	Low electron detachment energies

Table 14-2. Binding Energies ΔE_1 and ΔE_2, GIAO-SCF NICS and Electrophicity of

Cu_nH_n (n = 3-6).

Cluster	$\Delta E_1,^a$ kcal/mol	$\Delta E_2,^b$ kcal/mol	NICS, ppm	ω, eV
Cu_3H_3, D_{3h}	81.5	260.9	-8.4	1.595
Cu_4H_4, D_{4h}	137.0	376.1	-4.2	1.743
Cu_5H_5, D_{5h}	180.1	479.0	-1.4	2.040
Cu_6H_6, D_{6h}	217.5	576.2	-0.2	2.230

^{a} $\Delta E_1 = E(CuH)_n - nE(CuH)$
^{2} $\Delta E_1 = E(CuH)_n - n[E(Cu) + E(H)]$.
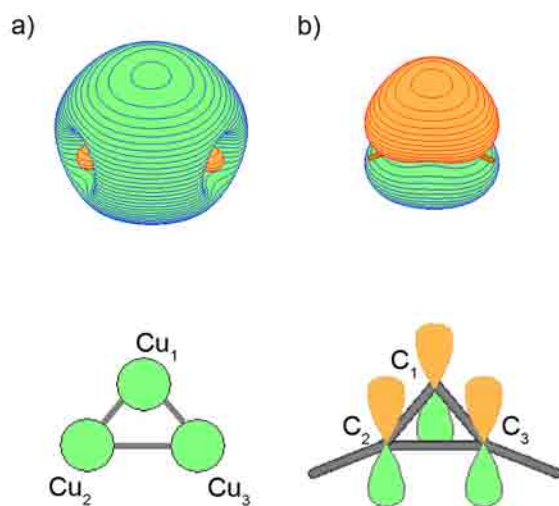
Figure 14-1. (a) The $3a_1$'-HOMO of Cu_3^+ and its schematic representation as a linear combination of 4s-AOs of Cu atoms, (b) $1a_2$"-HOMO of $C_3H_3^+$ and its schematic representation as a linear combination of $2p_z$-AOs of C atoms.
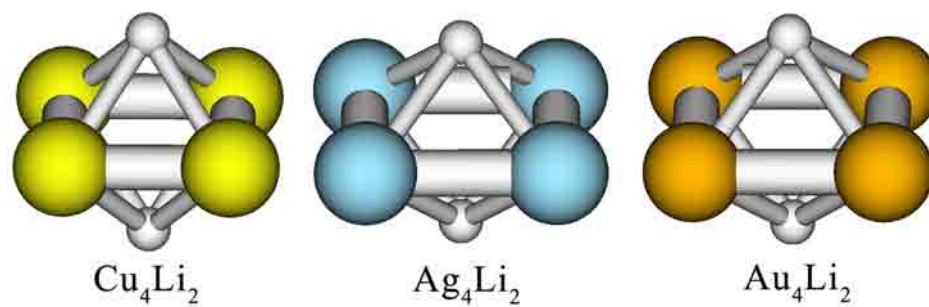
Figure 14-2. Optimized structures of Cu_4Li_2, Ag_4Li_2, and Au_4Li_2.[59]
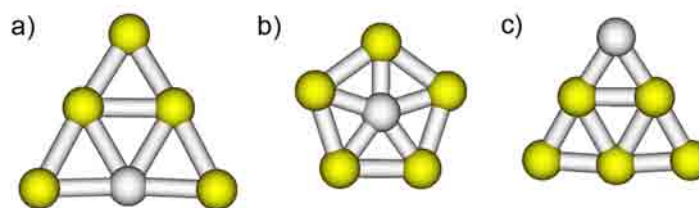
Figure 14-3. Three reported isomers of Au_5Zn^+.[58]
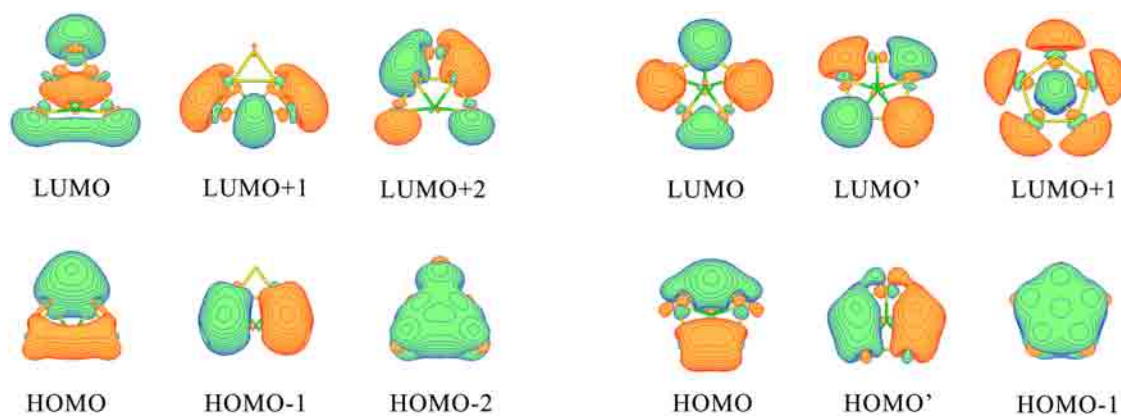
Figure 14-4. Pictures of valence MOs of Au_5Zn^+ isomers shown in Figure 14-3 a) and

b).
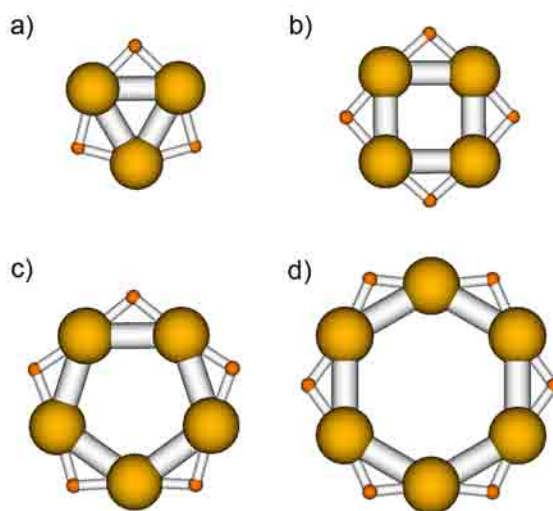
Figure 14-5. Optimized planar cyclic structures of Cu_nH_n clusters.[54]
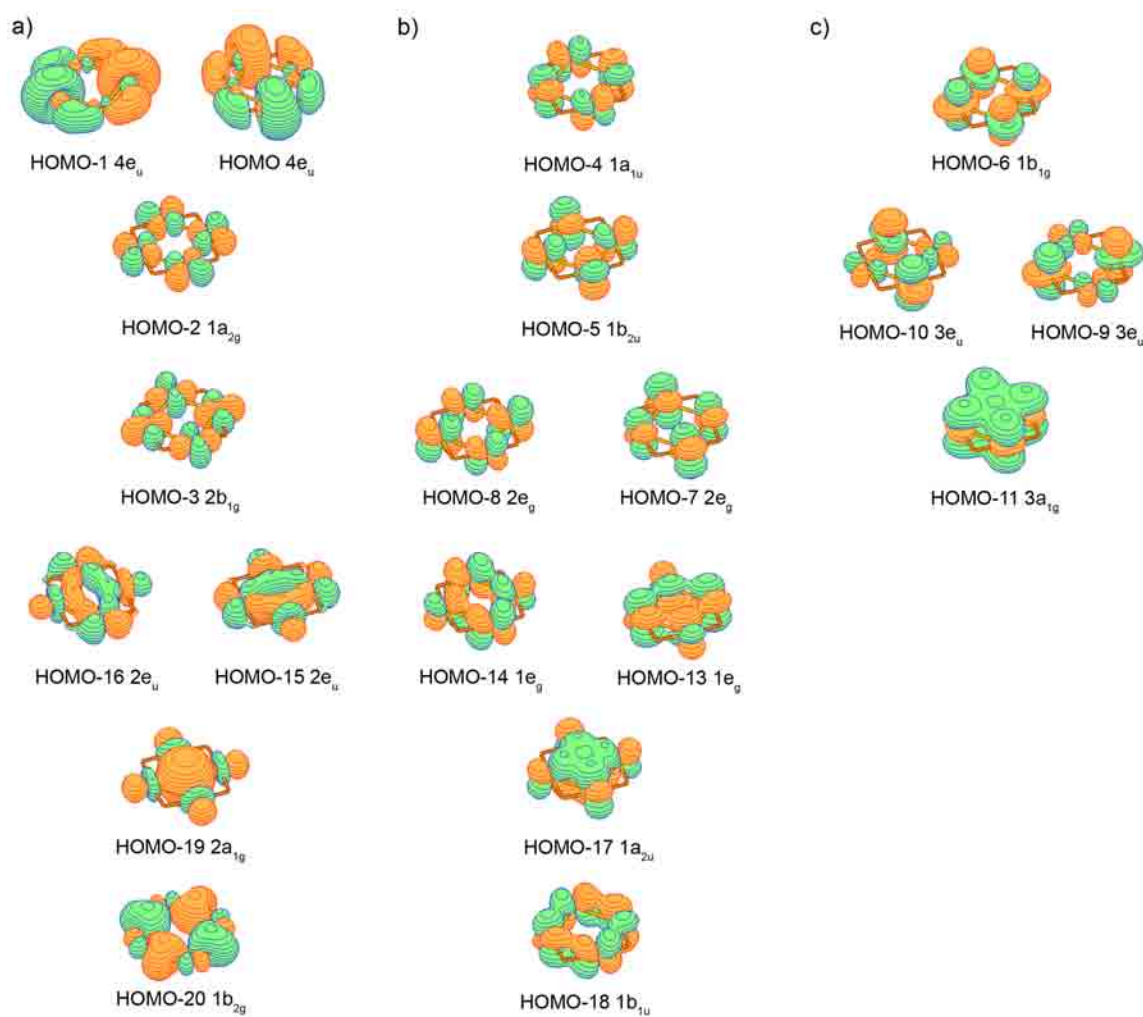
Figure 14-6. (a) σ-MOs, (b) π-MOs, and (c) δ-MOs composed out of d-AOs of Cu in Cu_4H_4 (D_{4h}, $^1A_{1g}$).

HOMO 1b$_{2g}$ HOMO-1 1a$_{2u}$ HOMO-2 2a$_{1g}$

HOMO-3 1b$_{1g}$ HOMO-4 1e$_u$ HOMO-4 1e$_u$ HOMO-5 1a$_{1g}$
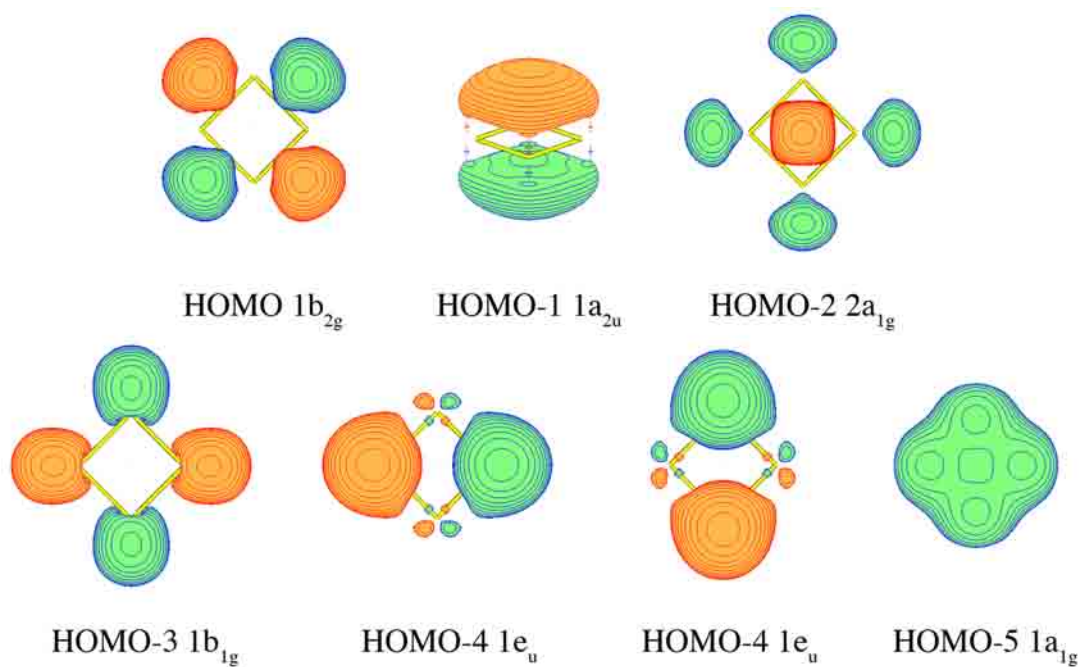
Figure 14-7. Valence molecular orbitals of Hg$_4^{6-}$.
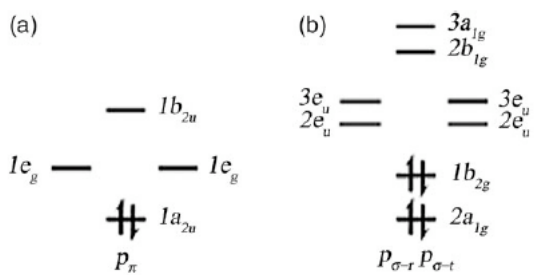
Figure 14-8. Molecular orbital diagram for a) π-MOs and b) σ-MOs for Hg$_4^{6-}$.
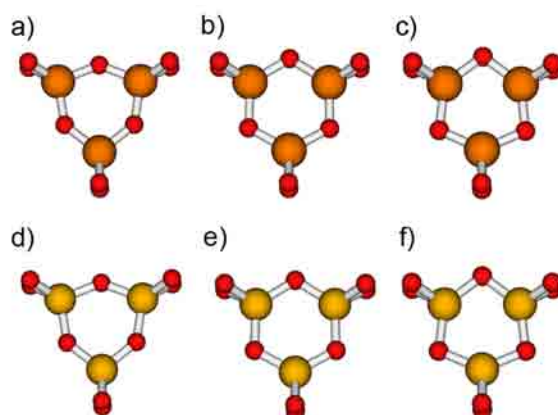
Figure 14-9. Optimized structures for M_3O_9 (a, d) $M_3O_9^-$ (b, e) and $M_3O_9^{2-}$ (c, f) (M = Mo, W) clusters.[64]
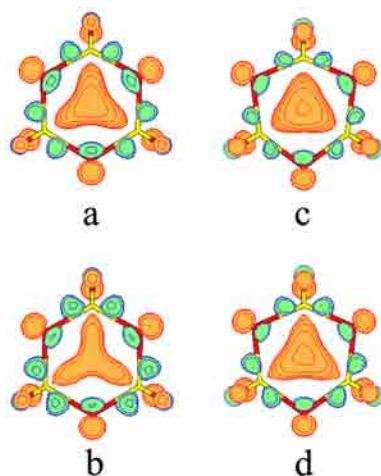
Figure 14-10. HOMOs in the $M_3O_9^-$ and $M_3O_9^{2-}$ species (M = Mo and W).[64]
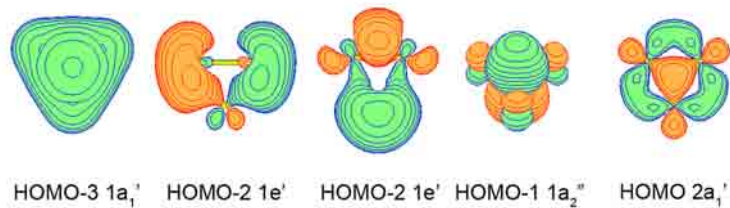
Figure 14-11. Valence MOs of X_3^- (X = Sc, Y, La) anions.
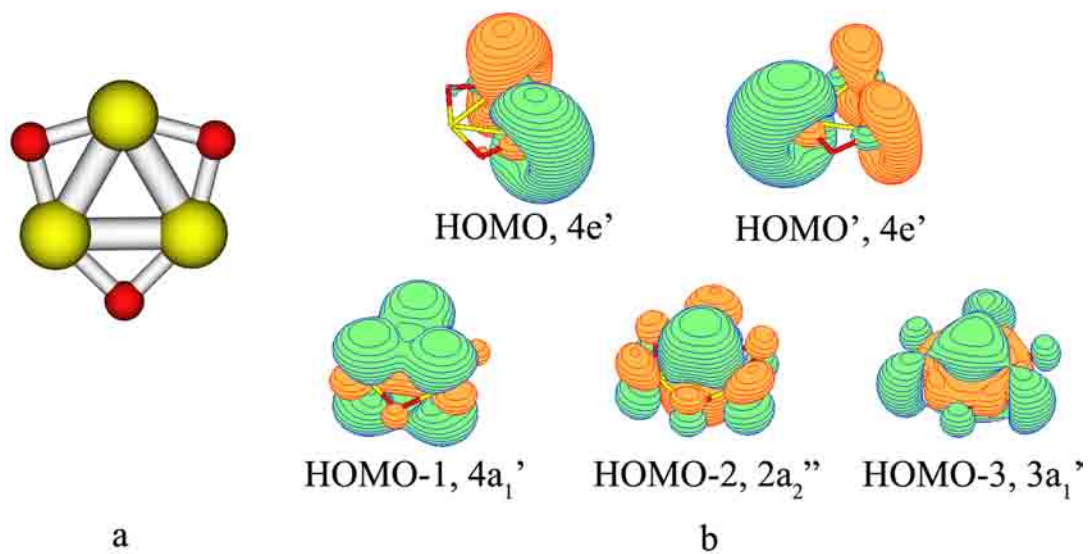
Figure 14-12. Optimized structure (a) and valence MOs (b) of $Ta_3O_3^-$.[65]
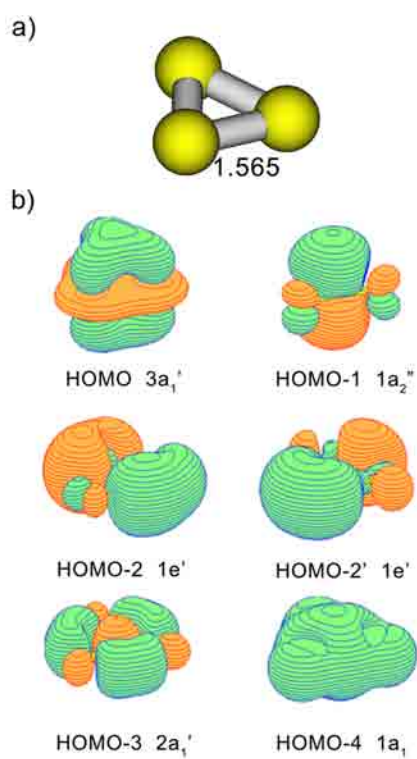
Figure 14-13. Optimized structure (a) and valence MOs (b) of the Hf_3 cluster in the D_{3h}, $^1A_1'$ state.

CHAPTER 15

RECENT ADVANCES IN ALL-TRANSITION METAL AROMATICITY AND

ANTIAROMATICITY[1]

Abstract

Though multiple bonding in transition metal compounds had been discussed in the literature for more than four decades, the discovery of aromaticity in all transition metal systems (cyclic systems composed out of transition metal atoms) was made only few years ago. In the compounds composed out of main group elements one may expect sigma-(σ-) and pi-(π-) aromaticity only. In all transition metal systems one may expect two new types of aromaticity: delta-(δ-) and fi-(ϕ-) in addition to σ- and π-aromaticity .

15-1. Introduction

Chemical bonding in transition metal compounds is more diverse and complicated compared to main group compounds due to participation of d- and f- atomic orbitals. In particular, in 1964, Cotton and co-workers published a milestone work on the $K_2[Re_2Cl_8]\cdot 2H_2O$ compound,[1] in which they showed the presence of a new type of a chemical bond – δ-bond between two Re atoms. This finding was the first example of the bond order of four. This paper and follow-up works led to the establishment of a new branch of inorganic chemistry involving multiple metal-metal bonding[2] with bond orders higher than three, the maximum allowed for main group molecules. Recently, Power and

---

[1] Coauthored by Alina P. Sergeeva, Boris B. Averkiev, and Alexander I. Boldyrev.

co-workers reported the synthesis of Ar'CrCrAr' [where Ar' is the bulky aryl group C_6H_3-2,6(C_6H_3-2,6-Pr^i_2)$_2$] with a quintuple bond ($s^2p^4d^4$) between two Cr atoms.[3] δ-bonds between two transition metal atoms suggests that there may exist multi-center transition metal species with completely delocalized cyclic δ-bond, thus raising the possibility of δ-aromaticity analogous to π- or σ-aromaticity in main group systems. Indeed, the first δ-delocalized bond and δ-aromaticity was recently discovered in the $Ta_3O_3^-$ cluster.[4] Averkiev and Boldyrev[5] theoretically predicted the first example of triple (σ-, π-, and δ-) aromaticity - Hf_3 cluster in the lowest singlet state. Tsipis, Kefalidis, and Tsipis[6] showed that the delocalized f electron density in the rings of planar isocyclic and heterocyclic uranium clusters could be associated with cyclic electron delocalization, which is a characteristic feature of aromaticity.

Thus, transition metal compounds have the striking feature of chemical bonding - the possibility of the multifold nature of aromaticity, antiaromaticity, and conflicting aromaticity.[7] When only s-atomic orbitals (AOs) are involved in chemical bonding, one may expect only σ-aromaticity or σ-antiaromaticity. If p-AOs are involved, σ-tangential (σ_t-), σ-radial (σ_r-), and π-aromaticity/antiaromaticity could occur. In this case, there can be multiple (σ- and π-) aromaticity, multiple (σ- and π-) antiaromaticity, and conflicting aromaticity (simultaneous σ-aromaticity and π-antiaromaticity or σ-antiaromaticity and π-aromaticity). If d-AOs are involved in chemical bonding, σ-tangential (σ_t-), σ-radial (σ_r-), π-tangential (π_t-), π-radial (π_r-), and δ-aromaticity/antiaromaticity could occur. In this case, there can be multiple (σ-, π-, and δ-) aromaticity, multiple (σ-, π-, and δ-)

antiaromaticity, and conflicting aromaticity (simultaneous aromaticity and antiaromaticity among the three σ-, π-, and δ-types). In the follow-up sections we discuss in details these new types of bonding as well as we show examples of chemical species manifesting these types of aromaticity.

Complicated nature of aromaticity in all transition metal cyclic systems can be understood more easily on simplified models – cyclic triatomic and tetratomic systems as examples of cyclic systems composed out of odd or even number of atoms, respectively. Counting rules for σ-, π-, δ-, and ϕ-aromaticity/antiaromaticity for both singlet/triplet coupled triatomic and tetratomic systems depend on the nature of atomic orbitals involved in the formation of corresponding bonding/antibonding molecular orbitals.

15-2. Model Consideration of σ-, π-, δ-, and ϕ-Aromaticity/Antiaromaticity

In order to develop a comprehensive understanding of chemical bonding in all-transition metal clusters we would like to present concise picture of delocalized bonding including s-, p-, d-, f-AO based σ-, π-, δ- and ϕ-aromaticity/antiaromaticity in model triatomic and tetratomic systems. The σ-, π, δ-, and ϕ-aromatic systems retain high symmetry structures whereas σ-, π-, δ-, and ϕ-antiaromatic systems should undergo Jahn-Teller distortion. When all bonding, partially bonding and antibonding MOs composed out of a particular type of AOs (s-, p-, d-, or f-) are completely occupied, those MOs do not contribute to bonding anymore, because all bonding effects will be cancelled by corresponding antibonding effects.

In Table 15-1 we present schematic molecular orbital diagrams, possible electronic configurations and Huckel's rules for s-, p-, d-, and f-AO based σ-aromaticity/antiaromaticity, p-, d-, and f-AO based π-aromaticity/antiaromaticity, d-, and f-AO based δ-aromaticity/antiaromaticity, and f-AO based ϕ-aromaticity/antiaromaticity of a singlet/triplet model triatomic system as a general example of odd-number cyclic systems. The same information for tetratomic system as a general example of even-number cyclic systems is listed in Table 15-2. In Figures 15-1 – 15-20 we give molecular orbital representation performed via Orbital Viewer 1.04[8] that can be found in the centre of the corresponding figure and the schematic representation of those orbitals in terms of atomic orbitals (to the left and to the right from molecular orbital representation).

15-2.1. s-, p-, d-, f-AO based σ-aromaticity/antiaromaticity

The simplest case is the s-AO based σ-aromaticity/antiaromaticity in a triatomic system. Out of three s-AOs (Figure 15-1) one can compose a completely bonding $1a_1'$-MO and two partially bonding/antibonding $1e'$-MOs. According to the 4n+2 Huckel's rule for aromaticity and 4n Huckel's rule for antiaromaticity, triatomic systems with the electronic configuration $1a_1'^{(2)}1e'^{(0)}$ are σ−aromatic and with the electronic configuration $1a_1'^{(2)}1e'^{(2)}$ (singlet coupling) are σ−antiaromatic. Whereas the triatomic system with electronic configuration $1a_1'^{(2)}1e'^{(2)}$ (triplet coupling) is σ−aromatic, thus satisfying the 4n Huckel's rule for triplet cases. Triplet coupling $1a_1'^{(1)}1e'^{(1)}$ electronic configuration should be considered as being σ-antiaromatic (Table 15-1).

In a tetratomic system out of four s-AOs (Figure 15-2) one can compose a completely bonding $1a_{1g}$-MO, two partially bonding/antibonding $1e_u$-MOs, and one completely antibonding $1b_{1g}$-MO. Similar to the triatomic systems (see above), tetratomic systems with the electronic configurations $1a_{1g}^{(2)}1e_u^{(0)}1b_{1g}^{(0)}$, $1a_{1g}^{(2)}1e_u^{(2)}1b_{1g}^{(0)}$ (triplet coupling) and $1a_{1g}^{(2)}1e_u^{(4)}1b_{1g}^{(0)}$ are σ–aromatic, with the electronic configuration $1a_{1g}^{(2)}1e_u^{(2)}1b_{1g}^{(0)}$ (singlet coupling) are σ–antiaromatic, according to the counting rule $4n+2/4n//4n/4n+2$ (Table 15-2). Triplet coupling $1a_{1g}^{(1)}1e_u^{(1)}$ electronic configuration should be considered as being σ-antiaromatic.

In the case of p-AO based σ-aromaticity/antiaromaticity in a cyclic triatomic system there are two types of p-AOs: p-sigma-radial ($p_{\sigma-r}$-) and p-sigma-tangential ($p_{\sigma-t}$-) AOs participating in delocalized bonding (Table 15-1 and Figure 15-3). The lowest-lying σ-MO ($1a_1'$) is completely bonding formed out of $p_{\sigma-r}$- AOs only, whereas the highest-lying one ($1a_2'$) is completely antibonding composed out of $p_{\sigma-t}$- AOs. The doubly degenerate $1e'$- and $2e'$-MOs are composed out of both $p_{\sigma-r}$- and $p_{\sigma-t}$-AOs. This is the reason why $p_{\sigma-r}$- and $p_{\sigma-t}$-MOs are presented as one set in Figure 15-3. The counting rules for aromaticity/antiaromaticity for σ-electrons in cyclic systems with the singlet//triplet coupling of electrons and odd number of vertices are $4n+2/4n//4n/4n+2$, respectively (Table 15-1).

For the cyclic tetratomic systems p-AO based σ-aromaticity/antiaromaticity is more complicated (Figure 15-4, Table 15-2). Now, the two lowest-lying σ-MOs ($1a_{1g}$ and $1b_{2g}$) are completely bonding and they are composed out of either $p_{\sigma-r}$- AOs ($1a_{1g}$) or $p_{\sigma-t}$-

AOs ($1b_{2g}$). The highest-lying ones are completely antibonding and they are also composed out of either $p_{\sigma\text{-r}}$- AOs ($1b_{1g}$) or $p_{\sigma\text{-t}}$- AOs ($1a_{2g}$). The four MOs ($1e_u$ and $2e_u$) in the σ-set that are located in between the completely bonding and antibonding MOs are doubly degenerate with bonding/antibonding characters. The $1e_u$- and $2e_u$-MOs are composed of both $p_{\sigma\text{-r}}$- and $p_{\sigma\text{-t}}$-AOs. On the basis of this mixing of the $p_{\sigma\text{-r}}$- and $p_{\sigma\text{-t}}$-AOs the counting rule for σ-electrons for singlet//triplet coupling cyclic systems with even number of vertices should be $4n+4/4n+2//4n+6/4n$ (Table 15-2) for aromaticity/antiaromaticity (in the simplest case of the occupation of just one $p_{\sigma\text{-r}}$- or one $p_{\sigma\text{-t}}$-MO the system is also aromatic).

d-AO based σ-aromaticity/antiaromaticity in a cyclic triatomic system is based on two types of d-AOs: $d_{\sigma\text{-r}}$- and $d_{\sigma\text{-t}}$-AOs participating in delocalized bonding (Figure 15-5). $d_{\sigma\text{-r}}$- AOs participate in the formation of the completely bonding lowest-lying σ-MO ($1a_1'$), whereas $d_{\sigma\text{-t}}$- AOs participate in the formation of the completely antibonding highest-lying σ-MO ($1a_2'$). Two doubly degenerate $1e'$- and $2e'$-MOs are composed out of both $d_{\sigma\text{-r}}$- and $d_{\sigma\text{-t}}$-AOs. The counting rules are $4n+2/4n//4n/4n+2$ for aromaticity/antiaromaticity for σ-electrons in cyclic systems with the singlet//triplet coupling of electrons and odd number of vertices (see Table 15-1).

There are also two types of d-AOs: $d_{\sigma\text{-r}}$- and $d_{\sigma\text{-t}}$-AOs participating in delocalized bonding which are responsible for d-AO based σ-aromatic/antiaromatic character in a cyclic tetratomic system (Table 15-2 and Figure 15-6). There are two lowest-lying completely bonding σ-MOs ($1a_{1g}$ and $1b_{2g}$) composed out of either $d_{\sigma\text{-r}}$- AOs ($1a_{1g}$) or $d_{\sigma\text{-t}}$-

AOs ($1b_{2g}$). Similarly, there are two highest-lying completely antibonding σ-MOs ($1b_{1g}$ and $1a_{2g}$) composed out of either $d_{\sigma-r}$- AOs ($1b_{1g}$) or $d_{\sigma-t}$- AOs ($1a_{2g}$). The four MOs ($1e_u$ and $2e_u$) in the σ-set that are located in between the completely bonding and antibonding MOs are doubly degenerate with bonding/antibonding characters. The $1e_u$- and $2e_u$-MOs are composed of both $d_{\sigma-r}$- and $d_{\sigma-t}$-AOs. The counting rules for σ-electrons for cyclic singlet//triplet coupling systems with even number of vertices should be $4n+4/4n+2//4n+6/4n$ for aromaticity/antiaromaticity (in the simplest case of the singlet coupling occupation of just one $d_{\sigma-r}$- or one $d_{\sigma-t}$-MO the system is also aromatic).

Cyclic triatomic system exhibiting f-AO based σ-aromaticity/antiaromaticity involves $f_{\sigma-r}$- and $f_{\sigma-t}$-AOs in delocalized bonding (Figure 15-7). The lowest-lying completely bonding ($1a_1'$) and the highest-lying completely antibonding ($1a_2'$) σ-MOs are formed out of either $f_{\sigma-r}$- AOs or $f_{\sigma-t}$- AOs, respectively. $1e'$- and $2e'$-MOs are composed out of both $f_{\sigma-r}$- and $f_{\sigma-t}$-AOs. The counting rules for aromaticity/antiaromaticity for σ-electrons in singlet//triplet coupled cyclic systems with odd number of vertices are $4n+2/4n//4n/4n+2$, respectively (see Table 15-1 for details). f-AO based σ-aromaticity/antiaromaticity in a cyclic tetratomic system involves $f_{\sigma-r}$- and $f_{\sigma-t}$-AOs in delocalized bonding (Table 15-2 and Figure 15-8). The two lowest-lying completely bonding ($1a_{1g}$ and $1b_{2g}$) and the two highest-lying completely antibonding ($1b_{1g}$ and $1a_{2g}$) σ-MOs are composed out of either $f_{\sigma-r}$- AOs ($1a_{1g}$, $1b_{1g}$) or $f_{\sigma-t}$- AOs ($1b_{2g}$, $1a_{2g}$). The four MOs ($1e_u$ and $2e_u$) in the σ-set have bonding/antibonding characters and are composed of both $f_{\sigma-r}$- and $f_{\sigma-t}$-AOs. The counting rules are $4n+4/4n+2//4n+6/4n$

(Table 15-2) for σ-electrons for cyclic singlet//triplet coupling systems with even number of vertices for aromaticity/antiaromaticity (the singlet coupled system is also aromatic in the simplest case of occupation of just one $f_{\sigma\text{-}r}$- or one $f_{\sigma\text{-}t}$-MO).

15-2.2. p-, d-, f-AO based π-aromaticity/antiaromaticity

In a triatomic system with the p-AO based π-aromaticity/antiaromaticity (Figure 15-9) there's one completely bonding $1a_2''$-MO and two partially bonding/antibonding $1e''$-MOs. Single-coupled triatomic systems with the electronic configuration $1a_2''^{(2)}1e''^{(0)}$ are π–aromatic and systems with the electronic configuration $1a_2''^{(2)}1e''^{(2)}$ are π–antiaromatic (see Table 15-1). Triple-coupled triatomic system with electronic configurations $1a_2''^{(2)}1e''^{(2)}$ and $1a_2''^{(1)}1e''^{(1)}$ are π–aromatic and π-antiaromatic, respectively (see Table 15-1).

The set of MOs composed out of four p-AOs in a tetratomic system is the following: a completely bonding $1a_{2u}$-MO, two partially bonding/antibonding $1e_g$-MOs, and one completely antibonding $1b_{2u}$-MO (Figure 15-10). Similar to the triatomic systems (see above) tetratomic systems with the electronic configurations $1a_{2u}^{(2)}1e_g^{(0)}1b_{2u}^{(0)}$, $1a_{2u}^{(2)}1e_g^{(2)}1b_{2u}^{(0)}$ (triplet coupling) and $1a_{2u}^{(2)}1e_g^{(4)}1b_{2u}^{(0)}$ are π–aromatic, with the electronic configurations $1a_{2u}^{(2)}1e_g^{(2)}1b_{2u}^{(0)}$ (singlet coupling) and $1a_{2u}^{(1)}1e_g^{(1)}1b_{2u}^{(0)}$ ((singlet coupling) are π–antiaromatic (Table 15-2).

In a cyclic triatomic system two types of d-AOs: $d_{\pi\text{-}r}$- and $d_{\pi\text{-}t}$-AOs are responsible for d-AO based π-aromaticity/antiaromaticity (Figure 15-11). The lowest-lying π-MO ($1a_2''$) is completely bonding formed out of only $d_{\pi\text{-}r}$- AOs, the doubly degenerate $1e''$-

and 2e"-MOs are composed out of both $d_{\pi\text{-}r}$- and $d_{\pi\text{-}t}$-AOs, and the highest-lying one

($1a_1$") is completely antibonding composed out of $d_{\pi\text{-}t}$- AOs. See Table 15-1 for the

counting rules and possible electronic configurations for aromaticity/antiaromaticity for

π-electrons in cyclic systems with the singlet//triplet coupling of electrons and odd

number of vertices.

Now, let's consider d-AO based π-aromaticity/antiaromaticity in cyclic tetratomic

systems (Figure 15-12). Cyclic tetratomic systems have eight MOs corresponding to the

d-AO based π-aromaticity/antiaromaticity: two completely bonding π-MOs ($1a_{2u}$ and $1b_{1u}$)

composed out of either $d_{\pi\text{-}r}$- AOs ($1a_{2u}$) or $d_{\pi\text{-}t}$- AOs ($1b_{1u}$), set of two partially

bonding/antibonding doubly degenerate MOs ($1e_g$ and $2e_g$) composed of both $d_{\pi\text{-}r}$- and $d_{\pi\text{-}t}$-AOs, and two completely antibonding MOs composed out of either $d_{\pi\text{-}r}$- AOs ($1b_{2u}$) or

$d_{\pi\text{-}t}$- AOs ($1a_{1u}$). The counting rules and possible electronic configurations for d-AO based

π-aromaticity/antiaromaticity can be found in Table 15-2.

In Table 15-1 and Figure 15-13 we summarized the case of f-AO based π-

aromaticity/antiaromaticity in a cyclic triatomic system. There are six π-MO formed out

of $f_{\pi\text{-}r}$- and $f_{\pi\text{-}t}$-AOs which are the following: completely bonding $f_{\pi\text{-}r}$- AO based $1a_2$",

doubly degenerate bonding/antibonding $f_{\pi\text{-}r}$- and $f_{\pi\text{-}t}$-AO based 1e"- and 2e", and finally

completely antibonding $f_{\pi\text{-}t}$- AO based $1a_1$" (see Table 1 for the counting rules and

possible electronic configurations for aromaticity/antiaromaticity).

Similar to cyclic triatomic systems there are two types of f-AOs: $f_{\pi\text{-}r}$- and $f_{\pi\text{-}t}$-AOs

participating   in   delocalized   bonding   in   the   case   of   f-AO   based π-

aromaticity/antiaromaticity in a cyclic tetratomic system (Figure 15-14). This case is similar to d-AO based π-aromaticity/antiaromaticity (see Table 15-2 for the counting rules and possible electronic configurations for f-AO based π-aromaticity/antiaromaticity in a cyclic tetratomic system).

15-2.3. d-, f-AO based δ-aromaticity/antiaromaticity

In the d-AO based δ-aromaticity/antiaromaticity in a triatomic system out of three d-AOs (Figure 15-15) one can compose a completely bonding $1a_1$'-MO and two partially bonding/antibonding $1e$'-MOs. The counting rules, symmetry of molecular orbitals and electronic configurations are like those in the case of s-AO based σ-aromaticity in a triatomic system (see Table 15-1, as well as Figure 15-1 and 15-15) .

Out of four d-AOs in a tetratomic system (Figure 15-16) one can compose a completely bonding $1a_{1g}$-MO, two partially bonding/antibonding $1e_u$-MOs, and one completely antibonding $1b_{1g}$-MO which participate in δ-aromaticity /antiaromaticity. Tetratomic systems with the electronic configurations $1a_{1g}^{(2)}1e_u^{(0)}1b_{1g}^{(0)}$, and $1a_{1g}^{(2)}1e_u^{(4)}1b_{1g}^{(0)}$, as well as with electronic configuration $1a_{1g}^{(2)}1e_u^{(2)}1b_{1g}^{(0)}$ (triplet coupling) are δ−aromatic. Tetratomic systems with the electronic configurations $1a_{1g}^{(2)}1e_u^{(2)}1b_{1g}^{(0)}$ (singlet coupling), and $1a_{1g}^{(1)}1e_u^{(1)}$ (triplet coupling) are δ−antiaromatic (See Table 15-2 and Figure 15-16 for details).

f-AO based δ-aromaticity/antiaromaticity in a cyclic triatomic system is based on $f_{\delta-r}$- and $f_{\delta-t}$-AOs (Table 15-1 and Figure 15-17). Similar to the cyclic triatomic systems exhibiting p-AO based σ-aromaticity/antiaromaticity, in case of f-AO based δ-

aromaticity/antiaromaticity there are six δ-MOs: $1a_1'$, $1e'$ and $2e'$, and $1a_2'$ which are completely bonding, partially bonding/antibonding, and completely antibonding, respectively (see Table 15-1 and Figures 15-3 and 15-17 for possible electronic configurations and the counting rules for aromaticity/antiaromaticity).

The $f_{\delta\text{-r}}$- and $f_{\delta\text{-t}}$- AOs are involved in f-AO based δ-aromaticity/antiaromaticity in cyclic tetratomic systems (Table 15-2 and Figure 15-18). There are eight δ-MOs, out of which $1a_{1g}$ and $1b_{2g}$ are completely bonding, $1e_u$ and $2e_u$ are partially bonding/anibonding, and $1b_{1g}$ and $1a_{2g}$ are completely antibonding. The counting rule for δ-electrons for singlet//triplet coupling cyclic systems with even number of vertices should be $4n+4/4n+2//4n+6/4n$ for aromaticity/antiaromaticity (in the simplest case of the occupation of just one $f_{\delta\text{-r}}$- or one $f_{\delta\text{-t}}$-MO the system is also aromatic).

15-2.4.   f-AO based ϕ-aromaticity/antiaromaticity

Finally, the f-AO based ϕ-aromaticity/antiaromaticity in a triatomic system is based on completely ϕ-bonding $1a_2''$-MO and two partially bonding/antibonding $1e''$-MOs (Figure 15-19). Applying Huckel's rules for aromaticity/antiaromaticity in cyclic triatomic systems, one can say that the system with the electronic configurations $1a_2''^{(2)}1e''^{(0)}$ and $1a_2''^{(2)}1e''^{(2)}$ (triplet coupling) are ϕ–aromatic, and with the electronic configurations $1a_2''^{(2)}1e''^{(2)}$ (singlet coupling) and $1a_2''^{(1)}1e''^{(1)}$ (triplet coupling) are ϕ–antiaromatic (Table 15-1).

As for f-AO based ϕ-aromaticity/antiaromaticity in tetratomic systems, there are four ϕ- MOs (Figure 15-20): completely bonding $1a_{2u}$, two degenerate partially

bonding/antibonding $1e_g$, and one completely antibonding $1b_{2u}$-MO. Having taken into account Huckel's rules for aromaticity/antiaromaticity in cyclic tetratomic systems, the systems with the electronic configurations $1a_{2u}^{(2)}1e_g^{(0)}1b_{2u}^{(0)}$, $1a_{2u}^{(2)}1e_g^{(2)}1b_{2u}^{(0)}$ (triplet coupling) and $1a_{2u}^{(2)}1e_g^{(4)}1b_{2u}^{(0)}$ can be said to be ϕ–aromatic, and the systems with the electronic configuration $1a_{2u}^{(2)}1e_g^{(2)}1b_{2u}^{(0)}$ (singlet coupling) - ϕ–antiaromatic (Table 15-2).

The above chemical bonding analysis on model triatomic and tetratomic systems can be used for assessing aromaticity/antiaromaticity in real molecules and clusters. However, hybridization may complicate this analysis. We will present below a few examples, where aromaticity/antiaromaticity in transition metal systems allows us to rationalize chemical bonding.

There have been very few examples on the aromaticity/antiaromaticity in all-transition metal cyclic systems reported in the literature to this day. In the following chapter we give detailed discussion on antiaromaticity/antiaromaticity in Au_3^+/Au_3^-, Na_2Zn_3, Hg_4^{6-}, $Mo_3O_9^{2-}$, Sc_3^-, Hf_3, and Ta_3^- clusters.

15-3. Examples of Aromatic/Antiaromatic Transition Metal Systems

We performed chemical bonding analysis in a few representative transition metal clusters using recently developed Adaptive Natural Density Partitioning (AdNDP) method.[9] The AdNDP method is based on the concept of the electron pair as the main element of chemical bonding models. Thus, it represents the electronic structure in terms of nc-2e bonds. With n spanning the interval from one to the total amount of atoms in the

particular atomic assembly, AdNDP recovers both Lewis bonding elements (1c-2e and 2c-2e objects, corresponding to the core electrons and lone pairs, and two-center two-electron bonds) and delocalized bonding elements, which are associated with the concepts of aromaticity and antiaromaticity. From this point of view, AdNDP achieves seamless description of systems featuring both localized and delocalized bonding without invoking the concept of resonance. Essentially, AdNDP is a very efficient and visual approach to the interpretation of the molecular orbital-based wave functions.

15-3.1. s-AO based σ-aromaticity and σ-antiaromaticity

There were a few works on the prototypical odd-number cyclic systems with s-AO based σ-aromaticity, namely the Li_3^+ (ref. 10-12) and the Cu_3^+ (ref. 12) clusters. In this chapter we would like to consider s-AO based σ-aromaticity/antiaromaticity in triatomic gold clusters Au_3^+ and Au_3^-, respectively.

Au_3^+, similar to Li_3^+ and Cu_3^+ clusters, has a D_{3h}, $^1A_1$' global minimum structure. Bonding in Au_3^+ is based on 6s-AOs of Au, because all the bonding and antibonding MOs composed out of 5d-AOs of Au are occupied, hence the contribution to bonding from 5d-AOs of Au is negligible (according to NBO analysis natural electronic configuration of Au_3^+ cluster is: $6s^{(0.71)}5d^{(9.93)}$ at B3LYP/LANL2DZ).   The AdNDP analysis reveals one 3c-2e σ-bond with occupation number (ON) of 2.00 electrons (2.00 |e|) composed out of 6s-AOs of three Au atoms (Figure 15-21a). It is completely bonding and it is responsible for σ-aromaticity in Au_3^+, according to the 4n+2 rule with n=0 (for

singlet coupling). The obtained 3c-2e σ-bond can be compared with the corresponding model molecular orbital $1a_1'$ (see Figure 15-1 and Table 15-1).

For σ-antiaromatic species (with ns-AOs participating in bonding) the counting rule is $4n$ (singlet coupling). The Au_3^- anion is a good example of σ-antiaromatic system with four 6s-electrons. The electronic configuration for the singlet state of Au_3^- at the D_{3h} symmetry is $1a_1''^{(2)}1e'^{(2)}$ (with the only contribution of 6s AOs to the bonding MOs, compare to Figure 15-1 and Table 15-1), and the triangular structure with the singlet electronic state must undergo the Jahn-Teller distortion towards linear $D_{\infty h}$ structure with a $1\sigma_g^{(2)}1\sigma_u^{(2)}$ valence electronic configuration and that is exactly what we found in our calculations. Two σ-delocalized MOs can be approximately localized into two 2c-2e bonds with ON = 2.00 |e| and the linear structure of Au_3^- can be formally considered as a classical structure (Figure 15-21b).

s-AO based σ-aromaticity in even-number cyclic systems namely M_4^{2-} (M = Cu, Ag, Au) dianions as parts of M_4Li_2 (M = Cu, Ag, Au) neutral species was studied by Wannere et al[13] and M_4X^- and M_4X_2 (M = Cu, Ag, Au; X=Li, Na) was studied by Lin et al.[14] s-AO based σ-aromaticity in the $cyclo$-M_nH_n (M = Cu, Ag, Au; n = 3-6), $cyclo$-$Au_3L_nH_{3-n}$ (L = CH_3, NH_2, OH, and Cl; n = 1-3), $cyclo$-$Cu_nAg_{k-n}H_n$ (n = 1-k, k = 3-5) clusters was studied by group of Tsipis.[15-18] We will not discuss these cases because their chemical bonding is similar to above Au_3^+ case and for those readers who would like to look into details we recommend consulting the original papers and the discussion in the recent review.[7]

15-3.2. p-AO based aromaticity and antiaromaticity

p-AOs participation in delocalized chemical bonding may lead to the phenomenon of double (σ- and π-) aromaticity. Chandrasekhar et al.[19] introduced simultaneous presence of σ- and π-aromaticity to explain the properties of the 3,5-dehydrophenyl cation. Simultaneous presence of aromaticity and antiaromaticity was first used by Martin-Santamaria and Rzepa[20] to explain chemical bonding in small carbon rings. Later the simultaneous presence of aromaticity and antiaromaticity was named as conflicting aromaticity.[21] Alexandrova et al.[22] have also shown an example of a doubly σ- and π-antiaromatic species – the B_6^{2-} dianion. p-AO based σ-aromaticity/antiaromaticity and p-AOs based double σ- and π-aromaticity and antiaromaticity was also found in transition metal systems.

Yong and Chi[23] have recently shown that a series of M_3^{2-}, NaM_3^-, Na_2M_3 (M = Zn, Cd, Hg) clusters have the M_3^{2-} D_{3h}, $^1A_1$' core, which is p-AOs π-aromatic. Thus, in all the M_3^{2-}, NaM_3^-, Na_2M_3 (M = Zn, Cd, Hg) systems bonding in the M_3^{2-} core is due to π-aromaticity only, without σ-bonding. Similar bonding pattern was previously reported for M_3^{2-}, NaM_3^-, Na_2M_3 (M = Be, Mg) systems by Kuznetsov and Boldyrev,[24] Chattaraj and Giri,[25] and Roy and Chattaraj.[26] We performed the AdNDP analysis of the Na_2Zn_3 cluster which revealed one 5c-2e π-bond composed out of 4p-AOs of three Zn atoms and 3s-AOs of two Na atoms with ON = 2.00 |e| (Figure 15-22). The 5c-2e π-bond is similar to 3c-2e model molecular orbital $1a_2$" if we exclude contribution from sodium atoms (Figure 15-9 and Table 15-1). 4s-AOs of Zn atoms are not responsible for bonding and

they form three lone pairs (one per each Zn atom) with ON = 1.90 |e|. Thus, the Na_2Zn_3 species as well as Zn_3^{2-} (with $1a_2$" occupied HOMO) and $NaZn_3^-$ are all π-aromatic with no contribution from σ-bonding.

The first example of a solid compound (Na_3Hg_2 amalgam) containing doubly σ- and π-aromatic transition metal cluster Hg_4^{6-} was discovered by Kuznetsov et al.[27] Formation of the Hg_4^{6-} cluster was puzzling since mercury has a closed shell electron configuration ($6s^{(2)}$) and therefore a neutral Hg_4 cluster is expected to be a van der Waals complex. The stability of the Hg_4^{6-} building block can be explained due to the fact that it is isoelectronic to the first all-metal aromatic cluster, Al_4^{2-}.[28] Bonding in Hg_4^{6-} is due to Hg 6p-AO based MOs and the completely occupied d-AOs of mercury do not contribute to the bonding. Figure 15-23 displays the bonding pattern obtained via AdNDP analysis of the square-planar Hg_4^{6-}.

The AdNDP analysis revealed four lone pairs on Hg atoms with ON = 1.94 |e|, as well as delocalized p-AO based 4c-2e σ-radial bond with ON = 2.00 |e|, p-AO based 4c-2e σ-tangential bond with ON = 2.00 |e|, and p-AO based 4c-2e π-bond with ON = 2.00 |e|. Thus Hg_4^{6-} should be considered as both p-radial-AO and p-tangential based σ-aromatic species. Therefore the Hg_4^{6-} cluster satisfies the 4n+4 counting rule for σ-aromaticity in cyclic systems with even numbers of atoms (see Table 15-2). In addition, Hg_4^{6-} should be considered as π-aromatic on the basis of the 4n+2 Huckel rule applied to its π-subsystem (see Table 15-2). Thus, Hg_4^{6-} is a doubly σ- and π-aromatic system. The p-AO based 4c-2e σ-radial and 4c-2e σ-tangential bonds can be compared to model

molecular orbitals $1a_{1g}$ and $1b_{2g}$, respectively (see Figure 15-4). One can compare the

p-AO based 4c-2e π-bond to the model molecular orbital $1a_{2u}$ (see Figure 15-10).

The finding of the double aromaticity in Hg_4^{6-} establishes a solid bridge between our gas-

phase studies of multiply aromatic clusters and bulk materials containing such species.

15-3.3. d-AO based aromaticity and antiaromaticity

Due to the more complicated nodal structure of d-AOs that can form δ-bond in

addition to σ- and π-bonds, transition-metal systems can provide a more diverse array of

aromaticity-antiaromaticity combinations. However, so far only few transition metal

systems with d-AO based aromaticity have been reported.

The first cases of d-AO based σ-aromaticity were reported by Huang et al.[29] in 4d

and 5d transition metal oxide clusters, $Mo_3O_9^-$ and $W_3O_9^-$, by combining photoelectron

spectroscopy and theoretical calculations. They found that the M_3O_9, $M_3O_9^-$, and $M_3O_9^{2-}$

(M = Mo, W) clusters all have D_{3h} structures and each metal atom is bonded to two

bridged O atoms and two terminal O atoms. We performed the AdNDP analysis for

$M_3O_9^{2-}$ cluster and the results are presented in Figure 15-24.

The following bonding pattern is revealed for the $Mo_3O_9^{2-}$ cluster: six 2c-2e Mo-O

σ-bonds with ON = 2.00 |e|, six 2c-2e Mo-O π-bonds with ON = 1.99 |e|, six 2c-2e Mo-O

σ-bonds with ON = 1.92 |e|, and one completely delocalized 3c-2e d-AO based σ_r-bond.

Thus, each terminal oxygen atom is bound to the closest molybdenum atom by both σ-

and π-bonds, each bridging oxygen atom is bound to the neighboring molybdenum atoms

by two σ-bonds, and the molybdenum atoms are bound to each other by completely

bonding 3c-2e σ-bond. According to the performed AdNDP analysis, $Mo_3O_9^{2-}$ species is σ-aromatic. The 3c-2e d-AO based $σ_r$-bond in the Mo_3 kernel is similar to the 3c-2e model d-AO based $1a_1$'σ-MO in Figure 15-5.

The first systems with d-AO based double (σ-and π-) aromaticity have been reported recently by Chi and Liu.[30] They demonstrated that the D_{3h} ($^1A_1$') structures are the global minimum structures for X_3^- (X = Sc, Y, La). All three species have the same valence electronic configuration $1a_1$'$^{(2)}1e$'$^{(4)}1a_2$''$^{(2)}2a_1$'$^{(2)}$, though the order of the MOs varies. The AdNDP analysis of the Sc_3^- cluster reveals the following bonding pattern: there are three 2c-2e Sc-Sc σ-bonds with ON = 1.99 |e| composed out of hybrid 4s,3d-AOs of Sc, one completely bonding 3c-2e d-radial based σ-bond with ON = 2.00 |e|, and one completely bonding 3c-2e d-radial based π-bond with ON = 2.00 |e| (Figure 15-25). Therefore the X_3^- (X = Sc, Y, La) clusters satisfy the 4n+2 counting rule for σ-aromaticity and the 4n+2 Huckel rule for π-aromaticity in cyclic systems with odd numbers of atoms (see Table 15-1). Thus, all three anions are d-orbital based doubly (σ- and π-) aromatic systems. The obtained via AdNDP method 3c-2e d-AO based $σ_r$-bond and 3c-2e d-AO based $π_r$-bond are similar to 3c-2e $1a_1$' and $1a_2$'' model molecular orbitals presented in Figures 15-5 and 15-11, respectively.

The first example of δ–aromaticity was found by Zhai et al.[4] in joint photoelectron spectroscopy and theoretical study. They showed that the $Ta_3O_3^-$ cluster possesses a global minimum with a perfect D_{3h} ($^1A_1$') planar triangular structure and that it's doubly π- and δ-aromatic species. Averkiev and Boldyrev[5] theoretically predicted the

first example of triple (σ-, π-, and δ-) aromaticity (Hf$_3$ in the D$_{3h}$, ^{1}A$_1$'

$1a_1'^{(2)}2a_1'^{(2)}1e'^{(4)}1a_2''^{(2)}3a_1'^{(2)}$ state). The results of the AdNDP analysis for this system are

presented in Figure 15-26. The following bonding pattern is revealed for the Hf$_3$ species:

three 2c-2e Hf-Hf σ-bonds with ON = 1.99 |e| are formed out of hybrid 6s,5d-AOs of Hf

atoms, and three completely delocalized bonds. They are: one completely bonding 3c-2e

d-radial based σ-bond with ON = 2.00 |e|, one completely bonding 3c-2e d-radial based

π-bond ON = 2.00 |e|, and one completely bonding 3c-2e d-AO based δ-bond ON = 2.00

|e|. Assignment of the triple (σ-, π-, and δ-) aromaticity can be made on the basis of the

4n+2 Huckel rule (odd number of atoms, see Table 1). One can find the correspondence

between 3c-2e d-AO based σ_r-bond, 3c-2e d-AO based π_r-bond, 3c-2e d-AO based δ-

bond and 3c-2e $1a_1$', $1a_2$", and $1a_1$' model molecular orbitals shown in Figures 15-5, 15-

11 and 15-15, respectively.

Wang et al.[31] presented joint photoelectron spectroscopy and theoretical study of

another example of transition metal Ta$_3^-$ cluster with triple (σ-, π-, and δ-) aromaticity.

They have shown that the lowest energy quintet state (D$_{3h}$, ^{5}A$_1$') has the following

electronic configuration: $1a_1'^{(2)}2a_1'^{(2)}1a_2''^{(2)}1e'^{(4)}1e''^{(2)}3a_1'^{(2)}2e'^{(2)}$. Out of these MOs, $1a_1$'

and 1e' are set of completely bonding and partially bonding/antibonding MOs formed out

of primarily 6s-AOs of tantalum atoms and should not contribute to bonding

significantly. $2a_1$' is a completely bonding MO formed out of d-sigma-radial (d$_{\sigma-r}$-) AOs

of tantalum atoms. The corresponding partially bonding/antibonding 2e'-MOs composed

out of d-sigma-radial (d$_{\sigma-r}$-) and d-sigma-tangential (d$_{\sigma-t}$-) AOs of tantalum atoms. These

doubly degenerate MOs are occupied by two electrons with triplet coupling and together with two electrons on $2a_1$' MO they satisfy the 4n rule for σ-aromaticity (triplet coupling) in odd number cyclic systems (see section 15-2.1 and Table 15-1). Similarly, $1a_2$" is a completely bonding MO formed out of d-pi-radial ($d_{\pi\text{-}r}$-) AOs of tantalum atoms. The corresponding partially bonding/antibonding $1e$"-MOs composed out of d-pi-radial ($d_{\pi\text{-}r}$-) and d-pi-tangential ($d_{\pi\text{-}t}$-) AOs of tantalum atoms. These doubly degenerate MOs are occupied by two electrons with triplet coupling and together with two electrons on $1a_2$" MO they satisfy the 4n rule for π-aromaticity (triplet coupling) in odd number cyclic systems (see section 15-2.2 and Table 15-1). Finally, $3a_1$' is a completely bonding δ-MO which is responsible for δ-aromaticity in this system (see section 15-2.3 and Table 15-1). Alvarado-Soto et al.[32,33] have discussed the concept of aromaticity in Re_3Cl_9, Re_3Br_9, $Re_3Cl_9^{2-}$, and $Re_3Br_9^{2-}$ clusters.

Though aromaticity in compounds containing a transition-metal atom has already been discussed for quite a long time, aromaticity in all-transition metal systems have been recognized only recently. There are examples of σ-, π-, and δ-aromaticity based on s-, p-, and d-AOs. We derived the counting rules for σ-, π-, δ-, and ϕ-aromaticity/antiaromaticity for both singlet/triplet coupled triatomic and tetratomic systems so that one could use those to rationalize aromaticity and antiaromaticity in all-transition metal systems. These rules can be easily extended for any cyclic systems composed out of odd or even number of atoms.

The concept of aromaticity, antiaromaticity and conflicting aromaticity is an important theoretical tool for deciphering chemical bonding in various known and novel chemical compounds containing transition metal atoms.

15-4 Summary

Aromaticity in compounds containing a transition-metal atom has already had a long history. Initially, Thorn and Hoffmann[34] proposed six-membered ring metallocyclic compounds, derivatives of benzene with one C-H moiety replaced by an isolobal transition-metal fragment. Three years later the first example of a stable, isolable metallobenzene — osmabenzene — was reported by Elliott et al.[35] Since then a large family of metallobenzenes have been synthesized and characterized.[36-38] Profilet et al.[39] reported first synthesis of dimetallobenzenes with two metal atoms incorporated into the benzene ring A thorough chemical bonding analysis of metallobenzene has been recently performed by Fernandez and Frenking.[40] However, in this review we demonstrated that aromaticity could be a powerful tool in explaining structure, stability and other molecular properties in cyclic systems composed of transition-metal atoms only.

It is clear that aromaticity and antiaromaticity could be very useful concepts in explaining structure, stability and other molecular properties of isolated and embedded clusters of transition metals and transition metal oxide clusters. The chemical bonding in transition metal clusters can come from s-AOs, p-AOs, and d-AOs, and can be expressed as a variety of multiple aromaticities and antiaromaticities as well as of conflicting aromaticities.

In a section 15-2 we considered models of σ-, π-, δ-, and φ-aromaticity/antiaromaticity based on a particular type (s-, p-, d-, or f-) of AOs in both even and odd number cyclic systems on an example of triatomic and tetratomic systems, respectively. One can compose σ-MOs out of s-AOs, as well as p-sigma-radial ($p_{\sigma-r}$-) and p-sigma-tangential ($p_{\sigma-t}$-) AOs, d-sigma-radial ($d_{\sigma-r}$-) and d-sigma-tangential ($d_{\sigma-t}$-) AOs, f-sigma-radial ($f_{\sigma-r}$-) and f-sigma-tangential ($f_{\sigma-t}$-) AOs participating in delocalized bonding. π-MOs can be composed out of p-AOs, as well as d-pi-radial ($d_{\pi-r}$-) and d-pi-tangential ($d_{\pi-t}$-) AOs, f-pi-radial ($f_{\pi-r}$-) and f-pi-tangential ($f_{\pi-t}$-) AOs participating in delocalized bonding. One can compose δ-MOs out of d-AOs, as well as f-delta-radial ($f_{\delta-r}$-) and f-delta-tangential ($f_{\delta-t}$-) AOs participating in delocalized bonding. Finally, φ-MOs can be composed out of f-AOs.

The counting rules for s-AO based σ-aromaticity, p-AO based π-aromaticity, d-AO based δ-aromaticity, and f-AO based φ-aromaticity are 4n+2/4n//4n/4n+2 rules for aromaticity/antiaromaticity (singlet//triplet coupling, respectively) for all cyclic structures. The counting rules for p-AO based σ-aromaticity, d-AO based σ-aromaticity, d-AO based π-aromaticity, f-AO based σ-aromaticity, and f-AO based π-aromaticity are 4n+2/4n//4n/4n+2 rules for aromaticity/antiaromaticity (singlet//triplet coupling, respectively) for cyclic structures with odd number of atoms. The counting rules for p-AO based σ-aromaticity, d-AO based σ-aromaticity, d-AO based π-aromaticity, f-AO based σ-aromaticity, and f-AO based π-aromaticity are 2,4n+4/4n+2//4n+6/4n rules for

aromaticity/antiaromaticity (singlet//triplet coupling, respectively) for cyclic structures with even number of atoms.

This model chemical bonding analysis for odd/even-number cyclic systems can be used for assessing aromaticity/antiaromaticity in real molecules and clusters. However, hybridization may complicate this analysis. For instance, in planar cyclic boron clusters the peripheral boron atoms participate in localized 2c-2e B-B σ-bonding and those bonds are formed out of hybridized 2p-sigma-tangential ($2p_{\sigma\text{-}t}$-) and 2s atomic orbitals. Therefore, $2p_{\sigma\text{-}t}$-AOs should be excluded from the delocalized σ-bonding. Thus, only 2p-sigma-radial ($2p_{\sigma\text{-}r}$-) AOs participate in the delocalized σ-bonding and the counting rule for σ-aromaticity becomes 4n+2/4n for all cyclic systems.[9,41,42]

In the section 15-3 of current work we presented a few examples of aromatic/antiaromatic transition metal systems. We have shown that triatomic gold clusters Au_3^+ and Au_3^- are s-AO based σ-aromatic and σ-antiaromatic, respectively. Na_2Zn_3 cluster was shown to have one 5c-2e π-bond composed out of 4p-AOs of three Zn atoms and 3s-AOs of two Na atoms, thus, it's a π-aromatic system with no contribution from σ-bonding in the Zn_3 kernel. The Hg_4^{6-} cluster is a doubly p-AO based both σ- and π-aromatic system. The $Mo_3O_9^{2-}$ species renders its d-radial-AO based σ-aromaticity. The Sc_3^- cluster is an example of a system with d-AO based double (σ-and π-) aromaticity with one completely bonding 3c-2e d-radial based σ-bond and one completely bonding 3c-2e d-radial π-bond.

The Hf_3 cluster was theoretically predicted to be the first example of triple (σ-, π-, and δ-) aromaticity in the lowest singlet state. The first experimentally observed triply aromatic system is Ta_3^- in the lowest quintet state.

Atomic f-AOs in lanthanide and actinide clusters offer additional possibility to form ϕ-bonds and thus could lead to systems with even richer variety of ϕ-aromaticity/antiaromaticity. Tsipis et al.[6] have recently presented the first evidence of f-AO participation in delocalized bonding.

We hope that the aromaticity, antiaromaticity and conflicting aromaticity concepts would stimulate theoretical analysis of chemical bonding in other known and novel chemical compounds containing transition metal atoms in clusters, nanoparticles, solid compounds and metallo-biomolecules.

References

(1) Cotton, F. A.; Curtis, N. F.; Harris, C. B.; Johnson, B. F. G.; Lippard, S. J.; Mague, J. T.; Robinson, W. R.; Wood, J. S. *Science* **1964**, *145*, 1305.

(2) Cotton, F. A.; Murillo, C. A.; Walton, R. A. *Multiple Bonds Between Metal Atoms*, 3rd. ed.; Springer, New York, **2005**.

(3) Nguyen, T.; Sutton, A. D.; Brynda, M.; Fettiger, J. C.; Long, G. J.; Power, P. P. *Science* **2005**, *310*, 844.

(4) Zhai, H. J.; Averkiev, B. B.; Zubarev, D. Y.; Wang, L. S.; Boldyrev, A. I. *Angew. Chem. Int. Ed.* **2007**, *46*, 4277.

(5) Averkiev, B. B.; Boldyrev, A. I. *J. Phys. Chem. A* **2007**, *111*, 12864.

(6) Tsipis, C. A.; Karagiannis, E. E.; Kladou, P. F.; Tsipis, A. C. *J. Am. Chem. Soc.* **2004**, *126*, 12916.

(7) Zubarev, D. Y.; Boldyrev, A. I. *J. Comput. Chem.* **2007**, *28*, 251.

(8) Manthey, D. *Orbital Viewer, 1.04*, http://www.orbitals.com/orb/ov.htm, **2004**.

(9) Zubarev, D. Y.; Boldyrev, A. I. *Phys. Chem. Chem. Phys.* **2008**, *10*, 5207.

(10) Alexandrova, A. N.; Boldyrev, A. I. *J. Phys. Chem. A* **2003**, *107*, 554.

(11) Havenith, R. W. A.; De Proft, F.; Fowler, P. W.; Geerlings, P. *Chem. Phys. Lett.* **2004**, *407*, 391.

(12) Yong, L.; Wu, S. D.; Chi, X. X. *Int. J. Quant. Chem.* **2007**, *107*, 722.

(13) Wannere, C. S.; Corminboeuf, C.; Wang, Z. X.; Wodrich, M. D.; King, R. B.; Schleyer, P. v. R. *J. Am. Chem. Soc.* **2005**, *127*, 5701.

(14) Lin, Y. C.; Sundholm, D.; Juselius, J.; Cui, L. F.; Li, X.; Zhai, H. J.; Wang, L. S. *J. Phys. Chem. A* **2006**, *110*, 4244.

(15) Tsipis, A. C.; Kefalidis, C. E.; Tsipis, C. A. *J. Am. Chem. Soc.* **2008**, *130*, 9144.

(16) Tsipis, A. C.; Stalikas, A. V. *New. J. Chem.* **2007**, *31*, 852.

(17) Tsipis, A. C.; Tsipis, C. A. *J. Am. Chem. Soc.* **2003**, *125*, 1136.

(18) Tsipis, A. C.; Tsipis, C. A. *J. Am. Chem. Soc.* **2005**, *127*, 10623.

(19) Chandrasekhar, J.; Jemmis, E. D.; Schleyer, P. v. R. *Tetrahedron Lett.* **1979**, *39*, 3707.

(20) Martin-Santamaria, S.; Rzepa, H. S. *Chem. Commun.* **2000**, *16*, 1503.

(21) Boldyrev, A. I.; Wang, L. S. *Chem. Rev.* **2005**, *105*, 3716.

(22) Alexandrova, A. N.; Boldyrev, A. I.; Zhai, H. J.; Wang, L. S.; Steiner, E.; Fowler, P. W. *J. Phys. Chem. A* **2003**, *107*, 1359.

(23) Yong, L.; Chi, X. X. *J. Mol. Struct. Theochem.* **2007**, *818*, 93.

(24) Kuznetsov, A. E.; Corbett, J. D.; Wang, L. S.; Boldyrev, A. I. *Angew. Chem. Int. Ed.* **2001**, *40*, 3369.

(25) Chattaraj, P. K.; Giri, S. *J. Mol. Struct. Theochem.* **2008**, *865*, 53.

(26) Roy, D. R.; Chattaraj, P. K. *J. Phys. Chem. A* **2008**, *112*, 1612.

(27) Kuznetsov, A. E.; Boldyrev, A. I. *Chem. Phys. Lett.* **2004**, *388*, 452.

(28) Li, X.; Kuznetsov, A. E.; Zhang, H. F.; Boldyrev, A. I.; Wang, L. S. *Science* **2001**, *291*, 859.

(29) Huang, X.; Zhai, H. J.; Kiran, B.; Wang, L. S. *Angew. Chem. Int. Ed.* **2005**, *44*, 7251.

(30) Chi, X. X.; Liu, Y. *Int. J. Quant. Chem.* **2007**, *107*, 1886.

(31) Wang, B.; Zhai, H. J.; Huang, X.; Wang, L. S. *J. Phys. Chem. A* **2008**, *112*, 10962.

(32) Alvarado-Soto, L.; Ramirez-Tagle, R.; Arratia-Perez, R. *Chem. Phys. Lett.* **2008**, *467*, 94.

(33) Alvarado-Soto, L.; Ramirez-Tagle, R.; Arratia-Perez, R. *J. Phys. Chem. A* **2009**, *113*, 1671.

(34) Thorn, D. L.; Hoffmann, R. *Nouv. J. Chim.* **1979**, *3*, 39.

(35) Elliot, G. P.; Roper, W. R.; Waters, J. M. *J. Chem. Soc., Chem. Commun.* **1982**, 811.

(36) Bleeke, J. R. *Chem. Rev.* **2001**, *101*, 1205.

(37) Wright, L. J. *Dalton. Trans.* **2006**, 1821.

(38) Landorf, W. C.; Haley, M. M. *Angew. Chem. Int. Ed.* **2006**, *45*, 3914.

(39) Profilet, R. D.; Fanwick, P. E.; Rothwell, I. P. *Angew. Chem. Int. Ed.* **1992**, *31*, 1261.

(40) Fernandez, I.; Frenking, G. *Chem. Eur. J.* **2007**, *13*, 5873.

(41) Alexandrova, A. N.; Boldyrev, A. I.; Zhai, H. J.; Wang, L. S. *Coord. Chem. Rev.* **2006**, *250*, 2811.

(42) Zubarev, D. Y.; Averkiev, B. B.; Zhai, H. J.; Boldyrev, A. I.; Wang, L. S. *Phys. Chem. Chem. Phys.* **2008**, *10*, 257.

Table 15-1. Schematic molecular orbital diagrams, possible electronic configurations and Huckel's rules for aromaticity/antiaromaticity of singlet/triplet model triatomic system as a general example of odd-number cyclic systems.

$\bigwedge$	Schematic molecular orbital diagram	Huckel's rule for aromaticity		Huckel's rule for antiaromaticity	
		singlet coupling	triplet coupling	singlet coupling	triplet coupling
s-AO based σ-aromaticit	— —$1e'$ —$1a_1'$	**4n+2** $\{1a_1'^{(2)}1e'^{(0)}\}$	**4n** $\{1a_1'^{(2)}1e'^{(2)}\}$	**4n** $\{1a_1'^{(2)}1e'^{(2)}\}$	**4n+2** $\{1a_1'^{(1)}1e'^{(1)}\}$
p-AO based σ-aromaticit	—$1a_2'$ — —$2e'$ — —$1e'$ —$1a_1'$	**4n+2** $\{1a_1'^{(2)}1e'^{(0)}\}$ $\{1a_1'^{(2)}1e'^{(4)}\}$ $\{1a_1'^{(2)}1e'^{(4)}2e'^{(4)}\}$	**4n** $\{1a_1'^{(2)}1e'^{(2)}\}$ $\{1a_1'^{(2)}1e'^{(4)}2e'^{(2)}\}$	**4n** $\{1a_1'^{(2)}1e'^{(2)}\}$ $\{1a_1'^{(2)}1e'^{(4)}2e'^{(2)}\}$	**4n+2** $\{1a_1'^{(1)}1e'^{(1)}\}$ $\{1a_1'^{(2)}1e'^{(3)}2e'^{(2)}\}$
p-AO based π-aromaticit	— —$1e''$ —$1a_2''$	**4n+2** $\{1a_2''^{(2)}1e''^{(0)}\}$	**4n** $\{1a_2''^{(2)}1e''^{(2)}\}$	**4n** $\{1a_2''^{(2)}1e''^{(2)}\}$	**4n+2** $\{1a_2''^{(1)}1e''^{(1)}\}$
d-AO based σ-aromaticit	—$1a_2'$ — —$2e'$ — —$1e'$ —$1a_1'$	**4n+2** $\{1a_1'^{(2)}1e'^{(0)}\}$ $\{1a_1'^{(2)}1e'^{(4)}\}$ $\{1a_1'^{(2)}1e'^{(4)}2e'^{(4)}\}$	**4n** $\{1a_1'^{(2)}1e'^{(2)}\}$ $\{1a_1'^{(2)}1e'^{(4)}2e'^{(2)}\}$	**4n** $\{1a_1'^{(2)}1e'^{(2)}\}$ $\{1a_1'^{(2)}1e'^{(4)}2e'^{(2)}\}$	**4n+2** $\{1a_1'^{(1)}1e'^{(1)}\}$ $\{1a_1'^{(2)}1e'^{(3)}2e'^{(2)}\}$
d-AO based π-aromaticit	—$1a_1''$ — —$2e''$ — —$1e''$ —$1a_2''$	**4n+2** $\{1a_2''^{(2)}1e''^{(0)}\}$ $\{1a_2''^{(2)}1e''^{(4)}\}$ $\{1a_2''^{(2)}1e''^{(4)}2e''^{(4)}\}$	**4n** $\{1a_2''^{(2)}1e''^{(2)}\}$ $\{1a_1''^{(2)}1e''^{(4)}2e'^{(2)}\}$	**4n** $\{1a_2''^{(2)}1e''^{(2)}\}$ $\{1a_2''^{(2)}1e''^{(4)}2e''^{(2)}\}$	**4n+2** $\{1a_2''^{(1)}1e''^{(1)}\}$ $\{1a_2''^{(2)}1e''^{(3)}2e''^{(2)}\}$
d-AO based δ-aromaticit	— —$1e'$ —$1a_1'$	**4n+2** $\{1a_1'^{(2)}1e'^{(0)}\}$	**4n** $\{1a_1'^{(2)}1e'^{(2)}\}$	**4n** $\{1a_1'^{(2)}1e'^{(2)}\}$	**4n+2** $\{1a_1'^{(1)}1e'^{(1)}\}$

f-AO based σ-aromaticity		4n+2	4n	4n	4n+2
	—— $1a_2'$				
	—— —— $2e'$	$\{1a_1'^{(2)}1e'^{(0)}\}$	$\{1a_1'^{(2)}1e'^{(2)}\}$	$\{1a_1'^{(2)}1e'^{(2)}\}$	$\{1a_1'^{(1)}1e'^{(1)}\}$
	—— —— $1e'$	$\{1a_1'^{(2)}1e'^{(4)}\}$ $\{1a_1'^{(2)}1e'^{(4)}2e'^{(4)}\}$	$\{1a_1'^{(2)}1e'^{(4)}2e'^{(2)}\}$	$\{1a_1'^{(2)}1e'^{(4)}2e'^{(2)}\}$	$\{1a_1'^{(2)}1e'^{(3)}2e'^{(2)}\}$
	—— $1a_1'$				

f-AO based π-aromaticity		4n+2	4n	4n	4n+2
	—— $1a_1''$				
	—— —— $2e''$	$\{1a_2''^{(2)}1e''^{(0)}\}$	$\{1a_2''^{(2)}1e''^{(2)}\}$	$\{1a_2''^{(2)}1e''^{(2)}\}$	$\{1a_2''^{(1)}1e''^{(1)}\}$
	—— —— $1e''$	$\{1a_2''^{(2)}1e''^{(4)}\}$ $\{1a_2''^{(2)}1e''^{(4)}2e''^{(4)}\}$	$\{1a_1''^{(2)}1e''^{(4)}2e'^{(2)}\}$	$\{1a_2''^{(2)}1e''^{(4)}2e''^{(2)}\}$	$\{1a_2''^{(2)}1e''^{(3)}2e''^{(2)}\}$
	—— $1a_2''$				

f-AO based δ-aromaticity		4n+2	4n	4n	4n+2
	—— $1a_2'$				
	—— —— $2e'$	$\{1a_1'^{(2)}1e'^{(0)}\}$	$\{1a_1'^{(2)}1e'^{(2)}\}$	$\{1a_1'^{(2)}1e'^{(2)}\}$	$\{1a_1'^{(1)}1e'^{(1)}\}$
	—— —— $1e'$	$\{1a_1'^{(2)}1e'^{(4)}\}$ $\{1a_1'^{(2)}1e'^{(4)}2e'^{(4)}\}$	$\{1a_1'^{(2)}1e'^{(4)}2e'^{(2)}\}$	$\{1a_1'^{(2)}1e'^{(4)}2e'^{(2)}\}$	$\{1a_1'^{(2)}1e'^{(3)}2e'^{(2)}\}$
	—— $1a_1'$				

f-AO based φ-aromaticity		4n+2	4n	4n	4n+2
	—— —— $1e''$				
	—— $1a_2''$	$\{1a_2''^{(2)}1e''^{(0)}\}$	$\{1a_2''^{(2)}1e''^{(2)}\}$	$\{1a_2''^{(2)}1e''^{(2)}\}$	$\{1a_2''^{(1)}1e''^{(1)}\}$

Table 15-2. Schematic molecular orbital diagrams, possible electronic configurations and Huckel's rules for aromaticity/antiaromaticity of singlet/triplet model tetratomic system as a general example of even-number cyclic systems.

	Schematic molecular orbital diagram	Huckel's rule for aromaticity		Huckel's rule for antiaromaticity	
		singlet coupling	triplet coupling	singlet coupling	triplet coupling
s-AO based σ-aromaticit	$-1b_{1g}$ $-$ $-1e_u$ $-1a_{1g}$	**4n+2** $\{1a_{1g}^{(2)}1e_u^{(0)}\}$ $\{1a_{1g}^{(2)}1e_u^{(4)}\}$	**4n** $\{1a_{1g}^{(2)}1e_u^{(2)}\}$	**4n** $\{1a_{1g}^{(2)}1e_u^{(2)}\}$	**4n+2** $\{1a_{1g}^{(1)}1e_u^{(1)}\}$
p-AO based σ-aromaticit	$-1a_{2g}$ $-1b_{1g}$ $-$ $-2e_u$ $-$ $-1e_u$ $-1b_{2g}$ $-1a_{1g}$	**2, 4n+4** $\{1a_{1g}^{(2)}1b_{2g}^{(0)}\}$ $\{1a_{1g}^{(2)}1b_{2g}^{(2)}\}$ $\{1a_{1g}^{(2)}1b_{2g}^{(2)}1e_u^{(4)}\}$ $\{1a_{1g}^{(2)}1b_{2g}^{(2)}1e_u^{(4)}2e_u^{(4)}\}$	**4n+2** $\{1a_{1g}^{(1)}1b_{2g}^{(1)}\}$ $\{1a_{1g}^{(2)}1b_{2g}^{(2)}1e_u^{(2)}\}$ $\{1a_{1g}^{(2)}1b_{2g}^{(2)}1e_u^{(4)}e_u^{(2)}\}$	**4n+6** $\{1a_{1g}^{(2)}1b_{2g}^{(2)}1e_u^{(2)}\}$ $\{1a_{1g}^{(2)}1b_{2g}^{(2)}1e_u^{(4)}2e_u^{(2)}\}$	**4n** $\{1a_{1g}^{(2)}1b_{2g}^{(1)}1e_u^{(1)}\}$ $\{1a_{1g}^{(2)}1b_{2g}^{(2)}1e_u^{(3)}2e_u^{(1)}\}$
p-AO based π-aromaticit	$-1b_{2u}$ $-$ $-1e_g$ $-1a_{2u}$	**4n+2** $\{1a_{2u}^{(2)}1e_g^{(0)}\}$ $\{1a_{2u}^{(2)}1e_g^{(4)}\}$	**4n** $\{1a_{2u}^{(2)}1e_g^{(2)}\}$	**4n** $\{1a_{2u}^{(2)}1e_g^{(2)}\}$	**4n+2** $\{1a_{2u}^{(1)}1e_g^{(1)}\}$
d-AO based σ-aromaticit	$-1a_{2g}$ $-1b_{1g}$ $-$ $-2e_u$ $-$ $-1e_u$ $-1b_{2g}$ $-1a_{1g}$	**2, 4n+4** $\{1a_{1g}^{(2)}1b_{2g}^{(0)}\}$ $\{1a_{1g}^{(2)}1b_{2g}^{(2)}\}$ $\{1a_{1g}^{(2)}1b_{2g}^{(2)}1e_u^{(4)}\}$ $\{1a_{1g}^{(2)}1b_{2g}^{(2)}1e_u^{(4)}2e_u^{(4)}\}$	**4n+2** $\{1a_{1g}^{(1)}1b_{2g}^{(1)}\}$ $\{1a_{1g}^{(2)}1b_{2g}^{(2)}1e_u^{(2)}\}$ $\{1a_{1g}^{(2)}1b_{2g}^{(2)}1e_u^{(4)}e_u^{(2)}\}$	**4n+6** $\{1a_{1g}^{(2)}1b_{2g}^{(2)}1e_u^{(2)}\}$ $\{1a_{1g}^{(2)}1b_{2g}^{(2)}1e_u^{(4)}2e_u^{(2)}\}$	**4n** $\{1a_{1g}^{(2)}1b_{2g}^{(1)}1e_u^{(1)}\}$ $\{1a_{1g}^{(2)}1b_{2g}^{(2)}1e_u^{(3)}2e_u^{(1)}\}$

		2, 4n+4	4n+2	4n+6	4n

d-AO based π-aromaticit

—$1a_{1u}$
—$1b_{2u}$
— —$2e_g$
— —$1e_g$
—$1b_{1u}$
—$1a_{2u}$

$\{1a_{2u}^{(2)}1b_{1u}^{(0)}\}$
$\{1a_{2u}^{(2)}1b_{1u}^{(2)}\}$
$1a_{2u}^{(2)}1b_{1u}^{(2)}1e_g^{(4)}$
$\{1a_{2u}^{(2)}1b_{1u}^{(2)}1e_g^{(4}$
$2e_g^{(4)}\}$

$\{1a_{2u}^{(2)}1b_{1u}^{(2)}1e_g^{(2}$
$)\}$
$1a_{2u}^{(2)}1b_{1u}^{(2)}1e_g^{(4)}2$
$e_g^{(2)}\}$

$\{1a_{2u}^{(1)}1b_{1u}^{(1)}\}$

$\{1a_{2u}^{(2)}1b_{1u}^{(2)}1e_g^{(2}$
$)\}$

$\{1a_{2u}^{(2)}1b_{1u}^{(2)}1e_g^{(4}$
$)2e_g^{(2)}\}$

$\{1a_{2u}^{(2)}1b_{1u}^{(1)}1e_g^{(1)}$
$\}$

$\{1a_{2u}^{(2)}1b_{1u}^{(2)}1e_g^{(3)}$
$2e_g^{(1)}\}$

		4n+2	4n	4n	4n+2

d-AO based δ-aromaticit

—$1b_{1g}$
— —$1e_u$
—$1a_{1g}$

$\{1a_{1g}^{(2)}1e_u^{(0)}\}$
$\{1a_{1g}^{(2)}1e_u^{(4)}\}$

$\{1a_{1g}^{(2)}1e_u^{(2)}\}$

$\{1a_{1g}^{(2)}1e_u^{(2)}\}$

$\{1a_{1g}^{(1)}1e_u^{(1)}\}$

		2, 4n+4	4n+2	4n+6	4n

f-AO based σ-aromaticit

—$1a_{2g}$
—$1b_{1g}$
— —$2e_u$
— —$1e_u$
—$1b_{2g}$
—$1a_{1g}$

$\{1a_{1g}^{(2)}1b_{2g}^{(0)}\}$
$\{1a_{1g}^{(2)}1b_{2g}^{(2)}\}$
$1a_{1g}^{(2)}1b_{2g}^{(2)}1e_u^{(4)}$
$\{1a_{1g}^{(2)}1b_{2g}^{(2)}1e_u^{(4}$
$2e_u^{(4)}\}$

$\{1a_{1g}^{(2)}1b_{2g}^{(2)}1e_u^{(2}$
$)\}$
$1a_{1g}^{(2)}1b_{2g}^{(2)}1e_u^{(4)}2$
$e_u^{(2)}\}$

$\{1a_{1g}^{(1)}1b_{2g}^{(1)}\}$

$\{1a_{1g}^{(2)}1b_{2g}^{(2)}1e_u^{(2}$
$)\}$

$\{1a_{1g}^{(2)}1b_{2g}^{(2)}1e_u^{(4}$
$)2e_u^{(2)}\}$

$\{1a_{1g}^{(2)}1b_{2g}^{(1)}1e_u^{(1)}$
$\}$

$\{1a_{1g}^{(2)}1b_{2g}^{(2)}1e_u^{(3)}$
$2e_u^{(1)}\}$

		2, 4n+4	4n+2	4n+6	4n

f-AO based π-aromaticit

—$1a_{1u}$
—$1b_{2u}$
— —$2e_g$
— —$1e_g$
—$1b_{1u}$
—$1a_{2u}$

$\{1a_{2u}^{(2)}1b_{1u}^{(0)}\}$
$\{1a_{2u}^{(2)}1b_{1u}^{(2)}\}$
$1a_{2u}^{(2)}1b_{1u}^{(2)}1e_g^{(4)}$
$\{1a_{2u}^{(2)}1b_{1u}^{(2)}1e_g^{(4}$
$2e_g^{(4)}\}$

$\{1a_{2u}^{(2)}1b_{1u}^{(2)}1e_g^{(2}$
$)\}$
$1a_{2u}^{(2)}1b_{1u}^{(2)}1e_g^{(4)}2$
$e_g^{(2)}\}$

$\{1a_{2u}^{(1)}1b_{1u}^{(1)}\}$

$\{1a_{2u}^{(2)}1b_{1u}^{(2)}1e_g^{(2}$
$)\}$

$\{1a_{2u}^{(2)}1b_{1u}^{(2)}1e_g^{(4}$
$)2e_g^{(2)}\}$

$\{1a_{2u}^{(2)}1b_{1u}^{(1)}1e_g^{(1)}$
$\}$

$\{1a_{2u}^{(2)}1b_{1u}^{(2)}1e_g^{(3)}$
$2e_g^{(1)}\}$

f-AO based δ-aromaticity

Energy level diagram:
$1a_{2g}$
$1b_{1g}$
$2e_u$
$1e_u$
$1b_{2g}$
$1a_{1g}$

2, 4n+4	4n+2	4n+6	4n
$\{1a_{1g}^{(2)}1b_{2g}^{(0)}\}$ $\{1a_{1g}^{(2)}1b_{2g}^{(2)}\}$ $\{1a_{1g}^{(2)}1b_{2g}^{(2)}1e_u^{(4)}\}$ $\{1a_{1g}^{(2)}1b_{2g}^{(2)}1e_u^{(4)}2e_u^{(4)}\}$	$\{1a_{1g}^{(1)}1b_{2g}^{(1)}\}$ $\{1a_{1g}^{(2)}1b_{2g}^{(2)}1e_u^{(2)}\}$ $\{1a_{1g}^{(2)}1b_{2g}^{(2)}1e_u^{(4)}2e_u^{(2)}\}$	$\{1a_{1g}^{(2)}1b_{2g}^{(2)}1e_u^{(2)}\}$ $\{1a_{1g}^{(2)}1b_{2g}^{(2)}1e_u^{(4)}2e_u^{(2)}\}$	$\{1a_{1g}^{(2)}1b_{2g}^{(1)}1e_u^{(1)}\}$ $\{1a_{1g}^{(2)}1b_{2g}^{(2)}1e_u^{(3)}2e_u^{(1)}\}$

f-AO based φ-aromaticity

Energy level diagram:
$1b_{2u}$
$1e_g$
$1a_{2u}$

4n+2	4n	4n	4n+2
$\{1a_{2u}^{(2)}1e_g^{(0)}\}$ $\{1a_{2u}^{(2)}1e_g^{(4)}\}$	$\{1a_{2u}^{(2)}1e_g^{(2)}\}$	$\{1a_{2u}^{(2)}1e_g^{(2)}\}$	$\{1a_{2u}^{(1)}1e_g^{(1)}\}$

Figure 15-1. s-AO based σ-MOs for model triatomic system.
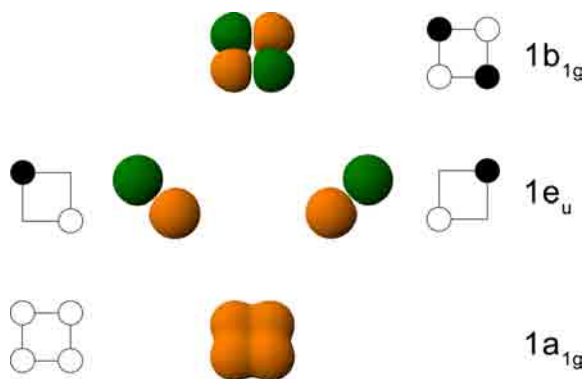
Figure 15-2. s-AO based σ-MOs for model tetratomic system.
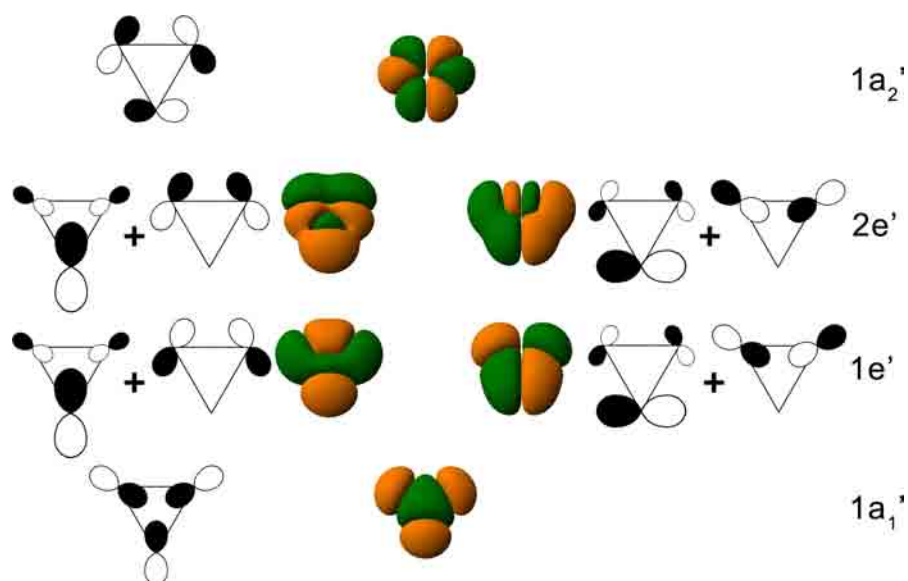
Figure 15-3. p-AO based σ-MOs for model triatomic system. Here and elsewhere molecular orbitals which are composed of both radial and tangential AOs are symbolically shown as a sum of two hypothetical MOs built out of either radial or tangential AOs.
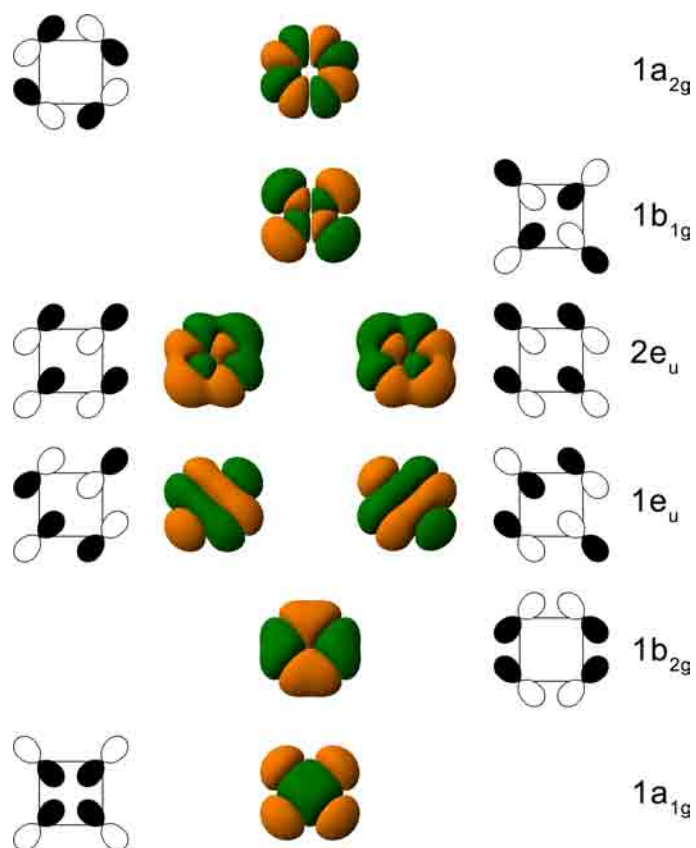
Figure 15-4. p-AO based σ-MOs for model tetratomic system.
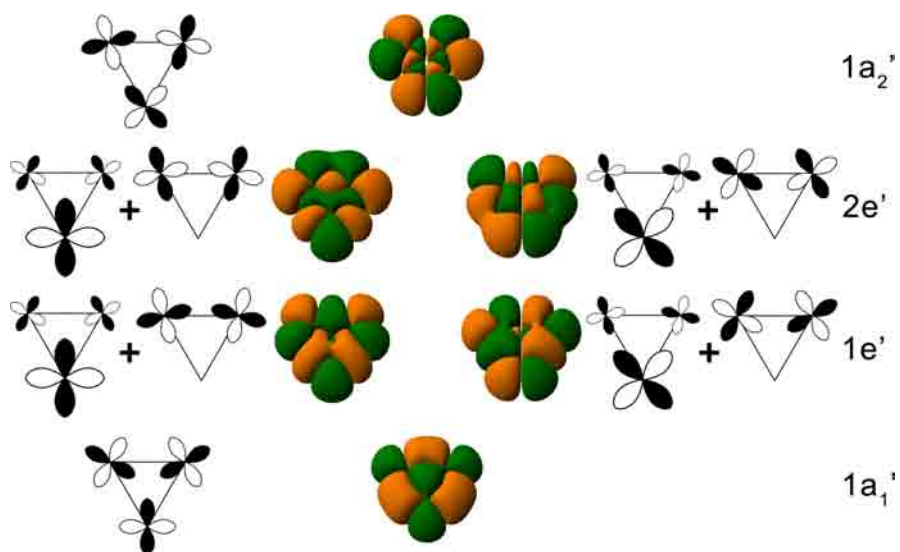
Figure 15-5. d-AO based σ-MOs for model triatomic system.
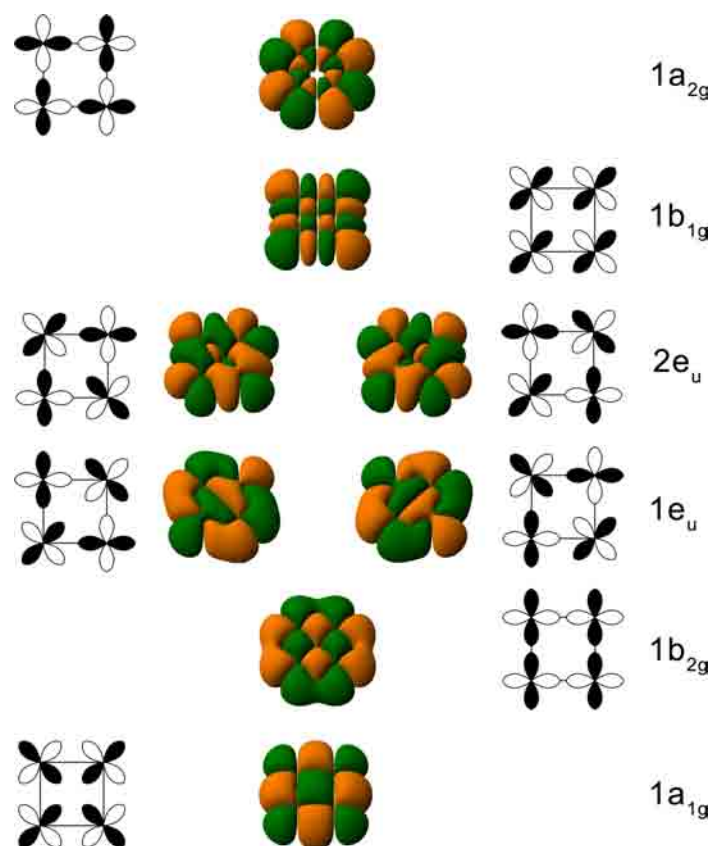
Figure 15-6. d-AO based σ-MOs for model tetratomic system.
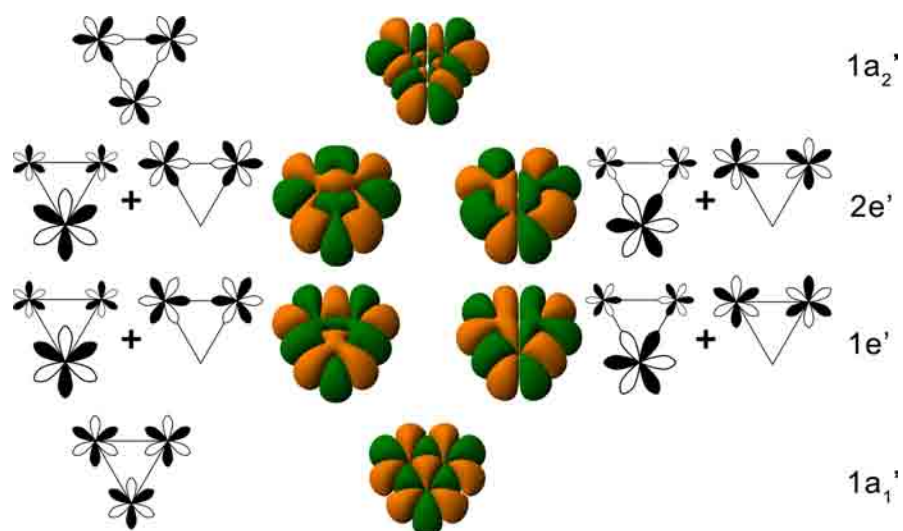
Figure 15-7. f-AO based σ-MOs for model triatomic system.
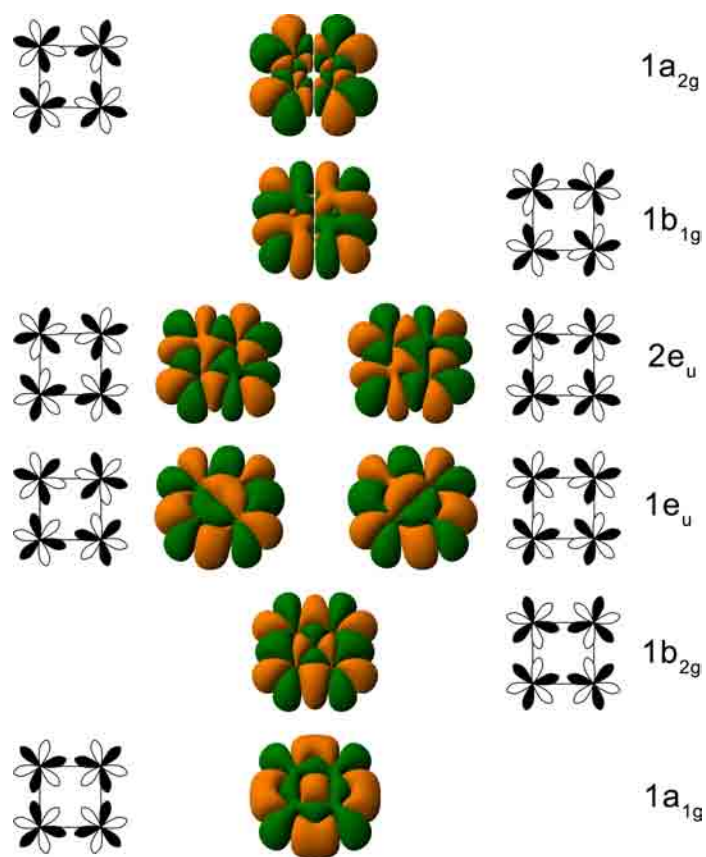
Figure15-8. f-AO based σ-MOs for model tetratomic system.
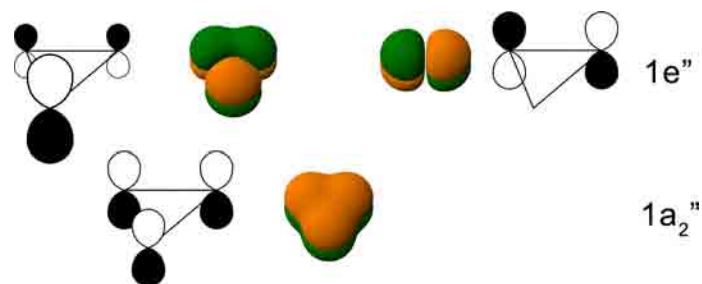
Figure15-9 p-AO based π-MOs for model triatomic system.
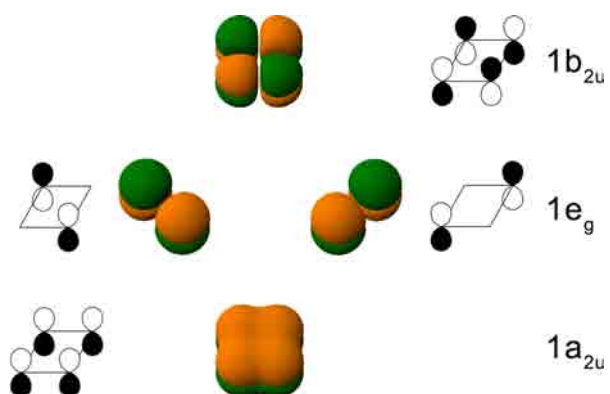
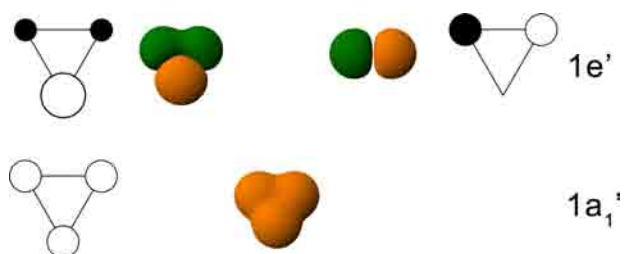**Figure15-10.** p-AO based π-MOs for model tetratomic system.
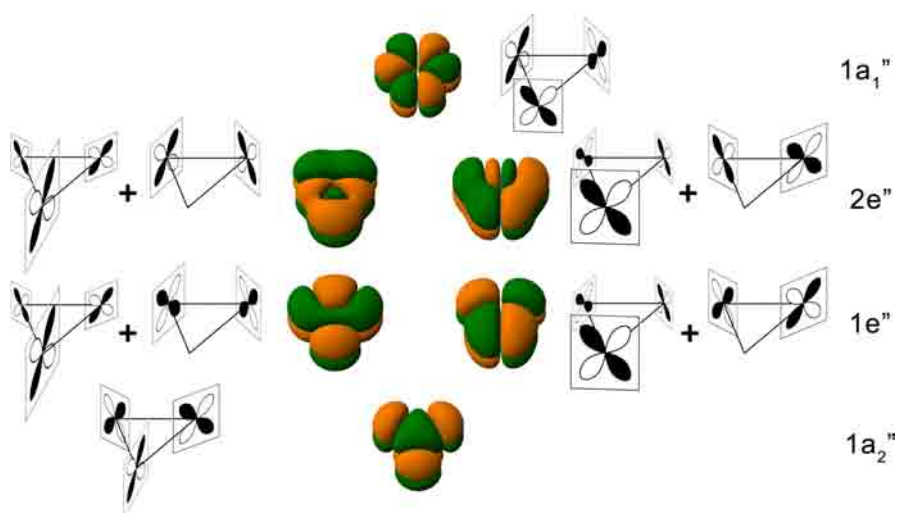
Figure15-11. d-AO based π-MOs for model triatomic system.
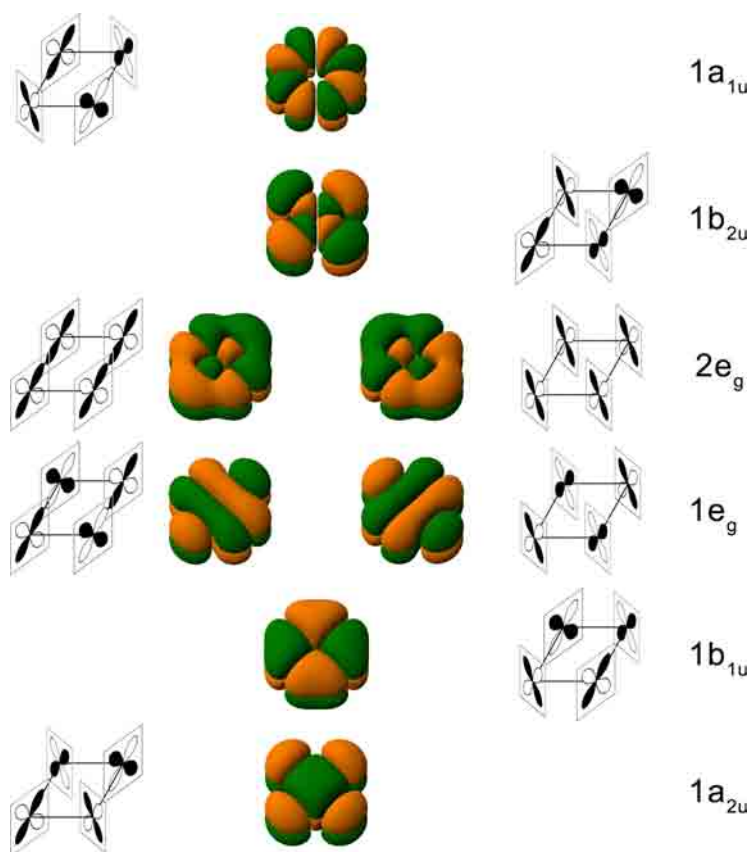
Figure15-12. d-AO based π-MOs for model tetratomic system.
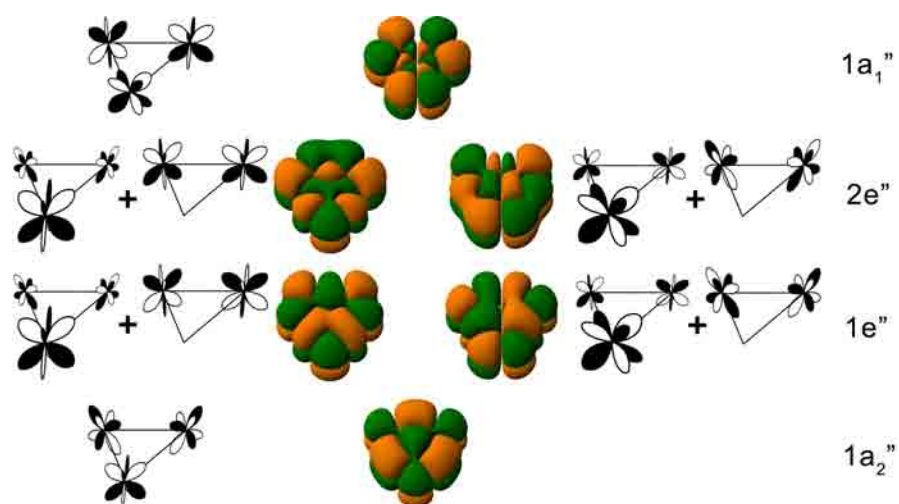
Figure15-13. f-AO based π-MOs for model triatomic system.
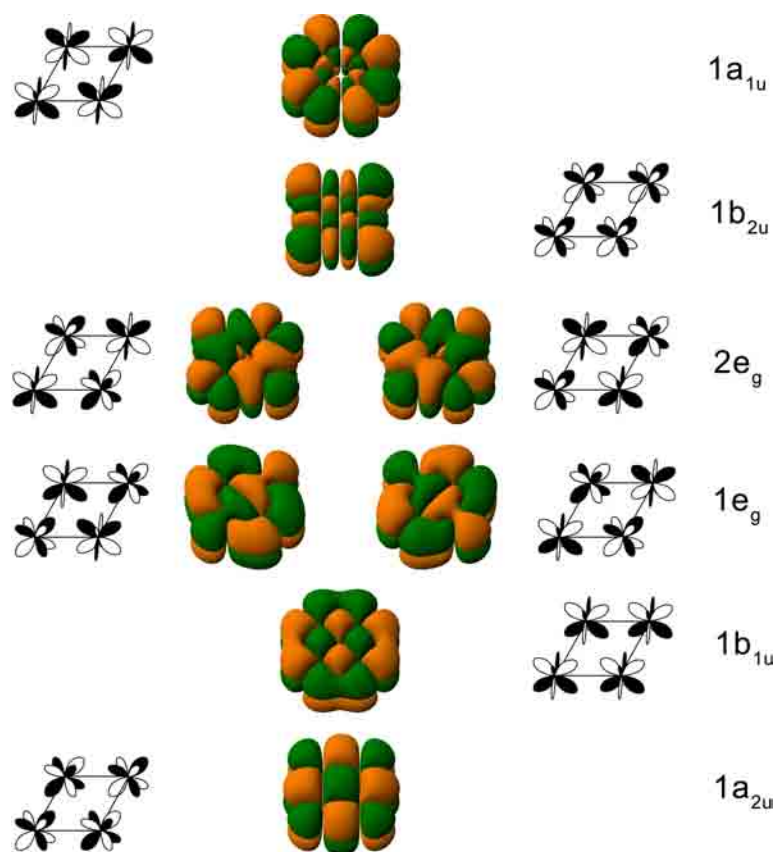
Figure15-14. f-AO based π-MOs for model tetratomic system.
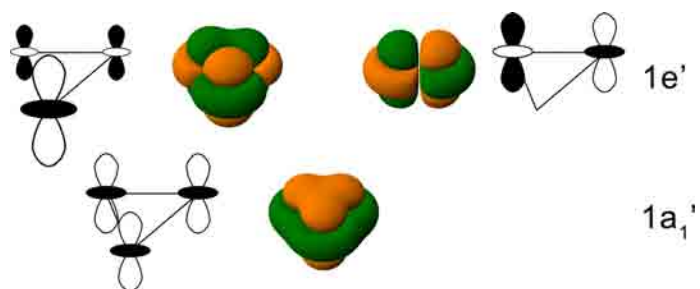
Figure15-15. d-AO based δ-MOs for model triatomic system.
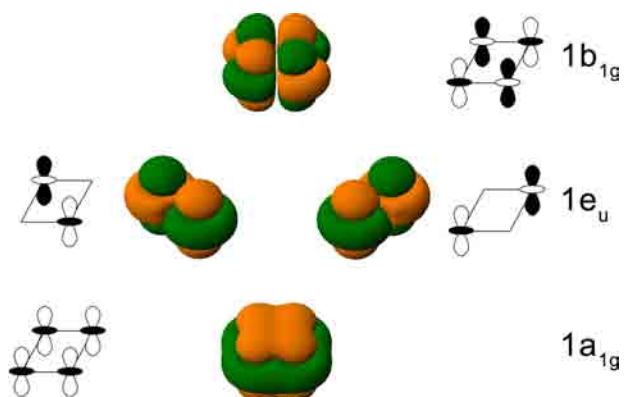
Figure15-16. d-AO based δ-MOs for model tetratomic system.
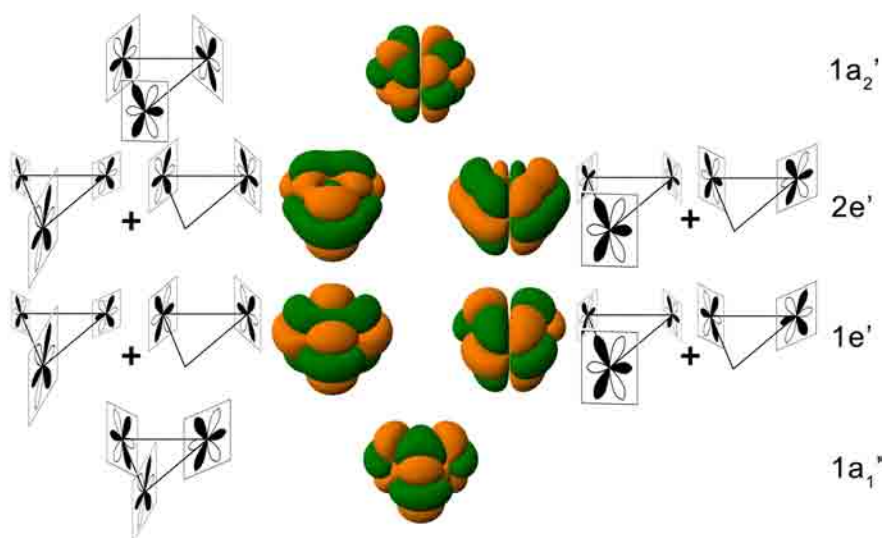
Figure15-17. f-AO based δ-MOs for model triatomic system.
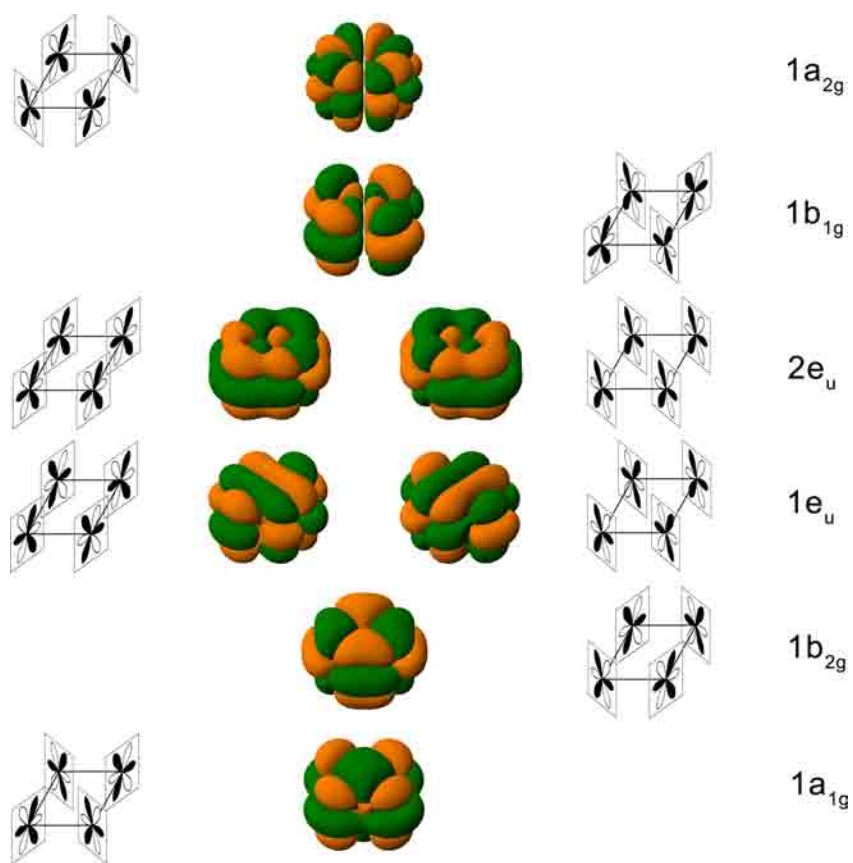
Figure15-18. f-AO based δ-MOs for model tetratomic system.
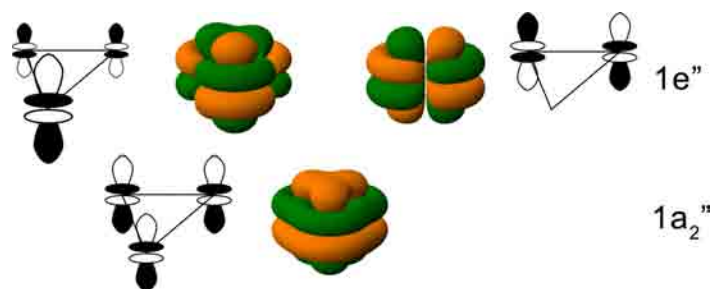
Figure15-19. f-AO based φ-MOs for model triatomic system.
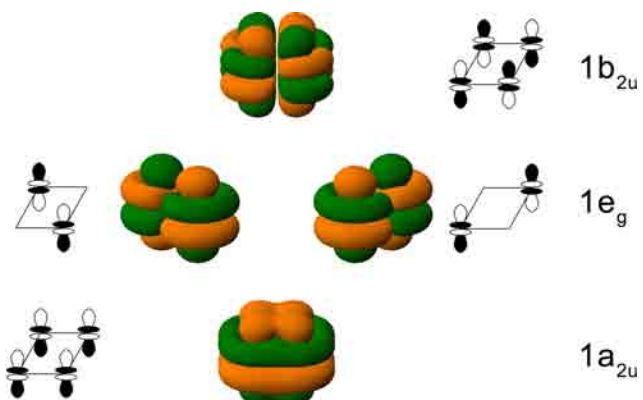
Figure15-20. f-AO based φ-MOs for model tetratomic system.
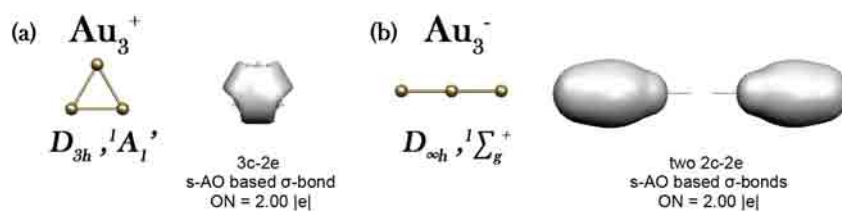
**Figure15-21.** (a) Geometric structure and 3c-2e s-AO based σ-bond of σ-aromatic Au_3^+ cluster; (b) Geometric structure and two 2c-2e s-AO based σ-bonds of σ-antiaromatic Au_3^- cluster.
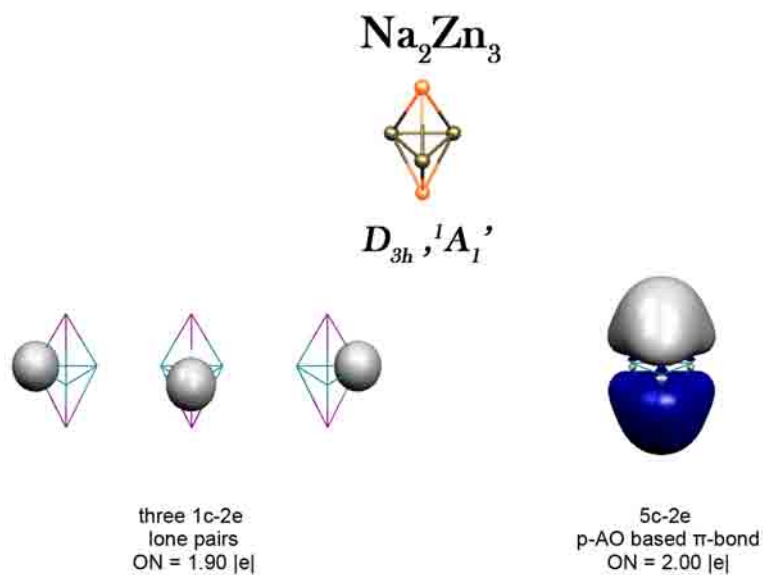
Figure15-22. Geometric structure, three 1c-2e lone pairs, and 5c-2e p-AO based π-bond of π-aromatic Na_2Zn_3 cluster.

$$Hg_4^{6-}$$

$$D_{4h}, {}^1A_{1g}$$

| four 1c-2e lone pairs ON = 1.94 \|e\| | 4c-2e p-AO based σ_r-bond ON = 2.00 \|e\| | 4c-2e p-AO based σ_t-bond ON = 2.00 \|e\| | 4c-2e p-AO based π-bond ON = 2.00 \|e\| |
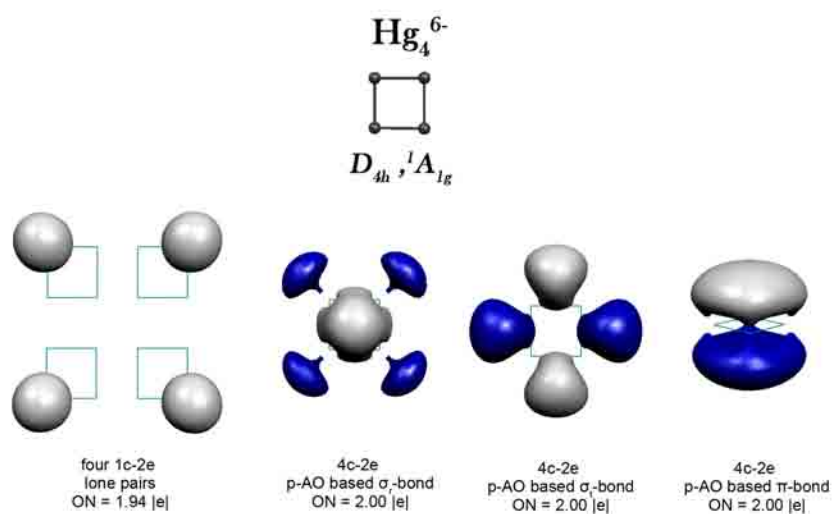
Figure 15-23. Geometric structure, four 1c-2e lone pairs, 4c-2e p-AO based σ_r-bond, 4c-2e p-AO based σ_t-bond, and 4c-2e p-AO based π-bond of doubly σ- and π-aromatic Hg_4^{6-} cluster.
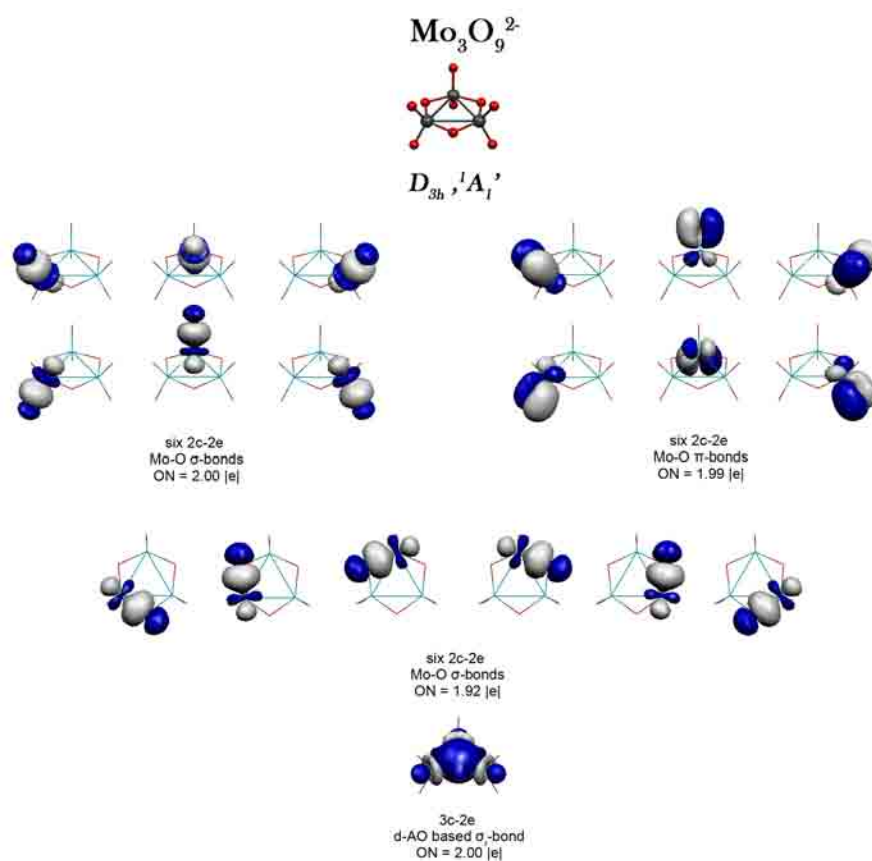
Figure15-24. Geometric structure, six 2c-2e Mo-O σ-bonds, six 2c-2e Mo-O π-bonds, six 2c-2e Mo-O σ-bonds, and 3c-2e d-AO based σ_r-bond of σ-aromatic $Mo_3O_9^{2-}$ cluster.
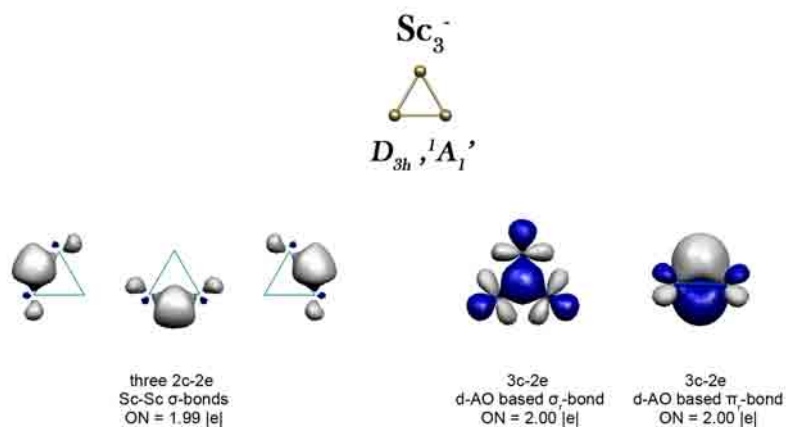
Figure15-25. Geometric structure, three 2c-2e Sc-Sc σ-bonds, 3c-2e d-AO based σ$_r$-bond, 3c-2e d-AO based π$_r$-bond of doubly σ- and π-aromatic Sc$_3^-$ cluster.
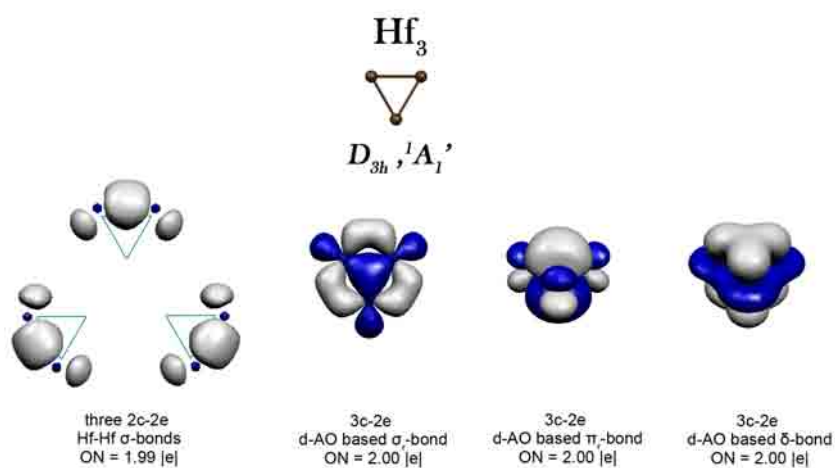
Figure15-26. Geometric structure, three 2c-2e Hf-Hf σ-bonds, 3c-2e d-AO based σ$_r$-bond, 3c-2e d-AO based π$_r$-bond, and 3c-2e d-AO based δ-bond of triply σ-, π- and δ-aromatic Hf$_3$ cluster.

CHAPTER 16

SUMMARY

The main result of dissertation is development of model of chemical bonding in clusters on example of Al_xN^- and Al_xN, mixed carbon-boron, and transition-metal clusters. This represents the first step toward rational design of nano- and subnano-structures with tailored properties.

This is the first systematic theoretical study of Al_xN and Al_xN^- clusters. It was shown that for small clusters Al-N interactions define the structure of clusters while increasing the number of Al atoms results in increasing of Al-Al interactions, which start to be important structure-forming factors in Al_5N^-. The global minimum structure of Al_5N^- is built upon the square-planar Al_4N^- structure with the additional Al atom boned to one of its four edges outside the first coordination layer. However, a 3D structure, which can be viewed as a tetrahedral Al_4 cluster bound to an AlN unit, was found to be a low-lying isomer and was also present in the PES spectra of Al_5N^-. For Al_6N^-, we found two close low-lying isomers, which appear to optimize both the Al-Al and Al-N interactions. For Al_7N^- and Al_7N, our study found only one dominating isomer in which the N atom has high coordination number of 6 and 7, respectively. Particularly for Al_7N, the seven Al atoms are all in the first coordination sphere and bound to the N atom, which seems to optimize Al-N interactions. We have also shown that the global minimum structures of the Al_6N^- and Al_7N^- can be viewed as being evolved from the N-centered Al_6N^{3-} octahedron.

For Al_8N^-, this Al_6N^{3-} octahedron is no longer found as a building block in the two lowest-lying isomers. Instead, the two lowest of Al_8N^- can both be viewed as a distorted Al_4N^- square bound to four additional Al atoms. Unlike the 3D structures of Al_6N^- and Al_7N^-, the Al-Al interactions seem to be dominating in Al_8N^-. Thus, the more complicated Al-Al and Al-N interactions in the larger Al_8N^- cluster are responsible for its structural diversity. It should also be pointed out that in all the low-lying isomers for Al_8N^- we found that the effective atomic charges on the N atom vary from -2.1 |e| to -2.5 |e|, indicating the formation of the nearly complete shell $2s^2 2p^6$ in the ionic limit (N^{3-}).

From our joint photoelectron spectroscopic and ab initio study we have demonstrated that carbon avoids central positions in CB_6^{2-}, CB_7^-, CB_8, and CB_8^-. We have developed a chemical bonding model (using AdNDP analysis), which explains why carbon avoids the central position in those species. According to this model, in the wheel type structures the central atom is involved in delocalized bonding only, while atoms at the periphery of the wheel structure are involved in both delocalized bonding and 2c-2e peripheral σ-bonding. The carbon atom is more electronegative than boron atoms and favors peripheral positions where it can participate in 2c-2e σ-bonding. Thus, wheel-type structures with a boron ring are not appropriate for designing planar molecules with a hypercoordinate central carbon. However, if the central atom is more electropositive than boron, then the wheel type structures are stable and can be either global minimum or low-lying isomers. AdNDP analysis of the chemical bonding in the CAl_4^{2-} dianion showed that in this case, the favorable central position of the carbon atom is due to essentially ionic bonding between a central carbon C^{4-} anion and an Al_4^{2+} cation with contributions

from delocalized σ-bonding and weakly delocalized π-bonding. In order to design a chemical species with a central hypercoordinate carbon atom, one should consider electropositive ligands, which would have lone pairs instead of forming 2c-2e peripheral bonds. Hence, we presented a chemical bonding model capable of rationalizing and predicting structures either with a boron ring or a central planar carbon.

We utilized the conception of aromaticity to transition metal systems. The striking feature of chemical bonding in transition-metal systems is the possibility of the multi-fold nature of aromaticity, antiaromaticity and conflicting aromaticity. If d atomic orbitals are involved in chemical bonding σ-tangential, σ-radial, π-tangential, π-radial and δ-aromaticity/antiaromaticity could occur. In this case, there can be multiple (σ-, π- and δ-) aromaticity, multiple (σ-, π- and δ-) antiaromaticity and conflicting aromaticity (simultaneous aromaticity and antiaromaticity involving σ, π and δ bonds).

Separate sets of counting rules have been proposed for cyclic transition-metal systems to account for the three types of d-AO aromaticity. $Ta_3O_3^-$ in $^1A_1'$ D_{3h} state was shown to be the first example of δ-aromatic compound. Hf_3 in $^1A_1'$ D_{3h} state is the first example of triply (σ, π, δ)-aromatic system. We believe that the ideas of aromaticity, antiaromaticity, and conflicting aromaticity will be valuable tools for understanding of the chemical bonding in transition-metal systems.

Coalescence Kick Method for finding global minima structure and low-lying isomers was implemented and tested. Tests showed that it works faster than other methodds and provides reliable results. It finds global minima even for such large clusters as B_{17}^- and B_{19}^- in reasonable time.

APPENDIX

PERMISSIONS

American Chemical Society's Policy on Theses and Dissertations

If your university requires a signed copy of this letter see contact information below.

Thank you for your request for permission to include **your** paper(s) or portions of text from **your** paper(s) in your thesis. Permission is now automatically granted; please pay special attention to the implications paragraph below. The Copyright Subcommittee of the Joint Board/Council Committees on Publications approved the following:

Copyright permission for published and submitted material from theses and dissertations
ACS extends blanket permission to students to include in their theses and dissertations their own articles, or portions thereof, that have been published in ACS journals or submitted to ACS journals for publication, provided that the ACS copyright credit line is noted on the appropriate page(s).

Publishing implications of electronic publication of theses and dissertation material
Students and their mentors should be aware that posting of theses and dissertation material on the Web prior to submission of material from that thesis or dissertation to an ACS journal <u>may</u> affect publication in that journal. Whether Web posting is considered prior publication may be evaluated on a case-by-case basis by the journal's editor. If an ACS journal editor considers Web posting to be "prior publication", the paper will not be accepted for publication in that journal. If you intend to submit your unpublished paper to ACS for publication, check with the appropriate editor prior to posting your manuscript electronically.

If your paper has **not** yet been published by ACS, we have no objection to your including the text or portions of the text in your thesis/dissertation in **print and microfilm formats**; please note, however, that electronic distribution or Web posting of the unpublished paper as part of your thesis in electronic formats might jeopardize publication of your paper by ACS. Please print the following credit line on the first page of your article: "Reproduced (or 'Reproduced in part') with permission from [JOURNAL NAME], in press (or 'submitted for publication'). Unpublished work copyright [CURRENT YEAR] American Chemical Society." Include appropriate information.

If your paper has already been published by ACS and you want to include the text or portions of the text in your thesis/dissertation in **print or microfilm formats**, please print the ACS copyright credit line on the first page of your article: "Reproduced (or 'Reproduced in part') with permission from [FULL REFERENCE CITATION.] Copyright [YEAR] American Chemical Society." Include appropriate information.

Submission to a Dissertation Distributor: If you plan to submit your thesis to <u>UMI or to another dissertation distributor</u>, you should not include the unpublished ACS paper in your thesis if the thesis will be disseminated electronically, until ACS has published your paper. After publication of the paper by ACS, you may release the <u>entire</u> thesis (**not the individual ACS article by itself**) for electronic dissemination through the distributor; ACS's copyright credit line should be printed on the first page of the ACS paper.

Use on an Intranet: The inclusion of your ACS unpublished or published manuscript is permitted in your thesis in print and microfilm formats. If ACS has published your paper you may include the manuscript in your thesis on an intranet that is <u>not</u> publicly available. Your ACS article cannot be posted electronically on a publicly available medium (i.e. one that is not password protected), such as but not limited to, electronic archives, Internet, library server, etc. The only material from your paper that can be posted on a public electronic medium is the article abstract, figures, and tables, and you may link to the article's DOI or post the article's author-directed URL link provided by ACS. This paragraph does not pertain to the dissertation distributor paragraph above.

Questions? Call +1 202/872-4368/4367. Send e-mail to copyright@acs.org or fax to +1 202-776-8112.   10/10/03, 01/15/04, 06/07/06

⊠aggiemail   Boris Averkiev <boris.averkiev@aggiemail.usu.edu>

AW: Form: Permission request
2 messages

Rights DE <RIGHTS-and-LICENCES@wiley-vch.de>   **Mon, Apr 6, 2009 at 12:33 AM**

To: "boris.averkiev@aggiemail.usu.edu" <boris.averkiev@aggiemail.usu.edu>

Dear Customer

Thank you for your request.

We hereby grant permission for the requested use expected that due credit is given to the original source.
For material published before 2007 additionally: Please note that the author's permission is also required.

Please note that we only grant rights for a printed version, but not the rights for an electronic/ online/ web/ microfiche publication, but you are free to create a link to the article in question which is posted on our website (http://www3.interscience.wiley.com)

If material appears within our work with credit to another source, authorisation from that source must be obtained.

Credit must include the following components:
- Books: Author(s)/ Editor(s) Name(s): Title of the Book. Page(s). Publication year. Copyright Wiley-VCH Verlag GmbH & Co. KGaA. Reproduced with permission.

- Journals: Author(s) Name(s): Title of the Article. Name of the Journal. Publication year. Volume. Page(s). Copyright Wiley-VCH Verlag GmbH & Co. KGaA. Reproduced with permission.

With kind regards

Bettina Loycke
****
Bettina Loycke
Copyright & Licensing Manager
Wiley-VCH Verlag GmbH & Co. KGaA
Boschstr. 12

Boschstr. 12
69469 Weinheim
Germany

Phone: +49 (0) 62 01- 606 - 280
Fax: +49 (0) 62 01 - 606 - 332
Email: rights@wiley-vch.de
_____

Wiley-VCH Verlag GmbH & Co. KGaA
Location of the Company: Weinheim
Chairman of the Supervisory Board: Stephen Michael Smith
Trade Register: Mannheim, HRB 432833
General Partner: John Wiley & Sons GmbH, Location: Weinheim
Trade Register Mannheim, HRB 432296
Managing Directors : Christopher J. Dicks, Bijan Ghawami, William Pesce

-----Ursprüngliche Nachricht-----
Von: boris.averkiev@aggiemail.usu.edu [mailto:boris.averkiev@aggiemail.usu.edu]
Gesendet: Sonntag, 5. April 2009 02:18
An: Rights DE
Betreff: Form: Permission request

Form: Permission request
Path: Service Permission Request
Language: en

Adress
First Name: Boris
Surname: Averkiev
Street: 684 1/2 East 400 North #2
Zip code: 84321
City: Logan, Utah
Country: USA
Fax: 1-(435) 797-3390
E-mail: boris.averkiev@aggiemail.usu.edu
Media Type: journal
Author or Editor:
ISBN:
Journal Title: Angew. Chem. Int. Ed
Journal Month: June
Journal Year: 2007
Journal Volume: 46
Media Type: journal
Page No: 4550 - 4553
Website or Intranet: no
University/Institute: Utah State University
Instructor: Boldyrev

Course: for PhD Dissertation
Wiley Author: yes

Rights DE <RIGHTS-and-LICENCES@wiley-vch.de>   **Mon, Apr 6, 2009 at 12:35 AM**

To: "boris.averkiev@aggiemail.usu.edu" <boris.averkiev@aggiemail.usu.edu>

Dear Customer

Thank you for your request.

We hereby grant permission for the requested use expected that due credit is given to the original source.
For material published before 2007 additionally: Please note that the author's permission is also required.

Please note that we only grant rights for a printed version, but not the rights for an electronic/ online/ web/ microfiche publication, but you are free to create a link to the article in question which is posted on our website (http://www3.interscience.wiley.com)

If material appears within our work with credit to another source, authorisation from that source must be obtained.

Credit must include the following components:
- Books: Author(s)/ Editor(s) Name(s): Title of the Book. Page(s). Publication year. Copyright Wiley-VCH Verlag GmbH & Co. KGaA. Reproduced with permission.

- Journals: Author(s) Name(s): Title of the Article. Name of the Journal. Publication year. Volume. Page(s). Copyright Wiley-VCH Verlag GmbH & Co. KGaA. Reproduced with permission.

With kind regards

Bettina Loycke
****
Bettina Loycke
Copyright & Licensing Manager
Wiley-VCH Verlag GmbH & Co. KGaA
Boschstr. 12
69469 Weinheim
Germany

Phone: +49 (0) 62 01- 606 - 280
Fax: +49 (0) 62 01 - 606 - 332

Email: rights@wiley-vch.de
_____

Wiley-VCH Verlag GmbH & Co. KGaA
Location of the Company: Weinheim
Chairman of the Supervisory Board: Stephen Michael Smith
Trade Register: Mannheim, HRB 432833
General Partner: John Wiley & Sons GmbH, Location: Weinheim
Trade Register Mannheim, HRB 432296
Managing Directors : Christopher J. Dicks, Bijan Ghawami, William Pesce

-----Ursprüngliche Nachricht-----
Von: boris.averkiev@aggiemail.usu.edu [mailto:boris.averkiev@aggiemail.usu.edu]
Gesendet: Samstag, 4. April 2009 01:23
An: Rights DE
Betreff: Form: Permission request

Form: Permission request
Path: Service Permission Request
Language: en

Adress
First Name: Boris
Surname: Averkiev
Street: 684 1/2 East 400 North #2
Zip code: 84321
City: Logan, Utah
Country: USA
Fax:
E-mail: boris.averkiev@aggiemail.usu.edu
Media Type: journal
Author or Editor:
ISBN:
Journal Title: Angew. Chem. Int. Ed
Journal Month: June
Journal Year: 2007
Journal Volume: 46
Media Type: journal
Page No: 4277-4280
Website or Intranet: no
University/Institute: Utah State University
Instructor: Boldyrev
Course: for PhD Dissertation
Wiley Author: yes

Boris Averkiev <boris.averkiev@aggiemail.usu.edu>

RE: Permission Request Form: Boris Averkiev

1 message

CONTRACTS-COPYRIGHT (shared) <Contracts-Copyright@rsc.org>   **Thu, Jun 25, 2009 at 12:50 AM**

To: "boris.averkiev@aggiemail.usu.edu" <boris.averkiev@aggiemail.usu.edu>

Dear Mr Averkiev

The Royal Society of Chemistry (RSC) hereby grants permission for the use of your paper(s) specified below in the printed and microfilm version of your thesis. You may also make available the PDF version of your paper(s) that the RSC sent to the corresponding author(s) of your paper(s) upon publication of the paper(s) in the following ways: in your thesis via any website that your university may have for the deposition of theses, via your university's Intranet or via your own personal website. We are however unable to grant you permission to include the PDF version of the paper(s) on its own in your institutional repository. The Royal Society of Chemistry is a signatory to the STM Guidelines on Permissions (available on request).

Please note that if the material specified below or any part of it appears with credit or acknowledgement to a third party then you must also secure permission from that third party before reproducing that material.

Please ensure that the thesis states the following:

Reproduced by permission of the PCCP Owner Societies

and include a link to the article on the Royal Society of Chemistry's website.

Please ensure that your co-authors are aware that you are including the paper in your thesis.

Regards

Gill Cockhead

Contracts & Copyright Executive

Gill Cockhead (Mrs), Contracts & Copyright Executive

Royal Society of Chemistry, Thomas Graham House

Science Park, Milton Road, Cambridge CB4 0WF, UK

Tel +44 (0) 1223 432134, Fax +44 (0) 1223 423623

http://www.rsc.org

-----Original Message-----
From: boris.averkiev@aggiemail.usu.edu [mailto:boris.averkiev@aggiemail.usu.edu]
Sent: 24 June 2009 22:39
To: CONTRACTS-COPYRIGHT (shared)
Subject: Permission Request Form: Boris Averkiev

  Name   : Boris Averkiev

Address :

 Department of Chemistry & Biochemistry

Utah State University

0300 Old Main Hill

Logan, UT 84322-0300

Tel   : 1 (435) 797-7507

Fax   : 1 (435) 797-3390

Email   : boris.averkiev@aggiemail.usu.edu

 I am preparing the following work for publication:

 Article/Chapter Title :

Journal/Book Title   : "GEOMETRY AND ELECTRONIC STRUCTURE OF DOPED CLUSTERS VIA THE COALESCENCE KICK METHOD"

Editor/Author(s)   : Boris Averkiev

Publisher   : Utah State University

I would very much appreciate your permission to use the following material:

Journal/Book Title   : Phys. Chem. Chem. Phys.

Editor/Author(s)   : Dmitry Yu. Zubarev, Boris B. Averkiev, Hua-Jin Zhai, Lai-Sheng Wang and Alexander I. Boldyrev

Volume Number   : 10

Year of Publication   : 2008

Description of Material :

Page(s)   : 257 - 267

Any Additional Comments   :

I would like to use this article co-authored by me, as a chapter in my PhD Dissertation entitled "GEOMETRY AND ELECTRONIC STRUCTURE OF DOPED CLUSTERS VIA THE COALESCENCE KICK METHOD"

AMERICAN INSTITUTE OF PHYSICS LICENSE
TERMS AND CONDITIONS

Jul 21, 2009

This is a License Agreement between Boris Averkiev ("You") and American Institute of Physics ("American Institute of Physics") provided by Copyright Clearance Center ("CCC"). The license consists of your order details, the terms and conditions provided by American Institute of Physics, and the payment terms and conditions.

All payments must be made in full to CCC. For payment instructions, please see information listed at the bottom of this form.

License Number	2211720614534
License date	Jun 18, 2009
Licensed content publisher	American Institute of Physics
Licensed content publication	Journal of Chemical Physics
Licensed content title	Planar nitrogen-doped aluminum clusters Al[sub x]N[sup -] (x = 3--5)
Licensed content author	Boris B. Averkiev, Alexander I. BoldyrevXi Li, Lai-Sheng Wang
Licensed content date	Sep 28, 2006
Volume number	125
Issue number	12
Type of Use	Thesis/Dissertation
Requestor type	Author (original article)
Format	Print and electronic
Portion	Excerpt (> 800 words)
Will you be translating?	No

Order reference number	1
Title of your thesis / dissertation	GEOMETRY AND ELECTRONIC STRUCTURE OF DOPED CLUSTERS VIA THE COALESCENCE KICK METHOD
Expected completion date	Jul 2009
Estimated size (number of pages)	326
Total	0.00 USD

Terms and Conditions

American Institute of Physics -- Terms and Conditions: Permissions Uses

American Institute of Physics ("AIP") hereby grants to you the non-exclusive right and license to use and/or distribute the Material according to the use specified in your order, on a one-time basis, for the specified term, with a maximum distribution equal to the number that you have ordered. Any links or other content accompanying the Material are not the subject of this license.

1. You agree to include the following copyright and permission notice with the reproduction of the Material: "Reprinted with permission from [FULL CITATION]. Copyright [PUBLICATION YEAR], American Institute of Physics." For an article, the copyright and permission notice must be printed on the first page of the article or book chapter. For photographs, covers, or tables, the copyright and permission notice may appear with the Material, in a footnote, or in the reference list.

2. If you have licensed reuse of a figure, photograph, cover, or table, it is your responsibility to ensure that the material is original to AIP and does not contain the copyright of another entity, and that the copyright notice of the figure, photograph, cover, or table does not indicate that it was reprinted by AIP, with permission, from another source. Under no circumstances does AIP, purport or intend to grant permission to reuse material to which it does not hold copyright.

3. You may not alter or modify the Material in any manner. You may translate the Material into another language only if you have licensed translation rights. You may not use the Material for promotional purposes. AIP reserves all rights not specifically granted herein.

4. The foregoing license shall not take effect unless and until AIP or its agent, Copyright Clearance Center, receives the Payment in accordance with Copyright Clearance Center Billing and Payment Terms and Conditions, which are incorporated herein by reference.

5. AIP or the Copyright Clearance Center may, within two business days of granting this license, revoke the license for any reason whatsoever, with a full refund payable to you. Should you violate the terms of this license at any time, AIP, American Institute of Physics, or Copyright Clearance Center may revoke the license with no refund to you. Notice of such revocation will be made using the contact information provided by you. Failure to receive such notice will not nullify the revocation.

6. AIP makes no representations or warranties with respect to the Material. You agree to indemnify and hold harmless AIP, American Institute of Physics, and their officers, directors, employees or agents from and against any and all claims arising out of your use of the Material other than as

specifically authorized herein.

7. The permission granted herein is personal to you and is not transferable or assignable without the prior written permission of AIP. This license may not be amended except in a writing signed by the party to be charged.

8. If purchase orders, acknowledgments or check endorsements are issued on any forms containing terms and conditions which are inconsistent with these provisions, such inconsistent terms and conditions shall be of no force and effect. This document, including the CCC Billing and Payment Terms and Conditions, shall be the entire agreement between the parties relating to the subject matter hereof.

This Agreement shall be governed by and construed in accordance with the laws of the State of New York. Both parties hereby submit to the jurisdiction of the courts of New York County for purposes of resolving any disputes that may arise hereunder.

Gratis licenses (referencing $0 in the Total field) are free. Please retain this printable license for your reference. No payment is required.

If you would like to pay for this license now, please remit this license along with your payment made payable to "COPYRIGHT CLEARANCE CENTER" otherwise you will be invoiced within 30 days of the license date. Payment should be in the form of a check or money order referencing your account number and this license number 2211720614534.
If you would prefer to pay for this license by credit card, please go to http://www.copyright.com/creditcard to download our credit card payment authorization form.

AMERICAN INSTITUTE OF PHYSICS LICENSE
TERMS AND CONDITIONS

Jul 21, 2009

This is a License Agreement between Boris Averkiev ("You") and American Institute of Physics ("American Institute of Physics") provided by Copyright Clearance Center ("CCC"). The license consists of your order details, the terms and conditions provided by American Institute of Physics, and the payment terms and conditions.

All payments must be made in full to CCC. For payment instructions, please see information listed at the bottom of this form.

License Number	2211720929300
License date	Jun 18, 2009
Licensed content publisher	American Institute of Physics
Licensed content publication	Journal of Chemical Physics
Licensed content title	Experimental and theoretical investigation of three-dimensional nitrogen-doped aluminum clusters Al[sub 8]N[sup -] and Al[sub 8]N
Licensed content author	Lei-Ming Wang, Wei Huang, Lai-Sheng Wang, et al.
Licensed content date	Apr 7, 2009
Volume number	130
Issue number	13
Type of Use	Thesis/Dissertation
Requestor type	Author (original article)
Format	Print and electronic
Portion	Excerpt (> 800 words)
Will you be translating?	No

Order reference number	2
Title of your thesis / dissertation	GEOMETRY AND ELECTRONIC STRUCTURE OF DOPED CLUSTERS VIA THE COALESCENCE KICK METHOD
Expected completion date	Jul 2009
Estimated size (number of pages)	326
Total	0.00 USD

Terms and Conditions

American Institute of Physics -- Terms and Conditions: Permissions Uses

American Institute of Physics ("AIP") hereby grants to you the non-exclusive right and license to use and/or distribute the Material according to the use specified in your order, on a one-time basis, for the specified term, with a maximum distribution equal to the number that you have ordered. Any links or other content accompanying the Material are not the subject of this license.

1. You agree to include the following copyright and permission notice with the reproduction of the Material: "Reprinted with permission from [FULL CITATION]. Copyright [PUBLICATION YEAR], American Institute of Physics." For an article, the copyright and permission notice must be printed on the first page of the article or book chapter. For photographs, covers, or tables, the copyright and permission notice may appear with the Material, in a footnote, or in the reference list.

2. If you have licensed reuse of a figure, photograph, cover, or table, it is your responsibility to ensure that the material is original to AIP and does not contain the copyright of another entity, and that the copyright notice of the figure, photograph, cover, or table does not indicate that it was reprinted by AIP, with permission, from another source. Under no circumstances does AIP, purport or intend to grant permission to reuse material to which it does not hold copyright.

3. You may not alter or modify the Material in any manner. You may translate the Material into another language only if you have licensed translation rights. You may not use the Material for promotional purposes. AIP reserves all rights not specifically granted herein.

4. The foregoing license shall not take effect unless and until AIP or its agent, Copyright Clearance Center, receives the Payment in accordance with Copyright Clearance Center Billing and Payment Terms and Conditions, which are incorporated herein by reference.

5. AIP or the Copyright Clearance Center may, within two business days of granting this license, revoke the license for any reason whatsoever, with a full refund payable to you. Should you violate the terms of this license at any time, AIP, American Institute of Physics, or Copyright Clearance Center may revoke the license with no refund to you. Notice of such revocation will be made using the contact information provided by you. Failure to receive such notice will not nullify the revocation.

6. AIP makes no representations or warranties with respect to the Material. You agree to indemnify and hold harmless AIP, American Institute of Physics, and their officers, directors, employees or agents from and against any and all claims arising out of your use of the Material

other than as specifically authorized herein.

7. The permission granted herein is personal to you and is not transferable or assignable without the prior written permission of AIP. This license may not be amended except in a writing signed by the party to be charged.

8. If purchase orders, acknowledgments or check endorsements are issued on any forms containing terms and conditions which are inconsistent with these provisions, such inconsistent terms and conditions shall be of no force and effect. This document, including the CCC Billing and Payment Terms and Conditions, shall be the entire agreement between the parties relating to the subject matter hereof.

This Agreement shall be governed by and construed in accordance with the laws of the State of New York. Both parties hereby submit to the jurisdiction of the courts of New York County for purposes of resolving any disputes that may arise hereunder.

Gratis licenses (referencing $0 in the Total field) are free. Please retain this printable license for your reference. No payment is required.

If you would like to pay for this license now, please remit this license along with your payment made payable to "COPYRIGHT CLEARANCE CENTER" otherwise you will be invoiced within 30 days of the license date. Payment should be in the form of a check or money order referencing your account number and this license number 2211720929300.
If you would prefer to pay for this license by credit card, please go to
http://www.copyright.com/creditcard to download our credit card payment authorization form.

SPRINGER LICENSE
TERMS AND CONDITIONS

Jul 21, 2009

This is a License Agreement between Boris Averkiev ("You") and Springer ("Springer") provided by Copyright Clearance Center ("CCC"). The license consists of your order details, the terms and conditions provided by Springer, and the payment terms and conditions.

All payments must be made in full to CCC. For payment instructions, please see information listed at the bottom of this form.

License Number	2212071302934
License date	Jun 18, 2009
Licensed content publisher	Springer
Licensed content publication	Russian Journal of General Chemistry
Licensed content title	Theoretical design of planar molecules with a nona- and decacoordinate central atom
Licensed content author	B. B. Averkiev
Licensed content date	Apr 1, 2008
Volume number	78
Issue number	4
Type of Use	Thesis/Dissertation
Portion	Full text
Number of copies	5
Author of this Springer article	Yes and you are a contributor of the new work
Country of republication	other
Order reference number	3
Title of your thesis / dissertation	GEOMETRY AND ELECTRONIC STRUCTURE OF DOPED CLUSTERS VIA THE COALESCENCE KICK METHOD
Expected completion date	Jul 2009
Estimated size(pages)	326
Total	0.00 USD

Terms and Conditions

Introduction
The publisher for this copyrighted material is Springer Science + Business Media. By clicking "accept" in connection with completing this licensing transaction, you agree that the following terms and conditions apply to this transaction (along with the Billing and Payment terms and conditions established by Copyright Clearance Center, Inc. ("CCC"), at the time that you opened your Rightslink account and that are available at any time at http://myaccount.copyright.com).

Limited License
With reference to your request to reprint in your thesis material on which Springer Science and Business Media control the copyright, permission is granted, free of charge, for the use indicated in your enquiry. Licenses are for one-time use only with a maximum distribution equal to the number that you identified in the licensing process.

This License includes use in an electronic form, provided it is password protected or on the university's intranet, destined to microfilming by UMI and University repository. For any other electronic use, please contact Springer at (permissions.dordrecht@springer.com or permissions.heidelberg@springer.com)

The material can only be used for the purpose of defending your thesis, and with a maximum of 100 extra copies in paper.

Although Springer holds copyright to the material and is entitled to negotiate on rights, this license is only valid, provided permission is also obtained from the (co) author (address is given with the article/chapter) and provided it concerns original material which does not carry references to other sources (if material in question appears with credit to another source, authorization from that source is required as well). Permission free of charge on this occasion does not prejudice any rights we might have to charge for reproduction of our copyrighted material in the future.

Altering/Modifying Material: Not Permitted
However figures and illustrations may be altered minimally to serve your work. Any other abbreviations, additions, deletions and/or any other alterations shall be made only with prior written authorization of the author(s) and/or Springer Science + Business Media. (Please contact Springer at permissions.dordrecht@springer.com or permissions.heidelberg@springer.com)

Reservation of Rights
Springer Science + Business Media reserves all rights not specifically granted in the combination of (i) the license details provided by you and accepted in the course of this licensing transaction, (ii) these terms and conditions and (iii) CCC's Billing and Payment terms and conditions.

Copyright Notice:
Please include the following copyright citation referencing the publication in which the material was originally published. Where wording is within brackets, please include verbatim.
"With kind permission from Springer Science+Business Media: <book/journal title, chapter/article title, volume, year of publication, page, name(s) of author(s), figure number(s), and any original (first) copyright notice displayed with material>."

Warranties: Springer Science + Business Media makes no representations or warranties with respect to the licensed material.

Indemnity
You hereby indemnify and agree to hold harmless Springer Science + Business Media and CCC, and their respective officers, directors, employees and agents, from and against any and all claims arising out of your use of the licensed material other than as specifically authorized pursuant to this license.

No Transfer of License
This license is personal to you and may not be sublicensed, assigned, or transferred by you to any other person without Springer Science + Business Media's written permission.

No Amendment Except in Writing
This license may not be amended except in a writing signed by both parties (or, in the case of Springer Science + Business Media, by CCC on Springer Science + Business Media's behalf).

Objection to Contrary Terms
Springer Science + Business Media hereby objects to any terms contained in any purchase order, acknowledgment, check endorsement or other writing prepared by you, which terms are inconsistent with these terms and conditions or CCC's Billing and Payment terms and conditions. These terms and conditions, together with CCC's Billing and Payment terms and conditions (which are incorporated herein), comprise the entire agreement between you and Springer Science + Business Media (and CCC) concerning this licensing transaction. In the event of any conflict between your obligations established by these terms and conditions and those established by CCC's Billing and Payment terms and conditions, these terms and conditions shall control.

Jurisdiction
All disputes that may arise in connection with this present License, or the breach thereof, shall be settled exclusively by the country's law in which the work was originally published.

v1.2

Gratis licenses (referencing $0 in the Total field) are free. Please retain this printable license for your reference. No payment is required.

If you would like to pay for this license now, please remit this license along with your payment made payable to "COPYRIGHT CLEARANCE CENTER" otherwise you will be invoiced within 30 days of the license date. Payment should be in the form of a check or money order referencing your account number and this license number 2212071302934.
If you would prefer to pay for this license by credit card, please go to
http://www.copyright.com/creditcard to download our credit card payment authorization form.
contact us referencing this license number 2212071302934 and noting the reason for cancellation..

Washington State University   **Pacific Northwest National Laboratory**

Department of Physics   Chemical & Materials Science Division
2710 University Drive   MS K8-88, P.O. Box 999
Richland, WA 99354-1671   3020 Q Street
                                            Richland, WA 99352

Lai-Sheng Wang
Professor & Affiliate Senior Chief Scientist

Tel: 509-371-6138
Fax: 509-371-6139
E-mail: ls.wang@pnl.gov
http://www.tricity.wsu.edu/~physics

April 14, 2009

Mr. Boris B. Averliv
Department of Chemistry
Utah State University

Dear Mr. Boris B. Averkiev

This letter is to confirm that you have my permission to use our nine joint papers as listed below:

1. "Planar Nitrogen-Doped Aluminum Clusters Al_xN^- (x=3-5)", J. Chem. Phys. 2006, 125, 124305-1-12.

2. "Probing the Structure and Bonding in Al_6N^- and Al_6N by Photoelectron Spectroscopy and Ab Initio Calculations", J. Phys. Chem. A, 2007, 111, 34-41.

3. "Experimental and Theoretical Evidence against Hypercoordinate Planar Carbon", Angew. Chem. Int. Ed. 2007, 46, 4277-4280.

4. "Delata-Aromaticity in $[Ta_3O_3]^-$", Angew. Chem. Int. Ed. 2007, 46, 12864-12866.

5. "Aromaticity and Antiaromaticity in Transition-Metal Systems", Phys. Chem. Chem. Phys. 2008, 10, 257-267.

6. "Photoelectron Spectroscopy and Ab Initio Study of the Structure and Bonding of Al_7N^- and Al_7N", J. Phys. Chem. A, 2008, 112, 1873-1879.

7. "Carbon Avoids Hypercoordination in CB_6^-, CB_6^{2-}, and $C_2B_5^-$ Planar Carbon-Boron Clusters", J. Am. Chem. Soc. 2008, 130, 9248-9250.

8. "Experimental and Theoretical Investigation of Three-Dimensional Nitrogen-Doped aluminum Clusters Al_8N^- and Al_8N", J. Chem. Phys. 2009, 130, 134303-1-7.

9. "Lessons from Experimental and Theoretical Investigations of CB_8^-: Towards Rational Design of Hypercoordinated Planar Chemical Species", submitted for publication.

in part or in full for preparation or presentation of your dissertation.

Sincerely yours,

Lai-Sheng Wang

Washington State University   **Pacific Northwest National Laboratory**

Department of Physics   *Chemical & Materials Sciences Division*
2710 University Drive, Richland, WA 99354   MS K8-88, P.O. Box 999, Richland, WA 99352

Hua-Jin Zhai, Ph.D.
Phone: 509-371-6148
Fax: 509-371-6139
E-mail: Hua-Jin.Zhai@pnl.gov

Boris B. Averkiev

Department of Chemistry and Biochemistry

Utah State University

Logan, Utah 84322

20 May, 2009

Dear Boris B. Averkiev
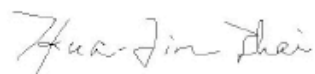
This letter is to confirm that you have my permission to use our common papers in part or in full for preparation or presentation of your PhD dissertation.

1. "Delta-Aromaticity in $[Ta_3O_3]^-$", *Angew. Chem. Int. Ed.* 2007, 46, 4277-4280.
2. "Aromaticity and Antiaromaticity in Transition-Metal Systems", *Phys. Chem. Chem. Phys.* 2008, 10, 257-267.

Sincerely,

Hua-Jin Zhai, Ph.D.

Boris Averkiev <boris.averkiev@aggiemail.usu.edu>   **Tue, Jun 9, 2009 at 1:44 PM**

To: wang <ls.wang@pnl.gov>

Dear Professor Wang,
Thank you very much for your letter of recommendation. Could you,
please, also send a recommendation letter to Professor
Gustavo E. Scuseria who agreed to consider my application as a
postdoctoral researcher?

Here is his information:
Gustavo E. Scuseria
Robert A. Welch Professor of Chemistry
Professor of Physics and Astronomy
Chemistry Department Vice Chair
Rice University
Houston, Texas 77005-1892
guscus@rice.edu | voice +1 713-348-4746
http://python.rice.edu/~guscus/

I also have one more question - do you have, by chance, e-mail address
of Doctor Xi Li. I need a permission from him to use our common papers
in my dissertation. I used e-mail li@rowland.harvard.edu, which I
found in Dima's dissertation, but he didn't reply. May be now he uses
different e-mail.

---

wang <ls.wang@pnl.gov>   **Wed, Jun 10, 2009 at 10:28 AM**

To: Boris Averkiev <boris.averkiev@aggiemail.usu.edu>

It's done. Good luck.

Xi Li is a professor at Fudan Univ in Shanghai. I do not have his e-mail. You may look it up on the
web.

19 May, 2009

Dear Mr. Boris B. Averkiev

This letter is to confirm that you have my permission to use our five common papers:

1. "CB_7^-: Experimental and Theoretical Evidence against Hypercoordinate Planar Carbon", Angew. Chem. Int. Ed. 2007, 46, 4550-4553.

2. "Photoelectron Spectroscopy and Ab Initio Study of the Structure and Bonding of Al_7N^- and Al_7N", J. Phys. Chem. A, 2008, 112, 1873-1879.

3. "Carbon Avoids Hypercoordination in CB_6^-, CB_6^{2-}, and $C_2B_5^-$ Planar Carbon-Boron Clusters", J. Am. Chem. Soc. 2008, 130, 9248-9250.

4. "Experimental and Theoretical Investigation of Three-Dimensional Nitrogen-Doped aluminum Clusters Al_8N^- and Al_8N", J. Chem. Phys. 2009, 130, 134303-1-7.

5. "Lessons from Experimental and Theoretical Investigations of CB_8^-: Towards Rational Design of Hypercoordinated Planar Chemical Species", submitted for publication.

in part or in full for preparation or presentation of your dissertation.

Sincerely

Lei-Ming Wang

05/19/09

19 May, 2009

Dear Mr. Boris B. Averkiev

This letter is to confirm that you have my permission to use our five common papers:

1. "CB_7^-: Experimental and Theoretical Evidence against Hypercoordinate Planar Carbon", Angew. Chem. Int. Ed. 2007, 46, 4550-4553.

2. "Photoelectron Spectroscopy and Ab Initio Study of the Structure and Bonding of Al_7N^- and Al_7N", J. Phys. Chem. A, 2008, 112, 1873-1879.

3. "Carbon Avoids Hypercoordination in CB_6^-, CB_6^{2-}, and $C_2B_5^-$ Planar Carbon-Boron Clusters", J. Am. Chem. Soc. 2008, 130, 9248-9250.

4. "Experimental and Theoretical Investigation of Three-Dimensional Nitrogen-Doped aluminum Clusters Al_8N^- and Al_8N", J. Chem. Phys. 2009, 130, 134303-1-7.

5. "Lessons from Experimental and Theoretical Investigations of CB_8^-: Towards Rational Design of Hypercoordinated Planar Chemical Species", submitted for publication.

in part or in full for preparation or presentation of your dissertation.

Sincerely

Dr. Wei Huang

UNIVERSITY OF CALIFORNIA, BERKELEY

BERKELEY · DAVIS · IRVINE · LOS ANGELES · RIVERSIDE · SAN DIEGO · SAN FRANCISCO   SANTA BARBARA · SANTA CRUZ

DEPARTMENT OF CHEMISTRY
BERKELEY, CALIFORNIA 94720-1460

April 03, 2009

Dear Mr. Boris B. Averkiev

This letter is to confirm that you have my permission to use our four common papers

1. "δ-Aromaticity in $[Ta_3O_3]^-$" (Angew. Chem. Int. Ed. 2007, 46, 12864-12866)

2. "CB_7^-: Experimental and Theoretical Evidence against Hypercoordinate Planar Carbon" (Angew. Chem. Int. Ed. 2007, 46, 4277-4280)

3. "Aromaticity and Antiaromaticity in Transition-Metal Systems" (Phys. Chem. Chem. Phys. 2008, 10, 257-267)

4. "Carbon Avoids Hypercoordination in CB_6^-, CB_6^{2-}, and $C_2B_5^-$ Planar Carbon-Boron Clusters" (J. Am. Chem. Soc. 2008, 130, 9248-9250)

in part or in full in preparation or presentation of your PhD dissertation.

Sincerely,

Dr. Dmitry Yu. Zubarev

Seth Call
Brigham Young University
1922 N 840 W
Provo, UT 84604
801-368-0565

Boris Averkiev
Department of Chemistry and Biochemistry
Utah State University
0300 Old Main Hill
Logan, UT 84322-0300
Fax: (435) 797-3390

Dear Boris,

I hereby give you permission to use our common paper in your dissertation:

Photoelectron Spectroscopy and Ab Initio Study of the Structure and Bonding of Al_7N-and Al_7N J. Phys. Chem. A, 2008, 112, 1873-1879

Good luck!

Sincerely,

Seth Call

Seth Call

22 May, 2009

Dear Mr. Boris B. Averkiev

This letter is to confirm that you have my permission to use our common work "Recent Advances in All-Transition Metal Aromaticity and Antiaromaticity" in part or in full in preparation or presentation of your PhD dissertation.

Sincerely,

A. P. Sergeeva

CURRICULUM VITAE

Boris Averkiev

Department of Chemistry & Biochemistry

Utah State University

0300 Old Main Hill

Logan, UT 84322-0300

Phone (435) 797-7507

boris.averkiev@aggiemail.usu.edu

EDUCATION

2009 - Ph.D. expected in 07.2009. Utah State University, Department of Chemistry and Biochemistry.

2005 – M.S. New Mexico Highlands University, Department of Natural Sciences.

1998 – M.S. Moscow Academy of Fine Chemical Technology, Moscow, Russia

1996 – B.S. Moscow Academy of Fine Chemical Technology, Moscow, Russia

AWARDS AND HONORS

2009 USU Graduate Research Assistant of the Year

2009 College of Science PhD Graduate Researcher of the Year

2008 - 2009 USU School of Graduate Studies Dissertation Fellowship

2008 Outstanding Graduate Student in Chemistry

PROFESSIONAL AFFILIATIONS

Member of American Chemical Society.

RESEARCH EXPERIENCE

2005-Present Thesis Research, Ph.D. Degree Research, Physical Chemistry, Supervisor: Dr. Alexander I. Boldyrev.

2002-2005 Thesis Research, M.S. Degree Research, Physical Chemistry, Supervisors: Dr. Tatiana V. Timofeeva, Dr. Mikhail Yu. Antipin.

1998-2002 Research Associate in Laboratory of X-ray analysis, Institute of Organoelement Compounds, Russian Academy of Sciences, Moscow, Russia.

EXPERIENCE AND SKILLS

Tools:

Ab Initio and DFT Quantum Chemical Methods, Molecular Mechanics, Genetic Algorithm, Monte Carlo, Crystal Structure Prediction.

Programs:

Gaussian, MOLPRO, ADF, SHELXTL - Structure Solution and Refinement Package, Cambridge Structural Database (CSD), Cerius2 Package, Material Studio.

Languages:

English (fluent), Russian (native)

C, C++, JAVA, HTML

Capabilities:

Electronic structure calculations

Multiconfigurational and relativistic methods

Small molecules and clusters: structure, spectroscopic properties

Analysis of chemical bonding

X-Ray Diffraction (Siemens P3/PC, Syntex $P2_1$, Bruker SMART, Enraf-Nonius CAD diffractometers) experimental technique, crystal structure solution and refinement.

SOFTWARE DEVELOPMENT

1) Program grouping all symmetrically equivalent reflections from X-ray experiment. This program tests the symmetry of crystal structure and reveals bad groups of equivalent reflections.

2) Working with Polymorph Predictor in New Mexico Highland University I realized that it has one problem – output predicted structures are not given in standard

setting, so it is rather difficult to compare predicted structures and experimental one. The program reads Polymorph predictor output file, converts unit cell parameters to standard setting and makes file with new parameters and coordinates for each predicted structure.

3) Method for the global minima search. This method is a modified famous "kick method", where all structures are generated by random positioning of atoms in space, with following geometry optimization. Many structures generated by kick method are consisted of many unconnected parts. It takes a lot of computational time to optimize them; some of them even stay unconnected after optimization. In the program the randomly generated structure is first modified by a coalescence procedure – all atoms gradually moving to the geometric center. When two atoms get connected, they are considered like one particle and for all next steps they are moving together as a whole particle. The procedure is finished when all atoms get connected in one cluster.

RESEARCH INTERESTS

- Quantum chemical investigation of small molecules and clusters
- Quantum chemical and experimental investigation of crystal structures
- General theory of chemical bonding in clusters
- Relativistic quantum chemistry
- Group theory
- Symmetry in quantum chemistry
- Symmetry of crystal structures
- Developing method, algorithm, and writing a program for global minimum search.

TEACHING AND MENTORING EXPERIENCE

Spring 2009 Teaching Assistant, Principles of Chemistry I (CHEM 1210), Utah State University.

July, 2008 Mentoring Intech Collegiate High School student Mahli Olson during Summer School.

Fall 2007 - Spring 2008 Mentoring first year graduate students Alina Sergeeva and Jared Olson, Utah State University.

June, 2007 Mentoring Intech Collegiate High School student Aaron Hooper during Summer School.

Spring 2005 Teaching Assistant, Chemistry for the Non-Scientist (CHEM 100), New Mexico Highlands University.

Fall 2004 Teaching Assistant, Chemistry for the Non-Scientist (CHEM 100), New Mexico Highlands University.

Fall 2004 Teaching Assistant, General Chemistry 1 (CHEM 211), New Mexico Highlands University.

Spring 2004 Teaching Assistant, Chemistry for the Non-Scientist (CHEM 100), New Mexico Highlands University.

Spring 2004 Teaching Assistant, Chemistry Laboratory 7 (CHEM 519), New Mexico Highlands University.

Fall 2004 Teaching Assistant, Chemistry for the Non-Scientist (CHEM 100), New Mexico Highlands University.

Spring 2003 Teaching Assistant, Chemistry Laboratory 2 (CHEM 216), New Mexico Highlands University.

PUBLICATIONS

Utah State University:

45. A. P. Sergeeva, B. B. Averkiev, A. I. Boldyrev, Recent Advances in All-Transition Metal Aromaticity and Antiaromaticity, In "Recent Advances in Metal-Metal Bonding" Structure and Bonding series, submitted for publication (Invited chapter).

44. L.-M. Wang, W. Huang, L. S. Wang, B. B. Averkiev, A. I. Boldyrev,
Experimental and Theoretical Investigation of 3-Dimensional Nitrogen-Doped Aluminum Clusters Al_8N^- and Al_8N, *J. Chem. Phys*. 130, 134303-1-7, **2009**.

43. B. B. Averkiev, D. Yu. Zubarev, L.-M. Wang, W. Huang, L. S. Wang, A. I. Boldyrev, Carbon Avoids Hypercoordination in CB_6^-, CB_6^{2-}, and $C_2B_5^-$ Planar Carbon-Boron Clusters, *J. Am. Chem. Soc*. 130, 9248-9250, **2008** (communication).

42. B. B. Averkiev, S. Call, A. I. Boldyrev, L. M. Wang, W. Huang, L. S. Wang, Photoelectron Spectroscopy and *Ab Initio* Study of the Structure and Bonding of Al_7N^- and Al_7N, *J. Phys. Chem. A* 112, 1873-1879, **2008** (cover page).

41. D. Yu. Zubarev, B. B. Averkiev, H.-J. Zhai, L. S. Wang, A. I. Boldyrev, Aromaticity and Antiaromaticity in Transition-Metal Systems *Phys. Chem. Chem. Phys.* 10, 257-267, **2008** (perspective article, cover page).

40. B. B. Averkiev, A. I. Boldyrev, Theoretical Design of Planar Molecules with 9- and 10-Coordinated Central Atom, *Russian Chemical Journal (Journal of the D.I. Mendeleev Russian Chemical Society)* 51, 87-90, **2007** (invited article).

39. B. B. Averkiev, A. I. Boldyrev, Hf_3 cluster is triply (σ-, π-, and δ-) aromatic in the lowest D_{3h}, $^1A_1'$ state, *J. Phys. Chem. A* 111, 12864-12866, **2007** (letter).

38. L.-M. Wang, W. Huang, B. B. Averkiev, A. I. Boldyrev, L. S. Wang, CB_7^-: Experimental and theoretical evidence against hypercoordinate planar carbon, *Angew. Chem. Int. Ed.* 46, 4550-4553, **2007**.

37. H.-J. Zhai, B. B. Averkiev, D. Yu. Zubarev, L. S. Wang, A. I. Boldyrev δ-Aromaticity in $[Ta_3O_3]^-$, *Angew. Chem. Int. Ed.* 46, 4277-4280, **2007**.

36. B. B. Averkiev, A. I. Boldyrev, X. Li, L. S. Wang, Probing the structure and bonding in Al_6N^- and Al_6N by photoelectron spectroscopy and ab initio calculations, *J. Phys. Chem. A*, 111, 34-41, **2007**.

35. B. B. Averkiev, A. I. Boldyrev, X. Li, L. S. Wang, Planar nitrogen-doped aluminum clusters Al_xN^- (x=3-5), *J. Chem. Phys.* 125, 124305-1-12, **2006**.

Laboratory of X-ray analysis, Institute of Organoelement Compounds:

34. Yu. G. Gololobov, I. R. Golding, M. A. Galkina, B. V. Lokshin, I. A. Garbuzova, P. V. Petrovskii, Z. A. Starikova, B. B. Averkiev, Reactions of distabilized beta-dicarbonyl sulfonium and iodonium ylides with isocyanates, *Russ. Chem. Bul.* 55, 883-891, **2006**.

33. N. Y. Kuznetsov, Z. A. Starikova, B. B. Averkiev, Y. N. Bubnov Synthesis of 6,7-benzo-3-borabicyclo[3.3.1]nonane and its 3-aza analog from 2-allylphenyl(diallyl)borane. Intramolecular arylboration of the C=C bond, *Russ. Chem. Bul.* 54, 678-683, **2005**.

32. A. B. Sheremetev, E. A. Ivanova, D. E. Dmitriev, V. O. Kulagina, B. B. Averkiev, M. Yu. Antipin, Synthesis of Macrocycles Incorporating Azo-bis(azofurazan) Framework, *J. Heterocycl. Chem.* 42, 803-810, **2005**.

31. I. L. Yudin, A. B. Sheremetev, B. B. Averkiev, M. Yu. Antipin, Furoxano[3,4-b]pyrazines: The first synthesis and X-ray structure, *J. Heterocycl. Chem.*, 42, 691-694, **2005**.

30. A. B. Sheremetev, N. S. Aleksandrova, D. E. Dmitriev, B. B. Averkiev, M. Yu. Antipin, Synthesis and X-ray study of novel azofurazan-annulated macrocyclic lactams, *J. Heterocycl. Chem.*, 42, 519-525, **2005**.

29. B. B. Averkiev, M. Yu. Antipin, A. B. Sheremetev, T. V. Timofeeva, Computer simulation of crystal structure for three furazan derivatives, *Cryst. Growth Des.* 5, 631-641, **2005**.

28. V. Tudor, V. C. Kravtsov, M. Julve, F. Lloret, Y. A. Simonov, B. B. Averkiev, M. Andruh, A new ferromagnetically coupled μ-alkoxo-μ-acetato copper(II) trinuclear complex: [Cu₃(H₂tea)(Htea)(CH₃COO)₂](ClO₄) (H₃tea = triethanolamine), *Inorg. Chim. Acta*, 358, 2066-2072, **2005**.

27. A. T. Soldatenkov, K. B. Polyanskii, A. V. Temesgen, N. D. Sergeeva, V. V. Vysotskaya, B. B. Averkiev, M. Yu. Antipin and N. N. Lobanov, Oxidative Reactions of Azines. 11. The Influence of Manganese Dioxide on the Reaction of Tetrahydropyridines with Formaldehyde: Synthesis and Molecular Structures of 3-Oxa-7-azabicyclo[3.3.1]- and 6-Oxa-2-azabicyclo[3.2.1]octanes, *Chem. Heterocycl. Compd.* 40, 641-649, **2004**.
26. A. F. Shidlovskii, A. S. Peregudov, B. B. Averkiev, M. Yu. Antipin, N. D. Chkanikov, Heterocyclization of 2-chloro-1-cyano-1-diethoxyphosphoryl-2-trifluoro-methylethylene and 2-chloro-2-chlorodifluoromethyl-1-cyano-1-diethoxyphosphoryl-ethylene, *Rus. Chem. Bul.* 53, 2060-2070, **2004**.

25. P. V. Pasternak, B. B. Averkiev, M. Yu. Antipin, A. S. Peregudov, N. D. Chkanikov, Synthesis and some heterocyclization reactions of new diethyl (1,1-difluoro-3,3-dicyano-2-trifluoromethylallyl)phosphonate and ethyl 3,3-dicyano-2-[(diethoxyphosphoryl)-difluoromethyl]acrylate, *J. Fluorine Chem.* 125, 1853–1868, **2004.**

24. T. V. Timofeeva, T. Kinnibrugh, O. Ya. Borbulevych, B. B. Averkiev, V. N. Nesterov, A. Sloan, M. Yu. Antipin, Vanishing polymorphism of (2E)-2-cyano-3-[4-(diethylamino)phenyl]prop-2-enethioamide: X-ray structural study and polymorph prediction, *Cryst. Growth Des.* 4, 1265-1276, **2004**.

23. L. N. Kuleshova, B. B. Averkiev, D. V. Gusev, K. Yu. Suponitskii, M. Yu. Antipin, Conformational polymorphism of N-(4-butoxyphenyl)-4-(4'-nitrophenyl)-2-thiazolamine, *Crystallogr. Rep.* 49, 798-806, **2004**.

22. A. B. Sheremetev, V. G. Andrianov, E. V. Mantseva, E. V. Shatunova, N. S. Aleksandrova, I. L. Yudin, D. E. Dmitriev, B. B. Averkiev, M. Yu. Antipin, Synthesis of secondary and tertiary aminofurazans, *Russ. Chem. Bul.* 53, 596-614, **2004**.

21. B. B. Averkiev, T. V. Timofeeva, A. B. Sheremetev, E. V. Shatunova, M. Yu. Antipin, Difurazano[3,4-b:3',4'-f]-4,5-diaza-1,8-dioxacyclododecine and an acyclic analogue, *Acta Cryst.* C60, o520-o523, **2004**.

20. A. B. Sheremetev, E. V. Shatunova, B. B. Averkiev, D. E. Dmitriev, V. A. Petukhov, M. Yu. Antipin, Chromophoric macrocycles from the oxidation of bis(aminofurazanylic) ethers of 1,2-diols, *Heteroat. Chem.* 15, 131-145, **2004**.

19. V. N. Yarovenko, A. A. Es'kov, G. V. Zatonsky, I. V. Zavarzin, M. M. Krayushkin, B. B. Averkiev, M. Yu. Antipin, Synthesis of azomethylene derivatives of 4-chloro-5H-1,2,3-dithiazole, *J. Heterocycl. Chem.*, 41, 37-43, **2004**.

18. A. B. Sheremetev, S. M. Konkina, I. L. Yudin, D. E. Dmitriev, B. B. Averkiev, M. Yu. Antipin, (Pyrrol-1-yl)furazans, *Russ. Chem. Bul.* 52, 1413-1418, **2003**.

17. B. B. Averkiev, M. Yu. Antipin, A. B. Sheremetev, T. V. Timofeeva, Four 3-cyanodifurazanyl ethers: potential propellants, *Acta Cryst*. C59. o383-o387, **2003**.

16. D. A. Lemenovskii, M. V. Makarov, V. P. Dyadchenko, A. E. Bruce, M. R. M. Bruce, S. A. Larkin, B. B. Averkiev, Z. A. Starikova, M. Yu. Antipin, Syntheses and crystal structures of ferrocenyl derivatives of biphenyl, *Russ. Chem. Bul.*, 52, 607-615, **2003**.

15. Yu. V. Tomilov, D. N. Platonov, B. B. Averkiev, E. V. Shulishov, O. M. Nefedov, Unusual formation of tetrahydropyridazine-3,4,5,6-tetracarboxylic and

pyrroletetracarboxylic esters upon decomposition of methyl diazoacetate in the presence of pyridine, *Russ. Chem. Bul.* 52, 187-191, **2003**.

14. E. V. Guseva, N. V. Volchkov, Y. V. Tomilov, B. B. Averkiev, O. M. Nefedov, Formation of cyclobutylidenepyrazolines by methanolysis of 6-(2,3,3-trifluorocyclobutenyl)-4,5-diazaspiro[2.4]hept-4-ene
Eur.J.Org.Chem. 492-495, **2003**.

13. B. Tashkhodzhaev, K. K. Turgunov, B. Usmanova, B. B. Averkiev, M. Yu. Antipin, Kh. M. Shakhidoyatov, Crystal and molecular structure of 2-oxo- and 2-thioxo-5,6-dimethyl-1H,3H-thieno[2,3-d]pyrimidin-4-ones, *J. Struct. Chem.* 43, 876–880, **2002**.

12. R. G. Kostyanovsky, V. Schurig, O. Trapp, K. A. Lyssenko, B. B. Averkiev, G. K. Kadorkina, A. V. Prisyanik, V. R. Kostyanovsky, Chiral 1-alkoxyaziridines: resolution, nitrogen inversion, structure and diastereomeric transformations, *Mendeleev Commun.* 12, 137-140, **2002**.

11. X.-J. Huang, G. H. Kuhn, V. N. Nesterov, B. B. Averkiev, B. Penn, M. Yu. Antipin, T. V. Timofeeva, (E)-(4-Hydroxyphenyl)(4-nitrophenyl)diazene, (E)-(4-methoxyphenyl)-(4-nitrophenyl)diazene and (E)-[4-(6-bromohexyloxy)phenyl](4-cyanophenyl)diazene, *Acta Cryst.* C58, o624-o628, **2002**.

10. M. N. Sultankhodzhaev, B. Tashkhodzhaev, B. B. Averkiev, M. Yu. Antipin, Secokaraconitine, a new diterpenoid alkaloid from Aconitum karacolicum, *Chem. Nat. Compd.* 38, 78-82, **2002**.

9. A. S. Golubev, P. V. Pasternak, A. F. Shidlovskii, L. N. Saveleva, B. B. Averkiev, S. P. Peregudov, N. D. Chkanikov, Synthesis and some heterocyclisation reactions of CF_2H- and CF_2Cl-substituted 1,dicyanoethylenes", *J. Fluorine Chem.* 114, 63-74, **2002**.

8. B. B. Averkiev, M. Yu. Antipin, I. L. Lidin, A. B. Sheremetev, X-ray structural study of three derivatives of dinitropyrazine, *J. Mol. Struct.* 606, 139-146, **2002**.

7. A. V. Bobrov, B. B. Averkiev, S. G. Zlotin, M. Yu. Antipin, Unusual scission of 3,7-dichlorobisisothiazolo[4,5-b:4',5'-e]pyrazine by nucleophiles, *Russ. Chem. Bul.* 50, 1287-1290, **2001**.

6. I. L. Yudin, S. M. Aronova, A. B. Sheremetev, B. B. Averkiev, M. Yu. Antipin, Facile and general synthesis of pyrrolo[2,3-b]pyrazines via 2-(dicyanoylidene)-3-halopyrazines, *Mendeleev Commun.* 11, 152-153, **2001**.

5. R. G. Kostyanovsky, V. R. Kostyanovsky, B. B. Averkiev, K. A. Lyssenko, P. E. Dormov, Bis-aziridinomethanes: synthesis, structure and properties, *Mendeleev Commun.* 11, 141-143, **2001**.

4. A. T. Soldatenkov, T. P. Khristoforova, A. W. Temesgen, B. N. Anissimov, B. B. Averkiev, L. N. Kuleshova, V. N. Khrustalev, M. Yu. Antipin, N. N. Lobanov, Oxidizing reactions of azines. 7. Imination of 4-aryl-1,2,3,6-tetrahydropyridines by arylamines in the presence of potassium permanganate. Molecular structure of 1-methyl-2-(4-nitrophenylimino)-4-phenyl-1,2,5,6-tetrahydropyridine, *Chem. Heterocycl. Compd.* 37, 715-722, **2001**.

3. R. G. Kostyanovsky, O. N. Krutius, I. A. Bronzova, D. A. Lenev, K. A. Lyssenko, B. B. Averkiev, Stereoregular self-assembling of diastereomeric bicyclic bis-lactam diesters, *Mendeleev Commun.* 11, 6-8, **2001**.

2. Yu. V. Tomilov, I. V. Kostyuchenko, E. V. Shulishov, B. B. Averkiev, M. Yu. Antipin, Different reactivities of regioisomeric azimines, adducts of phthalimidonitrene

with 5-bromospiro[1-pyrazoline-3,1'-cyclopropane], *Russ. Chem. Bul.* 49, 1919-1922, **2000**.

1. Yu. V. Tomilov, I. V. Kostyuchenko, E. V. Shulishov, B. B. Averkiev, M. Yu. Antipin, O. M. Nefedov, Formation and thermal decomposition of adducts of phthalimidonitrene with spiro(1-pyrazolinecyclopropanes), *Russ. Chem. Bul.* 48, 1316-1322, **1999**.

PRESENTATIONS AT PROFESSIONAL MEETINGS

5. (Poster) <u>B. B. Averkiev</u>, D, Yu. Zubarev, H. J. Zhai, L. S. Wang, A. I. Boldyrev, Multiple aromaticity, conflicting aromaticity, and multiple antiaromaticity in transition-metal systems, The 236th National American Chemical Society Meeting, Philadelphia, PA, August 17-21, **2008**.

4. (Poster) <u>B. B. Averkiev</u>, A. I. Boldyrev, L. S. Wang, Aromaticity and antiaromaticity in transition-metal systems, 22nd Austin Symposium on Molecular Structure, Austin, TX, 1-4 March, **2008**.

3. (Poster) <u>B. B. Averkiev</u>, A. I. Boldyrev, X. Li, L. S. Wang, Photoelectron spectroscopic and ab initio theoretical study of planar nitrogen doped aluminum clusters Al_3N^-, Al_4N^-, and Al_5N^-, 232nd National American Chemical Society Meeting, San Francisco, CA, September 10-14, **2006**.

2. (Poster) <u>B. B. Averkiev</u>, T. V. Timofeeva, A. B. Sheremetev, M. Yu. Antipin, The Structural Investigation of High Energetic Materials: Difurazanyl Ethers, American Crystallographic Association Meeting, Covington, KY, 26-31 July, **2003**.

1. (Poster) <u>B. B. Averkiev</u>, K. A. Lyssenko, M. Yu. Antipin, A. B. Sheremetev, I. L. Yudin, The crystal structure of furazane derivatives, II National Crystal Chemical Conference, Chernogolovka, Russia, 22-26 May, **2000**.